UNIVERSIDADE
BEIRA INTERIOR

Contribuição para o Estudo e Modelação do Comportamento de Vigas de Betão Estrutural à Torção Pura e Combinada

Mafalda Mangana Teixeira

Tese para obtenção do Grau de Doutor em
Engenharia Civil
(3º ciclo de estudos)

Orientador: Prof. Doutor Luís Filipe Almeida Bernardo

fevereiro de 2022

UNIVERSIDADE
BEIRA INTERIOR

Contribuição para o Estudo e Modelação do Comportamento de Vigas de Betão Estrutural à Torção Pura e Combinada

Mafalda Mangana Teixeira

(Versão final após defesa)

Composição do Júri:

Prof. Doutor João Paulo de Castro Gomes (Presidente)
Prof. Doutor Luís Filipe Almeida Bernardo (Orientador)
Prof. Doutor Bernardo Horowitz (Arguente)
Prof. Doutor Ricardo Carrazedo (Arguente)
Prof. Doutor Dario de Domenico (Arguente)
Prof. Doutor Jorge Miguel de Almeida Andrade (Vogal)

Provas Públicas realizadas a 14 de fevereiro de 2022

fevereiro de 2022

Esta tese foi desenvolvida no *Centre of Materials and Building Technologies* (C-MADE), entre 2017 e 2021.

Este trabalho foi submetido à Universidade da Beira Interior para defesa em prova pública.

C MADE
CENTRE OF MATERIALS
& BUILDING TECHNOLOGIES

UNIVERSIDADE
BEIRA INTERIOR

Agradecimentos

A realização desta tese não seria possível sem a colaboração e o contributo, de forma direta ou indireta, de algumas pessoas às quais quero aqui manifestar algumas palavras de agradecimento e reconhecimento.

Ao Professor Doutor Luís Filipe Almeida Bernardo, orientador científico desta tese, o meu mais sincero e profundo agradecimento, por todo o incentivo e encorajamento para continuar a fazer uma das coisas que mais gozo me dá na vida, estudar e aprender todos os dias; por toda a paciência e compreensão que a minha vida profissional obrigou a avançar e a recuar ao longo deste 3.º ciclo de estudos; por toda a generosidade e disponibilidade na transmissão de conhecimentos e experiência, não só na área da torção mas nas mais variadas áreas científicas; e, principalmente, pela amizade sempre demonstrada que não me fez desistir deste ciclo e me faz ter vontade de continuar a trabalhar em equipa.

Ao Professor Doutor Jorge Miguel de Almeida Andrade do Departamento de Engenharia Civil e Arquitetura da Universidade da Beira Interior, o meu agradecimento pela disponibilidade e apoio prestado na utilização dos seus aplicativos computacionais, bem como na implementação de alterações nos códigos para os modelos MVATM e GSVATM.

Ao Professor Doutor Sérgio Manuel Rodrigues Lopes do Departamento de Engenharia Civil da Universidade de Coimbra e investigador do *Center for Mechanical Engineering, Materials and Processes* (CEMMPRE), o meu agradecimento pelo seu apoio na realização do estudo que envolveu resultados experimentais do Laboratório de Ensaio de Materiais do referido departamento.

À minha família, em especial aos meus pais, Manuel e Lucília, e ao meu irmão Miguel, um profundo agradecimento por aceitarem as minhas escolhas, por me apoiarem incondicionalmente e por todo o carinho que me dão, que é tão importante para mim.

Ao Nelson, um especial agradecimento por todo o amor, amizade e carinho que todos os dias me oferece; por todo o apoio, paciência e compreensão demonstrados nos momentos mais difíceis, de pressão e de puro desânimo e por fazer com que a vida seja levada com mais descontração e alegria.

Resumo

Neste trabalho são apresentados vários contributos para o estudo e modelação do comportamento de vigas de betão estrutural à torção pura e à torção combinada com outros esforços internos (alguns casos). Todos os estudos apresentados focam o comportamento de vigas com secção transversal retangular (cheia e vazada).

Para a concretização do presente trabalho, procedeu-se à compilação de informação encontrada na literatura consultada sobre resultados experimentais de vigas de betão armado e pré-esforçado, ensaiadas primariamente à torção por diversos autores. O objetivo foi utilizar esta informação como base de validação para os vários estudos apresentados no presente trabalho.

Para a modelação do comportamento à torção de vigas de betão estrutural foram utilizados diversos modelos teóricos como base, nomeadamente: o *Modified Variable Angle Truss Model (*MVATM), o *Generalized Softened Variable Angle Truss Model* (GSVATM) e o *Combined Action Softened Truss Model* (CA-STM).

Para o MVATM foi proposta e validada a sua extensão para o cálculo do comportamento global à torção de vigas de betão pré-esforçado. Este trabalho deu origem a 1 artigo científico publicado numa revista internacional.

O GSVATM serviu de modelo base para o estudo comparativo das propostas de leis constitutivas médias para o betão à tração, encontradas na literatura consultada. O objetivo deste estudo foi identificar e avaliar a lei que melhor permite ao modelo prever o comportamento de vigas de betão armado em torção, para baixos níveis de carregamento, designadamente a transição entre o estado não fissurado e fissurado. Os resultados fizeram sobressair uma lei constitutiva média particular, a qual permite ao modelo obter a melhor aproximação dos resultados experimentais. Este trabalho deu origem a 1 artigo científico publicado numa revista internacional.

Para o CA-STM foi proposto um refinamento do modelo com uma solução de cálculo eficiente para a previsão do comportamento de vigas de betão armado sujeitas à torção combinada com flexão. Os resultados obtidos demonstraram que o refinamento proposto é adequado e que o novo procedimento de cálculo é mais simples e eficaz, com resultados bastante satisfatórios. Este trabalho deu origem a 1 artigo científico publicado numa revista internacional.

No âmbito do comportamento último de vigas de betão armado sujeitas à torção pura foi focado o estudo da ductilidade em torção. Para tal, foi proposta uma quantificação da ductilidade em torção e analisada a influência de vários parâmetros caracterizadores das vigas. Os resultados demonstraram que o tipo de secção transversal (cheia ou vazada), a classe de resistência do betão e a taxa total de armadura de torção são as variáveis de estudo que mais influenciam a ductilidade de uma viga de betão armado em torção. Foram também propostas orientações para a garantia da ductilidade em torção. Este trabalho deu origem a 1 artigo científico publicado numa revista internacional.

No que toca à verificação da segurança ao estado limite último das vigas de betão armado sujeitas à torção pura foi feito um estudo comparativo, envolvendo disposições normativas sobre torção de diversos documentos de dimensionamento de vigas de betão armado. O objetivo deste estudo foi verificar a sua fiabilidade para o cálculo do momento torsor resistente através da comparação com numerosos resultados experimentais. Os resultados demonstram que existe necessidade de rever alguns aspetos das disposições normativas para otimizar o dimensionamento de vigas de betão armado à torção. Este trabalho deu origem a 1 artigo científico publicado numa conferência internacional.

Por fim, tendo por base um estudo experimental previamente realizado e envolvendo vigas de alta resistência pré-esforçadas com secção vazada ensaiadas à torção, foi feito o estudo do comportamento registado e uma discussão dos resultados. Este trabalho deu origem a 1 artigo científico publicado numa revista internacional.

Palavras-chave

Vigas de Betão Estrutural; Torção; Pré-esforço; Flexão; Modelação do Comportamento Mecânico; Modelos da Analogia da Treliça Espacial; Avaliação Experimental; Resistência e Ductilidade; Documentos Normativos

Abstract

In this work, several contributions are presented for the study and modeling of structural concrete beams' behavior under pure torsion and combined with some other internal forces. All the presented studies focus on the behavior of beams with rectangular cross-sections (plain and hollow).

For this, experimental results of reinforced and prestressed concrete beams tested under torsion as the main loading, from several authors, were compiled. The aim was to use this information as a basis to validate several studies presented in this work.

To model the torsional behavior of structural concrete beams, several theoretical models were used as basis, namely: the Modified Variable Angle Truss Model (MVATM), the Generalized Softened Variable Angle Truss Model (GSVATM) and the Combined Action Softened Truss Model (CA-STM).

For the MVATM, an extension was proposed and validated in order to predict the global behavior of prestressed concrete beams under torsion. Based on this work, 1 scientific article was published in an international journal.

The GSVATM was used as a base model for perform a comparative study of the proposed smeared constitutive laws for tensile concrete found in the literature. The aim of this study was to evaluate and identify which law best allows the model to predict the behavior of reinforced concrete beams in torsion for low loading levels, namely the transition between the uncracked and cracked state. The results showed that there is a particular smeared constitutive law which allows the model to approximate better the experimental results. From the results of this work, 1 scientific article was published in an international journal.

For the CA-STM, a refinement of the model was proposed along with an efficient calculation solution to predict the behavior of reinforced concrete beams under torsion combined with bending. The obtained results showed that the proposed refinement is appropriate and the new calculation procedure is simpler and more efficient, with very satisfactory results. This work originated 1 scientific article published in an international journal.

For the ultimate torsional behavior of reinforced concrete beams, the study of ductility in torsion was particularly focused. For this, a quantification of the torsional ductility was proposed and the influence of several parameters, which characterize the beams, was analyzed. The results showed that the type of cross section (plain or hollow), the concrete compressive strength and the total ratio of torsional reinforcement are the variable studies which most influence the torsional ductility. Guidelines for ensuring torsional ductility were also proposed. Based on this study, 1 scientific article published in an international journal.

Regarding the safety for ultimate limit state of reinforced concrete beams under pure torsion, a comparative study was carried out involving the torsional guidelines from several normative documents. The aim of this study was to verify their reliability to predict the torsional strength by comparison with several experimental results. The results demonstrate that there is still a need to review some aspects of the normative guidelines to optimize the design of beams under torsion. This work originated 1 scientific article published in an international conference.

Finally, based on an experimental study previously carried out and involving pre-stressed high-strength beams with hollow section under torsion, a study on the behavior of such beams and a discussion of the results was carried out. This work originated 1 scientific article published in an international journal.

Keywords

Structural Concrete Beams; Torsion; Prestress; Bending; Modeling of the Mechanical Behavior; Space Truss Analogy Models; Experimental Evaluation; Strength and Ductility; Normative Documents

Lista de Publicações

Artigos incluídos nesta tese resultante do programa de investigação doutoral

Teixeira, M. M. and Bernardo, L. F. A. (2018). Ductility of RC beams under torsion. *Engineering Structures*. **168**: 759-769.https://doi.org/10.1016/j.engstruct.2018.05.021

Bernardo, L. F. A., and Teixeira, M. M. (2018). Modified softened truss-model for prestressed concrete beams under torsion. *Journal of Building Engineering*. **19**: 49-61. https://doi.org/10.1016/j.jobe.2018.04.024

Bernardo, L. F. A., Lopes, S. M. R. and Teixeira, M. M. (2020). Experimental Study on the Torsional Behaviour of Prestressed HSC Hollow Beams. *Applied Science*. **10**(2): 642. https://doi.org/10.3390/app10020642

Bernardo, L. F. A. and Teixeira, M. M. (2020). Refined softened-truss model with efficient solution procedure for reinforced concrete members under torsion combined with bending. *Structures*. **26**: 651-669. https://doi.org/10.1016/j.istruc.2020.04.055

Teixeira, M. M. and Bernardo, L. F. A. (2021). Evaluation of Smeared Constitutive Laws for Tensile Concrete to Predict the Cracking of RC Beams under Torsion with Smeared Truss Model. *Materials*. **14**(5): 1260. https://doi.org/10.3390/ma14051260

Teixeira, M. M. and Bernardo, L. F. A. (2021). Torsional strength of reinforced concrete beams – Evaluation of some codes of practice. *Concrete structures: New trends for eco-efficiency and performance*. Lisbon, June 2021. Fib Symposium. 2035-2046 pp.

Índice

Lista de Figuras

Capítulo 1

Capítulo 2

Modified softened truss-model for prestressed concrete beams under torsion

Evaluation of Smeared Constitutive Laws for Tensile Concrete to Predict the Cracking of RC Beams under Torsion with Smeared Truss Model

Refined softened-truss model with efficient solution procedure for reinforced concrete members under torsion combined with bending

Capítulo 3

Ductility of RC beams under torsion

Torsional Strength of Reinforced Concrete Beams – Evaluation of some Codes of Practice

Capítulo 4

Experimental Study on the Torsional Behavior of Prestressed HSC Hollow Beams

Lista de Tabelas

Capítulo 2

Modified softened truss-model for prestressed concrete beams under torsion

Evaluation of Smeared Constitutive Laws for Tensile Concrete to Predict the Cracking of RC Beams under Torsion with Smeared Truss Model

Refined softened-truss model with efficient solution procedure for reinforced concrete members under torsion combined with bending

Capítulo 3

Ductility of RC beams under torsion

Torsional Strength of Reinforced Concrete Beams – Evaluation of some Codes of Practice

Capítulo 4

Experimental Study on the Torsional Behavior of Prestressed HSC Hollow Beams

Lista de Acrónimos

ACI	*American Concrete Institute*
BA	Betão armado
BAR	Betão de alta resistência
BE	Betão estrutural
CA-STM	*Combined Action Softened Truss Model*
CEB	*Comité Européen du Béton*
C-MADE	*Centre of Materials and Building Technologies*
ELS	Estado Limite Serviço
ELU	Estado Limite Último
FA-STM	*Fixed Angle Softened Truss Model*
GSVATM	*Generalized Softened Variable Angle Truss Model*
MVATM	*Modified Variable Angle Truss Model*
PE	Pré-esforço
RA-STM	*Rotating Angle Softened Truss Model*
REBAP	Regulamento de Estruturas de Betão Armado e Pré-Esforçado
SMM	*Softened Membrane Model*
SMMT	*Softened Membrane Model for Torsion*
STA	*Space Truss Analogy*
STM	*Softened Truss Model*
UBI	Universidade da Beira Interior
VATM	*Variable Angle Truss Model*

Simbologia[1]

Letras latinas

C_1	Círculo de Mohr para o ensaio do betão à compressão uniaxial
C_2	Círculo de Mohr para o ensaio do betão à tração uniaxial
E_o	Módulo de elasticidade inicial do betão
f'_c	Resistência à compressão uniaxial do betão
f_r	Módulo de rotura reduzido para o betão
f'_t	Resistência à tração uniaxial do betão
T	Momento torsor; Momento torsor de rotura de uma viga pré-esforçada
T_b	Componente de flexão
T_{cr}	Momento torsor de fissuração
T_e	Momento torsor resistente elástico
T_n	Momento torsor resistente de uma viga de betão armado
T_{np}	Momento torsor resistente de uma viga de betão simples
T_p	Momento torsor plástico
T_t	Componente de torsão
T_u	Momento torsor resistente
T_y	Momento torsor de cedência de uma das armaduras de torção
x	Largura da secção transversal
y	Altura da secção transversal

Letras gregas

α	Coeficiente de Saint-Venant
α_p	Coeficiente plástico
ε	Extensão uniaxial
θ	Rotação transversal por unidade de comprimento
θ^I_{cr}	Rotação de torção correspondente a T_{cr}
θ_u	Rotação de torção correspondente a T_u
θ_y	Rotação de torção correspondente a T_y
ρ_{tot}	Taxa total de armadura de torção

[1] Simbologia referente ao Capítulo 1. A simbologia dos restantes capítulos encontra-se identificada nos respetivos artigos científicos.

σ	Tensão uniaxial
$\sigma_{máx}$	Tensão principal máxima de tração
τ	Tensão tangencial
$\tau_{máx}$	Tensão tangencial máxima de torção
γ	Factor de pré-esforço; Distorção

Capítulo 1

Enquadramento, revisão bibliográfica e objetivos do trabalho

O momento torsor constitui um dos quatro esforços internos (para além do momento fletor, esforço transverso e esforço axial) passíveis de ocorrer nas secções transversais de uma barra, como é o caso de uma viga de betão estrutural integrada numa estrutura para equilibrar um carregamento externo. Entende-se por momento torsor como a resultante dos momentos atuantes no centro de corte das secções transversais, sendo aqueles geralmente provocados por carregamentos excêntricos e que provocam a rotação dessas secções em torno do eixo axial do elemento. A resistência dos elementos estruturais a este esforço interno depende da rigidez da secção transversal e, no caso do betão estrutural, do estado comportamental (fissurado ou não fissurado). No dimensionamento de estruturas de betão é importante considerar os efeitos torsionais primários com vista a garantir um adequado comportamento para os Estados Limites (de Serviço e Último). Se tal objetivo é relativamente fácil de garantir antes de o betão fissurar, por aplicação das teorias clássicas da resistência dos materiais, já após a fissuração os estados internos de tensão para equilibrar o momento torsor e a deformação tornam a análise de uma viga de betão estrutural bastante mais complexa. Para este caso, modelos baseados em campos de tensões ou modelos de treliça têm-se revelado particularmente adequados.

1.1. A problemática da torção. Notas históricas.

Até meados do século XX, mesmo depois de o betão armado assumir um papel importante na conceção de estruturas, a torção era um fenómeno geralmente desprezado no processo de dimensionamento. Os códigos e regulamentos que regiam o dimensionamento de estruturas não incorporavam disposições específicas para o dimensionamento de secções à torção, remetendo para as disposições específicas de outros esforços internos, como a flexão e o esforço transverso, ou simplesmente não faziam menção a este esforço. Na época, era assumido que o momento torsor seria absorvido pela redistribuição de esforços que surgiam internamente numa estrutura em virtude da fendilhação, sendo a segurança garantida pelos elevados coeficientes de segurança à flexão estipulados pelos documentos normativos.

Porém, existia um caso particular onde era reconhecido que a torção apresentava um papel primário na resistência do elemento estrutural, o que mereceu a realização de ensaios e estudos específicos para determinar novas regras de dimensionamento. Tratava-se das designadas "estacas-parafuso" (*screwpiles*), elementos pré-fabricados construídos em betão e armados com uma armadura transversal helicoidal, os quais eram cravados no solo por meios mecânicos. Durante o processo de cravação eram introduzidos, simultaneamente, esforços de compressão e de torção no elemento.

A partir da Segunda Grande Guerra e com o advento de projetos arquitetónicos arrojados, os quais exigiam conceber estruturas com formas complexas e muitas vezes sujeitas a elevadas cargas excêntricas, os engenheiros projetistas começaram a sentir a falta de regras de dimensionamento específicas para a resistência à torção, tendo que, por vezes, se apoiar em estudos experimentais para avaliar a capacidade resistente de certos elementos estruturais. Foi o que aconteceu no caso de dois grandes projetos londrinos realizados na segunda metade da década de 40 do século passado e relatados por Armstrong [7] em 1956: a Ponte de *Waterloo* (Londres, 1945, Figura 1(a)) cujas cargas de projeto exercidas no tabuleiro originavam elevados momentos torsores nas vigas retangulares em caixão com três células (Figura 1(b) e 1(c)) [43]; e o *Royal Festival Hall* (Londres, 1951), onde foi necessário projetar uma viga triangular em caixão para apoiar a laje em consola do balcão superior do teatro (Figura 2(a) e 2(b)) [75].

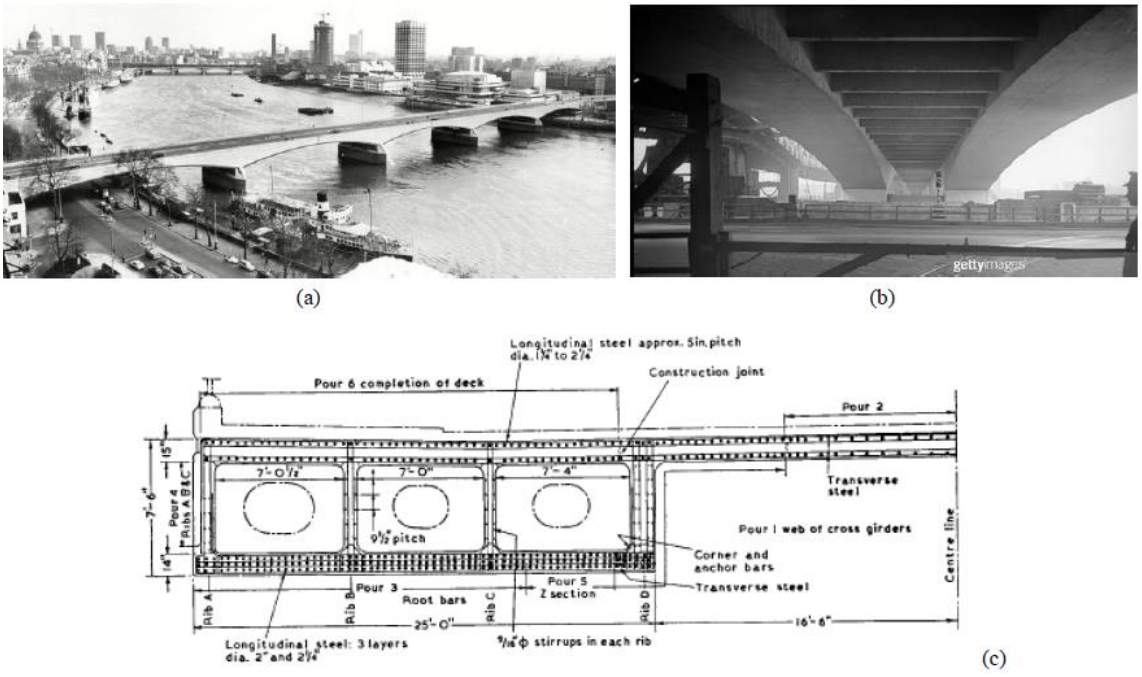

Figura 1. Ponte de *Waterloo*, Londres. (a) Registo fotográfico da ponte. (b) Pormenor da face inferior do tabuleiro. (c) Corte transversal do tabuleiro. [A] [D] [7].

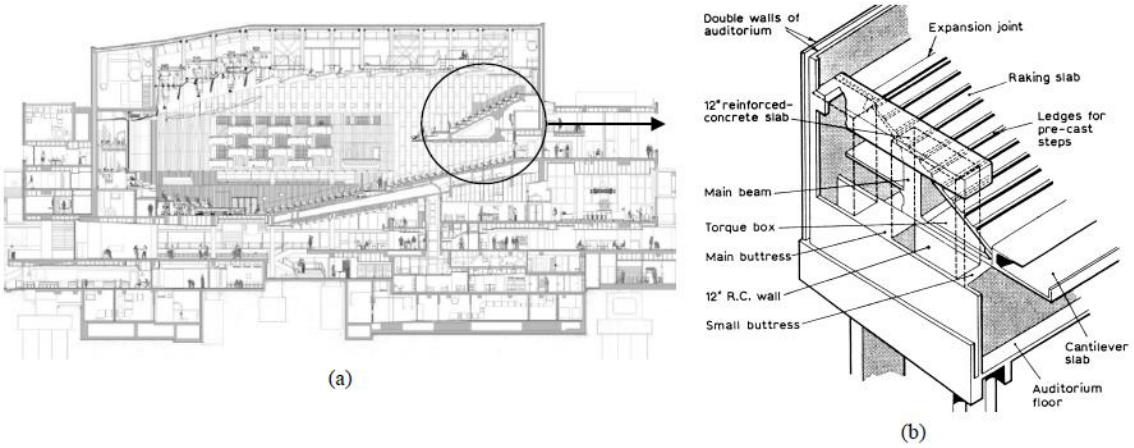

Figura 2. *Royal Festival Hall*, Londres. (a) Corte transversal do edifício. (b) Corte da viga triangular em caixão para apoiar a laje em consola. [75].

A partir daquela década de 40 verificou-se um "*boom*" de modernização na arquitetura. As estruturas, até então pensadas de forma plana, ganharam dimensões espaciais, formas complexas e irregulares que obrigaram, muitas vezes, a considerar nas estruturas carregamentos de grande excentricidade, não permitindo mais relegar os efeitos torsionais para um segundo plano e desprezar os seus efeitos torsores durante o processo de dimensionamento.

Outra dificuldade sentida muitas vezes pelos engenheiros de estruturas, ao serem confrontados com uma arquitetura arrojada, dizia respeito ao cálculo dos efeitos torsionais em estruturas estaticamente indeterminadas que, por vezes, se tornavam bastante fastidiosos e morosos. Felizmente, o rápido desenvolvimento das aplicações computacionais para a análise estrutural, ao longo das últimas décadas, veio facilitar este tipo de cálculo.

Na década de 60 do século passado, a substituição do método de dimensionamento de estruturas baseado nas tensões admissíveis, pelo método dos Estados Limites Últimos (ELU), veio reduzir os elevados fatores de segurança que conferiam a reserva necessária de resistência às estruturas para garantir a absorção dos efeitos torsionais, considerados até então como um efeito secundário.

São raros os casos práticos sobre problemas associados à fraca resistência à torção que tenham sido devidamente documentados. A Figura 3 [56] constitui um exemplo de um desses registos feito em 1964, na Florida (EUA), onde uma viga sofreu uma rotura devido à torção, por insuficiência de armadura. Esta viga, integrada numa estrutura de um edifício destinado a um parque de estacionamento, apresentava ao longo das suas faces uma fenda única helicoidal, típica de uma rotura frágil por torção.

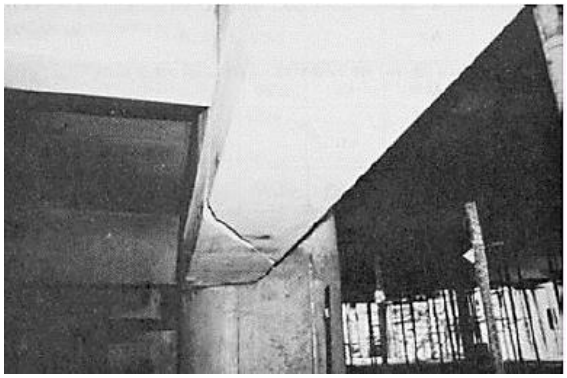

Figura 3. Rotura frágil por torção de uma viga num edifício [56].

Todos os fatores anteriormente referidos contribuíram para que, na comunidade científica, crescesse um sentimento de necessidade para que se estudasse adequadamente o comportamento das estruturas sujeitas à torção e definir regras de dimensionamento específicas para este esforço. Em resposta ao então amplo interesse mundial, em 1958 foi criada a Comissão 438 do *American Concrete Institute* (ACI 438) para promover investigação sobre esta temática e definir regras de dimensionamento para projeto de estruturas sujeitas à torção. Assim, no código ACI de 1971 (ACI 318-71 [1]) surgem, pela primeira vez, procedimentos para o dimensionamento de secções de betão armado à torção. Entre 1972 e 1977, no antigo *Comité Européen du Béton* (CEB), a Comissão V "Esforço Transverso – Torção" também desenvolveu extensos estudos sobre esta temática, culminando na incorporação de procedimentos de dimensionamento à torção, já baseados na teoria dos Estados Limites, na edição de 1978 do código modelo europeu (MC 78 [34]). Tendo por base este documento normativo, em Portugal, e no ano de 1983, surgiu o Regulamento de Estruturas de Betão Armado e Pré-Esforçado (REBAP [66]). Outros países, como a União Soviética e a Austrália, também deram o seu contributo para o estudo desta temática [56].

Desde então, inúmeros estudos foram realizados com vista ao melhor conhecimento do comportamento de estruturas de betão sujeitas a efeitos torsionais, em particular barras, e à definição de procedimentos adequados de dimensionamento para garantia de um comportamento adequado em Estado Limite de Serviço e Último. Hoje em dia, muitos desses procedimentos continuam a ser baseados em métodos semi-empíricos ou mesmo empíricos, ou tendo por base os resultados de programas experimentais pouco extensos, o que conduz à adoção de regras particulares de dimensionamento, diferentes nos documentos normativos adotados em vários países. Além disso, muitos aspetos hoje considerados importantes para um adequado comportamento estrutural, como sejam o comportamento em Serviço e a garantia de uma ductilidade na rotura, encontram-se ainda ausentes, ou deficientemente tratados, em muitos documentos normativos.

Muitas vezes, é necessário dimensionar elementos estruturais resistentes a elevados esforços de torção, na maioria dos casos combinados com outros esforços. Em geral, os regulamentos e códigos de dimensionamento prescrevem o dimensionamento dos elementos estruturais de forma separada para cada tipo de esforço e, posteriormente, prescrevem uma sobreposição de efeitos, eventualmente contemplada com uma verificação adicional da interação de esforços. Também nesta situação, o tratamento dos efeitos torsionais é ainda deficiente em muitos documentos normativos.

A problemática do dimensionamento à torção é ainda agravada com o desenvolvimento de novas técnicas de construção, como a utilização de pré-esforço ou de reforço estrutural, e com o surgimento de novos materiais, como betões de alta resistência e ultra alta resistência, betões leves ou betões com fibras, onde a investigação é ainda muito necessária e onde os documentos normativos carecem, muitas vezes, de disposições normativas.

1.2. Conceitos básicos para o tema investigado.

São raras as situações em que um elemento estrutural se encontra submetido à torção pura, sendo este esforço normalmente acompanhado por outros esforços internos. No entanto, existem casos práticos da engenharia de estruturas, como é o caso de pontes com curvatura pronunciada, de longos vãos ou estruturas geometricamente complexas, de edifícios que, sob o efeito das acções gravíticas e dinâmicas incorporam elementos estruturais, tais como vigas e/ou colunas, sujeitos a elevados momentos torsores, onde a torção pode constituir um esforço dominante ou primário e condicionar bastante o processo de dimensionamento [76] [83] [84].

No interesse do tema investigado, apresentam-se alguns conceitos considerados importantes para o presente trabalho.

1.2.1. Tipos de torção.

Os esforços de torção podem possuir diferentes graus de importância para o dimensionamento de estruturas, dependendo das condições em que a torção surge numa estrutura, da forma como a torção é absorvida pela secção transversal e/ou das consequências de a torção ser desprezada no dimensionamento.

Tendo por base a ligação entre elementos estruturais e a existência, ou não, de redundância em termos de estaticidade, é possível considerar dois tipos fundamentais de torção:

(i) Torção de Compatibilidade: são todos os efeitos torsionais que podem ser considerados como secundários face à compatibilidade de deformações entre elementos estruturais

(Figura 4(a)). Isto é, se o elemento sujeito à torção não possuir resistência suficiente a este esforço, a estrutura poderá sofrer deformações elevadas e fissuração excessiva, mas a estrutura não colapsará, mantendo-se em equilíbrio. Assim, este tipo de torção pode ser desprezado no dimensionamento da estrutura, desde que seja verificada a segurança da estrutura ao Estado Limite de Serviço (ELS), garantindo, por exemplo, a existência de uma armadura mínima de fissuração, em especial nas zonas de ligação entre elementos e no elemento em torção. Caso uma armadura mínima de torção não seja prevista numa viga de betão armado, a sua rigidez elástica de torção, no estado fissurado, decairá até 85% a 90% do seu valor inicial [51]. Em consequência da fissuração na zona de ligação e no elemento inicialmente em torção, parte dos esforços hiperestáticos são redistribuídos e a redução do esforço inicial de torção é "equilibrada" pelo aumento de outros esforços internos noutras secções, como a flexão e o esforço transverso. Para determinar os esforços internos de dimensionamento de uma estrutura, desprezando a torção de compatibilidade, é possível adotar modelos alternativos (Figura 4(b)), desde que garantido o bom comportamento em Serviço da estrutura. Este tipo de torção é comum surgir em pórticos correntes de edifícios, designadamente, nas ligações monolíticas entre elementos estruturais, como por exemplo, entre vigas (apoios indiretos, Figura 4), entre vigas de bordo e lajes de betão.

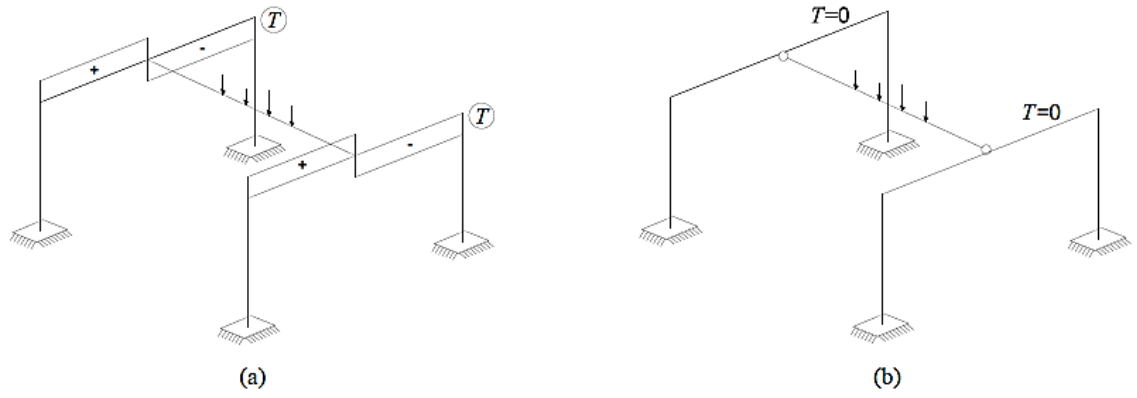

Figura 4. Exemplo esquemático de uma estrutura com torção de compatibilidade [6].

(ii) Torção de Equilíbrio: são todos os efeitos torsionais que são considerados primários e fundamentais para o equilíbrio da estrutura, ou de parte dela (Figura 5(a)). Ou seja, se o elemento sujeito à torção não possuir resistência suficiente a este esforço, a estrutura, ou parte dela, fica instável (Figura 5(b)). Este tipo de torção não pode ser desprezado no processo de dimensionamento, sendo obrigatória a verificação de segurança dos elementos envolvidos no ELU de resistência à torção.

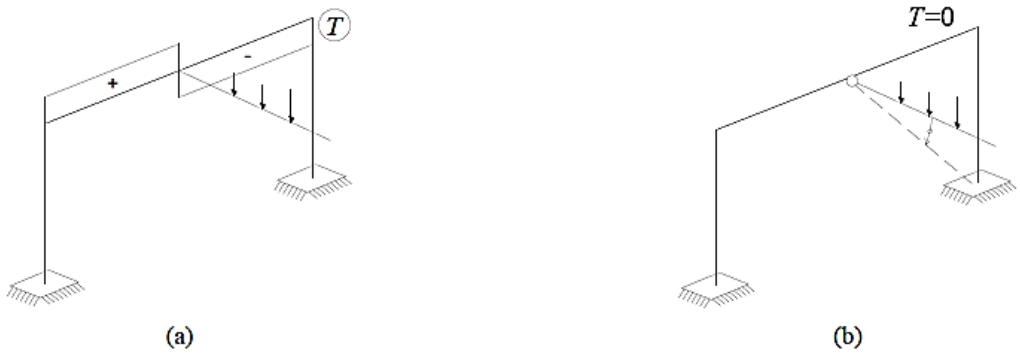

Figura 5. Exemplo esquemático de uma estrutura com torção de equilíbrio [6].

A Figura 6 apresenta dois exemplos de estruturas reais onde a torção de compatibilidade (Figura 6(a)) e a torção de equilíbrio (Figura 6(b)) ocorrem.

(a) (b)

Figura 6. Exemplos de estruturas reais com (a) torção de compatibilidade e (b) torção de equilíbrio [B] [C].

Conforme a secção transversal do elemento estrutural absorve os efeitos torsionais, é ainda possível considerar outros dois tipos fundamentais de torção:

(i) Torção Circulatória: também conhecida por torção de Saint-Venant, surge em secções em que a torção é fundamentalmente resistida por um fluxo circulatório de tensões tangenciais, designado por fluxo de corte. Este tipo de torção ocorre em secções correntemente utilizadas, como sejam secções circulares ou quadrangulares, podendo ser cheias ou vazadas (Figura 7(a)).

(ii) Torção de Empenamento: este tipo de torção surge principalmente em secções abertas de parede não espessa, onde o esforço torsional é fundamentalmente resistido por esforços secundários adicionais (momento fletor e esforço transverso), resultando no empenamento da secção (Figura 7(b)). O grau de empenamento pode ser controlado através da espessura das paredes, da configuração da viga e do tipo de carregamento [97]. Em toda a extensa literatura consultada no âmbito do presente trabalho não foi encontrado um modelo de dimensionamento plenamente satisfatório para elementos com secções de betão armado

sujeitos à torção com empenamento. Por essa razão, os documentos normativos incluem apenas disposições para o dimensionamento de elementos sujeitos à torção circulatória ou de Saint-Venant e, para o dimensionamento à torção com empenamento, remetem para a bibliografia especializada (por exemplo, os métodos de Walssow de 1964 [99], Grob de 1975 [50] ou Kovács de 1995 [35]).

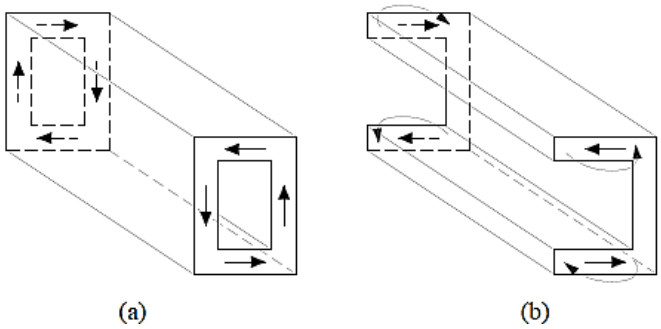

Figura 7. Exemplo esquemático de elementos com (a) torção circulatória e (b) torção com empenamento [13].

Pelo facto de as vigas usadas no projeto de estruturas correntes possuírem secção retangular cheia ou vazada, a torção com empenamento não será abordada no presente trabalho. Do mesmo modo, será dada relevância às vigas sujeitas a esforços de torção primários, para as quais se considera fundamental o seu dimensionamento à torção.

1.2.2. Comportamento de vigas de betão sujeitas à torção.

O comportamento global da zona crítica de uma viga de betão estrutural sujeita à torção pode ser representado por uma Curva $T - \theta$ (momento torsor *vs*. rotação transversal por unidade de comprimento). Esta curva pode ser determinada através de ensaios experimentais em laboratório e/ou calculada através de modelos matemáticos de comportamento que incorporam a não linearidade material. Atendendo a que o presente trabalho de investigação foca apenas o comportamento de vigas de secção retangular cheia ou vazada, as subsecções seguintes abordam apenas aspetos comportamentais deste tipo de vigas sujeitas à torção pura. Tais aspetos são evidenciados, fundamentalmente, pela observação experimental e com o suporte de conceitos-base teóricos e teorias simples para a sua compreensão.

1.2.2.1. Vigas de betão simples.

A Figura 8(a) representa o comportamento de duas vigas retangulares de betão simples (não armadas) ensaiadas à torção e cujos resultados foram publicados por Hsu em 1968 [51]. De acordo com as Curvas $T - \theta$ ilustradas naquela figura, para níveis baixos de carga o comportamento observado é praticamente linear. Já para níveis mais elevados de

carga as vigas tendem a perder o seu caráter de comportamento linear. Independentemente do tipo de viga de betão simples ensaiada, observa-se que a rotura é bastante frágil.

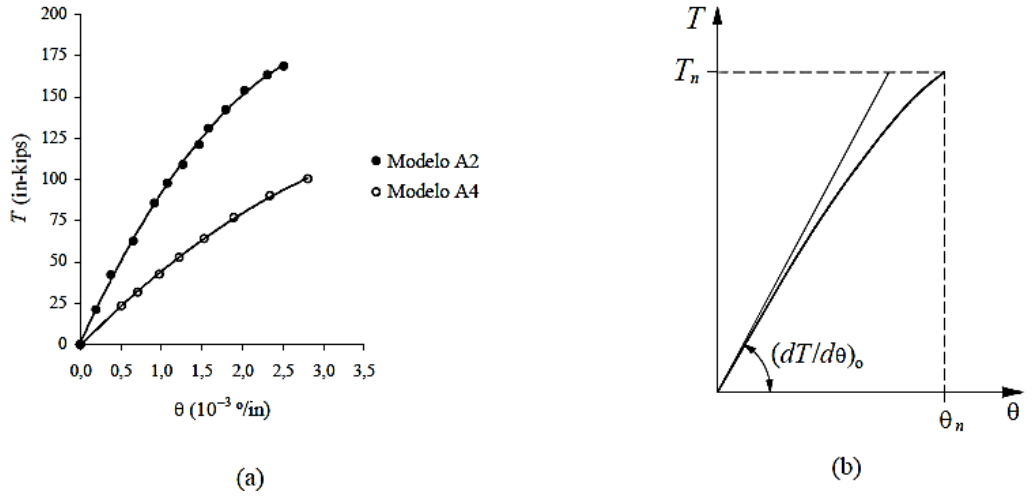

Figura 8. Curvas $T - \theta$ (a) experimentais e (b) teóricas para vigas de betão não armado [51]. (1 °/in = 39,37 °/m; 1 in-kips = 0,113 kNm)

No seu estudo, Hsu [51] percebeu que ao utilizar a teoria de Saint-Venant para determinar o módulo de elasticidade inicial do betão (E_0) das vigas à torção, este era muito próximo do E_0 obtido pela Curva $\sigma - \varepsilon$ do betão nos ensaios de compressão e tracção uniaxial (com σ a tensão unixial e ε a extensão, Figura 9). Assim, Hsu concluiu que a teoria de Saint-Venant pode descrever com precisão o comportamento das vigas de betão não armado sujeitas a carregamentos baixos de torção. Já para níveis elevados de carregamento, a Curva $T - \theta$ desvia-se da reta correspondente à rigidez de torção inicial, desviando-se por sua vez da previsão da teoria de Saint-Venant. Este fenómeno foi explicado por Hsu através da influência da microfissuração no betão, que se desenvolve ao longo das vigas antes de ser atingido o carregamento máximo. Apesar das suas observações, Hsu considerou que a teoria de Saint-Venant também pode descrever razoavelmente bem o comportamento de vigas sujeitas a elevados níveis de carregamento, desde que associados a algum tipo de módulo de elasticidade secante [56] (Figura 8(b)).

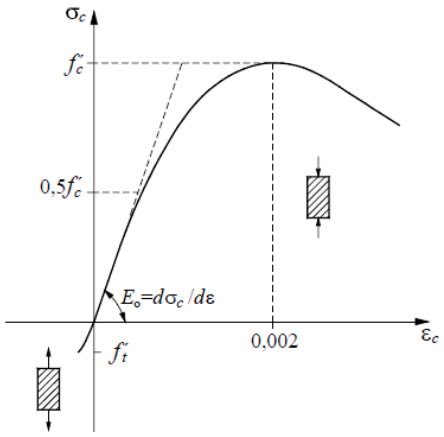

Figura 9. Curva $\sigma - \varepsilon$ uniaxial para o betão [13].

Quanto à resistência das vigas de betão não armado à torção, esta pode ser prevista através de três teorias, a saber:

(i) Teoria da Elasticidade: assumindo que a viga de betão não armado entra em rotura quando a tensão principal máxima de tração, $\sigma_{máx}$, é igual à resistência à tração do betão, f_t' (ou f_{ct}), a resistência da viga poderá ser determinada através da teoria de Saint-Venant. Assim, o momento torsor resistente elástico, T_e, pode ser calculado através da Eq. (1.1), onde x e y representam a largura e a altura da secção, e α o coeficiente de Saint-Venant).

$$T_e = \alpha x^2 y f_t' \tag{1.1}$$

A teoria elástica foi utilizada por Bach e Graf em 1912 [8], Young *et al.* em 1922 [100], Andersen em 1937 [5], Cowan em 1951 [40], Humphreys em 1957 [65] e Zia em 1961 [103]. Contudo, ensaios posteriores mostraram que a Eq. (1.1) subestima em cerca de 50% a resistência à torção das vigas [39] [56].

(ii) Teoria da Plasticidade: atendendo a que a teoria elástica subestima a resistência à torção, Nylander [80] suspeitou que a resistência extra registada experimentalmente poderia ser atribuída à plastificação do betão. Assumindo o mesmo critério de rotura e a plastificação total da secção, o momento torsor resistente plástico, T_p, pode ser calculado através da Eq. (1.2), com o coeficiente plástico $\alpha_p = 0{,}5 - x/(6y)$. Este coeficiente varia entre 1/3 e 1/2 e é cerca de 50% superior ao coeficiente α de Saint-Venant.

$$T_p = \alpha_p x^2 y f_t' \tag{1.2}$$

Contudo, esta teoria apresenta três falhas: *(a)* tendo em conta o critério de rotura, experimentalmente não é observado um comportamento plástico em betões à tração; *(b)* as vigas em betão simples possuem roturas bastante frágeis, não manifestando rotações

plásticas (Figura 9); *(c)* a teoria não considera o fator de escala, subestimando ou sobrestimando a resistência das vigas, consoante as dimensões da secção da viga.

(iii) Teoria da Flexão Enviesada (*Skew-Bending Theory*): face aos resultados insatisfatórios das duas anteriores teorias na previsão da resistência de vigas de betão simples sujeitas à torção, Hsu [53] suspeitou que o critério de rotura admitido nessas teorias estivesse incorreto. Após observação rigorosa do processo de rotura durante um ensaio, Hsu verificou que a fenda na face lateral (face maior da secção da viga), com cerca de 45º em relação ao eixo longitudinal, progrediu e abriu gradualmente na face de topo da viga até ao esmagamento do betão na face posterior (Figura 10). Este tipo de rotura é característico em vigas de betão simples sujeitas à flexão.

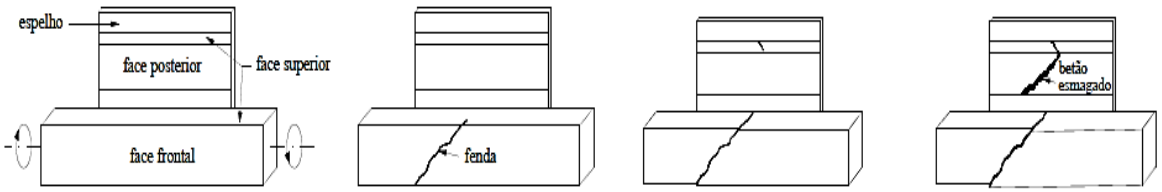

Figura 10. Mecanismo de rotura à torção de vigas de betão simples [13].

Tendo por base este mecanismo de rotura, Hsu deduziu uma equação para determinar a resistência à torção de vigas retangulares de betão simples, T_{np} (Eq. (1.3)), considerando duas componentes de vetores momento na superfície de rotura: a componente de torção, T_t (Figura 11(a)), e a componente de flexão, T_b (Figura 11(b)).

$$T_{np} = \frac{x^2 y}{3}(0{,}85 f_r) \tag{1.3}$$

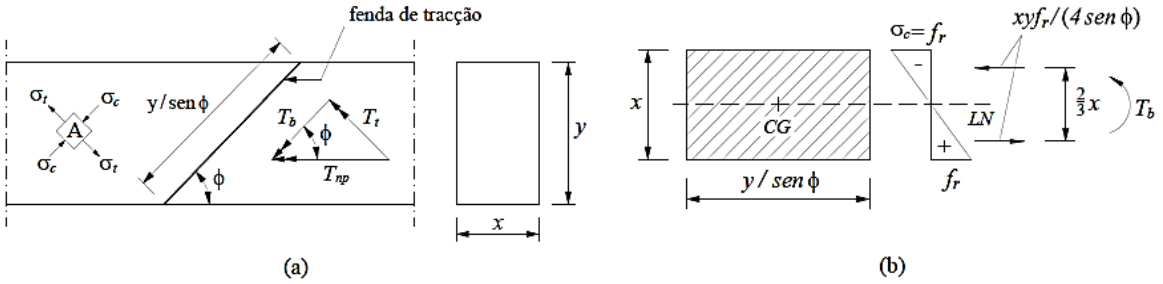

Figura 11. (a) Componentes do momento torsor e (b) Momento fletor resistente da secção de rotura [13].

A resistência T_{np} é deduzida a partir das condições de equilíbrio na secção de rotura, por aplicação da teoria elástica da flexão nessa secção, e tendo em conta a influência desfavorável da componente de torção, T_t, mediante a utilização de um módulo de rotura reduzido para o betão, f_r, determinado pela Eq. (1.4):

$$f_r = 21\left(1+\frac{10}{x^2}\right)\sqrt[3]{f_c'} \text{ para } x \geq 4\ in\ (10{,}2\ cm) \tag{1.4}$$

Note-se que esta equação é determinada em função de x, considerando, deste modo, o efeito de escala observado nos ensaios de torção [53]. As equações Eq. (1.3) e Eq. (1.4) devem ser utilizadas em unidades imperiais (1 in = 2,54 cm, 1 MPa = 145 psi).

Assim, a Eq. (1.3) introduziu um novo critério de rotura, o qual assume que a viga de betão simples entra em rotura quando a tensão de tração do betão na face maior, induzida pela componente de flexão T_b, atinge o módulo de rotura reduzido do betão.

1.2.2.2. Vigas com armadura longitudinal.

A Figura 12 representa o comportamento à torção pura de duas vigas armadas apenas longitudinalmente, uma com uma taxa de armadura elevada e outra com uma taxa de armadura reduzida. Na Figura 12, T_n e T_{np} indicam os momentos torsores resistentes de cada viga.

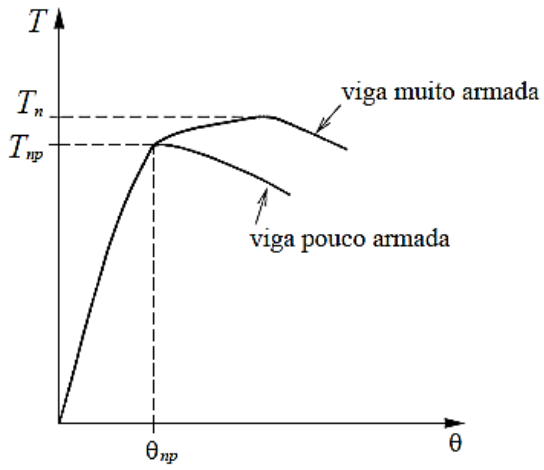

Figura 12. Curva $T-\theta$ típica de vigas sem armadura transversal [13].

Os comportamentos das duas vigas são praticamente iguais até ao ponto de fissuração, após o qual a viga com taxa de armadura reduzida entra instantaneamente em rotura e a viga com taxa de armadura elevada apresenta uma certa resistência adicional à torção, mas que raramente excede os 15% do momento torsor de fissuração [56]. Assim, conclui-se que a armadura longitudinal tem pouca influência na resistência à torção de vigas de betão. Esta observação mantém-se, independentemente da localização das armaduras na secção transversal [56]. A rigidez de torção destas vigas pode ser determinada através da teoria clássica de Saint-Venant para barras homogéneas.

Desprezando a pequena influência da armadura longitudinal, conclui-se que a rigidez de torção e a resistência à torção de uma viga de betão sem armadura transversal podem ser calculadas considerando a viga em análise como uma viga de betão simples (não armada).

1.2.2.3. Vigas com armadura longitudinal e transversal.

A Figura 13 representa uma curva comportamental típica para uma viga de betão armado, incorporando armadura longitudinal e transversal, com taxas de armadura moderadas e evidenciando algum comportamento dúctil na rotura. A curva $T - \theta$ pode ser dividida em três zonas de comportamento, desde o início do carregamento até à rotura da viga:

(i) Zona 1, Estado não fissurado: esta zona traduz o comportamento elástico linear da viga. Na curva $T - \theta$, a zona 1 encontra-se compreendida entre o ponto de origem da curva $T - \theta$ (0;0) e o ponto $(\theta_{cr}^{I}; T_{cr})$, (onde T_{cr} e θ_{cr}^{I} são, respetivamente, o momento torsor de fissuração e a rotação de torção correspondente a T_{cr}) e é representada, aproximadamente, por uma reta.

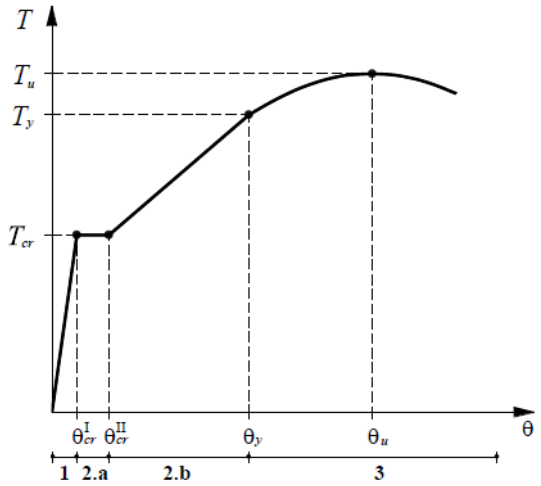

Figura 13. Curva $T - \theta$ típica para uma viga de betão armado sujeita à torção pura [13].

Nesta fase inicial, Hsu [56] observou que a taxa total de armadura de torção (ρ_{tot}) possui muito pouca influência na rigidez da viga, contribuindo apenas para um ligeiro aumento do momento torsor de fissuração à medida que a taxa de armadura aumenta. Deste modo, a viga comporta-se, essencialmente, como uma viga de betão simples. Como tal, a sua rigidez de torção, nesta zona de comportamento inicial, pode ser determinada através da teoria de Saint-Venant. Já para o cálculo de T_{cr} de uma viga de betão armado, Hsu [52] propôs uma expressão empírica para o efeito, Eq. (1.5), onde T_{np} representa a resistência à torção da mesma viga não armada.

$$T_{cr} = (1 + 4\rho_{tot})T_{np} \tag{1.5}$$

(ii) Zona 2, Estado fissurado: esta zona traduz o comportamento fissurado da viga antes da cedência das armaduras, o qual pode ser considerado aproximadamente elástico linear. Na curva $T-\theta$, a zona 2 encontra-se compreendida entre o ponto $(\theta_{cr}^{I}; T_{cr})$ e o ponto correspondente à cedência de, pelo menos, uma das armaduras de torção (longitudinal e transversal). Nas vigas de secção cheia, a zona 2 tem início com um aumento brusco da rotação para um valor do momento torsor aproximadamente constante e igual a T_{cr} (zona 2.a), desenvolvendo-se posteriormente de forma aproximada a uma reta (zona 2.b) até ao limite superior anteriormente referido. A extensão da zona 2.a é tanto maior quanto menor for a taxa de armadura de torção [51]. Experimentalmente, a zona 2.a não é registada em vigas de secção vazada, provavelmente por não existir, neste tipo de secções, uma capacidade pronunciada para a redistribuição transversal das tensões para o núcleo central de betão (o qual existe em vigas de secção cheia). Tal conduz a uma mobilização quase instantânea das armaduras de torção em vigas de secção vazada em consequência da fissuração [13]. Outro aspeto a realçar, é o facto de as vigas de secção vazada apresentarem um menor momento torsor de fissuração comparativamente às vigas similares de secção cheia. Tal deve-se à maior uniformidade de tensões ao longo da espessura da parede da secção, no caso da viga de secção vazada, comparativamente à "casca externa" da viga com secção cheia, na qual as tensões sofrem um maior gradiente. Quanto ao declive da reta na zona 2.b, que representa a rigidez de torção da viga no estado fissurado, Hsu verificou que esta é muito influenciada pela armadura, aumentando linearmente com a taxa total de armadura. Nesta zona de comportamento é também observado um aumento linear do comprimento da viga com o aumento do momento torsor [3] [96], mostrando, deste modo, a participação efetiva das armaduras longitudinais tracionadas no equilíbrio interno da viga.

(iii) Zona 3, Estado último*:* esta zona traduz o comportamento da viga após a plastificação das armaduras (comportamento não linear). Na curva $T-\theta$, a zona 3 começa no ponto $(\theta_y; T_y)$ correspondente à cedência de pelo menos uma das armaduras de torção, até ao ponto $(\theta_u; T_u)$ correspondente ao momento torsor resistente da viga. A rotura efetiva da viga dá-se por esmagamento do betão comprimido nas escoras (no caso de vigas com taxas de armadura de torção moderadas a elevadas) ou por rotura das armaduras tracionadas (no caso de vigas com taxas de armadura de torção muito baixas). Experimentalmente, observa-se que o comportamento em torção na Zona 3 de vigas de secção vazada não é completamente idêntico ao comportamento de vigas semelhantes de secção cheia [56]. Este facto deve-se, essencialmente, à ausência de núcleo de betão nas vigas de secção vazada, o que limita a capacidade de redistribuição de tensões para o interior da secção transversal. Consequentemente, as vigas de secção vazada apresentam menor ductilidade em torção.

A Figura 14 representa o comportamento de duas vigas com características idênticas (dimensões exteriores, materiais e taxas de armadura de torção), uma com secção cheia (Viga B4) e outra com secção vazada (Viga D4). Embora as duas vigas garantam resistências à torção praticamente idênticas, observa-se uma menor ductilidade na viga de secção vazada. Como já referido anteriormente, outra diferença notória é a que se pode constatar no comportamento das duas vigas na passagem do estado não fissurado para o estado fissurado. Em particular para a viga de secção vazada, observa-se um menor momento torsor de fissuração e a ausência visual do patamar horizontal imediatamente após a fissuração.

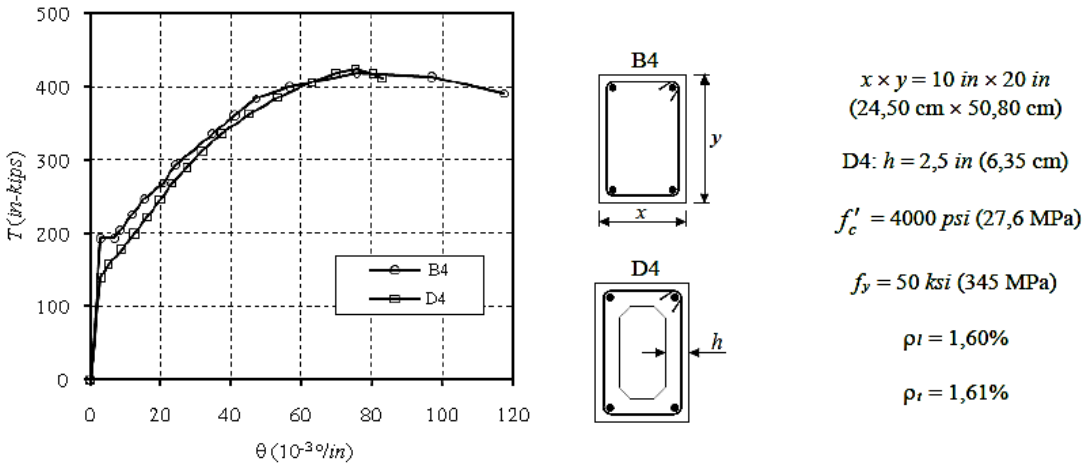

Figura 14. Influência do tipo de secção no comportamento global à torção pura [56].

1.2.2.4. Vigas com pré-esforço longitudinal e sem armadura transversal.

Tal como acontece numa viga de betão armado sujeito à flexão, a introdução de pré-esforço numa viga sujeita à torção aumenta a sua resistência à fissuração. O pré-esforço induz uma tensão de compressão adicional que, combinada com a tensão tangencial originada pelo momento torsor, resulta num estado de tensão biaxial (corte + compressão), atrasando assim a fissuração do betão. Além disso, Portanto, o pré-esforço pode também aumentar a resistência à torção e permitir que uma área maior da secção transversal do betão seja eficaz. Por estes motivos, o pré-esforço longitudinal constitui uma técnica correntemente utilizada em vigas submetidas a elevados esforços de torção, como, por exemplo, nas vigas de tabuleiro em pontes curvas [71].

Para avaliar a eficiência do pré-esforço no comportamento de uma viga à torção, é necessário definir um critério de rotura do betão em estado biaxial. A Figura 15(a) representa a tensão de pré-esforço longitudinal, σ, numa viga retangular sujeita a um momento torsor, T. Em cada uma das quatro faces da viga, um pequeno elemento de área "A" está sujeito a uma tensão tangencial, τ, devida à torção. Já nas faces laterais, este

elemento "A" está sujeito a uma tensão de compressão adicional, σ, devida ao pré-esforço. A Figura 15(b) representa as tensões biaxiais de um elemento "A" isolado a meia altura da superfície lateral da viga e a Figura 15(c) representa o estado de tensões desse mesmo elemento através do círculo de Mohr para as tensões.

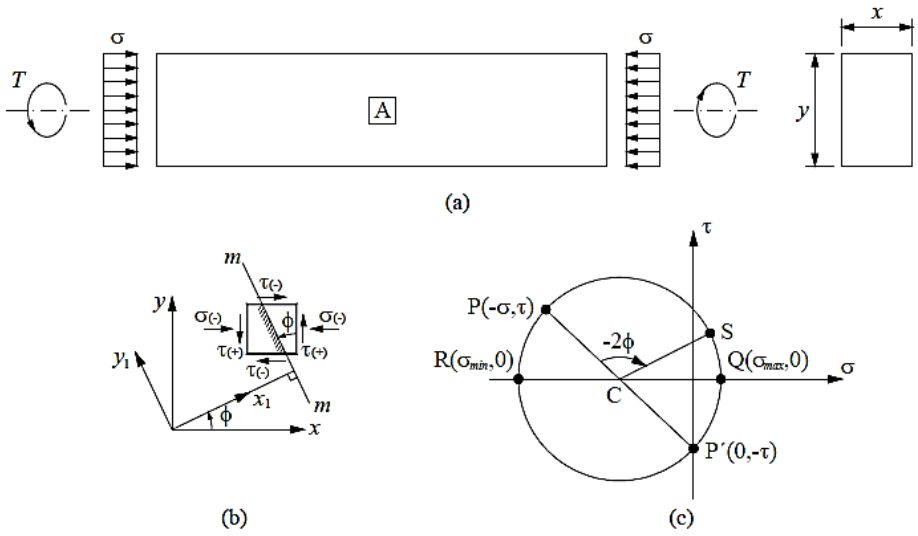

Figura 15. Estado de tensão de uma viga com pré-esforço sujeita à torção [13]: (a) viga, (b) elemento A, (c) círculo de Mohr.

No círculo de Mohr (Figura 15(c)), o estado de tensão numa face vertical do elemento "A" é representado pelo ponto P de coordenadas $(-\sigma\,;\,\tau)$ e o estado de tensão numa face horizontal do mesmo elemento é representado pelo ponto P' de coordenadas $(0\,;\,-\tau)$, onde a tensão normal devido ao pré-esforço é nula e a tensão de corte tangencial é considerada convencionalmente negativa. As tensões numa superfície arbitrária $m-m$ (Figura 15(b)), com ângulo ϕ medido no sentido contrário ao dos ponteiros do relógio em relação à superfície vertical, é representado pelo Ponto S.

A rotura do elemento "A" ocorre quando as tensões biaxiais atuantes atingem um valor crítico. A teoria de rotura de Mohr prevê que a rotura desse elemento ocorra devido ao deslizamento de um plano definido dentro do material. Este critério de rotura relaciona as tensões tangencial e normal desse plano com uma determinada função, designada por envolvente de rotura de Mohr, a qual constitui uma característica do material.

Uma vez que matematicamente é difícil expressar e aplicar a envolvente de rotura de Mohr, Cowan, em 1952 [41], propôs um critério de rotura para o betão mais simples. Considerando a simetria da envolvente de rotura de Mohr, Cowan substituiu a linha curva tangencial aos círculos de Mohr (na envolvente de rotura de Mohr) por duas linhas retas BD e DE (Figura 16). A linha reta BD é tangente em B ao círculo de Mohr C_1 para o ensaio do betão à compressão uniaxial e forma um ângulo de atrito interno (assumido) de 37º com o eixo

horizontal. Este critério é usado nos casos em que a rotura do betão é condicionada pela compressão. Já a linha vertical DE é tangencial ao círculo de Mohr C_2 para o ensaio do betão à tração uniaxial e este critério é usado nos casos em que a rotura do betão é condicionada pela tração.

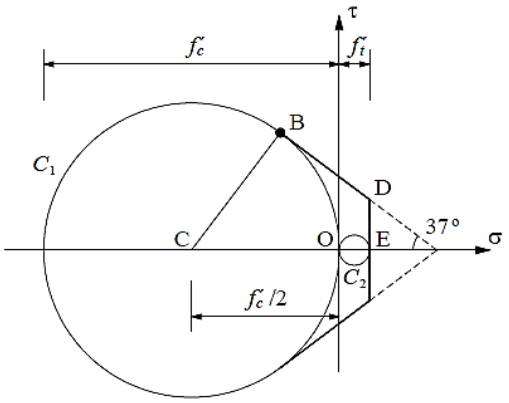

Figura 16. Envolvente de rotura de Cowan [41].

A partir deste critério de rotura é possível obter um fator de pré-esforço que define a relação entre a resistência de um elemento pré-esforçado e a resistência de um elemento sem pré-esforço. Este fator pode ser determinado através da teoria elástica, da teoria plástica ou da teoria da flexão enviesada.

Utilizando a teoria elástica (Saint-Venant) e para os casos em que a rotura do betão ocorra por compressão, o momento torsor de rotura de uma viga pré-esforçada, T, é determinado pela seguinte expressão:

$$T = \alpha x^2 y \tau_{máx} = \alpha x^2 y f_t' \sqrt{1 + \frac{\sigma}{f_t'}} = T_e \sqrt{1 + \frac{\sigma}{f_t'}} = T_e \gamma \qquad (1.6)$$

Onde $\tau_{máx}$ é a tensão tangencial máxima de torção no elemento "A" e o termo $\alpha x^2 y f_t'$ é o momento torsor elástico sem pré-esforço, T_e. Ou seja, a Eq. (1.6) determina que o momento torsor de rotura de uma viga pré-esforçada, T, é igual ao momento torsor de rotura de uma viga sem pré esforço, T_e, vezes um factor de pré-esforço, γ. Esta teoria foi utilizada por Cowan e Armstrong em 1955 [42] e Humphreys em 1957 [65] para determinar o factor de pré-esforço, γ.

Usando a teoria plástica proposta por Nylander em 1945 [80], e para os casos em que rotura do betão ocorra por tração, o momento torsor de rotura de uma viga pré-esforçada, T, é determinada pela seguinte expressão:

$$T = \alpha_p x^2 y \tau = \alpha_p x^2 y f_t' \sqrt{1 + \frac{\sigma}{f_t'}} = T_p \sqrt{1 + \frac{\sigma}{f_t'}} = T_p \gamma \tag{1.7}$$

Onde o termo $\alpha_p x^2 y f_t'$ é o momento torsor plástico sem pré-esforço, T_p. A Eq. (1.7) segue a mesma lógica da Eq. (1.6), determinando o momento torsor de rotura de uma viga pré-esforçada, T, através do momento torsor de rotura de uma viga sem pré esforço, T_p, vezes um factor de pré-esforço, γ.

Nas equações Eq. (1.6) e Eq. (1.7), o factor de pré-esforço, γ, baseia-se na resistência à tração uniaxial do betão, f_t'. Esta pode ser relacionada com a resistência à compessão, f_c', assumindo que $f_c'/f_t' = 10$ [56]. Ou seja:

$$\gamma = \sqrt{1 + 10 \frac{\sigma}{f_c'}} \tag{1.8}$$

A Eq. (1.8) foi validada por numerosos resultados experimentais realizados por Nylander em 1945 [80], Humphreys em 1957 [65] e Zia e McGee em 1974 [104].

Na teoria da flexão enviesada, Hsu integrou o mesmo fator de pré-esforço no cálculo do momento torsor resistente de vigas sem armadura transversal e com pré-esforço longitudinal uniforme [54].

1.2.2.5. Vigas de betão armado com pré-esforço longitudinal.

Tendo por base o modelo de treliça espacial com ângulo variável (*vide* Secção 1.3.2.1), Hsu e Mo [60] demonstraram que vigas de betão armado com pré-esforço longitudinal sujeitas à torção pura possuem um comportamento análogo ao de uma viga ordinária de betão armado, após a ocorrência de um fenómeno denominado por "descompressão do betão". Este fenómeno ocorre quando a força longitudinal de tração, proveniente da aplicação do momento torsor, equilibra a força de compressão no betão induzida pelo pré-esforço. A partir desse ponto, a armadura de pré-esforço passa a suportar inteiramente a força longitudinal de tração, uma vez que nesse momento a extensão na armadura ordinária e no betão é nula, comportando-se como uma viga de betão armado ordinária.

De acordo com estes autores, a localização da armadura de pré-esforço na secção transversal da viga (Figura 17) é indiferente. Desde que devidamente ancoradas nos topos da viga, uma armadura de pré-esforço centrada na secção (Figura 17(b)) participa de igual forma para a resistência dessa viga que uma armadura de pré-esforço localizada na região da espessura efetiva da secção (na "casca externa", (Figura 17(a)).

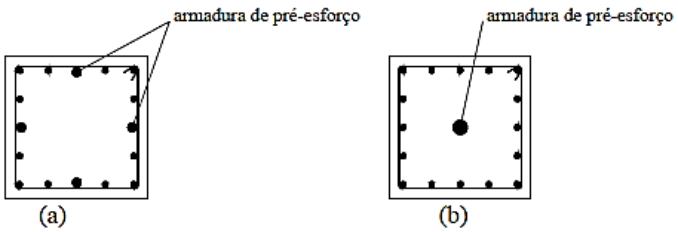

Figura 17. Localização da armadura de pré-esforço na secção transversal de uma viga [13].

Hsu e Mo [60] verificaram ainda que, quando a armadura de pré-esforço é exagerada, esta poderá conduzir ao esmagamento do betão muito antes de ocorrer o fenómeno de "descompressão do betão" e, consequentemente, a rotura da viga ocorre com uma extensão de compressão instalada nos varões longitudinais da armadura ordinária. Deste modo, o modelo de treliça espacial com ângulo variável deixa de ser válido nesta situação.

1.3 Modelos teóricos para determinar o comportamento global de vigas de betão à torção.

1.3.1. Notas históricas.

Os primeiros modelos propostos tiveram por base o estudo de barras homogéneas de betão à torção, os quais foram extrapolados para o caso das vigas de betão armado não fissurado sujeitas à torção. Navier, em 1826 [79], deduziu uma equação para barras homogéneas com secção retangular a partir da sua própria equação teórica para barras homogéneas com secção circular, assumindo que as tensões tangenciais eram proporcionais à distância ao eixo de torção. Contudo, a sua equação sobrestimava a rigidez de torção das barras retangulares em cerca de 20%.

Em 1855, Saint-Venant [91] apresentou uma solução para esta problemática, propondo substituir o momento torsor polar de inércia pela constante de torção de Saint-Venant, 18% inferior ao referido momento torsor. Com o advento das Séries de Fourier e da Teoria da Elasticidade desenvolvida por Cauchy [33], Saint-Venant desenvolveu a sua própria teoria para barras prismáticas sujeitas à torção. De acordo com a sua teoria, uma barra prismática sujeita à torção origina apenas tensões tangenciais circulatórias, sendo a parte externa da secção transversal a mais solicitada e a tensão nula no eixo de torção (no centro da secção transversal). Tendo por base a teoria de Saint-Venant, Bredt, em 1896 [32], derivou equações para determinar a secção transversal mais eficiente e económica para resistir à torção. O autor concluiu que essa secção é constituída por um tubo de parede fina com tensão uniforme [95].

Desde a segunda metade do século passado, várias teorias e modelos têm sido desenvolvidos para prever a resistência de elementos de betão estrutural sujeitos à torção pura e combinada. De todos aqueles modelos, destacam-se dois modelos físicos que serviram de base para posteriores desenvolvimentos: a Teoria da Flexão Enviesada (*Skew-Bending Theory*) e a Analogia da Treliça Espacial (*Space Truss Analogy*).

O Modelo da Teoria da Flexão Enviesada foi proposta por Hsu em 1968 [52], baseado no modelo de superfície espacial de rotura, para determinar a resistência de vigas de betão armado, com secção retangular cheia, sujeitas à torção pura. Este modelo foi formulado através de observações empíricas e permite prever a distribuição das tensões na secção transversal apenas na fase última do comportamento (rotura) da viga. Apesar do Modelo da Teoria da Flexão Enviesada apenas poder ser aplicado, de forma mais fidedigna, a vigas com secção retangular do tipo das usadas em edifícios e de dar origem a formulações complexas quando extrapolado para casos mais complexos, o mesmo foi desenvolvido ao longo de mais de duas décadas e teve uma influência considerável no estabelecimento das regras para o dimensionamento à torção em alguns códigos importantes, como o código do ACI até 1995. Dos estudos desenvolvidos com este modelo destacam-se os realizados por Hsu [52], McMullen e Warwaruk [74] e Elfgren *et al.* [45] para vigas sujeitas à torção combinada (flexão, esforço transverso e axial). Hoje em dia, as disposições dos códigos normativos para o dimensionamento de elementos de betão estrutural sujeitos à torção deixaram de ser baseadas neste modelo para passarem a basear-se no modelo da Analogia de Treliça Espacial. Por este motivo, o Modelo da Teoria da Flexão Enviesada não será abordado com maior profundidade no presente trabalho.

1.3.2. Analogia da Treliça Espacial (STA).

A Analogia da Treliça Espacial (*Space Truss Analogy* – STA) para vigas de betão armado sujeitas à torção foi desenvolvida por Rausch em 1929 [88] a partir do Modelo de Treliça a 45º de Ritter [89] e Morsh [77] (Figura 18). Estes autores simularam a fase pós-fissuração de um elemento de betão armado através de um modelo de treliça. De acordo com este modelo, numa viga de betão armado ao corte ocorre fissuração diagonal que divide o betão numa série de escoras, funcionando assim como uma treliça no plano de carga. As barras longitudinais (superiores e inferiores) constituem as cordas da treliça e as barras transversais e as escoras de betão constituem os elementos de equilíbrio da alma, sendo assumido um ângulo de 45º para a inclinação das escoras de betão. Através das equações de equilíbrio foram derivadas três equações para o cálculo das tensões nas armaduras (longitudinais e transversais) e nas escoras de betão a 45º.

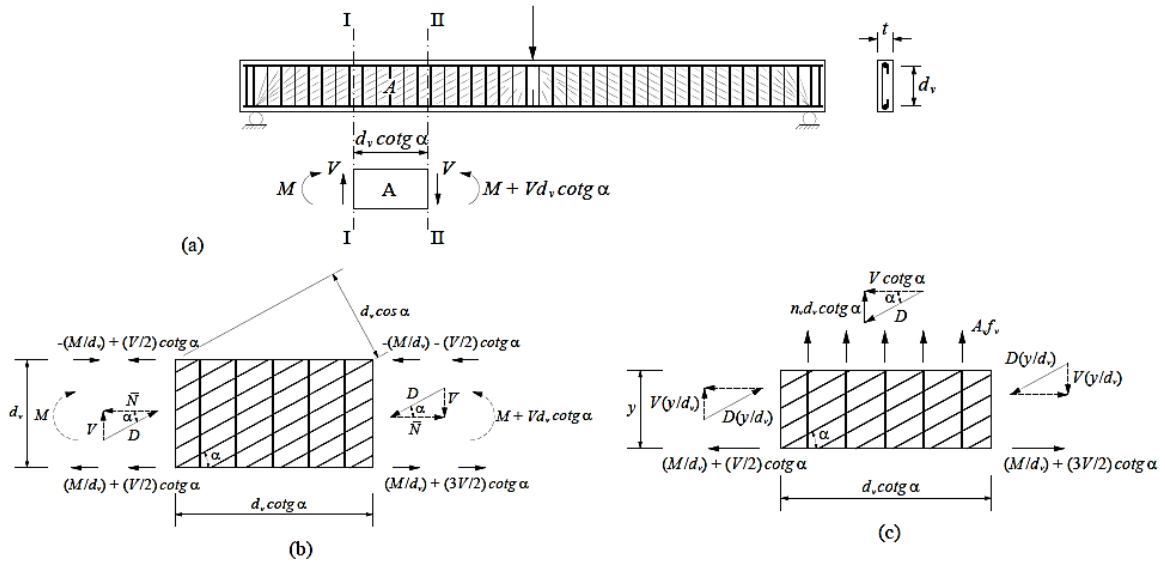

Figura 18. Análise de uma viga com base no modelo de treliça plana [56].

Rausch alargou o campo de aplicação do Modelo de Treliça a 45º e conjugou-o com a Teoria de Saint-Venant e a Teoria do Tubo Fino de Bredt, formulando, assim, o primeiro modelo físico coerente capaz de prever a resistência de elementos de betão armado sujeitos à torção. A Analogia da Treliça Espacial assume que uma viga de betão armado, após a fissuração, funciona como um tubo, sujeito a um fluxo circulatório de tensões de corte em torno do eixo de torção da viga, formando uma série de escoras inclinadas a 45º em relação ao eixo longitudinal, que interagem com a armadura longitudinal e transversal (Figura 19). Contudo, o modelo de Rausch não tem em conta alguns mecanismos resistentes, tais como: a resistência ao corte das escoras, a resistência adicional devido ao "efeito ferrolho" nas armaduras, a contribuição do núcleo de betão em secções cheias e a resistência do betão à tração [13]. Em resultado destas simplificações, foi experimentalmente observado que o modelo era pouco conservativo [39]. Como discutido seguidamente, a partir da segunda metade do século passado, a Analogia da Treliça Espacial foi sofrendo vários refinamentos e constitui, atualmente, o modelo base em numerosos códigos normativos, em particular do código modelo europeu desde 1978 e do código americano desde 1995.

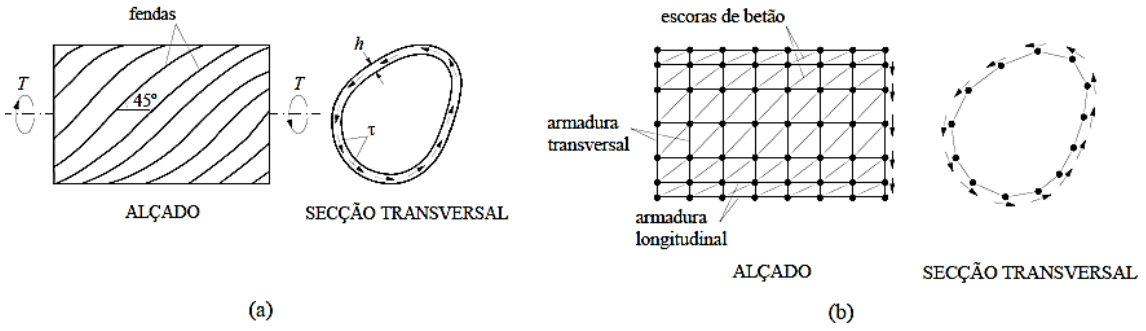

Figura 19. A Analogia da Treliça Espacial de Rausch [13] [56].

Com o objetivo de melhorar a precisão do modelo de Rausch, foram apresentadas várias propostas de modificação deste modelo, tendo estas resultado, basicamente, em três aproximações essenciais. A primeira aproximação assumiu que a armadura é apenas parcialmente eficiente [4] [39]. Para isso, a equação de Rausch foi multiplicada por um coeficiente de eficiência, λ, inferior ou igual à unidade. Esta aproximação foi seguida por Andersen em 1935 [4], Cowan em 1950 [39] e adotada pelo código ACI de 1971 [1] a 1995 [2]. A segunda aproximação reduziu a área da secção, *A*, assumindo que a linha média do fluxo de corte, que delimita essa nova área, coincide com a linha fechada que liga os centros geométricos dos varões longitudinais [72]. Esta aproximação foi seguida por Lampert e Thurlirmann em 1969 [72] e adotada pelo código modelo europeu de 1978 [34]. A terceira aproximação assumiu que a linha média do fluxo de corte coincide com a linha média do bloco equivalente das tensões de compressão nas escoras de betão [38]. Para a definição da espessura deste bloco é excluído o betão de recobrimento exterior à linha média de um varão transversal fechado (cinta). Contudo, o cálculo da profundidade do bloco equivalente das tensões de compressão não é rigoroso, pois não é tido em conta o efeito de "amolecimento" do betão ou *softening effect* [96]. Este efeito, observado pela primeira vez por Robinson e Demorieux em 1972 [90], refere-se à redução significativa da resistência do betão na escora devido à fissuração diagonal, efeito este não observado em ensaios de provetes cilíndricos sujeitos à compressão uniaxial [61]. Esta aproximação foi adotada por Collins e Mitchell em 1980 [38] e pelo código canadiano [94].

Pese embora estas três aproximações melhorassem a equação proposta por Rausch, verificaram-se algumas questões que comprometiam a sua utilização generalizada. A primeira questão prendia-se com o facto de este modelo e respetivas aproximações estarem calibradas apenas para vigas com secções pequenas, típicas das utilizadas em edifícios. A segunda questão prendia-se com os métodos empíricos considerados como pouco satisfatórios, segundo alguns autores, utilizados para modificar a equação de Rausch. Como tal, vários autores tentaram abordagens diferentes de melhoramento ao modelo de Rausch, tentando generalizar o modelo para o comportamento de vigas com secções pequenas e grandes, assim como para vigas com pré-esforço, abandonando, tanto quanto possível, o carácter empírico da correção da equação de Rausch. De entre estes modelos teóricos propostos, destaca-se o Modelo de Treliça com Ângulo Variável (*Variable Angle Truss Model* – VATM).

1.3.2.1. Modelos de Treliça de Ângulo Variável (VATM).

Em 1969, Lampert e Thurlirmann [72] generalizaram o modelo de treliça a 45º para vigas de betão armado sujeitas à torção, assumindo que o ângulo de inclinação das escoras de betão podia variar dos 45º e que a teoria da plasticidade seria aplicável, propondo, assim, o VATM. De acordo com o novo modelo proposto pelos referidos autores, o ângulo variável das escoras de betão é determinado pela magnitude das forças de cedência das armaduras transversais e longitudinais, explicando, deste modo, a observação experimental da cedência das armaduras de torção, mesmo quando estas não se encontram equilibradas. Os autores também observaram experimentalmente que uma superfície plana inicial (face exterior) da viga ensaiada se transforma numa superfície hiperbólica, após aplicação de um momento torsor, concluindo assim que as escoras de betão estão sujeitas à flexão e à compressão, simultaneamente. Desta observação, os autores derivaram duas condições adicionais de compatibilidade, onde a primeira condição relaciona a curvatura de flexão das escoras de betão com o ângulo de torção e a segunda condição relaciona a mesma curvatura com a extensão máxima de compressão à superfície da escora. Desta forma, o novo modelo consegue prever a resistência teórica de uma viga de betão armado à torção e também a respetiva deformação.

Em 1972, Elfgren [44] apresentou um modelo alternativo de treliça com ângulo variável tendo por base a analogia de Rausch, a teoria da plasticidade e a teoria do campo de trações de Wagner para vigas com alma fina de perfis metálicos [96]. O modelo proposto por este autor, denominado por Teoria da Plasticidade do Campo de Compressões (*Plasticity Compression Field Theory*), assume que o ângulo de inclinação das fissuras de betão é o mesmo que o ângulo de inclinação do campo de compressão. Contudo, o próprio autor reconheceu que o ângulo do campo de tensões de compressão não é igual ao ângulo real das fissuras, pelo facto de estas não "rodarem" continuamente em função da redistribuição das tensões.

Em 1973, Collins [37] apresenta outra abordagem do modelo de treliça com ângulo variável, tendo por base a compatibilidade de deformações do modelo de treliça. No seu modelo, denominado por Teoria do Campo Diagonal de Compressões (*Compatibility Compression Field Theory*), o ângulo do campo de tensões de compressão é determinado através de uma equação de compatibilidade. Já as condições de deformação são previstas através do círculo de Mohr.

Em todos os modelos anteriormente referidos foi adotada uma curva tensão (σ) – extensão (ε) convencional para o betão comprimido nas escoras, proveniente de ensaios de provetes cilíndricos à compressão axial. No entanto, por esta curva não incorporar o efeito de

amolecimento do betão, os modelos demonstraram ser pouco conservativos para a previsão teórica da resistência das vigas à torção.

Em 1985, Hsu e Mo [59] [60] [61] conseguem colmatar esta falha e propõem um novo refinamento do VATM, incorporando, pela primeira vez, leis constitutivas médias apropriadas para o betão à compressão e para as armaduras à tração. Para a primeira, a lei foi estabelecida a partir de ensaios experimentais controlados em painéis de betão armado sujeitos ao corte no plano, a fim de contabilizar o efeito do estado de tensão biaxial, o efeito das fissuras diagonais e a interação dos materiais componentes (betão e armadura). A lei constitutiva média adotada contabilizava, assim, o efeito de amolecimento bem como o efeito de "enrijecimento" (*stiffening effect*) do betão, este último para contabilizar a participação do betão em tração entre fissuras. Este modelo refinado do VATM mostrou-se capaz de prever adequadamente o valor da resistência real em torção de vigas de betão armado e pré-esforçadas e respetiva deformação. A Figura 20 ilustra um exemplo de modelo de treliça espacial com ângulo variável para uma viga com secção retangular vazada sujeita à torção pura. A secção é armada com quatro barras de canto idênticas e cintas espaçadas uniformemente.

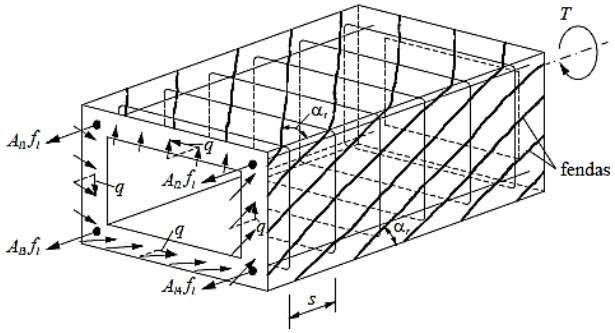

Figura 20. Modelo VATM para uma viga de secção retangular vazada sujeita à torção [56].

As previsões deste VATM refinado mostraram boa concordância com os resultados experimentais, nomeadamente na previsão da resposta das vigas à torção na fase final. Já para níveis de carga mais baixos, o modelo prevê uma resposta longe do comportamento real da viga, uma vez que assume que a viga se encontra completamente fissurada desde o início do carregamento e também por negligenciar a influência do núcleo de betão na resistência da viga [60] [61] (aspeto importante para secções cheias). Este facto pode ser observado no exemplo apresentado na Figura 21, onde se encontra representado o comportamento de uma viga de betão armado de resistência normal com secção cheia (viga M2) ensaiada à torção pura e respetiva previsão teórica do seu comportamento através do modelo VATM de Hsu e Mo [61].

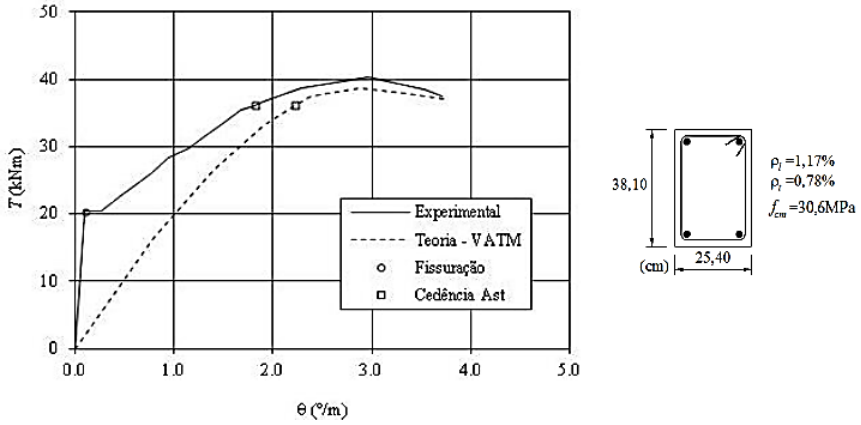

Figura 21. Exemplo de uma curva $T-\theta$ experimental e teórica calculada pelo VATM [61].

Quando comparado com modelos mais complexos propostos para vigas de betão armado sujeitas à torção, que por vezes envolvem um maior esforço computacional (*e.g.*, [9] [10] [78]), o VATM é reconhecido como um modelo mais simples e confiável para prever a resistência à torção das vigas, parâmetro crucial para o procedimento de verificação estrutural. Contudo, o VATM continua a possuir várias lacunas, tais como, a não consideração da resistência ao corte das escoras de betão, a influência do efeito "ferrolho" nas armaduras e a contribuição do betão à tração no comportamento das vigas para baixos níveis de carregamento. Nas últimas três décadas, este modelo tem sido amplamente melhorado e generalizado pelos investigadores, tendo sido propostos vários refinamentos ao VATM para vigas de betão armado e pré-esforçado (*e.g.*, [31] [60] [86] [98]), para vigas de betão armado sujeitas à torção combinada com outros esforços internos (*e.g.*, [48] [87] [93] [95]) e para vigas de betão armado sob torção e com restrição axial (*e.g.*, [28] [30]).

1.3.2.2. Modelos recentes baseados no VATM.

Entre 2008 e 2011, Bernardo e Lopes [25] [27] propuseram um dos primeiros modelos teóricos capaz de prever o comportamento global de vigas de betão armado sujeitas à torção pura. A aproximação teórica realizada por estes autores é composta por três fases de comportamento das vigas à torção, observadas experimentalmente, a saber:

(i) Estado I: fase de comportamento elástico-linear em regime não fissurado, caracterizada pelas teorias clássicas da torção adotadas por Hsu [56], *i.e.*, a teoria da elasticidade [91], a teoria da flexão enviesada [56] e a teoria do tubo fino de Bredt [32];

(ii) Estado II: fase de comportamento elástico-linear em regime fissurado, caracterizada pela analogia da treliça espacial com angulo de 45º para as escoras de betão e pelo comportamento linear dos materiais, modelo proposto por Hsu [55];

(iii) Estado III: fase de comportamento não linear, caracterizada pelo modelo de treliça com ângulo variável (VATM), modelo proposto por Hsu e Mo [59] [60] [61].

O modelo de Bernardo e Lopes foi ainda, então, pioneiro na previsão do comportamento à torção de vigas construídas com betões de alta resistência. Tais betões destacam-se dos betões de resistência normal pela maior durabilidade, elevadas propriedades mecânicas a curto prazo, reduzida tração e fluência, e melhor comportamento em Serviço. Segundo o código modelo europeu MC10 [36], um betão de alta resistência é um betão que, aos 28 dias de idade, possui, no mínimo, uma resistência característica ao ensaio de compressão de 50 MPa (Clausula 5.1.1). Abaixo desse valor, o betão é considerado de resistência normal. Devido às propriedades do betão de alta resistência, o comportamento das vigas à torção construídas com estes betões, para elevados carregamentos, é ligeiramente diferente do das vigas construídas com betões de resistência normal, possuindo um comportamento menos dúctil, mas uma maior capacidade de resistência à torção.

A Figura 22 mostra exemplos de previsões teóricas obtidas através do modelo proposto por Bernardo e Lopes (linha clara) e respetivos resultados experimentais (linha escura), referentes a vigas com secção cheia e vazada e vigas com betões de resistência normal e de alta resistência. As curvas $T - \theta$ mostram que o modelo de Bernardo e Lopes permite obter boas previsões do comportamento global das vigas à torção.

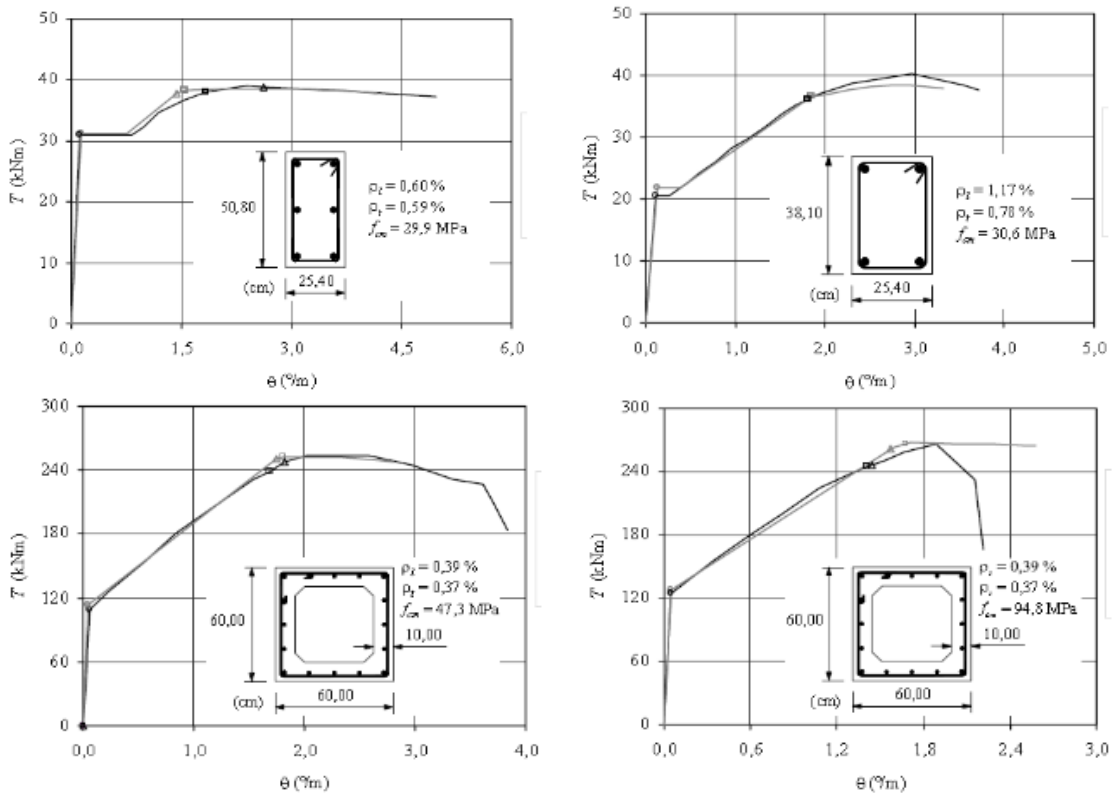

Figura 22. Curvas $T - \theta$ obtidas por Bernardo e Lopes [25] [27].

Pese embora a obtenção de bons resultados, o modelo de Bernardo e Lopes possui algumas limitações. A primeira limitação prende-se com o facto de o modelo ser pouco consistente face à utilização de três teorias distintas, com formulações próprias para cada fase de comportamento da viga. A transição entre as diversas teorias é feita através de critérios de ajustamento semi-empíricos baseados em observações experimentais disponíveis na literatura [25]. Os próprios autores reconhecem que o modelo seria mais satisfatório se fosse baseado numa única teoria. A segunda limitação prende-se com a não possibilidade de o modelo fornecer informação precisa sobre o estado de tensões e de deformações internas para baixos níveis de carregamento. Este facto deve-se à adoção dos critérios semi-empíricos de transição e de critérios de ajustamento da curva $T-\theta$ segundo o eixo das rotações, após o cálculo das várias fases de comportamento da viga. Estes ajustes fazem com que os parâmetros internos de cálculo deixem de ser válidos nos troços da curva $T-\theta$ posteriores aos troços ajustados. A falta de informação precisa sobre o estado de tensões e de deformações internas dos materiais compromete a utilização do modelo para a verificação da segurança das vigas ao Estado Limite de Serviço.

Em 2012, Andrade, Bernardo e Lopes [18], desenvolveram um modelo generalista para prever o comportamento global das vigas à torção, com base num único modelo, o VATM. Este novo modelo, designado por Modelo de Treliça com Ângulo Variável Modificado (*Modified Variable Angle Truss Model* – MVATM), consiste na modificação do VATM na fase de pré-fissuração da viga, de forma a adaptá-lo aos baixos níveis de carregamento. À semelhança do anterior modelo, o MVATM é composto por três fases de comportamento das vigas à torção, a saber:

(i) Estado não fissurado: a formulação do VATM é alterada de forma a incorporar a contribuição do betão tracionado nas equações de equilíbrio e a contribuição do núcleo de betão na rigidez das vigas com secção cheia;

(ii) Transição entre o estado não fissurado e o estado fissurado: é anulada a contribuição do betão tracionado, mantendo a contribuição do núcleo de betão nas vigas de secção cheia, de modo que as rotações sofram um acréscimo brusco para um momento torsor constante;

(iii) Estado fissurado: a contribuição do núcleo de betão (em vigas com secção cheia) vai diminuindo até atingir o momento torsor resistente, em resultado da propagação da fissuração e dos danos no betão. Para vigas de secção vazada, face à inexistência de um patamar horizontal na curva $T-\theta$ imediatamente após o momento torsor de fissuração, é realizado um pequeno ajuste na curva no troço pós-fissuração.

A Figura 23 mostra exemplos de previsões teóricas obtidas através do modelo proposto por Bernardo e Lopes, pelo MVATM e os respetivos resultados experimentais. As curvas $T - \theta$ mostram que o MVATM permite obter previsões muito próximas do modelo original de Bernardo e Lopes.

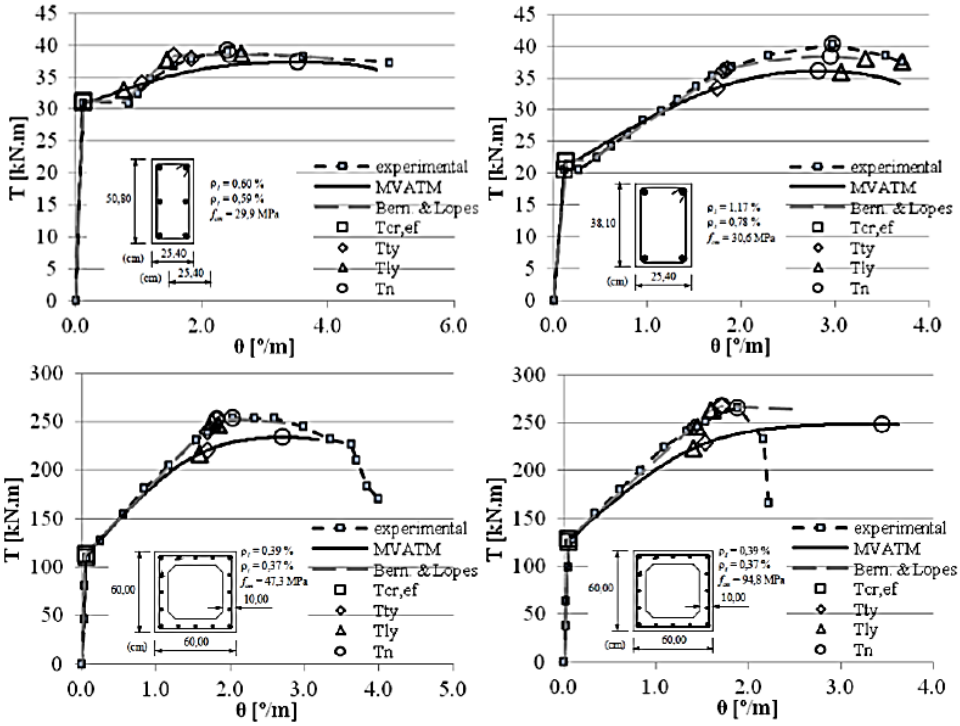

Figura 23. Curvas $T - \theta$ obtidas por Bernardo et. al [27].

Apesar do MVATM permitir boas previsões teóricas e ser teoricamente mais consistente que o modelo de Bernardo e Lopes [25] [27] por se basear em apenas num único modelo teórico, este modelo continua a não fornecer informações precisas sobre o estado interno de tensões e de deformações da viga na fase pós-fissuração. Esta situação deve-se ao facto de o modelo base (VATM) ser incapaz de prever corretamente o momento de fissuração e, em consequência, ser necessário recorrer a outra teoria para estabelecer o limite da fase não fissurada. Ainda assim, o MVATM foi validado tendo por base, essencialmente, os resultados de numerosos ensaios experimentais com vigas de betão armado sujeitas à torção. No Capítulo 3 do presente trabalho, uma extensão do MVATM é estudada e utilizada para o cálculo e análise do comportamento à torção de vigas de betão incorporando pré-esforço longitudinal.

Em 2015, Bernardo *et al.* [20] apresentam um novo modelo designado por Generalização do Modelo de Treliça Espacial com Ângulo Variável (*Generalized Softened Variable Angle Truss Model* – GSVATM), o qual constitui uma generalização do VATM. Tendo por base as modificações propostas por Jeng e Hsu ao modelo SMM (*Softened Membrane Model*, *vide*

Secção 1.3.2), o GSVATM incorpora um "tirante" perpendicular à escora de betão na reformulação do VATM, por forma a considerar a influência do betão à tração na resistência das vigas à torção. Para tal, o modelo incorpora uma nova lei constitutiva média para o betão à tração. O VATM constitui um caso particular do GSVATM, quando a resistência à tração do betão não é considerada. A Figura 24 apresenta exemplos de previsões teóricas obtidas através do modelo GSVATM e respetivas curvas experimentais.

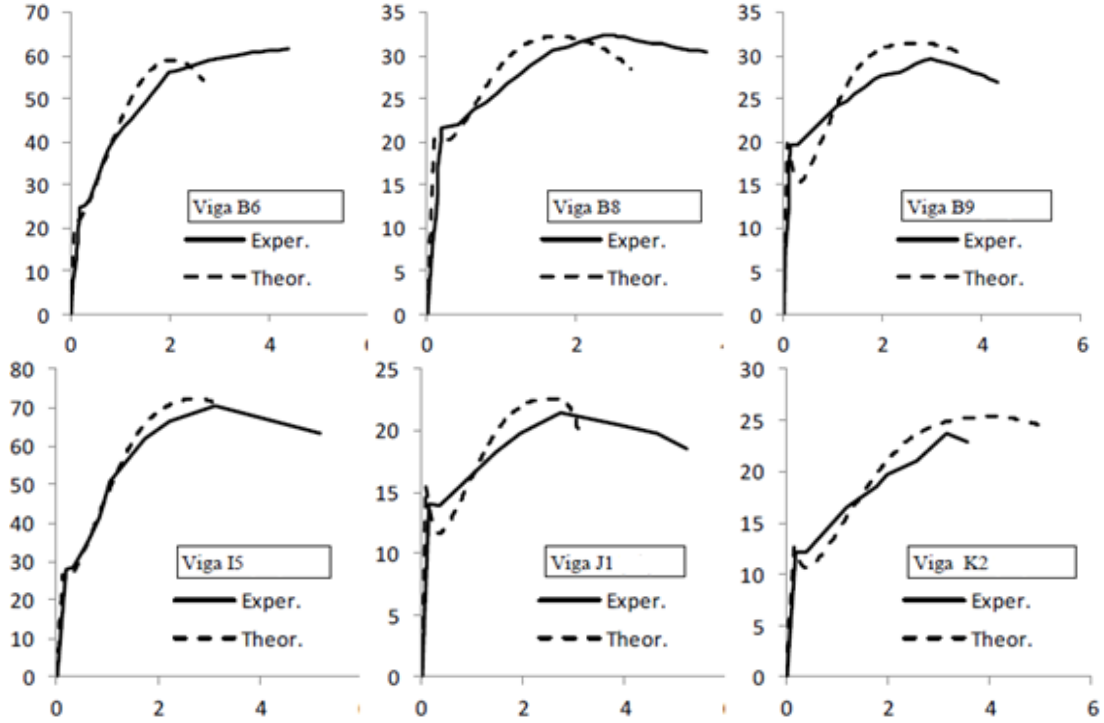

Figura 24. Curvas $T-\theta$ obtidas pelo GSVATM [20].

As curvas $T-\theta$ mostram que o novo modelo generalizado do VATM continua a ter alguma dificuldade na previsão do comportamento real da viga, bem como da sua rigidez, imediatamente após a fissuração, em especial para vigas com taxa de armadura pequena. De acordo com Bernardo *et al.* [20], o decréscimo do momento torsor após a fissuração deve-se à forma geométrica da curva $\sigma-\varepsilon$ adotada para a relação constitutiva média do betão à tração, em particular no ramo descendente pós-pico. Esta curva média, calibrada para ensaios de prismas de betão armado à tração uniaxial, não tem em conta os mecanismos suplementares que ocorrem em situações de corte, como por exemplo, o interbloqueamento dos agregados ou o "efeito ferrolho" das armaduras, o que leva a resultados teóricos desajustados em relação aos resultados experimentais para o caso da torção. No Capítulo 3 do presente trabalho, é feito um estudo comparativo de várias leis constitutivas médias do betão à tração encontradas na literatura consultada, a fim de verificar qual a lei que melhores resultados apresenta nesta zona comportamental de transição. Este estudo é importante porque as previsões dos modelos do tipo dos

anteriormente referidos dependem, fortemente, das leis constitutivas médias incorporadas no modelo. Este aspeto já tinha sido verificado e estudado por Bernardo *et al.* [16] [19] para as leis constitutivas médias para o betão à compressão e para as armaduras à tração a incorporar no MVATM. Para o GSVATM, ao incorporar uma lei constitutiva média do betão à tração adicional, é assim requerida uma avaliação similar.

O modelo original do GSVATM foi validado tendo apenas por base os resultados experimentais de vigas de betão armado com secção cheia à torção. Tal foi justificado pelos autores recorrendo a vários motivos. Em primeiro lugar, o número de resultados experimentais de vigas com secção vazada era ainda muito inferior aos de vigas com secção cheia. Em segundo lugar, como referido anteriormente (Secção 1.2.2.3), as vigas de secção vazada apresentam um comportamento diferente na transição do estado não fissurado para o estado fissurado, quando comparadas a vigas de secção cheia similar. Tendo por base resultados experimentais posteriores vocacionados para o estudo deste problema, bem como resultados experimentais adicionais com novas vigas (incluindo vigas com secção vazada e pré-esforço longitudinal, cujos resultados são apresentados no Capítulo 4 deste trabalho), o GSVATM foi posteriormente generalizado para vigas de secção vazada [14], para vigas de betão pré-esforçado [29] [95] [6] e para vigas com secção "T" [15]. Foi também recentemente formulada uma versão unificada do GSVATM [17].

1.3.3. Modelo de Treliça com Amolecimento para Membranas (STM).

Para simplificar o dimensionamento de estruturas complexas, vários autores têm desenvolvido diversos modelos analíticos para calcular a resistência dessas estruturas sujeitas a um determinado esforço ou conjunto de esforços atuantes, a partir de estruturas mais pequenas e simples que compõem as estruturas originais. Para muitas estruturas sujeitas, fundamentalmente, a esforços de membrana, essas estruturas mais simples podem ser representadas por elementos bidimensionais (2D), também denominados por placas ou painéis na literatura, sujeitas a tensões atuantes no seu plano (tensões de membrana).

Em 1988, Hsu [57] desenvolveu um modelo de cálculo a partir de resultados experimentais obtidos em diversos ensaios de painéis de betão armado sujeitos ao corte puro (Figura 25). Este modelo, designado por Modelo de Treliça com Amolecimento (*Softened Truss Model* – STM), tem por base o Modelo de Treliça Plana desenvolvido por Ritter e Mörsch [77] [89] e incorpora o efeito de amolecimento do betão [90]. Para o estado fissurado, o STM assume que a direção das fissuras é igual à direção das tensões internas principais de compressão do elemento de betão. Contudo, em 1993 [58], Hsu conclui que tal não acontece na realidade. No estado não fissurado, a direção da primeira fissura é, de facto, determinada pela direção das tensões principais. No entanto, com o aumento da carga, as novas fissuras

surgem orientadas em virtude da rotação da direção das tensões principais, rotação essa que acontece devido à redistribuição interna de tensões e das condições de compatibilidade. Esta observação é mais evidente em elementos com armaduras não equilibradas nas duas direções.

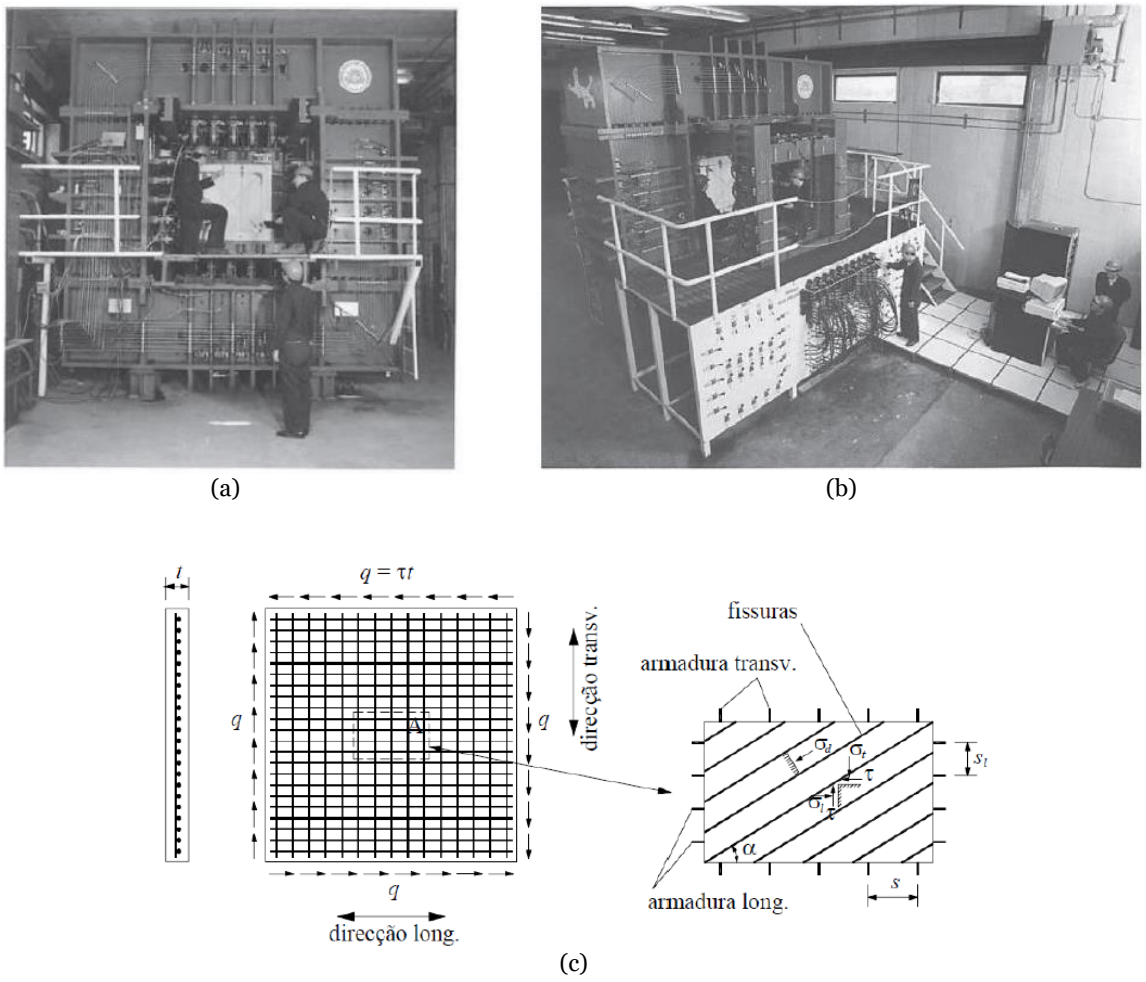

Figura 25. Ensaios de painéis de betão armado no *Universal Panel Tester* [58]: (a) vista norte, (b) vista sul. (c) Exemplo geral de uma placa sujeita ao corte [13].

Da conjugação dos estudos de Belarbi e Hsu em 1994 [11] e em 1995 [12], e também de Pang e Hsu em 1995 [81], surge um novo modelo designado por Modelo de Treliça com Amolecimento e Ângulo Rotacional (*Rotating-Angle Softened Truss Model* – RA-STM). Este modelo tem por base, de forma mais completa, os três princípios de Navier da mecânica dos materiais: o equilíbrio das tensões, a compatibilidade das deformações e as leis constitutivas médias dos materiais. Como tal, o modelo resulta da calibração das relações constitutivas médias do betão à tração e da incorporação do efeito de enrijecimento do betão [11], da calibração do coeficiente de amolecimento do betão [12] e da incorporação do "efeito de ferrolho" [81] na sua formulação. Em 1998, Zhang e Hsu [101] propuseram ainda a introdução de novas relações constitutivas médias para o betão à compressão. Uma vez que

as equações de equilíbrio e compatibilidade são formuladas num referencial cujos eixos coincidem com a direção principal das fissuras, igual à direção principal das tensões internas de compressão do elemento para qualquer nível de carregamento, o RA-STM não incorpora uma lei constitutiva média do betão ao corte. Na realidade, o betão apresenta uma pequena contribuição adicional ao corte devido ao "efeito ferrolho" nas armaduras e ao interloquemaneto dos agregados do betão ao longo das fissuras. Ainda assim, o RA-STM apresenta boas previsões teóricas globais comparadas com os resultados experimentais, sendo ainda um modelo amplamente utilizado para prever a resposta carga-deformação ao corte de painéis de betão armado e com pré-esforço [22] [23] [24].

Entre 1996 e 1997, Pang e Hsu [82], bem como Hsu e Zhang [63], desenvolveram um modelo diferente denominado de Modelo de Treliça com Amolecimento e Ângulo Fixo (*Fixed-Angle Softened Truss Model* – FA-STM). Como o próprio nome indica, o modelo assume um ângulo fixo, coincidente com o ângulo das direções principais dos esforços de tração e compressão externos aplicados no elemento, que define a orientação do sistema de coordenadas adotado para estabelecer as equações de equilíbrio e compatibilidade. Este modelo assume que a orientação das fissuras do elemento é perpendicular à direção principal do esforço de tração aplicado no elemento de betão armado, esforço esse constante. Após a fissuração do elemento, as armaduras começam a ser solicitadas e o sistema de coordenadas assumido para as tensões principais tende a desviar-se em virtude da rotação destas, implicando a necessidade de considerar tensões tangenciais nas equações de equilíbrio. Assim, para o cálculo da resistência do elemento aos esforços aplicados, foi incorporada uma lei constitutiva média do betão ao corte na formulação deste modelo, a qual foi calibrada tendo por base os resultados de ensaios de painéis ao corte. Comparativamente com RA-STM, o FA-STM possui um procedimento e uma formulação mais complexa.

Os modelos anteriores não preveem adequadamente o comportamento pós-pico da curva tensão tangencial (τ) – distorção (γ) das placas, particularmente pelo facto de o efeito de *Poisson* ser desprezado no estado fissurado. Para colmatar esta situação, em 2002, Hsu e Zhu [64] propuseram um refinamento ao FA-STM, desenvolvendo um novo modelo denominado por Modelo de Membrana com Amolecimento (*Softened Membrane Model* – SMM). Este modelo constitui um desenvolvimento do FA-STM e incorpora, na sua formulação, o designado coeficiente de Hsu/Zhu (equivalente ao coeficiente de *Poisson* para o estado fissurado [102]) bem como uma nova relação constitutiva média refinada para o betão ao corte. Quando comparado com os resultados dos modelos anteriores para painéis de betão armado sujeitos ao corte, o SMM prevê melhor o comportamento pós-pico [23].

1.3.3.1. Modelos com base no STM para vigas à torção pura.

Em 2009, Jeng e Hsu [69] apresentaram um novo modelo designado por Modelo de Membrana com Amolecimento para a Torção (*Softened Membrane Model for Torsion* – SMMT). Este modelo foi desenvolvido tendo por base a associação do SMM com a Teoria do Tubo Fino de Bredt, relacionando o fluxo de tensões de corte que atua num elemento de membrana (ou de parede da secção) e o momento torsor aplicado na secção, de modo a prever o comportamento global de vigas de betão armado com secção cheia sujeitas à torção. Neste modelo são incorporadas relações constitutivas médias do betão (à compressão, à tração e ao corte), permitindo incluir a contribuição do betão à tração na direção perpendicular às escoras, assim como o efeito da distorção devido ao corte no betão. Para calibrar o SMMT por forma a ser aplicável a vigas em torção na fase pré-fissurada, os autores propuseram, relativamente à formulação do SMM para painéis ao corte, a incrementação em 45% da rigidez pré-fissuração e da extensão para o pico de tensão na relação constitutiva média do betão à tração de Belarbi e Hsu [11]. Já para a fase última comportamental, os autores reduziram para 80% o coeficiente de Hsu/Zhu adotado no SMM.

A Figura 26 apresenta exemplos de previsões teóricas obtidas através do modelo SMMT (linha a traço interrompido) e respetivas curvas experimentais (linha contínua) de vigas ensaiadas à torção. As curvas $T - \theta$ mostram que o SMMT apresenta resultados bastante satisfatórios na previsão do comportamento das vigas à torção, em geral similares às previsões do GSVATM até ao momento torsor máximo.

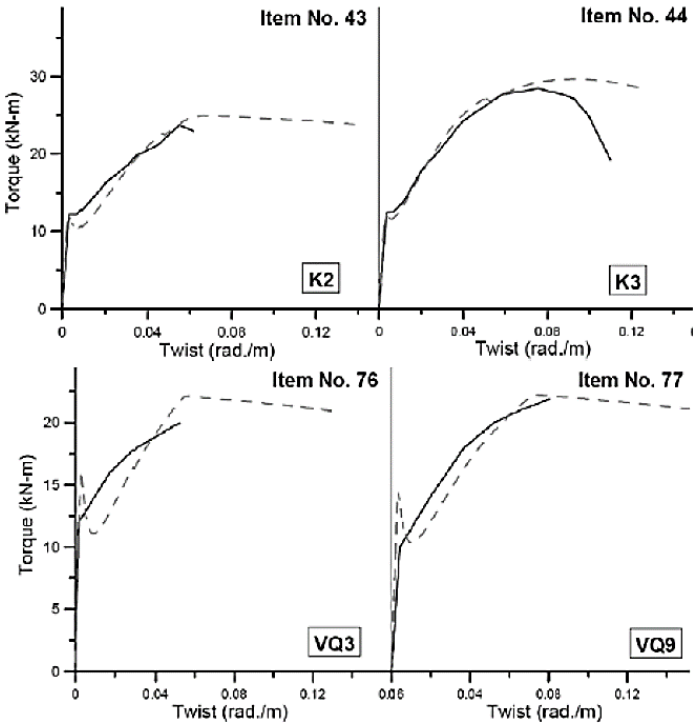

Figura 26. Curvas $T - \theta$ obtidas pelo SMMT [69].

Pese embora o SMMT seja um modelo consistente, por se basear num único modelo teórico, verifica-se existir alguma discordância entre as curvas $T-\theta$ teóricas e experimentais, imediatamente a seguir ao momento torsor de fissuração, de forma semelhante ao observado para o GSVATM. Também de forma semelhante ao explicado anteriormente para o GSVATM, o SMMT foi validado tendo por base apenas resultados experimentais de vigas com secção cheia.

Em 2013, Bernardo *et al.* [21] realizaram um estudo para analisar a validade do SMMT na previsão do comportamento de vigas com secção vazada sujeitas à torção. Os autores concluíram que o SMMT não fornece boas previsões para a fase pré-fissurada pelo facto de a correção à lei constitutiva média do betão à tração, adotada por Jeng e Hsu [69], não ser a mais adequada a este tipo de secções. Segundo Bernardo *et al.*, a rigidez da fase pré-fissurada e a extensão para o pico de tensão deveriam ser incrementados para 24% e não para 45%, como proposto por Jeng e Hsu. Assim, conclui-se que o SMMT necessita incorporar coeficientes empíricos de correção em função do tipo de secção a modelar.

Mais recentemente, o SMMT foi refinado e generalizado para vigas com pré-esforço [68] e para vigas com secção vazada [67].

1.3.3.2. Modelos com base no STM para vigas à torção combinada com outros esforços.

A consulta de literatura realizada no decurso deste trabalho revelou que existe um escasso número de modelos baseados em treliças com amolecimento capazes de prever adequadamente a resistência de elementos de betão armado sujeitos à torção combinada com outros esforços internos. A previsão do comportamento carga-deformação de um elemento estrutural nestas condições torna-se bastante mais complexa devido à interação que ocorre entre os vários esforços internos e à forma como cada esforço solicita as secções, em particular no estado fissurado.

Entre 2006 e 2009, Greene [47] e Greene e Belarbi [48] [49] propuseram um modelo com base no RA-STM, designado por Modelo de Treliça com Amolecimento para Ações Combinadas (*Combined Action Softened Truss Model* – CA-STM), capaz de prever o comportamento global de vigas de betão armado, com secção retangular cheia e vazada, sujeitas à torção combinada com flexão, esforço transverso e esforço axial. Este modelo simula a viga real em estudo através da combinação e compatibilização de quatro painéis de betão armado sujeitos a esforços de membrana, desprezando o núcleo de betão, no caso das vigas com secção cheia (Figura 27).

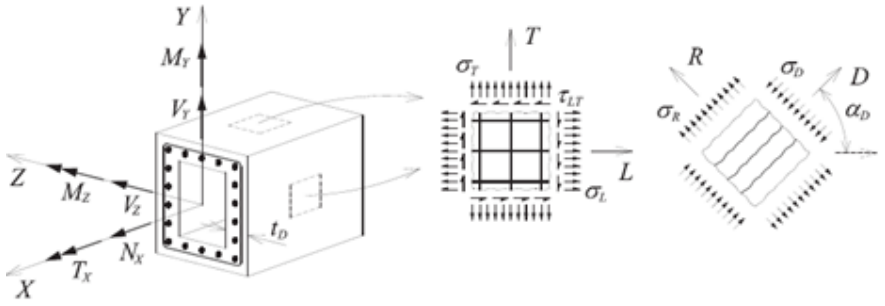

Paredes de BA. Elemento de BA 2D. Principais tensões.

Figura 27. Idealização de uma viga de betão armado pelo CA-STM.

A Figura 28 apresenta exemplos de previsões teóricas obtidas através do CA-STM e respetivas curvas experimentais de vigas ensaiadas à torção pura e vigas ensaiadas à torção combinada com flexão. As curvas $T-\theta$ e as curvas de interação mostram resultados satisfatórios na previsão do comportamento das vigas.

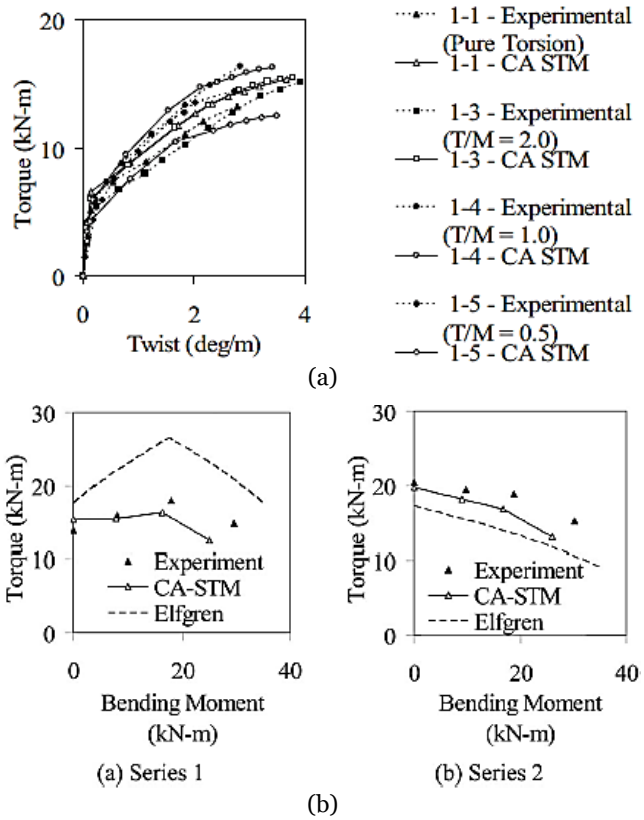

Figura 28. Curvas $T-\theta$ e de interação experimentais e teóricas determinadas pelo CA-STM [49]: (a) Torção pura; (b) Torção combinada com flexão.

O CA-STM foi validado pelos referidos autores tendo por base um número relativamente reduzido de resultados experimentais, particularmente para vigas sujeitas à torção combinada com flexão. Em adição, o seu procedimento de cálculo é complexo devido à característica intrínseca não linear das equações, as quais são resolvidas numericamente

baseando-se numa técnica de "tentativa e erro" que exige um grande esforço de cálculo, dado o número elevado de equações e variáveis envolvidas. Esta técnica de resolução faz com que o modelo perca alguma eficiência e estabilidade numérica devido ao grande número de estimativas iniciais que são necessárias para iniciar os cálculos.

Entre 2016 e 2017, Silva [92] e Silva *et al.* [93] propuseram um procedimento de cálculo mais eficiente para o CA-STM, capaz de prever o comportamento carga-deformação de vigas de betão armado solicitadas a diferentes combinações de esforços. Para tal, os referidos autores reformularam o procedimento de cálculo num sistema de equações não lineares com restrições, conseguindo, deste modo, reduzir o número de estimativas iniciais necessárias. Outra alteração empreendida no modelo original foi a de introdução de um algoritmo de otimização que permite resolver as equações não lineares sem recorrer à técnica original de "tentativa e erro". O modelo CA-STM, com o novo procedimento de cálculo, mostrou ser mais estável, exigindo menos esforço computacional de cálculo comparativamente ao procedimento de cálculo original. A Figura 29 mostra que, quando comparados com resultados experimentais e com o CA-STM original, o CA-STM com o novo procedimento de cálculo apresenta resultados teóricos bastante satisfatórios, principalmente na última fase de comportamento [93].

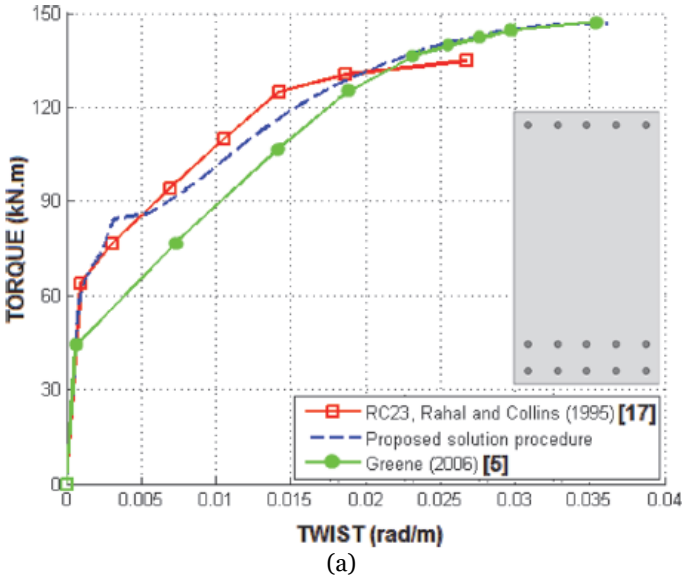

(a)

Figura 29. Curvas $T - \theta$ experimentais e teóricas determinadas com o CA-STM com o novo procedimento de cálculo de Silva et al. [93]: (a) Torção pura; (b) Torção combinada com esforço transverso.

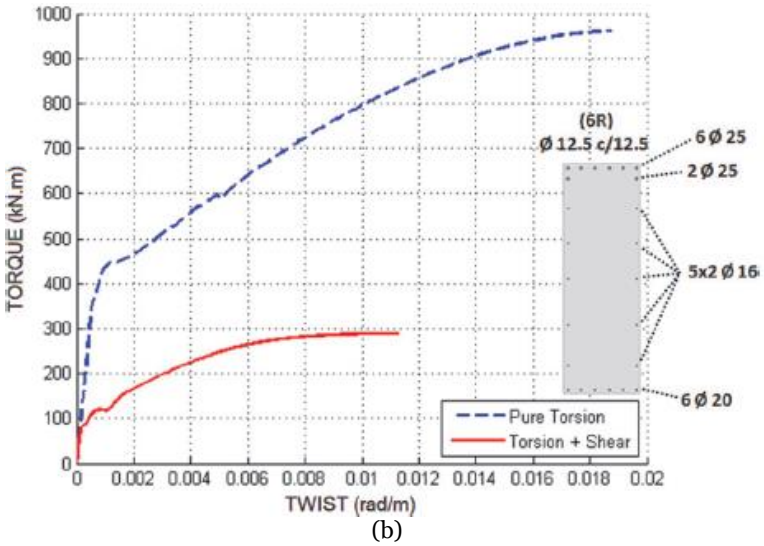

(b)

Figura 29. [cont.] Curvas $T-\theta$ experimentais e teóricas determinadas com o CA-STM com o novo procedimento de cálculo de Silva et al. [93]: (a) Torção pura; (b) Torção combinada com esforço transverso.

O CA-STM com o novo procedimento de cálculo foi validado tendo por base um número relativamente reduzido de resultados experimentais, envolvendo apenas vigas à torção pura e à torção combinada com esforço transverso. Tendo por base esta constatação, no Capítulo 3 é apresentada uma proposta de alteração ao procedimento de cálculo do CA-STM, reformulado de acordo com algumas propostas de Silva *et al.* [93], com vista ao seu refinamento para vigas de betão armado sujeitas à torção combinada com flexão. O modelo refinado proposto é validado tendo por base um número elevado de resultados experimentais de vigas de betão armado em torção combinada com flexão.

Foram recentemente propostos outros modelos melhorados tendo por base o SMM para torção com combinação de outros esforços, apresentando bons resultados [46] [70]. No entanto, observa-se novamente que, para a validação dos modelos, a combinação da torção com flexão é, em geral, preterida em relação a outras combinações de esforços internos.

1.4. Estado limite último de torção de vigas de betão armado. Ductilidade e resistência à torção.

A teoria da plasticidade faz hoje parte integrante da mecânica estrutural. A validade desta teoria pressupõe um comportamento dúctil da estrutura nas suas secções críticas, para que se possa adaptar à redistribuição lenta e gradual de esforços internos admissíveis no cálculo aos ELU, sem ocorrer uma rotura frágil nessas secções ou o seu colapso súbito. Se não for prevista uma redistribuição de esforços em projeto, a estrutura deve ainda assim ser dotada dessa capacidade para qualquer situação imprevista. Assim, a ductilidade pode ser definida

como a capacidade do material, secção, elemento estrutural ou estrutura estar sujeita a uma notável deformação inelástica sem uma perda apreciável da sua capacidade de carga.

No caso da torção, e atendendo a que o fenómeno principal associado a este esforço é o corte, a aplicação da teoria da plasticidade é ainda hoje questionável. É sabido que o betão simples (não armado) é um material frágil. Contudo, quando lhe é adicionada armadura em quantidade e com disposição adequada, a sua rotura não é tão frágil como poderia ser esperado. Já para níveis de carga elevada, a fissuração por corte apresenta uma influência direta na dissipação de energia interna, através de uma razoável deformação inelástica (efeito de amolecimento), tornando a rotura mais dúctil. Assim, para estes casos, a teoria da plasticidade torna-se numa escolha viável para analisar a capacidade resistente dos elementos estruturais à torção.

A Figura 30 ilustra dois casos exemplificativos, analisados numericamente, de vigas contínuas de dois tramos com eixo curvo sujeitas a uma carga distribuída uniforme, sem excentricidade em relação ao eixo da secção. A diferença entre os dois sistemas estruturais está no apoio central onde, no primeiro caso (Figura 30(a)) o apoio não restringe a deformação da viga à torção (rotação transversal), enquanto, no segundo caso (Figura 30(b)) o apoio central restringe essa mesma deformação. Em ambos os sistemas estruturais, os apoios de extremidade restringem a rotação de torção. O caso da Figura 30(a) é frequente em pontes, quando o apoio intermédio se localiza sob o eixo da viga do tabuleiro.

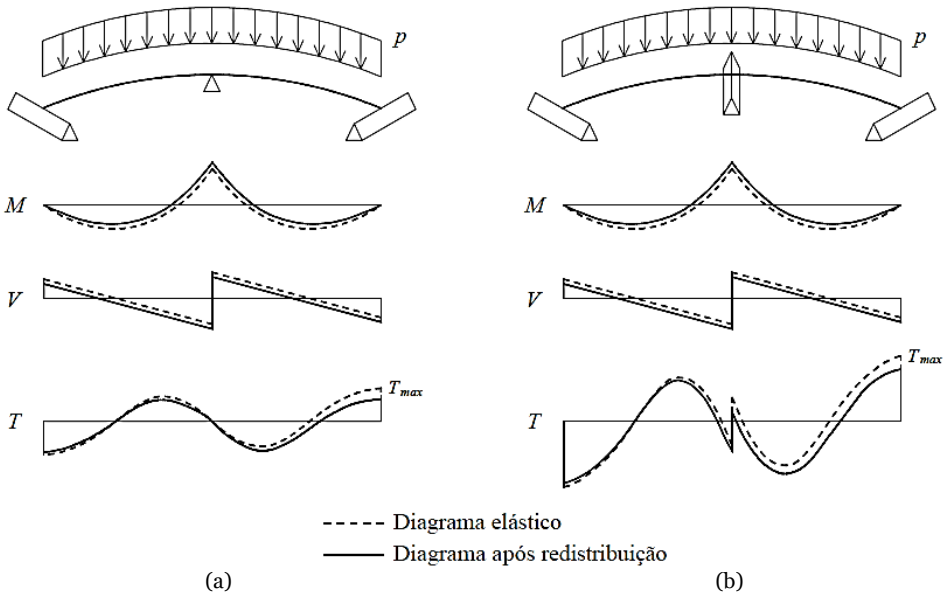

Figura 30. Redistribuição do diagrama dos momentos torsores elásticos em vigas contínuas com eixo curvo. (a) Rotação transversal livre no apoio central. (b) Rotação transversal restringida no apoio central. [73].

Nos apoios de extremidade, as armaduras são dimensionadas para o esforço máximo predominante, neste caso a torção (combinada com esforço transverso moderado e momento fletor nulo). Quando o momento torsor ultrapassa o momento torsor resistente das secções críticas, as vigas sofrem grandes deformações angulares nos apoios de extremidade, acompanhadas de uma redistribuição dos esforços internos elásticos (torsor, fletor e transverso) ao longo dos vãos. Se os apoios de extremidade não possuírem ductilidade suficiente para resistirem às acções imprevistas, a redistribuição de esforços decorrerá de forma brusca, plastificando a zona de extremidade e originando uma "rótula de torção". Esta situação obrigará a uma alteração do diagrama de momento torsor (Figura 31).

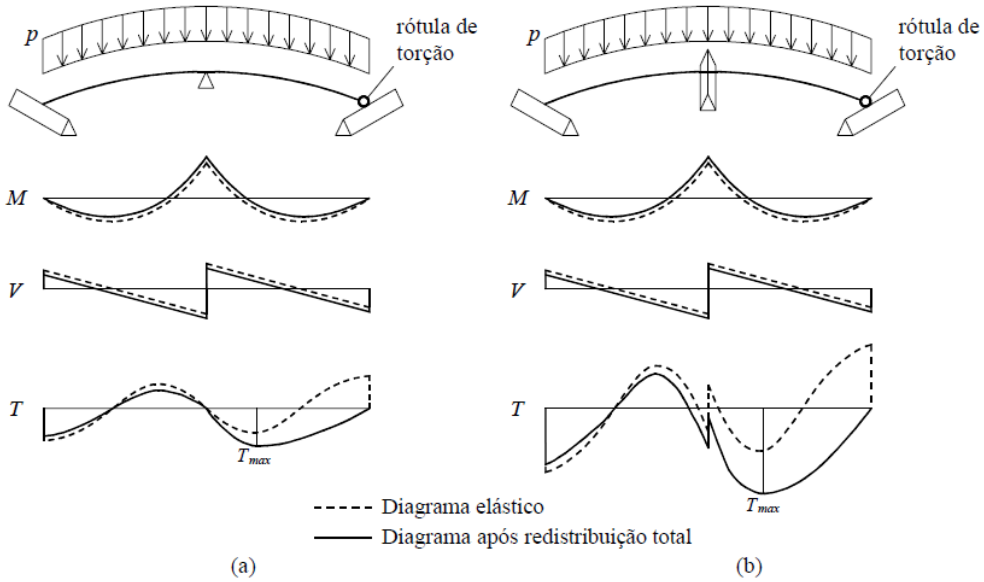

Figura 31. Redistribuição total do diagrama de momentos torsores [73].

A existência de "rótulas de torção" foi observada experimentalmente por Lopes e Bernardo [73], através do ensaio à torção de vigas de betão armado com secção vazada, tendo por base o registo das rotações transversais ao longo do eixo da viga, em numerosas secções pouco espaçadas (Figura 32). Essas medições revelaram que, para vigas que apresentaram um comportamento dúctil em torção, existem zonas localizadas com plastificação das armaduras de torção e comprimento médio igual à altura da secção transversal, onde se concentra a deformação da viga no estado último.

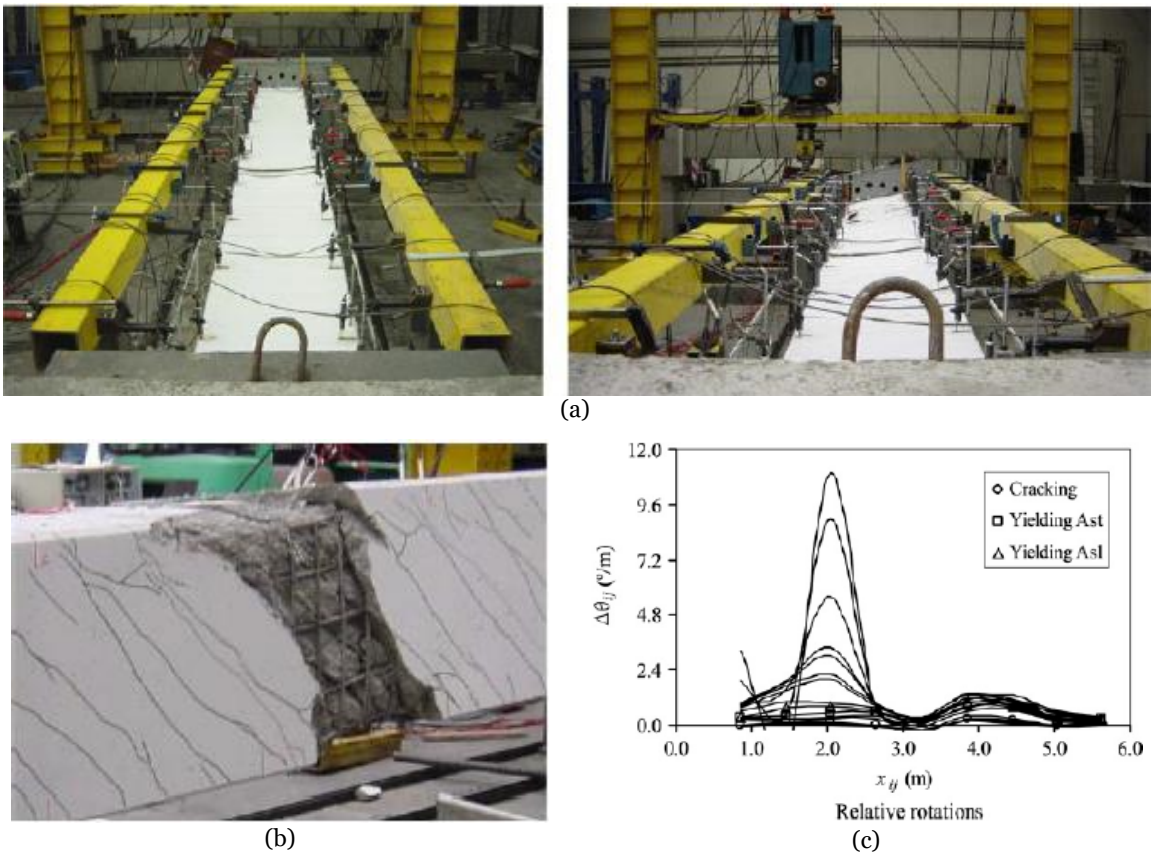

Figura 32. Ensaio experimenta [73]: (a) ensaio de uma viga à torção pura; (b) e (c) evidência experimental de uma "rótula de torção".

Fruto da nova redistribuição de esforços internos, surge um novo momento torsor máximo não previsto numa secção na zona do vão. Esta nova secção crítica em torção gera uma nova "rótula de torção" e a estrutura forma um mecanismo parcial de torção (Figura 33).

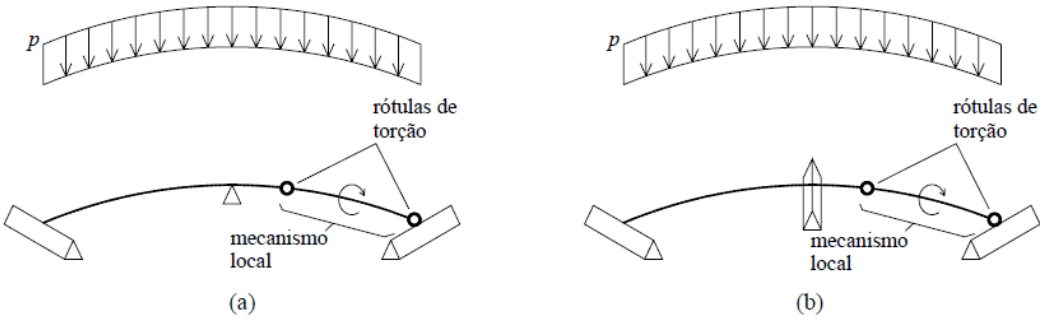

Figura 33. Mecanismo de torção resultante da redistribuição total do diagrama dos momentos torsores [73].

Existem casos documentados de colapsos de estruturas de pontes onde o esforço de torção demonstrou ser predominante na secção crítica. Um desses casos aconteceu em Northridge (USA) em 1994 (Figura 34), onde uma ponte com diretriz curva colapsou após um sismo de elevada intensidade. Este caso demonstra que é importante existir uma preocupação em

projeto de dotar as estruturas de um mínimo de ductilidade em torção, principalmente nas zonas críticas, para eventuais redistribuições de esforços inesperados.

Figura 34. Colapso estrutural de uma ponte rodoviária com eixo curvo [85].

Na literatura consultada são escassos os estudos que analisam especificamente a questão da ductilidade em torção de elementos estruturais. Em 1968, Hsu [52] [55] realizou um estudo experimental para averiguar a influência do núcleo central de uma viga de betão armado na rigidez de torção pós-fissuração e na resistência à torção. O autor ensaiou à torção pura, até à rotura, três vigas idênticas com geometria, materiais e taxas de armadura semelhantes. Das três vigas, uma era constituída por secção cheia e duas por secção vazada com espessuras de parede diferentes. Os resultados obtidos pelo autor encontram-se apresentados na Figura 35.

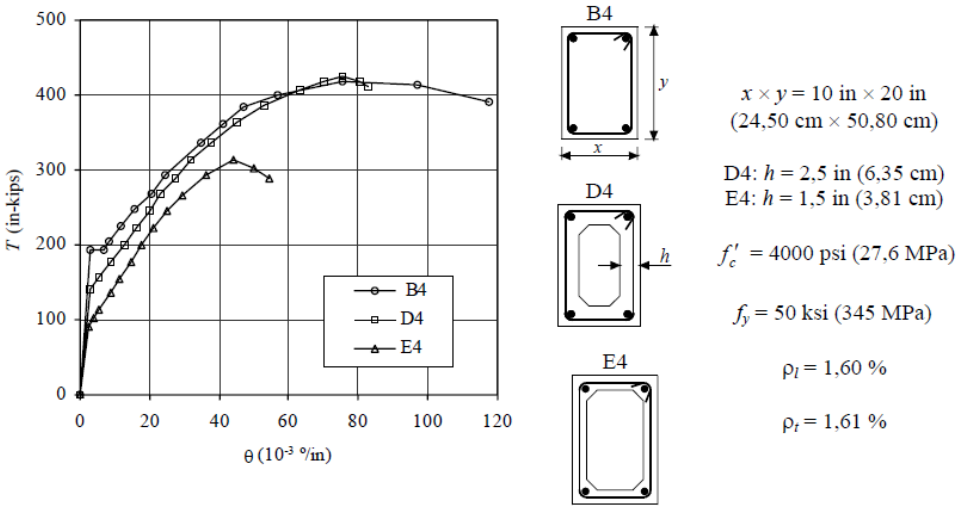

Figura 35. Influência do núcleo e espessura da parede da secção transversal no comportamento de uma viga de betão armado à torção pura [55].

Da observação do gráfico da figura anterior, em particular os resultados para as vigas B4 e D4 (a viga E4 sofreu uma rotura prematura por instabilidade das paredes finas) verifica-se

que, em maior ou menor grau, as vigas possuem um comportamento dúctil. No entanto, existe uma perda notória de ductilidade quando a secção da viga carece de um núcleo de betão (viga com secção vazada), sendo muito menor a sua capacidade em suster a carga sob deformações inelásticas.

Em 2003, Bernardo [13] também apresentou um estudo experimental com o objetivo de averiguar a influência da resistência do betão à compressão, f_{cm}, e da taxa de armadura, $\rho_{tot,m}$, na ductilidade e na capacidade de rotação plástica em torção de vigas com secção vazada de betão armado. O autor ensaiou onze vigas à torção pura até à rotura. As vigas possuíam dimensões idênticas, mas a resistência do betão à compressão e a taxa total de armadura de torção (com as armaduras longitudinal e transversal equilibradas) variaram. Dependendo da variável de estudo, as vigas foram agrupadas em séries com características semelhantes. Para este estudo, o autor definiu e quantificou um índice de ductilidade em torção. Os resultados obtidos pelo autor estão representados nas Figuras 36 e 37.

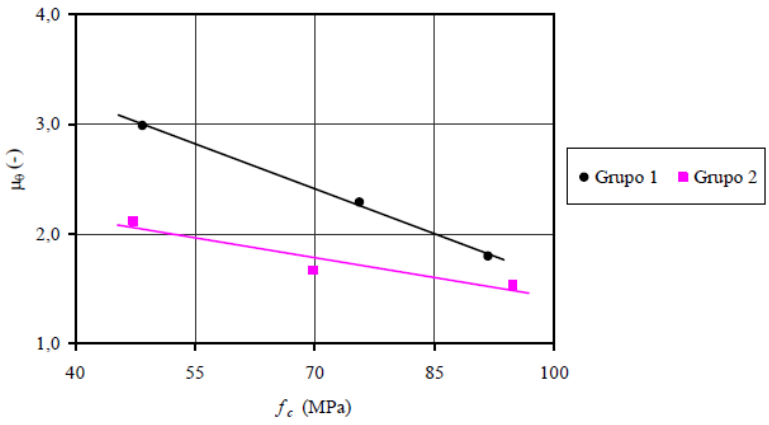

Figura 36. Influência do betão na ductilidade em torção [13].
(Grupo 1: $\rho_{tot,m}$ = 0,35 %, Grupo 2: $\rho_{tot,m}$ = 0,77 %)

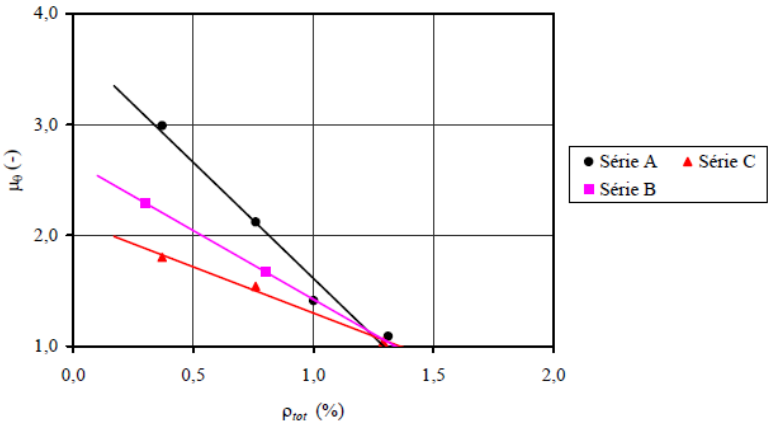

Figura 37. Influência da taxa de armadura na ductilidade em torção [13].
(Série A: f_{cm} = 49,2 MPa, Série B: f_{cm} = 72,4 MPa, Série C: f_{cm} = 992,7 MPa)

Este autor observou que a ductilidade em torção das vigas ensaiadas diminuía com o aumento da resistência do betão à compressão (para vigas com taxa de armadura constante) e com o aumento da taxa de armadura (para vigas com classes de resistência do betão semelhantes). Esta influência era mais expressiva para a variação da taxa de armadura para a qual foi observada, independentemente da classe do betão, um limite superior de cerca de 1,30% para garantir uma ductilidade mínima em torção.

A partir dos estudos anteriormente referidos, pode concluir-se que, à semelhança do procedimento usado para a flexão, para garantir uma ductilidade mínima em torção num elemento estrutural, este deve passar por um controlo de parâmetros, de entre os quais: (*i*) a escolha dos materiais (classe do betão à compressão e classe do aço) com características de ductilidade adequadas; (*ii*) a definição do tipo de secção (cheia ou vazada) e a limitação da espessura da secção transversal (para o caso das secções vazadas) do elemento solicitado; (*iii*) a adoção de uma taxa de armadura adequada, em particular com espaçamentos pequenos para garantir o confinamento do betão comprimido; e (*iv*) a limitação das tensões nas escoras de betão comprimido.

A fim de garantir uma ductilidade suficiente nos elementos estruturais, os engenheiros, geralmente, seguem regras de dimensionamento definidas em documentos normativos. No entanto, no que toca à problemática da torção, tais documentos revelam-se escassos na definição de regras de dimensionamento e de pormenorização específicas para garantir a ductilidade em torção para o ELU. Por exemplo, em alguns códigos de dimensionamento de estruturas de betão, a quantidade mínima de armadura de torção, considerada como um requisito básico, não se encontra definida. Já a armadura máxima de torção, em vários códigos, pode ser deduzida através da imposição de uma tensão máxima de compressão nas escoras de betão. À falta de disposições específicas para a torção, muitos códigos de dimensionamento remetem ainda para disposições específicas relacionadas com a armadura de flexão (para a armadura longitudinal) e de esforço transverso (para a armadura transversal). Tal constatação nos documentos normativos demonstra que existe ainda um longo trabalho de investigação por realizar no campo da torção.

Tendo por base o exposto anteriormente, no Capítulo 3 do presente trabalho é apresentado um estudo focado na ductilidade em torção de vigas de betão armado, onde é estudada a influência de várias propriedades geométricas e mecânicas das vigas, tendo por base numerosos resultados experimentais recolhidos na literatura. Em complemento do estudo anteriormente referido, no Capítulo 3 é ainda apresentado um estudo adicional com vista à verificação da adequação de vários documentos normativos de dimensionamento de

estruturas de betão com vista a prever o momento torsor resistente de um número elevado de vigas de betão armado sujeitas à torção.

1.5. Objetivo e justificação do trabalho.

A torção em vigas de betão estrutural continua a constituir um tema atual de investigação na área da mecânica estrutural. Desde o final do século passado têm vindo a ser publicados os resultados de diversos estudos que incorporam novos desenvolvimentos sobre a modelação do desempenho de vigas de betão estrutural submetidas à torção. Tais desenvolvimentos incluem, entre outros: o refinamento de modelos para prever o comportamento global de vigas de betão estrutural sujeitas à torção pura e à torção combinada com outros esforços internos; modelos de dimensionamento à torção de vigas executadas com betões não convencionais ou incorporando técnicas de reforço para melhorar o seu desempenho à torção; modelos que incluem o pré-esforço; modelos para contabilizar a influência do empenamento em secções abertas. Além disso, para a situação de interação de esforços internos, os procedimentos de verificação da segurança aos ELU das secções críticas das estruturas, geralmente prescritos pelos documentos normativos de dimensionamento de estruturas de betão, requerem o conhecimento prévio e individualizado do comportamento dessas secções críticas à torção.

O presente trabalho surge da necessidade de contribuir para o desenvolvimento de alguns estudos em curso na área da torção de vigas de betão estrutural. Assim, procedeu-se a estudos inseridos em três campos específicos, a saber:

1. Modelação do comportamento de vigas de betão estrutural sujeitas à torção pura ou combinada com outros esforços, em particular a acção do pré-esforço e da flexão (Capítulo 2).

Pese embora os recentes desenvolvimentos nesta área (*vide* Secção 1.3), continua a existir discrepância entre as previsões dos modelos teóricos propostos pela comunidade científica e os resultados observados em laboratório. Como tal, foram elaborados e publicados 3 artigos científicos, com os seguintes objetivos:

- Refinamento e validação do modelo MVATM [18] para o cálculo do comportamento global de vigas de betão armado com pré-esforço longitudinal (1 artigo em revista internacional). Na atualidade, a técnica do pré-esforço é amplamente utilizada em diversos tipos de sistemas e elementos estruturais, inclusive em vigas sujeitas a elevados momentos torsores. Quando aplicado de forma racional, o pré-esforço pode aumentar a resistência à fissuração e a rigidez de torção das vigas de betão. O pré-esforço também aumenta a resistência à

torção e permite que uma maior área da secção transversal do betão seja eficaz. Por essas razões afigura-se como necessário o desenvolvimento de um modelo confiável que preveja o comportamento global de vigas estruturais de betão sob torção, inclusive para baixos níveis de carregamento. A escolha do MVATM [18] para este estudo prendeu-se com o facto de este modelo ser um dos modelos teóricos em uso, desenvolvido na Universidade da Beira Interior, que melhores resultados tem demonstrado na previsão do comportamento das vigas em torção e para o qual a implementação do efeito do pré-esforço é relativamente simples [18].

- Estudo da lei constitutiva média do betão à tração para prever o momento torsor de fissuração de vigas de betão armado sujeitas à torção (1 artigo em revista internacional). No projeto de estruturas, os documentos normativos de dimensionamento obrigam à verificação da segurança das estruturas ao ELS. Para tal, é necessário conhecer com rigor o momento torsor de fissuração. Tal como para o MVATM, o GSVATM [20] (também desenvolvido na Universidade da Beira Interior) é um modelo capaz de prever o comportamento global de uma viga de betão estrutural sujeita à torção, desde o início do carregamento até à rotura. Contudo, na previsão da zona de transição entre o estado não fissurado e o estado fissurado da viga, este modelo afasta-se do comportamento real das vigas. Esta zona de transição é muito dependente da lei constitutiva média adotada para o betão à tração. Uma vez que, teoricamente, o GSVATM constitui um modelo mais consistente do que o MVATM, por incorporar diretamente na formulação a influência média do betão à tração na direção perpendicular às escoras de betão, entendeu-se ser importante contribuir para a resolução do problema anteriormente referido. Atendendo às várias leis constitutivas médias para o betão à tração encontradas na literatura consultada, existe a necessidade de verificar qual destas leis permitirá ao modelo aproximar, o melhor possível, do comportamento real das vigas em torção para baixos níveis de carregamento.

- Refinamento do procedimento de cálculo para o Modelo de Treliça com Amolecimento para Ações Combinadas e para elementos de betão armado sujeitos à torção combinada com flexão (1 artigo em revista internacional). Em muitos elementos estruturais de betão, a torção pode ser uma das acções principais a ser considerada em projeto. Contudo, na maioria dos casos, este esforço encontra-se combinado com outros esforços internos. Silva *et al.* [93] apresentou uma solução de cálculo alternativa baseada no procedimento de cálculo do CA-STM [48], reformulando-o como um sistema de equações não lineares com restrições e utilizando um algoritmo de otimização. Apesar de este modelo ter sido validado tendo por base poucos resultados experimentais relacionados com vigas de betão armado sujeitas à torção e à torção combinada com esforço transverso, os resultados revelaram-se satisfatórios [93]. No entanto, foram relatados alguns problemas numéricos relacionados

com a espessura máxima das paredes da secção transversal vazada efetiva. No presente trabalho são propostas algumas alterações ao procedimento do CA-STM, reformulando-o de acordo com algumas propostas de Silva *et al.* [93] e sendo os resultados teóricos comparados com numerosos resultados experimentais encontrados na literatura, para vigas sujeitas à torção combinada com flexão. Esta interação de esforços foi escolhida por se ter verificado que é uma das menos estudadas na literatura. Considerou-se, por isso, este ser o primeiro caso de combinação de esforços a estudar para validar o modelo refinado proposto, antes de se passar para outras condições de carregamento, em trabalho futuro.

2. Estudo do comportamento último das secções críticas de vigas de betão armado sujeitas à torção pura (Capítulo 3).

Para o dimensionamento à torção, os atuais documentos normativos revelam ainda algumas lacunas relacionadas com disposições específicas, em particular para garantir a ductilidade e o bom comportamento em serviço (*vide* Secção 1.4). Tal resulta na necessidade de existirem mais estudos especialmente focados nestes aspetos. Com vista a contribuir para este objetivo, foram elaborados e publicados 2 artigos científicos, com os seguintes objetivos:

- Estudo da ductilidade de vigas de betão armado sujeitas à torção (1 artigo em revista internacional). A redistribuição lenta e gradual dos esforços internos numa estrutura é fortemente dependente de uma adequada ductilidade nas suas regiões críticas, a qual permite evitar a formação de mecanismos súbitos. Ensaios anteriores mostram que, se corretamente dimensionadas e armadas, as vigas de betão armado evidenciam um comportamento dúctil na rotura, com formação de rótulas de torção [13]. Contudo, existe uma enorme escassez de estudos focados na ductilidade em torção de vigas de betão armado, não tendo sido encontrados na literatura quaisquer estudos especificamente vocacionados para o tema. Como tal, o estudo realizado tem como objetivo verificar a influência de diversas variáveis de estudo na ductilidade em torção de vigas de betão armado, designadamente: a resistência do betão à compressão; a taxa total de armadura de torção; o desequilíbrio de armaduras de torção (longitudinal *versus* transversal); o fator de escala (ratio entre a altura e largura da secção retangular); e o tipo de secção (secção cheia e vazada). O objetivo é contribuir para a inclusão futura nos documentos normativos de dimensionamento de estruturas cláusulas específicas à torção para garantir a ductilidade, à semelhança do que já acontece no caso da flexão.

- Verificação da fidelidade dos documentos normativos de dimensionamento de estruturas na previsão do momento torsor resistente de vigas de betão armado (1 artigo em congresso

internacional). Os códigos nacionais e normativos podem ter um caráter de lei em alguns países ou um caráter de recomendação em outros países. Apesar dos procedimentos para o dimensionamento à torção, incorporados em grande parte dos documentos normativos atuais, terem por base o mesmo modelo teórico (Analogia de Treliça Espacial), os cálculos a realizar diferem de documento para documento, designadamente em virtude das simplificações adotadas para facilitar os cálculos. Assim, com o presente estudo pretende-se fazer um ponto de situação atual sobre a fiabilidade de vários documentos normativos, reconhecidos e abrangentes do ponto de vista territorial, para a previsão da resistência à torção de vigas de betão armado. Para tal, as previsões normativas são comparadas com os valores obtidos experimentalmente em numerosos ensaios encontrados na literatura. Ao avaliar as eventuais discrepâncias observadas entre as previsões normativas e os resultados experimentais, pretende-se que este estudo possa servir de guia, quer para novos estudos, quer para o trabalho de comissões técnicas nas revisões futuras dos documentos normativos.

3. Contribuição para o aumento da base de dados de resultados experimentais de vigas de secção vazada com betões de alta resistência com pré-esforço longitudinal sujeitas à torção pura (Capítulo 4, 1 artigo em revista internacional).

1.6. Organização do documento.

Nesta secção apresenta-se, de forma sumária, a organização do presente documento.

No Capítulo 1 apresentou-se o enquadramento, uma revisão bibliográfica e os objetivos do trabalho elaborado ao longo do 3.º Ciclo de estudos conducente ao grau de Doutor em Engenharia Civil na Universidade da Beira Interior, com a apresentação de notas históricas, conceitos base ao tema da torção, revisão bibliográfica considerada de interesse e introdução das matérias específicas aos temas investigados.

No Capítulo 2 são apresentados 3 artigos científicos publicados em revistas internacionais, no âmbito da modelação do comportamento de vigas de betão estrutural sujeitas à torção pura e combinada. Um primeiro artigo propõe o refinamento do modelo MVATM para a previsão do comportamento de vigas pré-esforçadas longitudinalmente sujeitas à torção pura. Num segundo artigo, avaliam-se leis constitutivas médias para o betão à tração a serem implementadas na formulação do modelo GSVATM, para a previsão da zona de transição do estado não fissurado para o estado fissurado de vigas de betão armado sujeita à torção pura. O último artigo propõe um refinamento ao modelo CA-STM para a previsão do comportamento global de vigas de betão armado sujeitas à torção combinada com flexão.

No Capítulo 3 são apresentados 2 artigos científicos, um publicado em revista internacional e outro publicado em congresso internacional. Estes artigos estão direcionados para o ELU de vigas de betão armado sujeitas à torção pura. O primeiro artigo foca o estudo da ductilidade em torção. O segundo artigo faz um ponto de situação sobre a fiabilidade de vários documentos normativos de dimensionamento de estruturas atuais na previsão do momento torsor resistente de vigas de betão armado.

No Capítulo 4 é apresentado 1 artigo científico, publicado em revista internacional, onde se apresentam os resultados decorrentes de um estudo experimental previamente realizado e envolvendo vigas com secção vazada ensaiadas à torção, construídas com betão de alta resistência e incorporando pré-esforço longitudinal.

No Capítulo 5 resumem-se as principais conclusões apresentadas em cada artigo científico. São também apresentadas indicações e recomendações para futuros trabalhos de investigação no tema da torção em vigas de betão estrutural.

Bibliografia

[1] ACI Committee 318. (1971). *Building code requirements for reinforced concrete, (ACI 318-71)*. American Concrete Institute. Detroit.

[2] ACI Committee 318. (1995). *Building code requirements for reinforced concrete, (ACI 318-95)*. American Concrete Institute, Detroit.

[3] ACI Committee 363. (1984). The-state-of-the-art report on high-strength concrete. *Journal of the American Concrete Institute*. **81**: 364-411.

[4] Andersen, P. (1935). Experiments with concrete in torsion. *Transactions, ASCE*. **100**: 949-983 (citado em [13]).

[5] Andersen, P. (1937). Rectangular concrete sections under torsion. *Journal of the American Concrete Institute*. **34**(1): 1-11.

[6] Andrade, J. M. A. (2011). *Modelação do comportamento global de vigas sujeitas à torção. Generalização da analogia da treliça espacial com ângulo variável.* Tese de Doutoramento em Engenharia Civil. Universidade da Beira Interior, Covilhã, Portugal. 512 pp.

[7] Armstrong, S. (1956). The strength of concrete members in combined bending and torsion. *Proceedings of a symposium of the strength of concrete structures, Session B: Paper 2*. London, May 1956, Cement and Concrete Association. pp. 101-122.

[8] Bach, B. and Graf, O. (1912). *Versuche uber die widerstands fahigkeit von beton und eisenbeton gegen verdrehung (Investigation of torsional strength of concrete and reinforced concrete)*. Deutscher Ausschuss fur Eisenbeton, Helf 16. Wilhelm Ernst. Berlin (em Alemão, citado em [56]).

[9] Bairan Garcia, J. M. and Mari Bernat, A. R. (2006a). Coupled model for the non-linear analysis of anisotropic sections subjected to general 3D loading. Part 1: Theoretical formulation. *Computers & Structures*. **84**: 2254-2263.

[10] Bairan Garcia, J. M. and Mari Bernat, A. R. (2006b). Coupled model for the non-linear analysis of anisotropic sections subjected to general 3D loading. Part 2: Implementation and validation. *Computers & Structures*. **84**: 2264-2276.

[11] Belarbi, A. and Hsu, T. T. C. (1994). Constitutive laws of concrete in tension and reiforcing bars stiffened by concrete. *Structural Journal of American Concrete Institute*. **91**(4): 465-474 (citado em [6]).

[12] Belarbi, A. and Hsu, T. T. C. (1995). Constitutive laws of softened concrete in biaxial tension-compression. *Structural Journal of American Concrete Institute*. **92**(5): 562-573.

[13] Bernardo, L. F. A. (2003). *Torção em vigas em caixão de betão de alta resistência*. Tese de Doutoramento em Engenharia Civil. Universidade de Coimbra, Coimbra, Portugal. 692 pp.

[14] Bernardo, L. F. A. (2019a). Generalized softened variable angle truss model for RC hollow beams under torsion. *Materials*. **12**(13): 2209.

[15] Bernardo, L. F. A. (2019b). Modeling the full behavior of reinforced concrete flanged beams under torsion. *Applied Sciences*. **9**(13): 2730.

[16] Bernardo, L. F. A. and Andrade, J. M. A. (2017). Prestressed concrete beams under torsion – Extension of the VATM and evaluation of constitutive relationships. *Structural Engineering and Mechanics*. **61**(5): 577-592.

[17] Bernardo, L. F. A. and Andrade, J. M. (2020). A unified softened truss model for RC and PC beams under torsion. *Journal of Building Engineering*. **32**: 101467.

[18] Bernardo, L. F. A., Andrade, J. M. A. and Lopes, S. M. R. (2012a). Modefied variable angle truss-model for torsion in reinforced concrete beams. *Materials and Structures*. **45**(12): 1877-1902.

[19] Bernardo, L. F. A., Andrade, J. M. A. and Lopes, S. M. R. (2012b). Softened truss model for reinforced NSC and HSC beams under torsion: a comparative study. *Engineering Structures*. **42**: 278-296.

[20] Bernardo, L. F. A, Andrade, J. M. A. and Nunes, N. C. G. (2015). Generalized softened variable angle truss-model for reinforcement concrete beams under torsion. *Materials and Structures*. **48**: 2169-2193.

[21] Bernardo, L. F. A, Andrade, J. M. A. and Oliveira, L. A. P. (2013). Reinforced and prestressed concrete hollow beams under torsion. *Journal of Civil Engineering and Management*. **19**(S1): S141-S152.

[22] Bernardo, L. F. A, Cerquido, B. M. D., Silva, J. R. B. and Horowitz, B. (2018). Efficient refined rotating-angle softened truss model procedure to analyze reinforced concrete membrane elements. *Structural Concrete*. **19**(6): 1971-82.

[23] Bernardo, L. F. A., Filho, B. M. V. C. and Horowitz B. (2020). Predicting the behavior of prestressed concrete membrane elements by refined rotating-angle softened-truss model with efficient solution procedure. *Structural Concrete*. **21**(3): 934–948.

[24] Bernardo, L. F. A, Lyrio, A. R. B., Silva, J. R. B. and Horowitz, B. (2018). Refined softened truss model with efficient solution procedure for prestressed concrete membranes. *Journal of Structural Engineering*. **144**(6): 04018045.

[25] Bernardo, L. F. A. and Lopes, S. M. R. (2008). Behavior of concrete beams under torsion – NSC plain and hollow beams. *Materials and Structures*. **41**(6): 1143-1167.

[26] Bernardo, L. F. A. and Lopes, S. M. R. (2009). Torsion in HSC hollow beams: strength and ductility analysis. *ACI Structural Journal*. **106**(1): 39-48.

[27] Bernardo, L. F. A. and Lopes, S. M. R. (2011). Theoretical behavior of HSC sections under torsion. *Engineering Structures*. **33**(12): 3702-3714.

[28] Bernardo, L. F. A., Taborda, C. S. B. and Andrade, J. M. A. (2015). Ultimate torsional behavior of axially restrained RC beams. *Computers and Concrete*. **16**(1): 67-97.

[29] Bernardo, L. F. A., Taborda, C. S. B. and Andrade, J. M. A. (2018). Generalized softened variable angle truss-model for PC beams under torsion. *International Journal of Concrete Structures and Materials*. **12**(62).

[30] Bernardo, L. F. A., Taborda, C. S. B. and Gama, J. M. R. (2015). Parametric analysis and torsion design charts for axially restrained RC beams. *Structural Engineering and Mechanics*. **55**(1): 1-27.

[31] Bhatti, M. A. and Almughrabi, A. (1996). Refined model to estimate torsional strength of reinforced concrete beams. *Journal of the American Concrete Institute*. **93**(5): 614-622.

[32] Bredt, R. (1896). Kristische bermerkungen zur drehungselatizitat. *Zeitschrift des Vereines Deutscher Ingenieure*. **40**(28): 785-790; **40**(29): 813-817 (in German, citado em [20]).

[33] Cauchy, A. (1828). *Sur les équations qui expérimentent les conditions d'equilibre ou les lois de mouvement intérieur d'un corps solide*. Exercices de mathématique. Paris (citado em [56]).

[34] CEB-FIP. (1983). *Model code for concrete structures*. 3rd edition. CEB-FIP International Recommedations. Paris.

[35] CEB-FIB. (1995). *Ultimate limit state design models. A state-of-art report*. Bulletin d'Information N.º 223.

[36] CEB-FIP. (2013). *Model code for concrete structures 2010*. Comité Euro-International du Béton – Fédération Internationale du Betón. Suisse.

[37] Collins, M. P. (1973). *Torque-twist characteristics of reinforced concrete beams*. Inelasticity and Non-Linearity in Structural Concrete, Study No. 8. University of Waterloo Press, Waterloo. Ontario, Canada. pp. 211-232.

[38] Collins, M.P. and Mitchell, D. (1980). Shear and torsion design of prestressed and non-prestressed concrete beams. *Journal of the Prestressed Concrete Institute*. **25**(5): 32-100.

[39] Cowan, H. J. (1950). Elastic theory for torsional strength of rectangular reinforced concrete beams. *Magazine of Concrete Researc.* **2**(4): 3-8.

[40] Cowan, H. J. (1951). Tests of torsional strength and deformation of rectangular reinforced concrete beams. *Concrete and Constructional Engineering*. **46**(2): 51-59.

[41] Cowan, H. J. (1952). Strength of reinforced concrete under the action of combined stresses at the representation of the criterion of failure by a space model. *Nature*. **169**: 663 pp. (citado em [56]).

[42] Cowan, H. J. and Armstrong, S. (1955). Experiments on the strength of reinforced and prestressed concrete beams and of concrete-encased steel joists in combined bending and torsion. *Magazine of Concrete Reserch*. **7**(19): 3-20.

[43] Cuerel, J. (1948). New Waterloo Bridge at London. *International Association for Bridge and Structural Engineering, 3rd Congress*. Liège, 1948. pp. 367-380.

[44] Elfgren, L. (1972). *Reinforced concrete beams loaded in combined torsion, bending and shear*. Publication 71:3, Division of Concrete Structures, Chalmers University to Technology. Goteborg, Sweden. 249 pp.

[45] Elfgren L., Karlsson I. and Losberg A. (1974). Torsion-bending-shear interaction for concrete beams. *Journal Structures Division*. **100**(8): 1657–76.

[46] Ganganagoudar, A., Mondal, T. G. and Prakash, S. S. Improved softened membrane model for reinforced concrete circular bridge columns under torsion. *Journal of Bridge Engineering*. **21**(7): 1–12.

[47] Greene, G. G. Jr. (2006). *Behavior of reinforced concrete girders under cyclic torsion and torsion combined with shear: experimental investigation and analytical models*. Ph.D. Theses. Department of Civil Engineering, University of Missouri-Rolla, USA.

[48] Greene, G. and Belarbi, A. (2009a). Model for RC members under torsion, bending and shear. I: Theory. *Journal of Engineering Mechanics*. **135**(9): 961-969.

[49] Greene, G. and Belarbi, A. (2009b). Model for RC members under torsion, bending and shear. II: Model application and validation. *Journal of Engineering Mechanics*. **135**(9): 970-977.

[50] Grob, J. (1975). *Traglast von stäbe mit dunnwandigen offenen querschnitten*. Eidgenössische Technische Hochschule (ETH), Institut fur Baustatik und Konstruktion. Zurich (em Alemão, citado em [35]).

[51] Hsu, T. T. C. (1968a). Torsion of structural concrete – A summary of pure torsion. *Torsion of Structural Concrete, SP-18*. American Concrete Institute, Detroit. Vol. 18. pp 165-178.

[52] Hsu, T. T. C. (1968b). Torsion of structural concrete – Behavior of reinforced concrete rectangular members. *Torsion of Structural Concrete, SP-18*. American Concrete Institute, Detroit. Vol. 18. pp. 261-306.

[53] Hsu, T. T. C. (1968c). Torsion of structural concrete – Plain concrete rectangular sections. *Torsion of Structural Concrete, SP-18*. American Concrete Institute, Detroit. Vol. 18. pp. 203-238.

[54] Hsu, T. T. C. (1968d). Torsion of structural concrete – Uniformly prestressed rectangular members without web reinforcement. *Journal of the Prestressed Concrete Institute*. **13**(2): 34-44.

[55] Hsu, T. T. C. (1973). Post-cracking torsional rigidity of reinforced concrete sections. *Journal of the American Cocrete Institute*. **70**(5): 352-360.

[56] Hsu, T. T. C. (1984). *Torsion of reinforced concrete*. Van Nostrand Reinhold Company.

[57] Hsu, T. T. C. (1988). Softened truss model theory for shear and torsion. *Structural Journal of the American Concrete Institute*. **85**(6): 624-635.

[58] Hsu, T. T. C. (1993). *Unified theory of reinforced concrete*. CRP Press Inc., Boca Raton. Florida.

[59] Hsu, T. T. C. and Mo, Y. L. (1985a). Softening of concrete in torsional members – Design recommendations. *Journal of the American Concrete Institute*. **82**(4): 443-452 (citado em [6]).

[60] Hsu, T. T. C. and Mo, Y. L. (1985b). Softening of concrete in torsional members – Prestressed concrete. *Journal of the American Concrete Institute*. **82**(5): 603-615.

[61] Hsu, T. T. C. and Mo, Y. L. (1985c). Softening of concrete in torsional members - Theory and tests. *Journal of the American Concrete Institute*. **82**(3): 290-303 (citado em [13]).

[62] Hsu, T. T. C. and Mo, Y. L. (2010). *Unified theory of concrete structures*. Wiley.

[63] Hsu, T. T. C and Zhang, L. X. (1997). Nonlinear analysis of membrane elements by fixed-angle softened-truss model. *Structural Journal of the American Concrete Institute*. **94**(5): 483-492.

[64] Hsu, T. T. C. and Zhu, R. R. H. (2002). Softened membrane model for reinforced concrete elements in shear. *Structural Journal of the American Concrete Institute*. **99**(4): 460-469.

[65] Humphreys, R. (1957). Torsional properties of prestressed concrete. *The Structural Engineer*. **35**(6): 213-224.

[66] INCM. (1983). *Regulamento de estruturas de betão armado e pré-esforço*. Imprensa Nacional, Casa da Moeda. Lisboa.

[67] Jeng, C. H. (2015). Unified softened membrane model for torsion in hollow and solid reinforced concrete members: Modeling precracking and postcracking behavior. *Journal of Structural Engineering*. **141**(10).

[68] Jeng, C. H., Chiu, H. J. and Chen, C. S. (2010). Modelling the initial stresses in prestressed concrete members under torsion. *Structures Congress*; ASCE: Orlando, USA. pp. 1773-1781.

[69] Jeng, C. H. and Hsu, T. T. C. (2009). A softened membrane model for torsion in reinforced concrete members. *Engineering Structures*, **31**: 1944-1954.

[70] Kothamuthyala, S. R., Thammishetti, N., Prakash, S. S. and Vyasarayani, C.P. (2019). Optimization-based improved softened membrane model for rectangular reinforced concrete members under combined shear and torsion. *Journal of Structural Engineering*. **145**(2).

[71] Laffranchi, M. (1999). Zur Konzeption Gekrümmter Brücken. *IKB Report*. Institut für Baustatik und Konstruktion, Zürich, Switzerland (in Germany).

[72] Lampert, P. and Thurlimann, B. (1969). *Torsionsversuche an stahlbetonbalken (Torsion tests of reinforced concrete beams)*. Bericht, Nr. 6506-2, Institut fur Baustatik, ETH. Zurich (em Alemão, citado em [6]).

[73] Lopes, S. M. R. and Bernardo, L. F. A. (2009). Twist behavior of high-strength concrete hollow beams – Formation of plastic hinges along the length. *Engineering Structures*. **31**(1): 138-149.

[74] McMullen A. E. and Warwaruk J. (1970). Concrete beams in bending, torsion and shear. *Journal of the Structural Divisio*n. **96**(5): 885–903.

[75] Measor, E. O. and New, D. H. (1951). The design and construction of the Royal Festival Hall, South Bank. *Journal of the Institution of Civil Engineers*, **36**(7): pp. 241-318.

[76] Mondal T. G. and Prakash S. S. (2016). Nonlinear finite element analysis of RC bridge columns under torsion with and without axial compression. *Journal of Bridge Engineering*. **21**(2): 13.

[77] Morsh, E. (1906). *Der eisenbetonbau, seine theorie und anwendung*. 2nd ed., Verlag von Konrad Wittmer. Stuttgart. (traduzido para inglês por Goodrich, E. P. (1909). McGraw-Hill Book Co. New York).

[78] Mostofinejad, D. and Behzad, T. S. (2011). Nonlinear modeling of RC beams subjected to torsion using smeared crack model. *Procedia Engineering*. **14**: 1447-1454.

[79] Navier, C. L. (1826). *Résumé des leçons données à l'école des ponts et chaussées sur l'application de la mécanique à l'établissement des machines. Première partie, contentant les leçons sur la résistance des matériaux et sur l'établissement des construction*. Article V – de la résistance d'un corps prismatique à la torsion, pp. 71-76. Article VI – de la résistance d'un corps prismatique à la ruprure causée par la torsion, pp. 76-80. Paris.

[80] Nylander, H. (1945). *Vridning vridningsinspanning vid betongkongstruktioner (Torsion and torsional restraint of concrete structures)*. Stantens Kommitté för Byggnadsforskning, Bulletin No. 3. Stockholm.

[81] Pang, X. B. and Hsu, T. T. C. (1995). Behavior of reinforced concrete membrane elementes in shear. *Structural Journal of American Concrete Institute*. **92**(6): 665-679.

[82] Pang, X. B. and Hsu, T. T. C. (1996). Fixed angle softened-truss model for reinforced concrete. *ACI Structural Journal*. **93**(2): 197-207 (citado em [69]).

[83] Prakash S. S., Belarbi A. and You Y.-M. (2010). "Seismic performance of circular RC columns subjected to axial force, bending, and torsion with low and moderate shear. *Engineering Structures*. **32**(1): 46–59.

[84] Prakash S. S., Li Q. and Belarbi A. (2013). Behavior of circular and square reinforced concrete bridge columns under combined loading including torsion. *ACI Structural Journal*. **109**(3): 317–28.

[85] Priestley, M. J. N., Seible, F. and Wang, C. M. (1994). The northridge earthquake of January 17, 1994 – Damage analysis of selected freeway bridges. *Report No. SSRP – 94/06*, University of California, San Diego.

[86] Rahal, K. N. and Collins, M. P. (1996). Simple model for predicting torsional strength of reinforced and Prestressed concrete sections. *Journal of the American Concrete Institute*. **93**(6): 658-666.

[87] Rahal, K. N. and Collins, M. P. (2003). Combined torsion and bending in reinforced and Prestressed concrete beams. *ACI Structural Journal*. **100**(2): 157-165.

[88] Rausch, E. (1929). *Berechnung des eisenbetons gegen verdrehung (Design of reinforced concrete in torsion)*. Ph.D Thesis. Berlin. 53 pp. (em Alemão, citado em [56]).

[89] Ritter, W. (1899). *Die bauweise hennebique*. Schweizerishe Bauzeitung. Zurich.

[90] Robinson, J. R. and Demorieux, J. M. (1968). Essais de traction-tompression sur modèles d'ame de poutre en beton arme. *IRABA Report*, *Institut de Recherches Appliquees du Betons de L'Ame*, Part 1, 44 pp. (citado em [62]).

[91] Saint-Venant, B. de. (1856). *Mémoire sur la torsion des prismes, (lu à l'Académie le 13 juin 1853) – Mémoires des savants étranger – Mémoires das divers savants à l'Académie des Sciences, de l'Institut Impérial de France et imprime par son ordre*. Vols. 14. Imprimerie Impériale. Paris. (citado em [56]).

[92] Silva, J. R. B. (2016). Procedimento eficiente de análise de secções em concreto armado usando o modelo de treliça com amolecimento. Dissertação de Mestrado em Engenharia Civil. Universidade Federal de Pernambuco, Recife, Brasil.

[93] Silva, J. R. B., Horowitz, B. and Bernardo, L. F. A. (2017). Efficient analysis of beam sections using softened truss model. *ACI Structural Journal*. **114**(3): 765–74.

[94] Standards Council of Canada. (2004). *Design of concrete structure for buildings, CAN3-A23.3-04*. Canadian Standards Association. Rexdale. Toronto, Canada.

[95] Taborda, C. S. B. (2012). *Efeito do confinamento axial no comportamento de vigas de betão estrutural sujeitas à torção*. Dissertação de Mestrado em Engenharia Civil. Universidade da Beira Interior, Covilhã, Portugal. 198 pp.

[96] Wagner, H. (1929). Ebene blechwandttrager mit sehr dunnem stegblech (Flat Sheet Metal Girders with Very Thin Metal Web*). Zeitshrift fur Flugtechnik und Motoluftschiffahr*. **20**(8 to 12). (em Alemão, citado em [56]).

[97] Waldren, P. (1988). The significance of warping torsion in the design of straight concrete box girder bridges. *Canadian Journal of Civil Engineering*, **15**: 879-889.

[98] Wang, W. and Hsu, T. T. C. (1997). Limit analysis of reinforced concrete beams subjected to pure torsion. *Journal of Structure Engineering*. **123**(1): 86-94.

[99] Wlassow, W. S. (1964). *Dünnwandige elastische stäbe*. Verly fur Bauwesen. Berlin (em Alemão, citado em [35]).

[100] Young, C. R., Sagar, W. L. and Hughes, C. A. (1922). Torsional strength of rectangular sections of concrete, plain and reinforced. Bulletin No. 9. University of Tornoto, School of Engineering. Toronto (citado em [56]).

[101] Zhang, L. X. and Hsu, T. T. C. (1998). Behavior and analysis of 100 MPa concrete membrane elements. *Journal of Structural Engineering*. **124**(1): 24-34, 1998.

[102] Zhu, R. R. H. and Hsu, T. T. C. (2002). Poisson effect in reinforced concrete membrane elements. *Structural Journal of American Concrete Institute*. **99**(5): 631-640 (citado em [69]).

[103] Zia, P. (1961). Torsional strength of prestressed concrete members. *Journal of the American Concrete Institute*. **57**(9): 1337-1359.

[104] Zia, P. and McGee, W. D. (1974). Torsion design of prestressed concrete. *Journal of the Prestressed Concrete Institute*. **19**(2): 46-65.

[A]<http://i.dailymail.co.uk/i/pix/2013/07/15/article-2364712-0000931100000CB2-300_634x341.jpg>, acedido em dezembro de 2016.

[B] < https://images.app.goo.gl/kWzea7p7ybwR6cFj6>, acedido em junho de 2021.

[C] <https://images.app.goo.gl/W4KnmwoLpSjJh72r9>, acedido em abril de 2021.

[D]<http://www.gettyimages.pt/evento/june-20th-waterloo-bridge-taken-down-70-yrs-ago-50823300?#underneath-the-newly-constructed-waterloo-bridge-london-picture-id3349298>, acedido em dezembro de 2016.

Capítulo 2

Modelação do comportamento de vigas de betão estrutural sujeitas à torção pura e combinada

Neste capítulo são apresentados três artigos científicos, publicados em revistas internacionais, no âmbito da modelação do comportamento de vigas de betão estrutural sujeitas à torção pura e combinada. Apresenta-se lista de artigos que integram o presente capítulo:

Bernardo, L. F. A., and Teixeira, M. M. (2018). Modified softened truss-model for prestressed concrete beams under torsion. *Journal of Building Engineering*. **19**: 49-61. https://doi.org/10.1016/j.jobe.2018.04.024

Teixeira, M. M. and Bernardo, L. F. A. (2021). Evaluation of Smeared Constitutive Laws for Tensile Concrete to Predict the Cracking of RC Beams under Torsion with Smeared Truss Model. *Materials*. **14**(5): 1260. https://doi.org/10.3390/ma14051260

Bernardo, L. F. A. and Teixeira, M. M. (2020). Refined softened-truss model with efficient solution procedure for reinforced concrete members under torsion combined with bending. *Structures*. **26**: 651-669. https://doi.org/10.1016/j.istruc.2020.04.055

Journal of Building Engineering 19 (2018) 49–61

Contents lists available at ScienceDirect

Journal of Building Engineering

journal homepage: www.elsevier.com/locate/jobe

Modified softened truss-model for prestressed concrete beams under torsion

L.F.A. Bernardo[a,*], M.M. Teixeira[b]

[a] Assistant Professor with Aggregation, University of Beira Interior, C-MADE - Centre of Materials and Building Technologies, Covilhã, Portugal
[b] PhD Student, University of Beira Interior, C-MADE - Centre of Materials and Building Technologies, Covilhã, Portugal

ARTICLE INFO

Keywords:
Prestress Concrete
Beams
Torsion
Softened Truss-Model

ABSTRACT

This article presents a computation procedure developed to predict the global behaviour of prestressed concrete (PC) beams under pure torsion. This computation procedure constitutes an extension of a theoretical model previously proposed, the Modified Variable Angle Truss-Model (MVATM) for Reinforced Concrete (RC) beams under torsion. The modifications incorporated in the MVATM and the calculation procedure are presented. The obtained theoretical predictions are compared with experimental results available in the literature. It is shown that the proposed computation procedure provides good predictions for the global behaviour of PC beams under torsion, including for low loading stages.

1. Introduction

Since the beginning of last century, several theoretical models have been developed to model the behaviour of Reinforced Concrete (RC) beams under torsion. Among those models, the Space Truss Analogy (STA) has a highest historical value and constitutes the base model of the European Model Code since 1978 and also the ACI Code since 1995. From the second half of the last century, successive developments of the STA have been proposed by several authors. However, the Variable Angle Truss Model (VATM) proposed by Hsu and Mo in 1985 [1,2], was the one that firstly aimed to unify the torsion design of small and large sections as well as RC and Prestressed Concrete (PC) beams under torsion. One of the major innovation of VATM was the incorporation of a softened stress (σ) - strain (ε) relationship for the concrete in the struts instead of a conventional σ - ε relationship for uniaxial compression.

VATM is able to predict the general state of the beam throughout the entire loading history.

However, since VATM assumes an extensively cracked state from the beginning of loading and also neglects the influence of the concrete core for plain beams, good results are observed only for high loading stages [1,2]. Further studies also shown that appropriates σ - ε relationships for the materials constitute an key parameter for VATM to be able to provide good results for high loading stages, both for RC and PC beams under torsion [3,4].

In the last three decades, new versions of the VATM have been proposed for RC and PC beams under pure torsion [5–7], for RC beams under torsion combined with other internal forces [8–11] and for axially restrained RC beams under torsion [12,13]. Other advanced analytical models not directly based on the STA have also been proposed by other authors, for instance [14,15], including for concrete members under torsion combined with other internal forces [16,17]. Also alternative models which combine two different models to calculate the pre-cracking and the post-cracking behaviour of RC beams under torsion have been proposed [18,19]. This results to an abrupt transfer from the first to the second model which can be observed in the torque (T) – twist (θ) curves. This option is justified because it is experimentally observed that the torsional behaviour of a RC beam comprises two distinct regions: the pre-cracked stage and the post-cracked stage. The different character of the response in these regions reveals the different nature of the load resisting mechanism in each case. However, such option can be considered theoretically less satisfactory and a model mainly based on a single theory is preferable.

When compared with many of the previously referred alternative models, it can be stated that the mathematical treatment and the solution procedure of the VATM is simpler. Furthermore, VATM provides a simpler physical understanding of the torsional behaviour of structural concrete beams after cracking.

Also, many of the previously referred models are only able to compute accurately the ultimate torsional behaviour of RC beams. Nowadays, it is recognized that good predictions for low loading stages are also important to be obtained in order to check the serviceability limit states, such as the deformation (twist) of the beam and the stress/strain levels in the materials. Nowadays, prestress technique is widely used in many structures, including in members with high torsional loading. It is well known that prestress, if rationally applied, increases the resistance to cracking and the stiffness of concrete beams, including

* Correspondence to: Universidade da Beira Interior, Departamento de Engenharia Civil e Arquitetura, Edifício II das Engenharias, Calçada Fonte do Lameiro, 6201-001 Covilhã, Portugal
E-mail address: lfb@ubi.pt (L.F.A. Bernardo).

https://doi.org/10.1016/j.jobe.2018.04.024
Received 18 August 2017; Received in revised form 23 April 2018; Accepted 23 April 2018
Available online 27 April 2018
2352-7102/

for torsion. This is because prestress induces a compressive stress state which, in combination with the shear stress induced by the torsional moment, results in a biaxial stress state which delays the concrete cracking. Prestress also increases the torsional strength and allow for a larger area of the concrete cross section to be effective.

For all these reasons, new and reliable theoretical models are still need to predict de global behaviour of structural concrete beams under torsion, including for PC beams and for low loading stages.

To solve these issues, Jeng and Hsu in 2009 [20], Jeng *et al.* in 2010 [21] and Jeng in 2014 [22] proposed the Softened Membrane Model for Torsion (SMMT) to model RC and PC beams under torsion. This model can predict the entire $T - \theta$ curve of the beams under torsion, including for low loading stages. Since SMMT constitutes an extension of the Softened Membrane Model (SMM) for RC membrane elements under shear [23], the mathematical treatment and the solution procedure is more complex when compared with VATM.

For this reason, Bernardo *et al.* in 2012 [24] and in 2015 [25] proposed new developments for the original VATM. These models were called the Modified Variable Angle Truss Model (MVATM) and the Generalized Softened Variable Angle Truss Model (GSVATM), respectively. As for the SMMT, MVATM and GSVATM are also able to predict the entire $T - \theta$ curves of RC beams under torsion, including for low loading stages. Recently, the GSVATM was also extended to PC beams under torsion [11,26] and similar conclusions were drawn.

For all these models, good agreement with experimental results were observed. However, both SMMT and GSVATM still don´t predict with accuracy the T - θ curves in the post-cracked ascending branch for low loading levels. Therefore, these models don´t allow to predict very well the torsional stiffness, the twist of the beam or the stress/strain in the materials in the post-cracked stage for low loading levels. This drawback is important in case one wants to check the behaviour of the beams under torsion for the serviceability limit states.

When compared with SMMT and GSVATM, the MVATM from Bernardo *et al.* in 2012 [24] shown to give very good results for the T - θ curve in the post-cracked ascending branch for low loading levels.

Based on the foregoing, in this study the MVATM [24] is extended to cover PC concrete beams under torsion with uniform longitudinal prestress. The modifications in the original VATM formulation [1,2], which lead to the extended MVATM for PC beams, are presented. The solution procedure is also developed and presented. The predictions obtained from the proposed theoretical model are compared with some experimental results of reference PC beams under torsion, which results are available in the literature.

2. Variable angle truss model for beams with longitudinal prestress

The computation of the theoretical T - θ curve from the VATM [1,2] (Fig. 1) requires 3 equilibrium equations to compute the torque, T, the effective thickness, t_d, of the wall (concrete strut) of the equivalent tubular section and the angle of the inclined concrete struts, α, from the horizontal axis of the beam (Eqs. (1)–(3) in Table 1). The VATM [1,2] also requires 3 compatibility equations to compute the strains of the transversal reinforcement, ε_t, the strains of the longitudinal reinforcement, ε_l, and the twist, θ (Eqs. (4)–(6) in Table 1).

The stress in the concrete diagonal struts, f_d, is defined as the average stress of a non-uniform compressive stress diagram (Fig. 1). To characterize the concrete in compression in the diagonal struts, a σ - ε relationship is adopted to account for the softening effect due to cracking caused by tensile stresses in the perpendicular direction to the compressive field (Eqs. (7) to (12) in Table 2). Parameter k_1, to calculate the stress in the concrete diagonal struts (Eqs. (13)–(16) in Table 2), is obtained by integrating numerically Eqs. (7) and (8).

Based on an extensive comparative analysis with experimental results, Bernardo *et al.* in 2012 [3] and Bernardo and Andrade in 2017 [4] found that, to provide good predictions for the ultimate stage, VATM

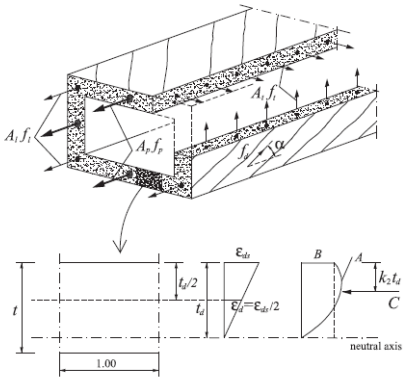

Fig. 1. – VATM: strains and stresses in the concrete struts.

Table 1
Equations of VATM for beams with longitudinal prestress.

Variable Angle Truss Model with softening effect

Equilibrium equations [1,2]:

$$T = 2A_o t_d \sigma_d \sin\alpha \cos\alpha \quad (1)$$

$$\cos^2\alpha = \frac{A_l f_l + A_p f_p}{p_o \sigma_d t_d} \quad (2)$$

$$t_d = \frac{A_l f_l + A_p f_p}{p_o \sigma_d} + \frac{A_t f_t}{s \sigma_d} \quad (3)$$

Compatibility equations [1,2]:

$$\varepsilon_t = \left(\frac{A_o^2 f_d}{p_o T \mathrm{tg}\alpha} - \frac{1}{2}\right)\varepsilon_{ds} \quad (4)$$

$$\varepsilon_l = \left(\frac{A_o^2 f_d}{p_o T \mathrm{cotg}\alpha} - \frac{1}{2}\right)\varepsilon_{ds} \quad (5)$$

$$\theta = \frac{\varepsilon_{ds}}{2 t_d \sin\alpha \cos\alpha} \quad (6)$$

where:
A_o = area limited by the center line of the flow of shear stresses, which coincides with the center of the strut's thickness (t_d): $A_o = (x - t_d)(y - t_d)$ (x and y are the outer dimensions of the cross section);
p_o = perimeter of area A_o: $p_o = 2(x - t_d) + 2(y - t_d)$;
f_d = stress in the diagonal concrete strut;
A_l, A_p = total area of the longitudinal ordinary and prestress reinforcement, respectively;
A_t = area of one unit of the transversal reinforcement;
s = spacing of the transversal reinforcement;
ε_d = compressive strain in the strut direction;
ε_{ds} = maximum compressive strain in the external surface in the strut direction;
f_l; f_p = longitudinal ordinary and prestress reinforcement stress, respectively;
f_t = transversal reinforcement stress.

should incorporates the σ - ε relationship for compressed concrete in struts proposed by Belarbi and Hsu in 1991 [27] (Table 2 - Eqs. (7) and (8)) with softening factors for the maximum stress in concrete (β_σ) and for the corresponding strain (β_ε) proposed by Zhang and Hsu in 1998 [28] (Table 2 - Eqs. (9)–(12)). VATM should also incorporates the σ - ε relationship for ordinary reinforcement in tension proposed by Belarbi and Hsu in 1995 [29] (Table 3 – Eqs. (17)–(20)) and the σ - ε relationship for prestress reinforcement in tension proposed by Ramberg-Osgood, as presented in [1] (Table 4 – Eqs. (21) and (22)).

Table 3 also presents the equations to calculate the strain in the

Table 2
σ - ε relationship for concrete in compression.

Equations for σ - ε curve [27,28]:

$$f_{c2} = \beta_\sigma f'_c \left[2\left(\frac{\varepsilon_{c2}}{\beta_\varepsilon \varepsilon_o}\right) - \left(\frac{\varepsilon_{c2}}{\beta_\varepsilon \varepsilon_o}\right)^2 \right] \text{if} \varepsilon_{c2} \le \beta_\varepsilon \varepsilon_o \quad (7)$$

$$f_{c2} = \beta_\sigma f'_c \left[1 - \left(\frac{\varepsilon_{c2} - \beta_\varepsilon \varepsilon_o}{2\varepsilon_o - \beta_\varepsilon \varepsilon_o}\right)^2 \right] \text{if } \varepsilon_{c2} > \beta_\varepsilon \varepsilon_o \quad (8)$$

$$\beta_\sigma = \beta_\varepsilon = \frac{R(f'_c)}{\sqrt{1 + \frac{400\varepsilon_{c1}}{\eta'}}} \quad (9)$$

$$\eta = \frac{\rho_l f_{sly}}{\rho_t f_{sty}} \quad (10)$$

$$\begin{cases} \eta \le 1 \Rightarrow \eta' = \eta \\ \eta > 1 \Rightarrow \eta' = 1/\eta \end{cases} \quad (11)$$

$$R(f'_c) = \frac{5.8}{\sqrt{-f'_c\,(\text{MPa})}} \le 0.9 \quad (12)$$

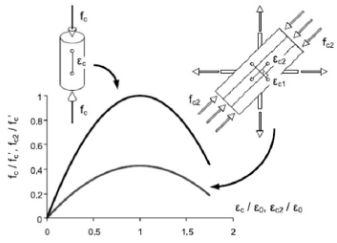

Equations for the stress in the concrete diagonal struts [1,2] (Fig. 4):

$$f_d = k_1 \beta_\sigma f'_c \quad (13)$$

$$A = \beta_\sigma f'_c \quad (14)$$

$$B = k_1 \beta_\sigma f'_c \quad (15)$$

$$C = k_1 \beta_\sigma f'_c\, t_d \quad (16)$$

where:
f'_c = concrete compressive strength (uniaxial);
ε_o = strain corresponding to f'_c;
ε_{c1} = tensile strain in the perpendicular direction of the strut;
ρ_l;ρ_t = longitudinal and transversal reinforcement ratio, respectively (see Section 5.1);
f_{sly}, f_{sty} = longitudinal and transversal reinforcement yielding stress, respectively.

prestress reinforcement (Eqs. (23)–(26)) by using the concept of decompression of the concrete, which occurs when the strain in the ordinary longitudinal reinforcement (initially in compression due to prestress) becomes zero due to the increasing torque. At decompression, the strain in the prestress reinforcement is equal to the strain at decompression ε_{dec}.

For PC beams, parameter η (Table 2, Eq. (10)) must also account for the resistance force in the longitudinal prestress reinforcement:

$$\eta = \frac{\rho_l f_{sly} + \rho_{pl} f_{pl0.1\%}}{\rho_t f_{sty}} = \frac{A_l f_{sly} + A_{pl} f_{pl0.1\%}}{\frac{u}{s} A_t f_{sty}} \quad (27)$$

Table 3
σ - ε relationship for ordinary reinforcement in tension.

Equations for σ - ε curve [29]:

$$f_s = \frac{0.975 E_s \varepsilon_s}{\left[1 + \left(\frac{1.1 E_s \varepsilon_s}{f_{sy}}\right)^m\right]^{\frac{1}{m}}} + 0.025 E_s \varepsilon_s \quad (17)$$

$$m = \frac{1}{9B - 0.2} \le 25 \quad (18)$$

$$B = \frac{1}{\rho}\left(\frac{f_{cr}}{f_{sy}}\right)^{1.5} \quad (19)$$

$$f_{cr} = 3.75\sqrt{f'_c\ (psi)} \quad (20)$$

where:
E_s = Young's modulus of the ordinary reinforcement;
f_{cr} = concrete tensile strength;
ρ = reinforcement ratio (see Eqs. (34) and (35));
f_{sy} = reinforcement yielding stress.

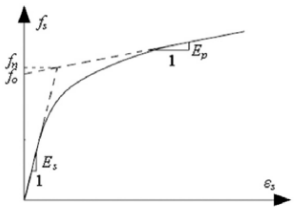

Table 4
σ - ε relationship for prestress reinforcement in tension.

Equations for σ - ε curve [1]:

$$f_p = E_p \varepsilon_p \text{ for } \varepsilon_p \le \varepsilon_{p0.1\%} = f_{p0.1\%}/E_p \quad (21)$$

$$f_p = \frac{E_p \varepsilon_p}{\left[1 + \left(\frac{E_p \varepsilon_p}{f_{pl}}\right)^{4.38}\right]^{\frac{1}{4.38}}} \text{ for } \varepsilon_{p0.1\%} < \varepsilon_p \le \varepsilon_{pu} \quad (22)$$

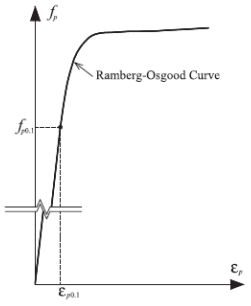

Strain in the longitudinal prestress reinforcement [1]:

$$\varepsilon_p = \varepsilon_{dec} + \varepsilon_l \quad (23)$$

$$\varepsilon_{dec} = \varepsilon_{pi} + \varepsilon_{li} \quad (24)$$

$$\varepsilon_{pi} = \frac{f_{pi}}{E_p} \quad (25)$$

$$\varepsilon_{li} = \frac{A_p f_{pi}}{A_l(E_s - E_c) + (A_c - A_h - A_p)E_c} \quad (26)$$

where:
E_p = Young´s modulus of the prestress reinforcement;
E_c = Young´s modulus of the concrete;
A_c = area limited by the external perimeter of the section;
A_h = hollow area of the section (for plain sections: Ah = 0);
f_{pi} = initial stress due to prestress in the prestress reinforcement;
f_{pu} = ultimate stress of the prestress reinforcement;
$f_{p0.1\%}$ = conventional stress of the prestress reinforcement;
ε_{ps} = strain in the prestress reinforcement;
ε_{dec} = strain in the prestress reinforcement at concrete´s decompression;
ε_{pi} = inicial tensile strain in the prestress reinforcement;
ε_{li} = inicial compressive strain in the longitudinal ordinary reinforcement;
$\varepsilon_{p0.1\%}$ = strain corresponding to $f_{p0.1\%}$.

$$\rho_{pl} = \frac{A_p}{A_c} \quad (28)$$

Where:

ρ_{pl} = longitudinal prestress reinforcement ratio;
ρ_l = longitudinal ordinary reinforcement ratio (see Eq. (34));
ρ_t = transversal ordinary reinforcement ratio (see Eq. (35));
u = perimeter of the transversal ordinary reinforcement ($u = 2x_1 + 2y_1$, with x_1 and y_1 the minor and major dimension of the hoop).

Since unknown and interdependent variables exit to start the calculation procedure, an iterative calculation algorithm needs to be used to compute the points of the T - θ curve (see flowchart in Fig. 2).

The theoretical failure of the beam under torsion is defined when the maximum compressive strain on the surface of concrete struts, ε_{ds} (Fig. 1), or when the tensile strain for the torsion reinforcement, ε_s, reaches there conventional values for failure point (ε_{cu} and ε_{su}, respectively). In this study, these values were defined from Eurocode 2 [30].

3. *T* - θ curve

In general, the results from experimental tests on beams (with current reinforcement ratios) under pure torsion up to failure lead to a typical $T - \theta$ curve, as illustrated in Fig. 3. This curve shows 3 different zones (zone 1, 2 and 3 of Fig. 3). After cracking, plain beams suffer a sudden increase of twist (Zone 2.a). Experimental tests shows that this behavioural zone is practically inexistent in hollow beams [31].

Several key points and properties of the $T - \theta$ curve presented in Fig. 3 will be used for comparative analysis in this study (Section 6).

4. Reference PC beams

The theoretical results from the MVATM will be compared with the results of tested PC beams under pure torsion (uniform longitudinal prestress) which are available in literature. In this study, in addition to the twelve PC beams used by Jeng *et al.* in 2010 [21] (tests reported from [32]), five additional beams were incorporated [2,33,34]. The experimental results of such beams can be considered trustworthy for comparative analysis with respect to the global behaviour. In fact, not all the experimental results available in literature can be used for this purpose. For instance, in some experimental studies the authors present the average twist for all the beam length, and not the twist of the critical zone. For slender beams, theoretical twists based on a section analysis cannot be directly compared with these experimental twists. For these reason, the beams reported by Wafa *et al.* in 1995 [35] where not included in this study (neither in [21]). A more detailed discussion about this subject can be found in [18].

Table 5 summarizes the properties of the reference PC beams used in this study, namely: the external width (x) and height (y) of the cross section, the thickness of the walls of the cross hollow sections (t), the distances between centerlines of legs of the hoops (x_1 and y_1), the area of longitudinal reinforcement (A_{sl}), the distributed area of one unit of

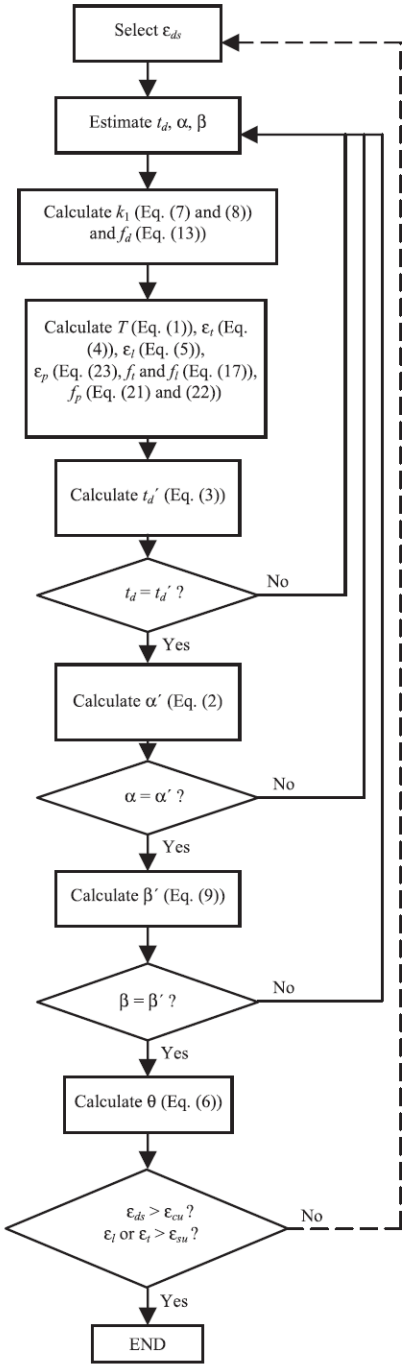

Fig. 2. Flowchart to compute T - θ for PC beams (VATM) [2].

the transversal reinforcement (A_{st} / s, where s is the longitudinal spacing of transversal reinforcement), the area of longitudinal prestress reinforcement (A_p), the average concrete compressive strength (f_{cm}), the average yielding stress of longitudinal and transversal reinforcement (f_{lym} and f_{tym}), the proportional conventional limit stress to 0.1% ($f_{p0,1\%}$) and the initial stress for the prestress reinforcement (f_{pi}).

5. Modified variable angle truss model for PC beams

5.1. Zone 1 (Non-cracked state)

To correct the formulation of the VATM for Zone 1 (Fig. 3) it is necessary to know the cracking torque (T_{cr}) to set the upper limit of the non-cracked state.

In previous studies, Bernardo and Lopes [18,19,36] found that Bredt's Thin Tube Theory, with some corrections proposed by Hsu and Mo in 1985 [2], is appropriate to compute T_{cr} regardless of the beam type (RC or PC, plain or hollow). For RC rectangular hollow sections (f'_c in *psi*, t in *in.* and A_c in *in.*^{2}):

$$T_{cr} = 2A_c t(2.5\sqrt{f'_c}) \tag{29}$$

In Eq. (29), A_c is the area limited by the outer perimeter of the section (including hollow area) and t is the thickness of the wall. Hsu in 1984 [37] showed that Eq. (29) could also be applied to RC rectangular plain sections by taking $t = 1.2A_c/p_c$, with p_c (in *in.*) the outer perimeter of the cross section. Bernardo and Lopes in 2011 [19] showed that Eq. (29) should be multiplied by 0.85 when $f'_c > 50$MPa.

Eq. (29) must also be corrected for PC beams. Hsu in 1984 [37] showed that Cowan´s failure criterion [38] can be used to correct Eq. (29) through a simple prestress factor, γ:

$$\gamma = \sqrt{1 + 10\frac{\sigma}{f'_c}} \tag{30}$$

In Eq. (30), σ is the concrete stress due to prestress. Then, for PC beams the cracking torque (T_{cr}^p) is computed as follows:

$$T_{cr}^p = T_{cr}\gamma = T_{cr}\sqrt{1 + 10\frac{\sigma}{f'_c}} \tag{31}$$

Hsu [37] proposed an empirical equation to compute the effective cracking torque ($T_{cr,ef}$) to account for the influence of the torsional reinforcement (ρ_l and ρ_t are the longitudinal an transversal reinforcement ratio, respectively):

$$T_{cr,ef} = [1 + 4\rho_{tot}]T_{cr} \tag{32}$$

$$\rho_{tot} = \rho_l + \rho_t \tag{33}$$

$$\rho_l = \frac{A_{sl}}{A_c} \tag{34}$$

$$\rho_t = \frac{A_{st}u}{A_c s} \tag{35}$$

If prestress reinforcement is bonded to the concrete and if it is located in the outer area of the concrete section, then ρ_l must be substituted by $\rho_{l,tot}$:

$$\rho_{l,tot} = \frac{A_{sl} + nA_p}{A_c} \approx \frac{A_{sl} + A_p}{A_c} \tag{36}$$

In Eq. (36), n is the ratio between Young´s modulus for prestress and ordinary steel ($n = E_p/E_s \approx 1$).

The twist θ and the torsional stiffness for non-cracked state is calculated from the MVATM, which should incorporate the contribution of the concrete in tension (neglected in VATM) and also the contribution of the concrete core for plain sections.

To maintain consistency with VATM, an equivalent hollow section is assumed for the non-cracked state (Fig. 4(a)). The influence of the concrete core will be introduced latter. From ACI 318–14 [39], for plain sections the equivalent thickness for the wall (h_{eq}) is equal to $0.75A_{cp}$ / p_{cp}, where A_{cp} is the area limited by the outer perimeter p_{cp} of the cross section.

Parameter h_{eq} will be only used to calculate some properties of the

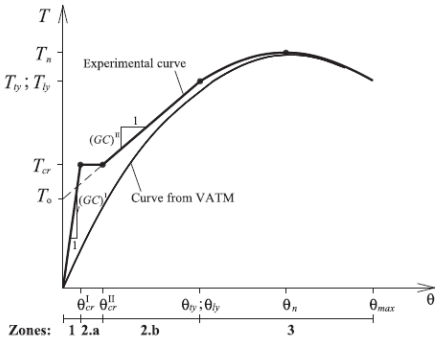

T_{cr} = Cracking torque
θ_{cr}^{I} = Twist corresponding to T_{cr} (non-cracked state)
θ_{cr}^{II} = Twist corresponding to T_{cr} (cracked state)
T_o = Ordinate at the origin of the T - θ equivalent straight line for Zone 2.b
T_{ly} = Torque corresponding to yielding of longitudinal reinforcement
θ_{ly} = Twist corresponding to T_{ly}
T_{ty} = Torque corresponding to yielding of transversal reinforcement
θ_{ty} = Twist corresponding to T_{ty}
T_n = Resistance torque
θ_n = Twist corresponding to T_n
θ_{max} = Maximum twist at beam´s failure
$(GC)^I \equiv K_t^I$ = torsional stiffness in non-cracked state
$(GC)^{II} \equiv K_t^{II}$ = torsional stiffness in cracked state

Fig. 3. Typical T - θ curves.

section. To compute the T – θ curve, parameter t_d (thickness of the struts) will be used to maintain consistency with VATM.

In non-cracked state, it is assumed that the torsional reinforcement has no influence on the position of the center line of the shear flow. Thus, A_o is considered equal to the area limited by the center line of the equivalent thickness of the wall (Fig. 4(b)):

$$A_o = (x - h_{eq})(y - h_{eq}) \tag{37}$$

The perimeter of the center line of the shear flow p_o is calculated as follows (Fig. 4(b)):

$$p_o = 2(x - h_{eq}) + 2(y - h_{eq}) \tag{38}$$

In previous studies, the well-known elastic torsional analysis of structural concrete beams has been successfully extended by using tension softening of concrete, that is, by incorporating an additional smeared σ - ε relationships for concrete in tension in the model [16,17,20–22,25]. This technique was successfully applied for plain concrete in torsion with arbitrary (non-rectangular) cross-section [16,17] and also for RC and PC beams in torsion [10–22,25,40] for the prediction of the elastic behaviour and the ultimate or cracking torsional moment, respectively. In the present study, the same technique used in the MVATM for RC beams is adopted to extend the model to PC beams. In the non-cracked state, the influence of the concrete in tension is directly introduced in the longitudinal and transversal equilibrium equations of VATM. For this purpose, the PC section is homogenized for both longitudinal and transversal directions by assuming the equivalent thickness h_{eq} of the concrete in tension as effective to carry the forces

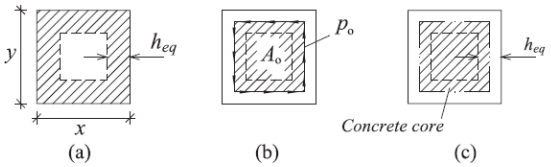

Fig. 4. Equivalente hollow section for non-cracked state (plain section) and concrete core.

together with the reinforcement. Since the original equilibrium equations in the VATM are written with respect to the forces in the reinforcement (Eqs. (2) and (3) in Table 1), the area of concrete in tension is "transformed" into an equivalent steel area. Fig. 5(a) and Fig. 5(b) illustrate the effective area of concrete in tension in the longitudinal and transversal direction, respectively. Thus, the total longitudinal force ($F_{l,tot}$) and the total distributed transversal force ($F_{t,tot}$) are computed as follows:

$$F_{l,tot} = A_{lh} f_l = (A_l + n_c A_{cl,eq} + n_p A_p) f_l \tag{39}$$

$$F_{t,tot} = A_{th} f_t / s = (A_t + n A_{ct,eq}) f_t / s \tag{40}$$

$$A_{cl,eq} = xy - (x - h_{eq})(y - h_{eq}) \tag{41}$$

$$A_{ct,eq} = s h_{eq} \tag{42}$$

In the above equations, $n = E_c/E_s$ is the ratio between Young´s

Table 5
Properties of reference PC beams.

Beam	Section type	x cm	y cm	t cm	x_1 cm	y_1 cm	A_{st} cm^2	A_{st} / s cm^2/m	A_p cm^2	f_{cm} MPa	f_{lym} MPa	f_{tym} MPa	$f_{p0,1\%}$ (MPa)	f_{pi} (MPa)
P2 [34]	Hollow	35.6	43.2	8.9	31.2	38.9	5.58	7.35	4.63	32.9	407	407	1476	1145
D1 [33]	Hollow	60.0	60.0	11.4	54.3	54.2	23.75	11.22	4.20	80.8	724	715	1670	640
D2 [33]	Hollow	60.0	60.0	11.5	55.5	55.5	23.75	11.22	5.60	58.8	724	715	1670	1100
P3 [34]	Plain	35.6	43.2	–	29.2	36.8	4.26	7.35	1.16	34.0	328	328	1476	1145
P8 [2]	Plain	25.4	38.1	–	21.6	34.3	5.16	22.58	9.58	31.0	334	336	959	690
PA1R [32]	Plain	25.4	25.4	–	22.2	22.2	2.84	4.48	0.93	43.6	435	310	1638	1207
PA2 [32]	Plain	25.4	25.4	–	21.6	21.6	5.16	7.74	1.50	45.6	483	310	1663	1207
PA3 [32]	Plain	25.4	25.4	–	21.9	21.9	8.00	7.93	2.06	41.8	389	435	1744	1303
PA4 [32]	Plain	25.4	25.4	–	21.9	21.9	11.36	11.00	2.97	42.2	419	435	1709	1303
PB1 [32]	Plain	17.8	35.6	–	14.6	32.4	2.84	4.48	0.93	45.8	435	310	1638	1207
PB2 [32]	Plain	17.8	35.6	–	14.0	31.8	5.16	7.74	1.50	45.8	483	310	1663	1207
PB3 [32]	Plain	17.8	35.6	–	14.3	32.1	8.00	7.51	2.06	45.5	389	435	1744	1303
PB4 [32]	Plain	17.8	35.6	–	14.3	32.1	11.36	10.21	2.97	45.5	419	435	1709	1303
PC1 [32]	Plain	14.6	43.8	–	11.4	40.6	2.84	4.48	0.93	42.2	435	310	1638	1207
PC2 [32]	Plain	14.6	43.8	–	10.8	40.0	5.16	6.90	1.50	45.1	483	310	1663	1207
PC3 [32]	Plain	14.6	43.8	–	11.1	40.3	8.00	6.79	2.06	41.3	389	435	1744	1303
PC4 [32]	Plain	14.6	43.8	–	11.1	40.3	11.36	9.53	2.97	42.1	419	435	1709	1303

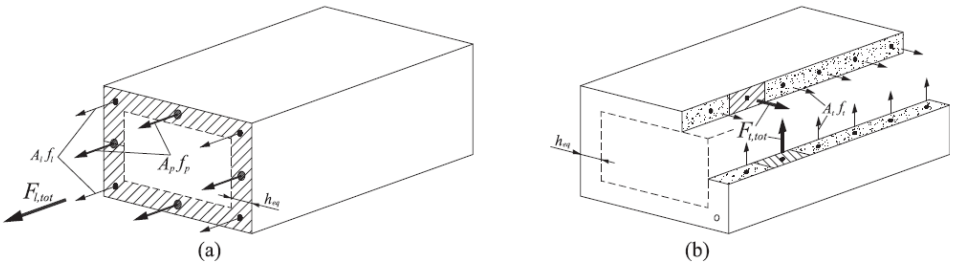

Fig. 5. Participating areas of concrete in tension.

modulus for concrete and ordinary steel, A_{lh} and A_{th} are the homogenized steel areas in the longitudinal and transversal direction, respectively, $A_{cl,eq}$ and $A_{ct,eq}$ are the equivalent area of effective concrete in tension for the longitudinal and transversal direction, respectively.

For the non-cracked state and for PC beams, the method presented in Section 2 (VATM) to calculate the strain in the longitudinal prestress reinforcement, ε_p, in order to calculate the stress, f_p, must be corrected because in this stage the beam is actually not cracked. Moreover, a load range exists for which the beam has not yet reached the decompression of concrete. Before decompression, the strain of the longitudinal prestress reinforcement is calculated as follows:

$$\varepsilon_p = \varepsilon_{pi} + \varepsilon'_l \tag{43}$$

$$\varepsilon_{pi} = \frac{f_{pi}}{E_p} \tag{44}$$

$$\varepsilon'_l = -\varepsilon_{li} + \varepsilon_l \tag{45}$$

$$\varepsilon_{li} = \frac{A_p f_{pi}}{A_l(E_s - E_c) + (A_c - A_h - A_p)E_c} \tag{46}$$

The effective strain in the longitudinal ordinary reinforcement, ε'_l, is calculated accounting that an initial compressive strain ε_{li} exists due to prestress. The strain in the longitudinal reinforcement ε_l induced by the torsional moment T is calculated based on Eq. (5) (Table 1).

The outer fiber of the concrete strut has an initial compressive strain ε_{dsi} due to prestress. Assuming a 45 degrees angle for the struts for non-cracked state, ε_{dsi} can be estimated as follows (Fig. 6):

$$\varepsilon_{dsi} \approx \frac{\varepsilon_{li}}{cos45} \tag{47}$$

ε_{dsi} must be added to the input value ε_{ds} in the iterative computational procedure in order to calculate the effective strain ε'_{ds} (Eq. (48)) to initialize the calculation procedure.

$$\varepsilon'_{ds} = \varepsilon_{ds} + \varepsilon_{dsi} \tag{48}$$

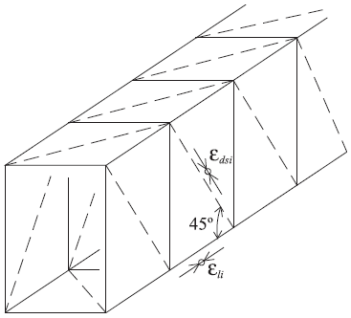

Fig. 6. Inicial compressive strain in concrete strut due to prestress.

Summarizing, from the original formulation of VATM presented in Section 2 and Table 1, the MVATM for PC beams under torsion incorporates the following changes:

- Parameters A_o and p_o are calculated using Eqs. (37) and (38), respectively;
- Equilibrium Eqs. (2) and (3) from Table 1 are rewritten (Eqs. (49) and (50)) to incorporate the total longitudinal force $F_{l,tot}$ (Eq. (39)) and the total distributed transversal force $F_{t,tot}$ (Eq. (40)):

$$\cos^2\alpha = \frac{F_{l,tot}}{p_o \sigma_d t_d} \tag{49}$$

$$t_d = \frac{F_{l,tot}}{p_o \sigma_d} + \frac{F_{t,tot}}{\sigma_d} \tag{50}$$

- The value to initialize the iterative calculation procedure is ε'_{ds} (Eq. (48));
- The calculation procedure ends when the torsional moment is higher than $T_{cr,ef}$ from Eq. (32).

It is also assumed that the influence of the concrete core in plain sections only influences the torsional stiffness of the beam. For this, the torsional stiffness of the concrete core alone is added to the torsional stiffness of the equivalent hollow section in order to correct the twists θ. The following steps are implemented:

1. From the calculation procedure and for each increment of ε'_{ds}, obtain the point (θ;T);
2. Calculate an equivalent secant torsional stiffness;

$$K_{t,eq} = T/\theta \tag{51}$$

3. Using Theory of Elasticity with some corrections [24], calculate the torsional stiffness of the concrete core: $K_{t,c} = 0.292E_c C$.
4. Calculate the equivalent total torsional stiffness of the full section, $K_{t,eq,tot}$:

$$K_{t,eq,tot} = K_{t,eq} + K_{t,c} \tag{52}$$

5. Calculate the corrected twist θ_{cor}, based on $K_{t,eq,tot}$ (Eq. (52)). This leads to the final point (θ_{cor}; T) for the theoretical T - θ curve;

$$\theta_{cor} = T/K_{t,eq,tot} \tag{53}$$

To calculate $K_{t,c}$, the dimensions of the concrete core are defined assuming some overlap between the equivalent hollow section and the section of the concrete core in order to account for the real connection [24]. The considered overlap area is limited by the center line of the equivalent thickness of the wall (Fig. 4(c)). Thus, the "external" dimensions of the rectangular concrete core are x - h_{eq} / 2 and y - h_{eq} / 2.

Based on the foregoing, an iterative calculation procedure is used to compute the T - θ curve for non-cracked state (Zone 1 of Fig. 3). The flowchart for the calculation algorithm is illustrated in Fig. 7(a) (hollow

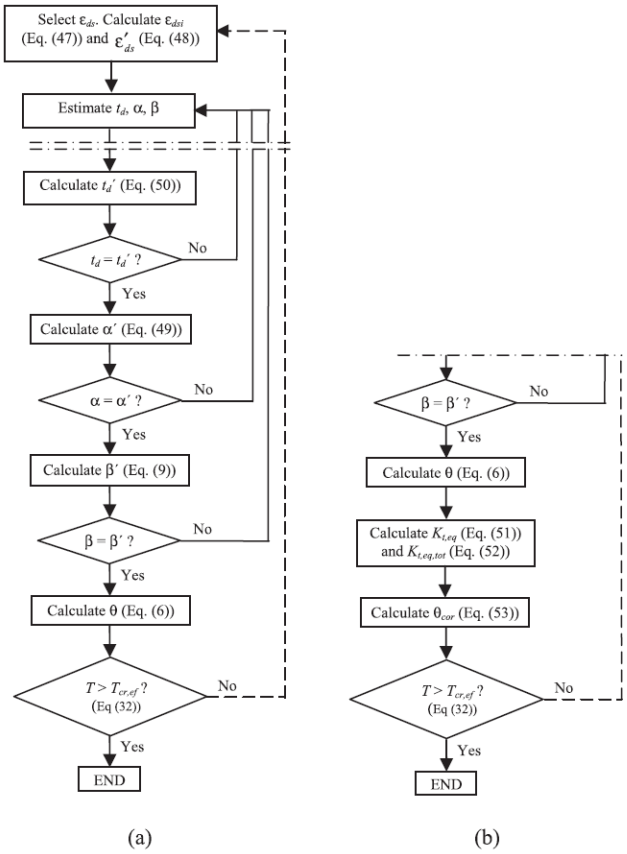

Fig. 7. – Flowchart to compute T - θ curve (zone 1 – non-cracked state) – MVATM for PC beams: (a) hollow sections and (b) plain sections.

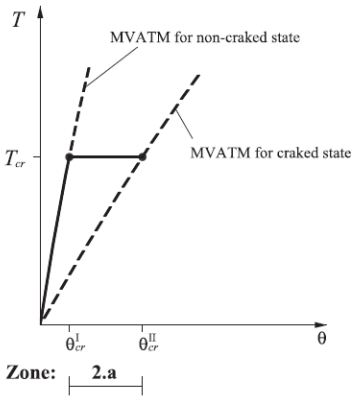

Fig. 8. – Simulation of Zone 2.a (plain beams).

sections) and Fig. 7(b) (plain sections). Only the new part of the flowchart from the original MVATM [24], in order to include PC beams, is presented in Fig. 7.

5.2. Zone 2.a (Cracked state)

The calculation of Zone 2.a of the T - θ curve (Fig. 3) from MVATM, as presented in Section 5.1, accounts for the concrete cracking. When the effective cracking torque ($T_{cr,ef}$) is reached, the effective concrete in tension is no longer considered for the equilibrium in the longitudinal and transversal direction. This will cause an instantaneous increase of the twist, as it is observed experimentally (mainly for plain beams). Moreover, for plain beams the influence of the concrete core still exists after cracking [18].

For this new stage, MVATM no longer uses the equivalent hollow section (with h_{eq}) for non-cracked state. After the cracking of the beam, the effective wall thickness is considered equal to t_d (effective thickness of the concrete struts). Then, the center line of the shear flow is now assumed to be located at t_d / 2, as for VATM (Table 1).

Summarizing, in order to compute Zone 2.a, MVATM from non-cracked state (Section 5.1) incorporates the following changes:

- Parameters A_o and p_o are calculated as for VATM (see Table 1);
- Eqs. (49) and (50) are substituted by the original equilibrium Eqs. (2) and (3);
- From the theoretical T - θ curve calculated for cracked state (based on the earlier changes), only the point for $T_{cr,ef}$ is retained to compute Zone 2.a.

If the longitudinal prestress reinforcement is located in the area near

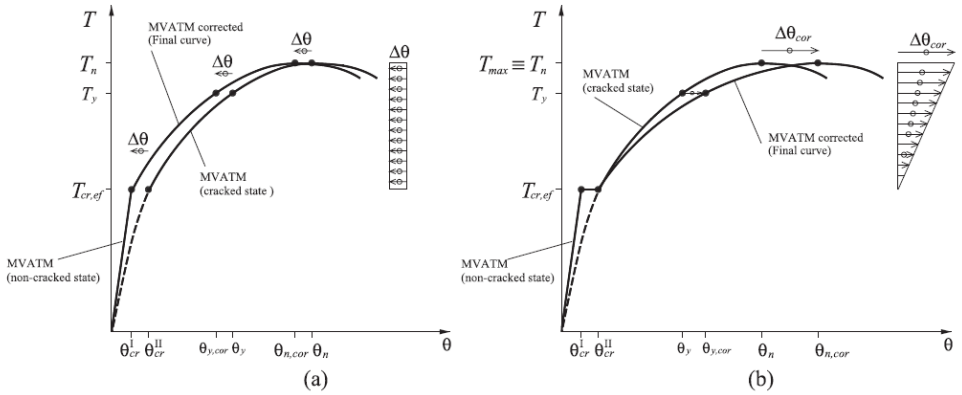

Fig. 9. – Corrections of T – θ curves (Zone 2.b): (a) hollow sections and (b) plain sections.

Table 6
Comparative analysis for the cracking torque and torsional stiffness (non-cracked state).

Beam	$K^I_{t,exp}$ kN.m²/°	$K^I_{t,th}$ kN.m²/°	$K^I_{t,exp}$ /$K^I_{t,th}$	$T_{cr,exp}$ kN.m	$T_{cr,th}$ kN.m	$T_{cr,exp}$ /$T_{cr,th}$
P2 [34]	419.1	307.6	1.36	58.0	44.6	1.30
D1 [33]	2656.2	2383.1	1.11	172.9	278.9	0.62
D2 [33]	2499.1	2108.8	1.19	184.7	248.9	0.74
P3 [34]	197.1	350.6	0.56	41.2	44.9	0.92
P8 [2]	189.9	152.3	1.25	45.2	26.9	1.68
PA1R [32]	9.6	70.7	0.14	18.5	17.4	1.06
PA2 [32]	19.2	73.8	0.26	21.7	20.1	1.08
PA3 [32]	31.6	72.9	0.43	24.4	22.1	1.10
PA4 [32]	57.4	74.9	0.77	26.3	25.7	1.02
PB1 [32]	11.5	54.9	0.21	15.4	16.4	0.94
PB2 [32]	30.3	56.5	0.54	17.8	18.7	0.96
PB3 [32]	74.1	57.3	1.29	20.7	20.9	0.99
PB4 [32]	45.1	58.7	0.77	21.9	24.2	0.91
PC1 [32]	22.5	40.6	0.55	13.3	14.8	0.89
PC2 [32]	38.3	42.7	0.90	16.6	17.2	0.96
PC3 [32]	64.2	41.9	1.53	17.0	18.9	0.90
PC4 [32]	61.6	43.1	1.43	21.6	22.1	0.98
		$\bar{x}$ =	0.84		$\bar{x}$ =	1.00
		s =	0.46		s =	0.23
		cv =	54%		cv =	23%

$\bar{x}$

Table 7
Comparative analysis for the torsional stiffness and ordinate at the origin (cracked state).

Beam	$K^{II}_{t,exp}$ kN.m²/°	$K^{II}_{t,th}$ kN.m²/°	$K^I_{t,exp}$ /$K^I_{t,th}$	$T_{o,exp}$ kN.m	$T_{o,th}$ kN.m	$T_{o,exp}$ /$T_{o,th}$
P2 [34]	18.0	22.1	0.82	55.5	52.4	1.06
D1 [33]	140.3	206.4	0.68	163.8	139.2	1.18
D2 [33]	171.9	222.9	0.77	172.0	134.8	1.28
P3 [34]	7.7	6.9	1.11	39.6	51.6	0.77
P8 [2]	17.4	10.6	1.64	41.1	42.6	0.97
PA1R [32]	1.1	0.8	1.38	18.4	17.1	1.07
PA2 [32]	4.1	5.2	0.80	19.8	18.4	1.07
PA3 [32]	5.3	6.6	0.81	22.9	19.8	1.15
PA4 [32]	5.8	7.9	0.74	24.3	23.0	1.05
PB1 [32]	1.6	0.9	1.81	15.6	16.0	0.98
PB2 [32]	4.3	5.0	0.86	17.0	16.1	1.06
PB3 [32]	5.2	5.6	0.92	18.9	17.7	1.07
PB4 [32]	8.2	7.5	1.09	20.5	19.5	1.05
PC1 [32]	2.1	1.3	1.58	12.5	14.0	0.89
PC2 [32]	4.9	3.9	1.26	15.5	14.6	1.06
PC3 [32]	6.1	4.7	1.30	15.0	15.4	0.97
PC4 [32]	7.7	6.0	1.29	17.7	17.4	1.02
		$\bar{x}$ =	1.11		$\bar{x}$ =	1.04
		s =	0.35		s =	0.11
		cv =	32%		cv =	11%

to the external perimeter, in this new stage the total longitudinal reinforcement ratio is also computed from Eq. (36). The strain in the prestress reinforcement is calculated according to Section 5.1. The strains in the transversal and longitudinal ordinary reinforcement are calculated from Eq. (4) and Eq. (5), respectively.

Based on the foregoing, the iterative calculation procedure of Section 5.1 is corrected to compute the T - θ curve for the cracked state and for $T_{cr,ef}$. The flowchart for the calculation algorithm to compute the new T - θ curve for cracked state is the same as illustrated in Fig. 7(a) (hollow sections) and Fig. 7(b) (plain sections), with t_d' and α′calculated from Eq. (2) and Eq. (3), respectively.

The target of this section is illustrated in Fig. 8. Zone 2.a corresponds to a horizontal landing, with $T = T_{cr,ef}$ and $\theta^I_{cr} \le \theta \le \theta^{II}_{cr}$. θ^I_{cr} and θ^{II}_{cr} corresponds to the abscissa of the intersection point between the horizontal landing for $T = T_{cr,ef}$ and the theoretical T - θ curve computed with MVATM for non-cracked state (Section 5.1) and with MVATM for cracked state (present section), respectively.

5.3. Zones 2.b and 3 (Cracked and ultimate states)

As discussed in Section 1, the theoretical T - θ curve computed with VATM does not fit accurately with the experimental results for Zone 2.b (see Fig. 3). In addition to the explanation related with cracking, for plain beams part of the observed deviations can be explained because VATM neglects the influence of the concrete core in the torsional stiffness after cracking [18,19].

The theoretical T - θ curve from MVATM for cracked state, as presented in Section 5.2, cannot be used to draw the entire T - θ curve for Zone 2.b and 3, since it fully incorporates the influence of the concrete core for plain sections. Bernardo and Lopes [18,19], based on theoretical simulations of zone 2.b by using the torsional Hsu´s model for cracked state [41], found that the influence of the concrete core to the cracked torsional stiffness decreases as the torsional moment increases (from $T_{cr,ef}$). This influence is residual in the ultimate stage and can be neglected. In order to correct the torsional stiffness calculated with MVATM for cracked state (Section 5.2), from $T_{cr,ef}$ to the maximum toque T_n, the following methodology is adopted:

- Calculate the entire T - θ curve from $T_{cr,ef}$ with MVATM for cracked state (Section 5.2). The torsional moments of this T - θ curve are considered the final ones and only the twists θ are corrected;
- From $T_{cr,ef}$ to T_n the influence of the concrete core is gradually reduced by reducing linearly the “external” dimensions of the concrete

Table 8
Comparative analysis for the resistance torque and correspondent twist (ultimate state).

Beam	$T_{n,exp}$ kN.m	$T_{n,th}$ kN.m	$T_{n,exp}$ / $T_{n,th}$	$\theta_{n,exp}$ °/m	$\theta_{n,th}$ °/m	$\theta_{n,exp}$ /$\theta_{n,th}$
P2 [34]	87.1	80.3	1.08	2.8	1.9	1.51
D1 [33]	396.0	428.8	0.92	1.7	2.0	0.87
D2 [33]	447.7	409.9	1.09	1.9	1.8	1.08
P3 [34]	55.8	64.1	0.87	3.1	2.6	1.19
P8 [2]	61.8	61.6	1.00	1.9	1.7	1.10
PA1R [32]	21.8	19.6	1.11	3.0	3.9	0.76
PA2 [32]	29.3	28.7	1.02	2.9	2.9	0.98
PA3 [32]	34.0	33.0	1.03	2.7	2.7	0.98
PA4 [32]	37.4	36.8	1.02	2.9	2.3	1.27
PB1 [32]	22.2	18.8	1.18	4.5	4.3	1.05
PB2 [32]	27.5	27.1	1.01	2.7	3.2	0.87
PB3 [32]	32.6	30.8	1.06	3.1	3.0	1.03
PB4 [32]	37.6	34.0	1.11	2.6	2.6	1.02
PC1 [32]	19.7	18.0	1.10	5.2	4.7	1.12
PC2 [32]	28.6	24.2	1.18	3.4	3.6	0.93
PC3 [32]	32.8	26.9	1.22	4.7	3.3	1.44
PC4 [32]	38.5	30.1	1.28	3.8	2.9	1.33
		$\bar{x}$ =	1.08		$\bar{x}$ =	1.09
		s =	0.10		s =	0.20
		cv =	10%		cv =	19%

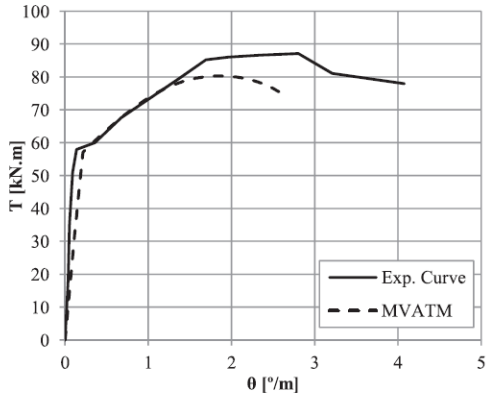

Fig. 10. T - θ curves: Beam P2 [34].

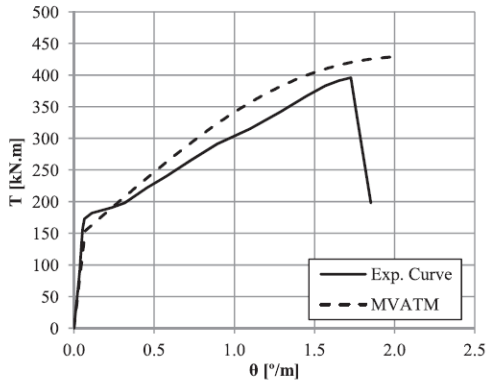

Fig. 11. T - θ curves: Beam D1 [33].

core (considering the fully dimensions for $T_{cr,ef}$ and no dimensions at all for T_n). Then, from point (θ_{cr}^{II}; $T_{cr,ef}$) all the points of T - θ curve are corrected along the θ axis.

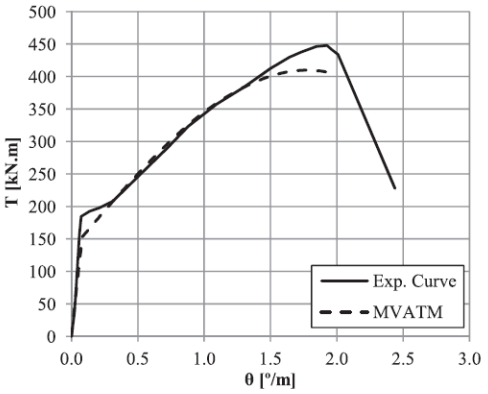

Fig. 12. T - θ curves: Beam D2 [33].

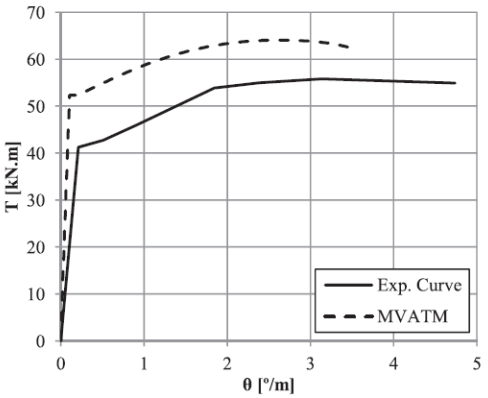

Fig. 13. T - θ curves: Beam P3 [34].

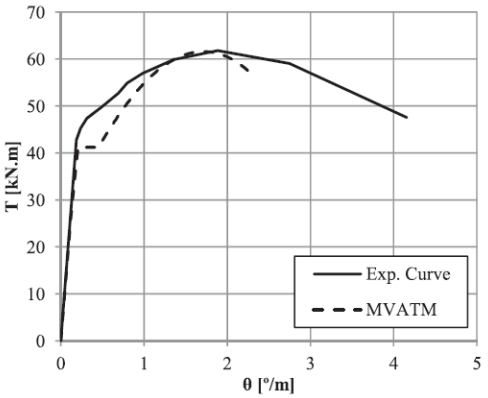

Fig. 14. T - θ curves: Beam P8 [2].

Fig. 9(b) shows that the correction method for θ (plain beams) consists to add increasing values from $T_{cr,ef}$ to T_n, assuming a linear variation, to simulate the decreasing of stiffness due to the loss of concrete core influence.

For hollow beams, all the T - θ curve is calculated with MVATM for cracked state (Section 5.2), since no concrete core exists. However, since a theoretical "small" Zone 2.a ($\Delta\theta$) always exists, a small

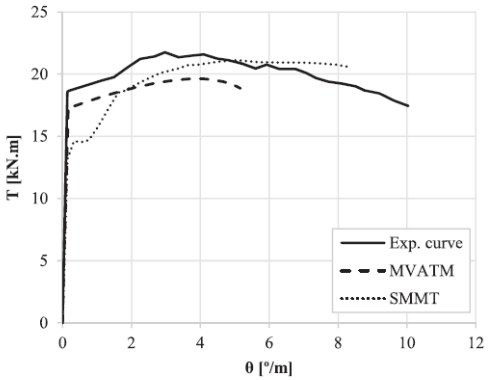

Fig. 15. T - θ curves: Beam PA1R [32].

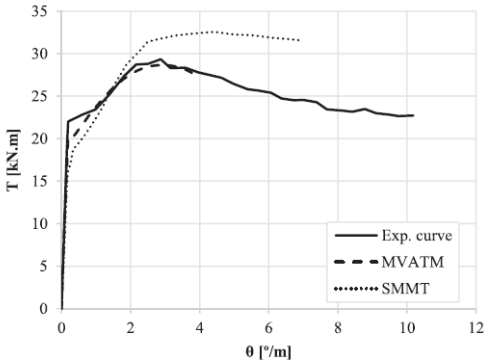

Fig. 16. T - θ curves: Beam PA2 [32].

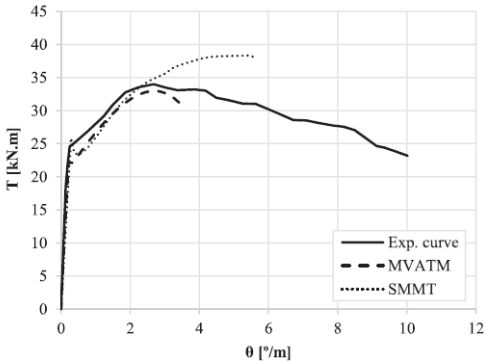

Fig. 17. T - θ curves: Beam PA3 [32].

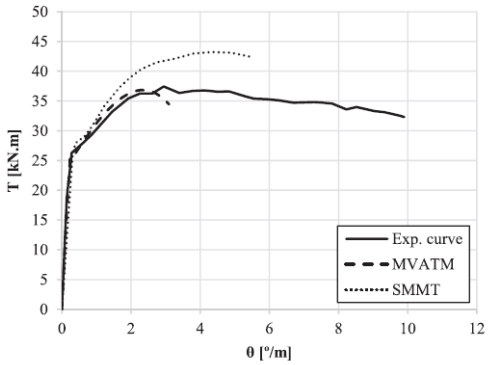

Fig. 18. T - θ curves: Beam PA4 [32].

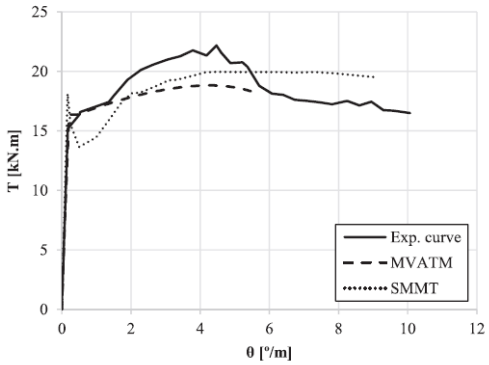

Fig. 19. T - θ curves: Beam PB1 [32].

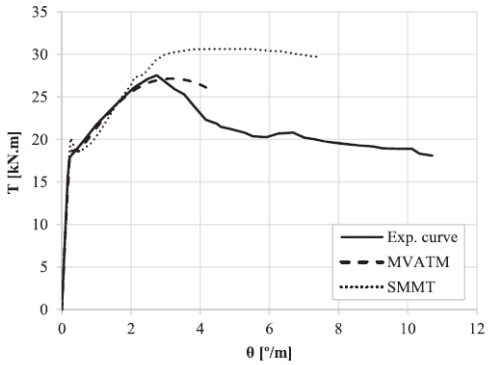

Fig. 20. T - θ curves: Beam PB2 [32].

correction is need because such zone is not experimentally observed for hollow beams [31]. Then, all the points of the T - θ curve from (θ_{cr}^{II}; T_{cr}), are translated to the left by $\Delta\theta$ (Fig. 9(a)).

6. Comparative analysis with reference PC beams

Based on Section 5, a final calculation procedure was implemented to calculate the full theoretical T - θ curve of PC beams under torsion. The resultant theoretical predictions from MVATM for the T - θ curves are compared with the experimental ones from reference PC beams and also, for some beams, with the theoretical predictions from Jeng *et al.* [21] by using SMMT.

6.1. Zone 1 (Non-cracked state)

To check the validity of MVATM for non-cracked state, the secant torsional stiffness is used for comparison. This parameter is computed as follows (were θ_{cr} is the twist corresponding to $T_{cr,ef}$):

$$K_i^1 = \frac{T_{cr,ef}}{\theta_{cr}} \tag{54}$$

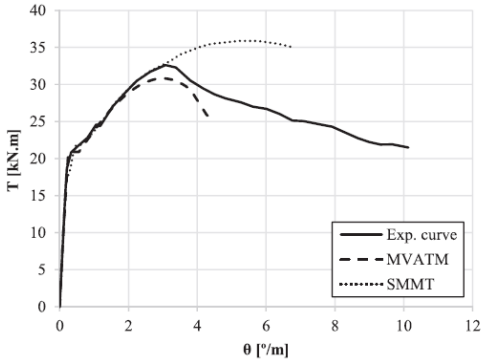

Fig. 21. T - θ curves: Beam PB3 [32].

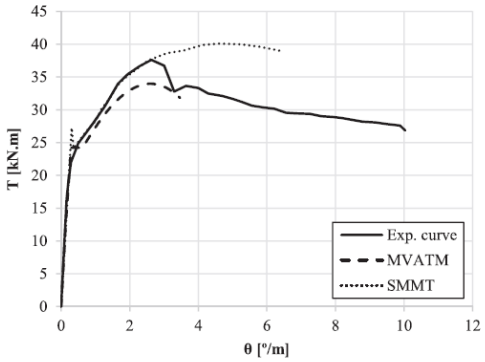

Fig. 22. T - θ curves: Beam PB4 [32].

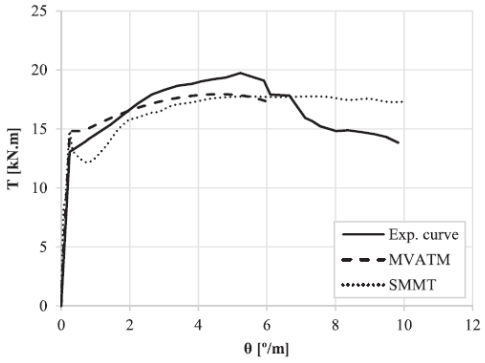

Fig. 23. T - θ curves: Beam PC1 [32].

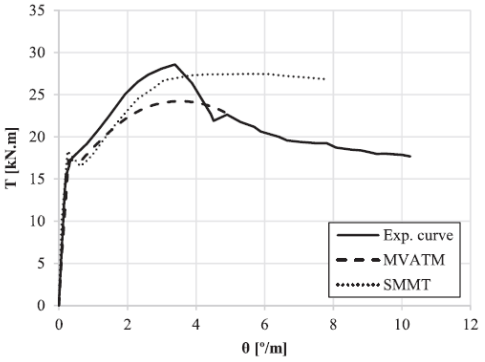

Fig. 24. T - θ curves: Beam PC2 [32].

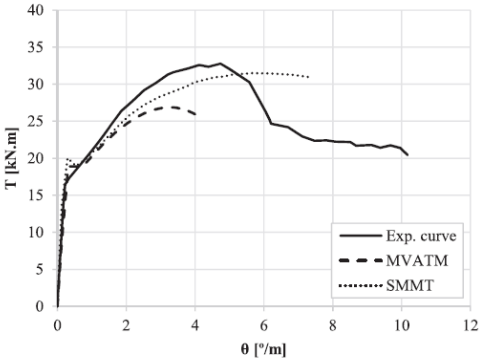

Fig. 25. T - θ curves: Beam PC3 [32].

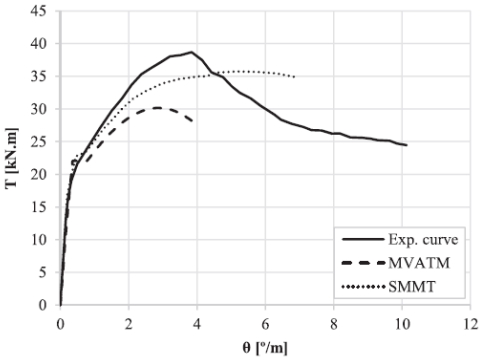

Fig. 26. T - θ curves: Beam PC4 [32].

Table 6 presents, for each reference beam, the experimental value of torsional stiffness ($K_{t,\exp}^{I}$) and cracking torque ($T_{cr,exp}$), and the corresponding theoretical values ($K_{t,th}^{I}$ and $T_{cr,th}$ respectively). The ratios $K_{t,\exp}^{I}/K_{t,th}^{I}$ and $T_{cr,exp}/T_{cr,th}$ are also presented, as well as the corresponding average value $\bar{x}$, sample standard deviation s and coefficient of variation cv.

Table 6 shows that the torsional stiffness in non-cracked state is somewhat overestimated ($\bar{x} = 0.84$). On the other hand, the estimations for the cracking torque are apparently very good ($\bar{x} = 1.00$). However, the variability of the results are somewhat high for the cracking torque ($cv = 23\%$), still acceptable, and very high for the torsional stiffness ($cv = 54\%$). Since the values of the twists are very small at this stage, the observed high dispersion for the torsional stiffness can be considered less important.

In general, the results from Table 6 agree with the results from previous studies which used alternative theoretical models [21,33,36].

6.2. Zones 2.b (Cracked state)

This section summarizes the results for the torsional stiffness in cracked state (K_t^{II}) and for the ordinate at the origin (T_0, see Fig. 3) of the straight line representing the equivalent torsional stiffness in

cracked state for Zone 2.b. K_t^{II} and T_0 were estimated from a linear regression of the theoretical and experimental T - θ curve points corresponding to Zone 2.b. Parameter T_0 measure the "position" of the T - θ curve in the graph, which is related with the correct evaluations on the internal stress and deformation states.

Table 7 presents, for each reference beam, the experimental value of the torsional stiffness in cracked state ($K_{t,exp}^{II}$) and the ordinate at the origin ($T_{o,exp}$), their correspondent theoretical values ($K_{t,th}^{II}$ and $T_{o,th}$), as well as the ratios $K_{t,exp}^{II}/K_{t,th}^{I}$ and $T_{0,exp}/T_{0,th}$, and also the statistical parameters ($\bar{x}$, s and cv).

Table 7 shows that the prediction of the torsional stiffness in cracked state (K_t^{II}) is good ($\bar{x} = 1.11$) but the dispersion of the results is high ($cv = 32\%$). This latter is probably related with the difficulty to draw objectively the approximate straight line representing the equivalent torsional stiffness in cracked state. Nevertheless, the results are not very bad. Table 7 also shows that the estimations of the ordinate at the origin (T_o) are good ($\bar{x} = 1.04$) and the dispersion of the results are quite acceptable ($cv = 11\%$).

Based on the results above, MVATM seems to be quit acceptable to estimate the main characteristics of Zone 2.b for PC beams under torsion.

6.3. Zone 3 (Ultimate state)

Table 8 presents, for each reference beam, the experimental values of the resistance torque ($T_{n,exp}$) and the corresponding twist ($\theta_{n,exp}$), and their corresponding theoretical values ($T_{n,th}$, $\theta_{n,th}$). Table 8 also presents the ratios $T_{n,exp}/T_{n,th}$ and $\theta_{n,exp}/\theta_{n,th}$, as well as the statistical parameters ($\bar{x}$, s and cv).

Table 8 shows that the estimations of the resistance torque (T_n) are good ($\bar{x} = 1.08$) and the dispersion of the results are quite acceptable ($cv = 10\%$). The estimations for the ultimate twist (θ_n) are also good ($\bar{x} = 1.09$) although the dispersion of the results are higher ($cv = 19\%$), still acceptable.

6.4. T - θ curves

Figs. 10 to 26 present the experimental and theoretical T - θ curves for the reference beams analyzed in this article. Figs. 15 to 26 also include the theoretical curves from Jeng *et al.* [21], based on the SMMT for PC beams, for comparison.

Figs. 10 to 26 shows that, for most of the beams, the theoretical T - θ curves obtained from MVATM are generally close to the correspondent experimental curves. In general, MVATM also provides good predictions, namely for the ultimate state, as for the SMMT [21]. Moreover, MVATM generally capture better the post-cracking behaviour of the beams.

7. Conclusions

In this study, the theoretical model MVATM for RC beams under torsion is extended to cover PC concrete beams under torsion. Based on the proposed modifications of the MVATM, a calculation procedure was established and implemented to compute the full theoretical T - θ curve for plain or hollow PC beams under torsion.

It was shown that MVATM provides good results when its predictions are compared with the experimental results of PC beams under torsion and also with another theoretical model (SMMT).

MVATM can be considered a good contribution in the attempt to generalize the STA in order to make it able to predict accurately the full behaviour of PC beams under torsion.

References

[1] T.T.C. Hsu, Y.L. Mo, Softening of concrete in Torsional members – theory and tests, J. Am. Concr. Inst. 82 (3) (1985) 290–303.

[2] T.T.C. Hsu, Y.L. Mo, Softening of concrete in Torsional members – Prestressed concrete, J. Am. Concr. Inst. 82 (5) (1985) 603–615.

[3] L.F.A. Bernardo, J.M.A. Andrade, S.M.R. Lopes, Softened truss model for reinforced NSC and HSC beams under torsion: a comparative study, Eng. Struct. 42 (2012) 278–296.

[4] L.F.A. Bernardo, J.M.A. Andrade, Prestressed concrete beams under torsion – Extension of the VATM and evaluation of constitutive relationships, Struct. Eng. Mech., Int. J. 61 (5) (2017) 577–592.

[5] K.N. Rahal, M.P. Collins, Simple model for predicting torsional strength of reinforced and Prestressed concrete sections, J. Am. Concr. Inst. 93 (6) (1996) 658–666.

[6] M.A. Bhatti, A. Almughrabi, Refined model to estimate Torsional strength of reinforced concrete beams, J. Am. Concr. Inst. 93 (5) (1996) 614–622.

[7] W. Wang, C.T.T. Hsu, Limit analysis of reinforced concrete beams subjected to pure torsion, J. Struct. Eng. 123 (1) (1997) 86–94.

[8] J. Silva, B. Horowitz, L. Bernardo, Efficient procedure to analyze RC beam sections using the softened truss model, ACI Struct. J. 114 (3) (2017) 765–774.

[9] G.G. Greene, A. Belarbi, Model for RC members under torsion, bending, and shear. I: theory, J. Eng. Mech. 135 (9) (2009) 961–969.

[10] K.N. Rahal, M.P. Collins, Combined torsion and bending in reinforced and Prestressed concrete beams, ACI Struct. J. 100 (2) (2003) 157–165.

[11] C.S.B. Taborda, Generalization of the VATM and GSVATM to model structural concrete beams under torsion combined with uniforme axial stress state", PhD Thesis, department of civil engineering and architecture, Faculty of Engineering of University of Beira Interior, Covilhã, Portugal, 2017 (in Portuguese).

[12] L.F.A. Bernardo, C.S.B. Taborda, J.M.A. Andrade, Ultimate torsional behaviour of axially restrained RC beams, Comput. Concr., Int. J. 16 (1) (2015) 67–97.

[13] L.F.A. Bernardo, C.S.B. Taborda, J.M.R. Gama, Parametric analysis and torsion design charts for axially restrained RC beams, Struct. Eng. Mech., Int. J. 55 (1) (2015) 1–27.

[14] A.S. Alnauimi, P. Bhatt, Direct design of hollow reinforced concrete beams. Part I: design procedure, Struct. Concr. 5 (4) (2004) 139–146.

[15] J.M. Bairan Garcia, A.R. Mari Bernat, Shear-bending-torsion interaction in structural concrete members: a nonlinear coupled sectional approach, Arch. Comput. Methods Eng. 14 (3) (2007) 249–278.

[16] C.G. Karayannis, Smeared crack analysis for plain concrete in torsion, J. Struct. Eng. 126 (6) (2000) 638–645.

[17] C.G. Karayannis, C.E. Chalioris, Experimental validation of smeared analysis for plain concrete in torsion, J. Struct. Eng. 126 (6) (2000) 646–653.

[18] L.F.A. Bernardo, S.M.R. Lopes, Behaviour of concrete beams under torsion – NSC plain and hollow beams, Mater. Struct. 41 (6) (2008) 1143–1167.

[19] L.F.A. Bernardo, S.M.R. Lopes, Theoretical behaviour of HSC sections under torsion, Eng. Struct. 33 (12) (2011) 3702–3714.

[20] C.-H. Jeng, T.T.C. Hsu, A softened membrane model for torsion in reinforced concrete members, Eng. Struct. 31 (2009) 1944–1954.

[21] C. Jeng, H. Chiu, C. Chen, Modeling the initial stresses in prestressed concrete members under torsion, Struct. Congr. 2010 (2010) 1773–1781.

[22] C.H. Jeng, Unified softened membrane model for torsion in hollow and solid reinforced concrete members: modeling precracking and postcracking behavior, J. Struct. Eng. 141 (10) (2015).

[23] T.T.C. Hsu, R.R.H. Zhu, Softened membrane model for reinforced concrete elements in shear, ACI Struct. J. 99 (4) (2002) 460–469.

[24] L.F.A. Bernardo, J.M.A. Andrade, S.M.R. Lopes, Modified variable angle truss-model for torsion in reinforced concrete beams, Mater. Struct. 45 (12) (2012) 1877–1902.

[25] L.F.A. Bernardo, J.M.A. Andrade, N.C.G. Nunes, Generalized softened variable angle truss-model for reinforced concrete beams under torsion, Mater. Struct. 48 (7) (2015) 2169–2193.

[26] L.F.A. Bernardo, C.S.B. Taborda, J.M.A Andrade, Generalized Softened Variable Angle Truss Model for PC Beams Under Torsion, Int. J. Concr. Struct. Mater. (2018) (under review).

[27] A. Belarbi, T.C. Hsu, Constitutive Laws of Softened Concrete in Biaxial Tension-Compression, Research Report UHCEE 91-92, Univ. of Houston, Houston, Texas, 1991.

[28] L.X. Zhang, T.C. Hsu, Behaviour and analysis of 100 MPa concrete membrane elements, J. Struct. Eng. 124 (1) (1998) 24–34.

[29] A. Belarbi, T.C. Hsu, Constitutive laws of Softened concrete in biaxial tension-compression, Struct. J. Am. Concr. Inst. 92 (5) (1995) 562–573.

[30] NP EN 1992-1 – 1, Eurocode 2: Design of Concrete Structures - Part 1: General Rules and Rules for Buildings, 2010.

[31] L.F.A. Bernardo, S.M.R. Lopes, Torsion in HSC hollow beams: strength and ductility analysis, ACI Struct. J. 106 (1) (2009) 39–48.

[32] W.M. El_Degwy, A.E. McMullen, Prestressed concrete tests compared with torsion theories, PCI J. 30 (5) (1985) 96–127.

[33] L.F.A. Bernardo, J.M.A. Andrade, L.A.P. Oliveira, Reinforced and prestressed concrete hollow beams under torsion, J. Civil. Eng. Manag. 19 (S1) (2013) S141–S152.

[34] D. Mitchell, M.P. Collins, The behavior of structural concrete beams in pure torsion, Civil. Eng. Publ. No (1974) (74-06, Department of civil Engineering, University of Toronto).

[35] F.F. Wafa, S.A. Shihata, S.A. Ashour, A.A. Akhtaruzzaman, Prestressed high-strength concrete beams under torsion, J. Struct. Eng. 121 (9) (1995) 1280–1286.

[36] S.M.R. Lopes, L.F.A. Bernardo, Theoretical model for the mechanical behavior of pre-stressed beams under torsion, Cogent Eng. 1 (1) (2014) 943934.

[37] T.T.C. Hsu, Torsion of Reinforced Concrete, Van Nostrand Reinhold Company, 1984.

[38] H.J. Cowan, Strength of reinforced concrete under the action of combined stresses at the representation of the criterion of failure by a space model, Nature 169 (1952) (663 pp).

[39] ACI Committee 318, Building Code Requirements for Reinforced Concrete, (ACI318-14), American Concrete Institute, 2014.

[40] C.G. Karayannis, C.E. Chalioris, Strength of prestressed concrete beams in torsion, Struct. Eng. Mech., Int. J. 10 (2) (2000) 165–180.

[41] T.T.C. Hsu, Post-cracking torsional rigidity of reinforced concrete sections, J. Am. Concr. Inst. 70 (5) (1973) 352–360.

materials

MDPI

Article

Evaluation of Smeared Constitutive Laws for Tensile Concrete to Predict the Cracking of RC Beams under Torsion with Smeared Truss Model

Mafalda Teixeira and Luís Bernardo *

Centre of Materials and Building Technologies (C-MADE), Department of Civil Engineering and Architecture, University of Beira Interior, 6201-001 Covilhã, Portugal; mafalda.m.teixeira@ubi.pt
* Correspondence: lfb@ubi.pt

Abstract: In this study, the generalized softened variable angle truss-model (GSVATM) is used to predict the response of reinforced concrete (RC) beams under torsion at the early loading stages, namely the transition from the uncracked to the cracked stage. Being a 3-dimensional smeared truss model, the GSVATM must incorporate smeared constitutive laws for the materials, namely for the tensile concrete. Different smeared constitutive laws for tensile concrete can be found in the literature, which could lead to different predictions for the torsional response of RC beams at the earlier stages. Hence, the GSVATM is used to check several smeared constitutive laws for tensile concrete proposed in previous studies. The studied parameters are the cracking torque and the corresponding twist. The predictions of these parameters from the GSVATM are compared with the experimental results from several reported tests on RC beams under torsion. From the obtained results and the performed comparative analyses, one of the checked smeared constitutive laws for tensile concrete was found to lead to good predictions for the cracking torque of the RC beams regardless of the cross-section type (plain or hollow). Such a result could be useful to help with choosing the best constitutive laws to be incorporated into the smeared truss models to predict the response of RC beams under torsion.

Keywords: RC beams; torsion; generalized softened variable angle truss-model (GSVATM); tensile concrete; smeared constitutive law; cracking torque; cracking twist

Citation: Teixeira, M.; Bernardo, L. Evaluation of Smeared Constitutive Laws for Tensile Concrete to Predict the Cracking of RC Beams under Torsion with Smeared Truss Model. *Materials* **2021**, *14*, 1260. https://doi.org/10.3390/ma14051260

Academic Editor: Lizhi Sun

Received: 16 February 2021
Accepted: 4 March 2021
Published: 7 March 2021

1. Introduction

In the second half of the last century, the Space Truss Analogy (STA) was successively refined in order to better predict the response of structural concrete beams under torsion. Nowadays, modern truss-based models can be considered reliable, comprehensive and unified analytical models. They are able to simulate the complex 3-dimensional features of the torsional phenomenon, including the nonlinear behavior and the interaction between the material components of the beam in all loading stages. Models based on the STA constitute the basis models for most codes of practice to establish the design procedures for torsion and still continue to be improved and extended [1,2].

A STA-based model assumes that a reinforced concrete (RC) beam under torsion behaves like a cracked thin tube, where the external torque is resisted through a transversal circulatory shear flow. The tube is modeled with a spatial truss, which includes longitudinal and transverse steel reinforcement under tension interacting with inclined concrete struts under compression. The model satisfies the three Navier's principles of the mechanics of materials, namely, stress equilibrium, strain compatibility and constitutive laws.

Among the STA-based models that have been developed, one of the most commonly used and extended is the Variable-Angle Truss Model (VATM), which was originally proposed by Hsu and Mo in 1985 [3]. This model incorporated for the first time smeared constitutive laws, or smeared stress (σ)—strain (ε) relationships, for both tensile steel reinforcement embedded in concrete and compressive concrete. Such constitutive laws

are established from controlled experimental tests on RC panels under in-plane shear, in order to account for, on average (considering an area sufficiently wide to include several cracks), the effect of the biaxial stress state in the principal direction of stresses, the effect of cracking, the interaction between the material components, and both the softening and stiffening effects. The Universal Panel Tester at the University of Houston is one of the testing devices which has most contributed to the establishment of smeared constitutive laws for smeared truss models [4].

Despite being a nonlinear model with an incremental and iterative calculation procedure, the VATM is relatively simple to implement, having access to programming languages in a computer. The model allows us to calculate the full response of RC beams under torsion, namely the torque (M_T)–twist (θ) curve. The predictions from the VATM showed good agreement with experimental results, namely when predicting the response of RC beams under torsion at the ultimate stage [3,5,6]. When compared with more complex models also proposed for the RC beam under torsion, which sometimes involve large computational effort (for instance [7–10]), the VATM is recognized as a simpler and more reliable model for predicting the torsional strength of RC beams under torsion, which is one of the most important key parameters for design. It should also be mentioned that smeared approaches, such as the VATM, constitute an alternative approach to local ones in which the local fracture properties are directly accounted for, such as in the numerical models from [11,12]. In smeared approaches, smeared constitutive laws for the materials are incorporated into the model. Such models have been shown to be reliable, on average, for modeling the global behavior of structural elements, such as for the RC beams under torsion.

The VATM has been extended for prestress concrete (PC) beams [13] and also for axially restrained RC beams [14,15]. The VATM was also improved in order to reliably predict the response of RC beam under torsion for the low loading stages, namely the transition between the uncracked stage and the cracked stage. This was achieved by incorporating into the model the contribution of the tensile concrete (neglected in the VATM) through an additional smeared σ—ε constitutive law in the perpendicular direction to the concrete struts. The new model, called generalized softened variable angle truss-model (GSVATM), was proposed in 2015 for RC solid beams under torsion [16]. The predictions from the GSVATM showed good agreement with experimental results for all loading stages. The GSVATM was recently extended for PC beams [17], hollow RC beams [18] and RC flanged beams [19]. A unified version of the model was also recently proposed [2].

The predictions from any smeared truss model, such as the VATM or the GSVATM, strongly depend on the smeared σ—ε relationships for the materials. This important aspect was previously demonstrated by Bernardo et al. in 2012 [20] for the prediction of the torsional strength and corresponding twist for the RC beams under torsion. The study aimed to find the most reliable smeared σ—ε relationships for the materials, among the several ones found in the literature, to be incorporated into the VATM to better predict the ultimate response of RC beams under torsion. The best constitutive laws found in [20], for both the concrete in compression and steel reinforcement in tension, were posteriorly incorporated in the GSVATM [16]. Bernardo et al. in 2012 [20] did not include in their study the prediction of the key parameters for the low loading stages because, as referred to before, the predictions from the VATM were shown to be in good agreement with the experimental results only for the ultimate stage. This is mainly because the model assumes that the member has been fully cracked since the beginning of loading, which is not true.

For design, it is also important to reliably predict the behavior for the low loading levels. The current codes of practice compel us to check the structural members for both the serviceability and ultimate limit states. For the first one, it is important that the cracking torque is known. As previously referred to, the GSVATM is able to predict the full response of the RC beams under torsion, including the transition between the uncracked stage and the cracked stage. The prediction of such a transition zone highly depends on the smeared constitutive law for the tensile concrete. As for the other constitutive laws referred to

(for concrete in compression and steel reinforcement in tension), different proposals of smeared constitutive laws for tensile concrete can be found in the literature. To the best of the authors' knowledge, no previous study was found with the aim of checking such constitutive laws in smeared truss models, in order to evaluate which features allow the model to give the best predictions for the low loading stages. Usually, researchers working with smeared truss models use their own smeared constitutive laws or choose them based on the proposals from other studies.

In this study, the GSVATM is used to check some proposed smeared constitutive laws for tensile concrete found in the literature. The GSVATM was the chosen model because, as previously stated, it is able to predict the full response of the RC beams under torsion for all loading stages. In addition, this model was proposed by the corresponding author [16] and has also been successfully used in previous studies [2,17–19,21]. The chosen parameters to be studied are the cracking torque and the corresponding twist. The theoretical predictions of such parameters are compared with the experimental results from several reported tests on RC beams under torsion. Only RC beams with rectangular sections are studied because they constitute the current solution used in practice. In addition, the number of reported experimental results in the literature for such beams is much higher than for other typologies such as PC beams or beams with a flanged cross-section.

2. The Generalized Softened Variable Angle Truss-Model

For the sake of the readers of this article, a brief description of the GSVATM is presented. The GSVATM was initially proposed for RC plain beams under torsion [16]. Recently, the model was extended and unified for RC hollow beams under torsion [18]. Details about the assumptions of the model, the derivation of the equations and the justification of the calculation solution procedure can be found [16,18].

According to the GSVATM, a cracked RC thin beam element under a vertical shear force V, which induces a shear flow q in the cross-section, is modeled with a smeared plain truss analogy, as illustrated in Figure 1. The behavior of the RC thin beam is governed by Equations (1) to (5). The smeared plain truss incorporates inclined concrete struts (with compressive force C) with an angle α to the longitudinal axis, and perpendicular concrete ties (with tensile force T). The corresponding stress fields are denoted by σ_2^c and σ_1^c, respectively. The meanings of the parameters are (see Figure 1): R is the resultant force, β is the angle of R to the force C, γ is the angle of R to the longitudinal axis, t_c is the width of the cross-section and d_v is the distance between centers of the longitudinal bars.

$$R = \sqrt{C^2 + T^2} \tag{1}$$

$$\beta = \arctan(T/C) \tag{2}$$

$$\gamma = \alpha + \beta \tag{3}$$

$$C = \sigma_2^c t_c d_v \cos\alpha \tag{4}$$

$$T = \sigma_1^c t_c d_v \sin\alpha \tag{5}$$

An equivalent cracked RC hollow beam under a torque M_T, as illustrated in Figure 2, is modeled as the union of four thin beam elements as in Figure 1. Each thin beam constitutes a wall of the RC hollow beam. As a result of this union, the torque M_T induces a circulatory shear flow q and the beam can be modeled with a smeared spatial truss analogy. The center line of the circulatory shear flow q coincides with the center line of the walls. The behavior of the RC hollow beam is governed by equilibrium equations, Equations (6) to (8), and compatibility equations, Equations (9) to (12). If $\gamma = \alpha + \beta > 90°$, Equation (7) must be multiplied by (-1). The previous equations account for the strain gradient along the walls' thickness due to the bidirectional opposite curvatures induced by bending (Figure 3).

$$M_T = \frac{2AR\sin\gamma}{d_v} \tag{6}$$

$$t_c = \frac{A_{sl} f_{sl}}{\sigma_2^c p} \frac{\cos\beta}{\cos\alpha \cos\gamma} \text{ for } \gamma = \alpha + \beta \leq 90^\circ \tag{7}$$

$$\alpha = \arctan\left(\frac{\sqrt{F^2(\tan\beta)^2 + F(\tan\beta)^4 + F + (\tan\beta)^2}}{F(\tan\beta)^2 + 1}\right) \text{ with } F = \frac{A_{st} f_{st} p}{A_{sl} f_{sl} s} \tag{8}$$

$$\varepsilon_{st} = \left(\frac{A_0^2 \sigma_2^c \sin\gamma}{p M_T \cos\beta \tan\alpha \sin\alpha} - \frac{1}{2}\right) \varepsilon_{2s}^c \tag{9}$$

$$\varepsilon_{sl} = \left(\frac{A_0^2 \sigma_2^c \sin\gamma}{p M_T \cos\beta \cot\alpha \sin\alpha} - \frac{1}{2}\right) \varepsilon_{2s}^c \tag{10}$$

$$\theta = \frac{\varepsilon_{2s}^c}{2 t_c \sin\alpha \cos\alpha} \tag{11}$$

$$\varepsilon_{1s}^c = 2\varepsilon_1^c = 2\varepsilon_{sl} + 2\varepsilon_{st} + \varepsilon_{2s}^c \tag{12}$$

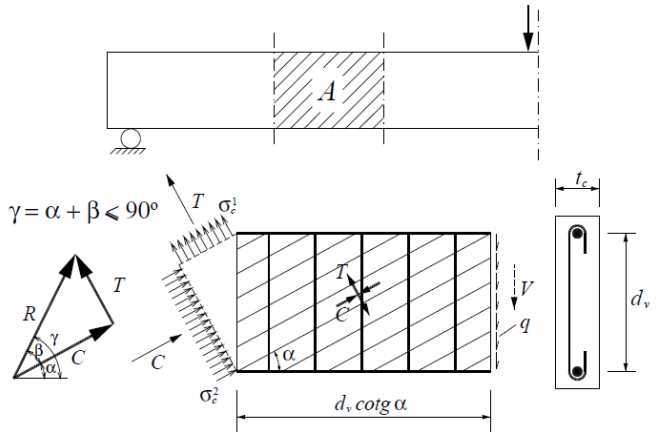

Figure 1. Reinforced concrete (RC) thin beam element [18].

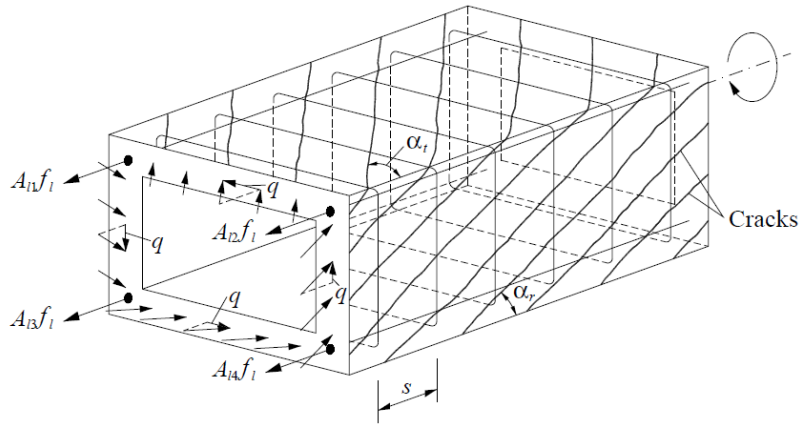

Figure 2. RC hollow beam element [18].

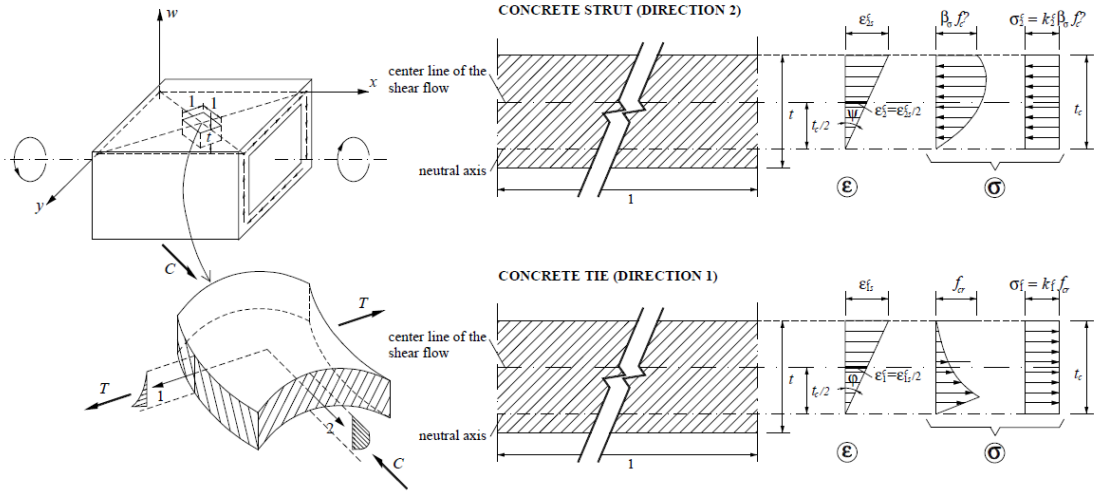

Figure 3. Curvatures and strain gradient in the walls [18].

In the previous equations (see Figures 2 and 3), t_c is the effective thickness of the concrete strut and tie in the walls, $A = (x - t_c)(y - t_c)$ and $p = 2(x - t_c) + 2(y - t_c)$ are the area enclosed and the perimeter of the center line of the shear flow q (with x the minor and y the major outer dimension of the beam's cross-section), respectively, A_{sl} is the total area of the longitudinal reinforcement, A_{st} is the area of one rebar of the transverse reinforcement, s is the longitudinal spacing of the transverse reinforcement, f_{sl} and f_{st} are the tensile stresses in the longitudinal and transverse reinforcement, respectively, ε_{sl} and ε_{st} are the tensile strains in the longitudinal and transverse reinforcement, respectively, ε^c_{2s} and ε^c_{1s} are the strains at the outer fiber of the concrete strut and concrete tie, respectively, ε^c_1 is the average strain in the concrete tie, and θ is the twist per unit length.

As referred to in the introduction section, the GSVATM incorporates smeared σ—ε relationships to model the behavior of the compressive concrete in the struts, the tensile concrete in the ties and the tensile longitudinal and transverse steel reinforcement (rebars embedded in concrete). For the RC beams under torsion, some suitable smeared σ—ε relationships were previously found by Bernardo et al. in 2012 [20] and are also used in this study. For the compressive concrete, the smeared σ—ε relationship proposed by Belarbi and Hsu in 1995 [22] (Equations (13) and (14)) with softening factor $\beta_* = \beta_\sigma = \beta_\varepsilon$, for both the peak stress and corresponding strain, proposed by Zhang and Hsu in 1998 [23] (Equations (15) to (18)) are used. For the steel reinforcement in tension, the smeared σ—ε relationship proposed by Belarbi and Hsu in 1994 [24] (Equations (19) to (21)) is used.

The meaning of the parameters are: f'_c is the average uniaxial concrete compressive strength, ε_o is the strain corresponding to f'_c, ε^c_2 is the average strain in the concrete strut (Figure 3), ρ_l and ρ_t are the longitudinal ($\rho_l = A_{sl}/A_c$, with $A_c = xy$) and transverse ($\rho_t = A_{st}u/A_c s$, with $u = 2x + 2y$) reinforcement ratios, respectively, f_{ly} and f_{ty} are the yielding stresses for the longitudinal and transverse reinforcement, respectively, f_{cr} is the tensile concrete strength, ε_{cr} is the strain corresponding to f_{cr}, f_s and ε_s are the stress and strain in the steel reinforcement (longitudinal or transversal), respectively, E_s is the Young's Modulus for steel reinforcement, f_y is the yielding stress of steel reinforcement (longitudinal or transversal) and ρ is the reinforcement ratio (longitudinal or transversal).

$$\sigma^c_2 = \beta_\sigma f'_c \left[2\left(\frac{\varepsilon^c_2}{\beta_\varepsilon \varepsilon_o}\right) - \left(\frac{\varepsilon^c_2}{\beta_\varepsilon \varepsilon_o}\right)^2 \right] \text{ if } \varepsilon^c_2 \leq \beta_\varepsilon \varepsilon_o \quad (13)$$

$$\sigma_2^c = \beta_\sigma f_c' \left[1 - \left(\frac{\varepsilon_2^c - \beta_\varepsilon \varepsilon_o}{2\varepsilon_o - \beta_\varepsilon \varepsilon_o}\right)^2\right] \text{ if } \varepsilon_2^c > \beta_\varepsilon \varepsilon_o \quad (14)$$

$$\beta_* = \beta_\sigma = \beta_\varepsilon = \frac{R(f_c')}{\sqrt{1 + \frac{400\varepsilon_1^c}{\eta'}}} \quad (15)$$

$$\eta = \frac{\rho_l f_{ly}}{\rho_t f_{ty}} \quad (16)$$

$$\begin{cases} \eta \leq 1 \Rightarrow \eta' = \eta \\ \eta > 1 \Rightarrow \eta' = 1/\eta \end{cases} \quad (17)$$

$$R(f_c') = \frac{5.8}{\sqrt{f_c'(\text{MPa})}} \leq 0.9 \quad (18)$$

$$f_s = \frac{0.975 E_s \varepsilon_s}{\left[1 + \left(\frac{1{,}1 E_s \varepsilon_s}{f_y}\right)^m\right]^{\frac{1}{m}}} + 0.025 E_s \varepsilon_s \quad (19)$$

$$m = \frac{1}{9B - 0.2} \leq 25 \quad (20)$$

$$B = \frac{1}{\rho}\left(\frac{f_{cr}}{f_y}\right)^{1.5} \quad (21)$$

For the tensile concrete, the smeared σ—ε relationships checked in this study are presented in more detail in the Section 3. However, in order to present the equations for some correction coefficients and also the flowchart with the calculation procedure for the GSVATM, the following general and common form of the equations are written ($F(\ldots)$ stands for "function of ... "):

$$\sigma_1^c = E_c \varepsilon_1^c \text{ if } \varepsilon_1^c \leq \varepsilon_{cr} \quad (22)$$

$$\sigma_1^c = F(f_{cr}; \varepsilon_1^c) \text{ if } \varepsilon_1^c > \varepsilon_{cr} \quad (23)$$

In Equation (22), which models the linear–elastic stage before cracking, E_c is the Young's Modulus for the concrete. Based on the proposals from previous studies [9,25,26], and in order to unify the GSVATM for both the RC plain and the hollow beams under torsion, and also to improve the predictions from the model for the low loading stages, in 2019 Bernardo [18] presented a set of equations (Equations (24) to (29)) to compute the parameters ε_{cr} and E_c, accounting for the correction coefficients μ and λ. These equations apply for all smeared σ—ε relationships for tensile concrete presented in the Section 3 and checked in this study.

$$\varepsilon_{cr} = 0.00008\mu \quad (24)$$

$$E_c = 3875\lambda\sqrt{f_c' \text{ (MPa)}} \quad (25)$$

$$\mu = \lambda = 1.45 \text{ (RC solid beams)} \quad (26)$$

$$\mu = \lambda = 0.93 \text{ (RC thin-walled hollow beams)} \quad (27)$$

$$\mu = \lambda = 1.20 \text{ (RC thick-walled hollow beams and } f_c' \leq 48 \text{ MPa)} \quad (28)$$

$$\mu = \lambda = 1.129 \text{ (RC thick-walled hollow beams and } f_c' > 48 \text{ MPa)} \quad (29)$$

The classification of the RC hollow beams into "thin wall" or "thick wall" [26] is done during the calculation procedure of the GSVATM. The RC hollow beam is firstly calculated as an equivalent RC plain beam until both the cracking torque $M_{Tcr,plain}$ and the corresponding value for the effective wall's thickness $t_{c,cr,plain}$ are computed. Then, the following classification applies (with t being the real thickness of the wall of the RC hollow beam):

- if $t \leq 0.91 t_{c,cr,plain}$ the RC hollow beam has a "thin wall";

- if $t > 0.91 t_{c,cr,plain}$ the RC hollow beam has a "thick wall".

Then, the beam is recalculated considering the real cross-section (hollow).

For the RC beams under torsion, average stresses σ_2^c (Equation (30)) and σ_1^c (Equation (31)) are computed for the concrete strut and tie, respectively, accounting for the section type through the correction coefficient η (Equations (32) to (35)). This simplification is assumed because the real stress diagrams along the effective wall's thickness t_c are not uniform due to the strain gradient (Figure 3). The coefficients k_2^c and k_1^c are computed from the numerical integration of the smeared σ—ε relationships.

$$\sigma_2^c = \eta k_2^c \beta_\sigma f_c' \tag{30}$$

$$\sigma_1^c = \eta k_1^c f_{cr} \tag{31}$$

$$\eta = 1 \text{ (RC solid beams)} \tag{32}$$

$$\eta = 0.033\sqrt{f_c' \text{ (MPa)}} + 0.73 \text{ (RC thin-walled hollow beams)} \tag{33}$$

$$\eta = 0.0938\sqrt{f_c' \text{ (MPa)}} + 0.43 \text{ (RC thick-walled hollow beams and } f_c' \leq 48 \text{ MPa)} \tag{34}$$

$$\eta = \frac{8.45}{\sqrt{f_c' \text{ (MPa)}}} + 0.17 \text{ (RC thick-walled hollow beams and } f_c' > 48 \text{ MPa)} \tag{35}$$

To solve the nonlinear procedure of the GSVATM, an algorithm incorporating a trial-and-error technique was implemented using the programming language Delphi (see flowchart in Figure 4) [16,18]. For each iteration, the input parameter $\varepsilon_{2s}^c = 2\varepsilon_2^c$ (strain at the outer fiber of the concrete strut) is incremented in order to compute each solution point to draw the theoretical M_T—θ curve. The calculation procedure ends when the assumed failure strains for the materials is reached, either for concrete in compression (ε_{cu}) or for steel reinforcement in tension (ε_{su}). In this study, European code Eurocode 2 was used to define the conventional failure strains for the materials.

3. Smeared Constitutive Laws for Tensile Concrete

This section presents eight smeared σ—ε relationships for tensile concrete proposed in previous studies (laws *l*1 to *l*8), so that they can be implemented in the GSVATM and checked (Section 4). In a previous study, it was showed that these relationships are suitable to be implemented in smeared truss models, such as the GSVATM, to account for the contribution of the tensile concrete [27].

Some of the presented smeared σ—ε relationships for tensile concrete were proposed based on the experimental results from concrete panels under shear. In such cases, the average stress σ_1^c in the tensile concrete after cracking ($\varepsilon_1^c > \varepsilon_{cr}$) is usually obtained from the equilibrium of the stress fields applied to the panels by separating the average stresses in both the tensile steel reinforcement and the tensile concrete. The other smeared σ—ε relationships for tensile concrete were proposed by refining the previous ones in order to improve the predictions of the used smeared models.

For all presented smeared σ—ε relationships for tensile concrete, two equations are written. The first one aims to model the tensile behavior of the concrete before cracking and is equal for all smeared constitutive laws:

$$\sigma_1^c = E_c \varepsilon_1^c \text{ if } \varepsilon_1^c \leq \varepsilon_{cr} \tag{36}$$

The second equation aims to model the tensile behavior of the concrete after cracking, and accounts for the tension softening (the influence of the cracks) and the tension stiffening (the retention of concrete tensile stress due to the interaction with steel reinforcement).

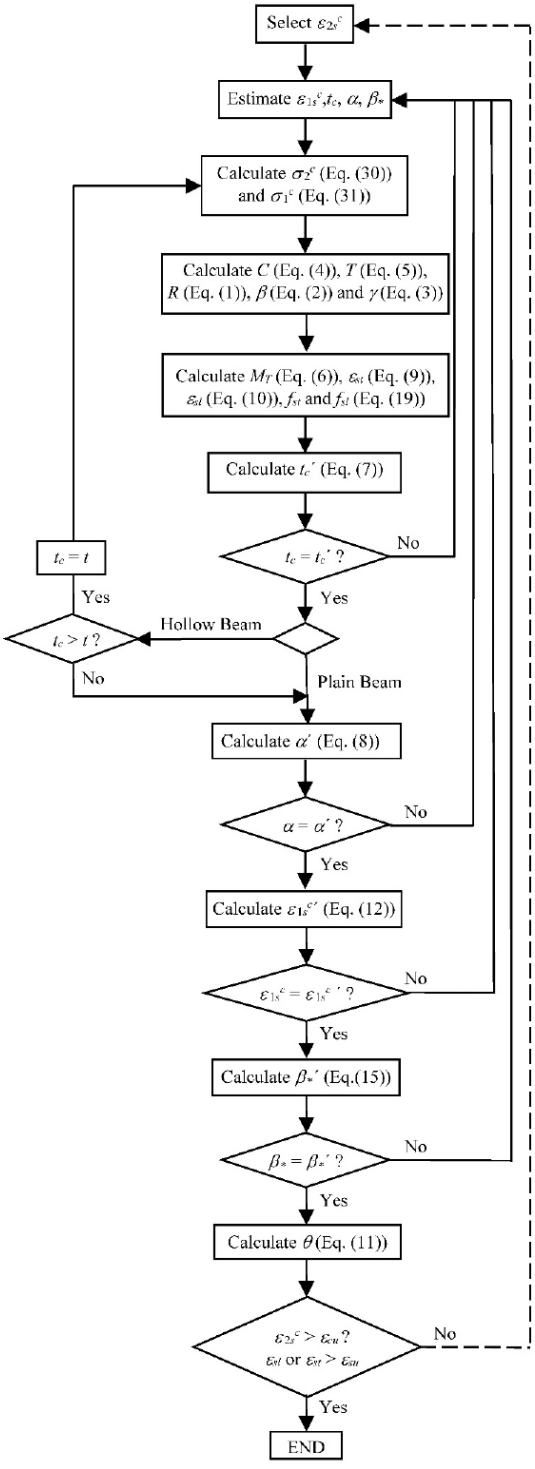

Figure 4. Flowchart.

As presented in Section 2, parameters ε_{cr} and E_c are computed according to Equations (24) and (25), which apply for all the presented smeared σ—ε relationships. Further, for all presented equations, the symbology was adapted to the same one used in the previous section.

3.1. Law l1—Cervenka in 1985

In 1985, Cervenka proposed a smeared model for cracked RC panels. In this model, the author implemented the following equation for the descending branch of the smeared σ—ε relationships for tensile concrete [28]:

$$\sigma_1^c = f_{cr}\left[1 - \left(\frac{\varepsilon_1^c}{c}\right)^{k_2}\right] \text{ if } \varepsilon_1^c > \varepsilon_{cr} \tag{37}$$

Parameter c is the average tensile strain (ε_1^c) for which the principal tensile stress can be considered null. The author observed that c ranges between 0.004 and 0.005. For this study, the average value (0.0045) was considered. The exponent k_2 is related with the curvature shape of the descending branch of the σ—ε curve after the peak tensile stress. Cervenka proposed to consider $k_2 = 0.5$.

3.2. Law l2—Vecchio and Collins in 1986

In 1986, based on several experimental results from RC panels under shear performed at the University of Toronto, Vecchio and Collins proposed the smeared model called Modified Compression Field Theory. For this model, the following postpeak smeared σ—ε relationship for tensile concrete was proposed [29]:

$$\sigma_1^c = \frac{f_{cr}}{1 + \sqrt{200\varepsilon_1^c}} \text{ if } \varepsilon_1^c > \varepsilon_{cr} \tag{38}$$

3.3. Law l3—Hsu in 1991

In 1991, Hsu [30] proposed an efficient algorithm for his softened truss model theory to analyze the nonlinear behavior of concrete membrane elements. For this model, a refined version of the postpeak smeared σ—ε relationship for tensile concrete from Vecchio and Collins in 1986 [29] was proposed:

$$\sigma_1^c = \frac{f_{cr}}{1 + \sqrt{\frac{\varepsilon_1^c - \varepsilon_{cr}}{0.005}}} \text{ if } \varepsilon_1^c > \varepsilon_{cr} \tag{39}$$

3.4. Law l4—Belarbi and Hsu in 1994

Based on experimental studies on RC panels under shear performed at the University of Houston, Belarbi and Hsu in 1994 [24] proposed Equation (40) for the descending branch of the smeared constitutive law for tensile concrete.

$$\sigma_1^c = f_{cr}\left(\frac{\varepsilon_{cr}}{\varepsilon_1^c}\right)^{0.4} \text{ if } \varepsilon_1^c > \varepsilon_{cr} \tag{40}$$

3.5. Law l5—Collins and Colaborators in 1996

In 1996, Collins et al. [31] proposed a postpeak smeared constitutive law for tensile concrete slightly different from the one proposed by Vecchio and Collins in 1986 [29]:

$$\sigma_1^c = \frac{f_{cr}}{1 + \sqrt{500\varepsilon_1^c}} \text{ if } \varepsilon_1^c > \varepsilon_{cr} \tag{41}$$

3.6. Law l6—Vecchio in 2000

The Disturbed Stress Field Model for RC was proposed by Vecchio in 2000 [32]. For this model, the author proposed a somewhat more complicated postpeak smeared constitutive law for tensile concrete, in order to account more precisely for the tension stiffening. The author proposed two equations, with a maximum condition, to also account indirectly for the level of reinforcement ratio (Equations (42) to (45)). When a low (high) reinforcement ratio exists, tension softening (stiffening) is more relevant.

$$\sigma_1^c = \max\left(f_{c1}^a; f_{c1}^b\right) \text{ if } \varepsilon_1^c > \varepsilon_{cr} \tag{42}$$

$$f_{c1}^a = f_{cr}\left(1 - \frac{\varepsilon_1^c - \varepsilon_{cr}}{\varepsilon_{ts} - \varepsilon_{cr}}\right) \tag{43}$$

$$f_{c1}^b = \frac{f_{cr}}{1 + \sqrt{c_t \varepsilon_1^c}} \tag{44}$$

$$\varepsilon_{ts} = 2.0\frac{G_f}{f_{cr} L_r} \tag{45}$$

Parameter ε_{ts} represents the terminal strain, which depends on the fracture energy (G_f), assumed to be constant and equal to 75 N/m by Vecchio, and also on half of the distance between cracks (L_r). Parameter c_t can be simply considered equal to 200 for small members or for members incorporating steel reinforcement grids with very small spacing, and 500 for large members. For this study, L_r was infered from the experimental data of the used reference beams (Section 4).

3.7. Law l7—Bentz in 2005

In 2005, Bentz proposed Equations (46) and (47) for the smeared postpeak tension stiffening relationship of tensile concrete [33].

$$\sigma_1^c = \frac{f_{cr}}{1 + \sqrt{3.6 M \varepsilon_1^c}} \text{ if } \varepsilon_1^c > \varepsilon_{cr} \tag{46}$$

$$M = \frac{A_c}{\sum \phi \pi} \tag{47}$$

Parameter M (in "mm" units) accounts for the effective tensile concrete area around the rebars (A_c) and for the rebars' diameter (ϕ). For this study, A_c was computed considering the effective thickness of the concrete tie (t_c), which is computed from the GSVATM.

3.8. Law l8—Stramandinoli and Rovere in 2008

In 2008, for the nonlinear analysis of reinforced concrete members, Stramandinoli and Rovere proposed equations for the postpeak smeared constitutive law for tensile concrete [34] (Equations (48) to (50)). The law accounts directly for the longitudinal reinforcement ratio ρ.

$$\sigma_1^c = f_{cr} e^{-\alpha\left(\frac{\varepsilon_1^c}{\varepsilon_{cr}}\right)} \text{ if } \varepsilon_1^c > \varepsilon_{cr} \tag{48}$$

$$\alpha = 0.017 + 0.255(n\rho) - 0.106(n\rho)^2 + 0.016(n\rho)^3 \tag{49}$$

$$n = \frac{E_s}{E_c} \tag{50}$$

3.9. Comparison between the Smeared Constitutive Laws

For comparison, Figure 5 illustrates the smeared σ—ε curves for tensile concrete for each of the proposals presented in the previous subsections. The curves were computed considering the same arbitrary and typical cross-section with current materials.

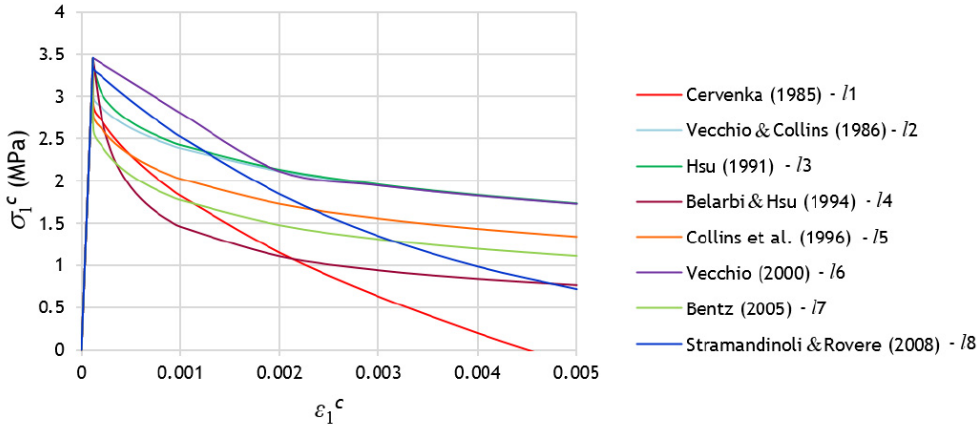

Figure 5. Comparison between the smeared constitutive laws.

After the peak stress, namely for the descending branch, Figure 5 shows high variability between the σ—ε curves. In spite of the peak stress coincides for all the curves, it should be noted that the referred variability will influence the calculation of the cracking torque and corresponding twist with the GSVATM. This is because, as previously referred, the tensile stress σ_1^c computed from Equation (31) represents an average stress since the real stress diagram along the effective tie's thickness is not uniform due to the strain gradient (Figure 3). The representative concrete tensile stress in the GSVATM (σ_1^c) does not coincide with the maximum tensile stress. Hence, the strain ε_1^c corresponding to the effective cracking torque in the M_T—θ curve computed with the GSVATM does not coincide with the strain ε_{cr} corresponding to the peak stress in the smeared σ—ε curves for tensile concrete. This is illustrated in Figure 6, where an example of M_T—θ and corresponding σ—ε curves for tensile concrete, computed with the GSVATM, are presented. The highlighted point in the curves (with marker " ●") corresponds to the effective cracking torque, which is reached for a strain $\varepsilon_1^c > \varepsilon_{cr}$, i.e., in the descending branch of the smeared σ—ε curve for tensile concrete. This explains why different smeared σ—ε curves for tensile concrete incorporated in the GSVATM will lead to different coordinates for the cracking torque (cracking torque and corresponding twist).

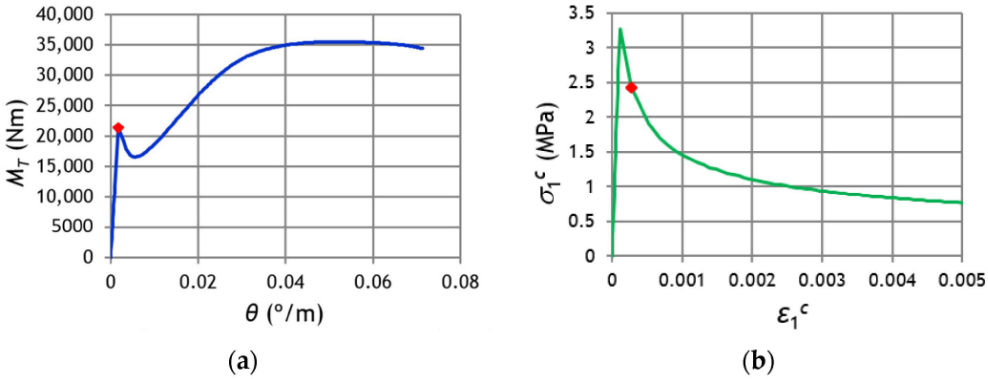

Figure 6. Location of the effective cracking point.

4. Comparison with Experimental Results

For this study, the experimental results of 103 RC beams tested under torsion were collected from the literature. Both RC beams with plain and hollow rectangular cross section were considered. These beams were selected based on criteria related to minimum requirements from codes of practice (for instance, the beams should incorporate a minimum torsional reinforcement, the spacing between rebars should not exceed the maximum allowed, etc.) in order to ensure a typical behavior under torsion. A detailed discussion on such applied criteria can be found in [21]. For the RC plain beams, the data were collected from the following studies: Hsu in 1968 [35], McMullen and Rangan in 1978 [36], Koutchkali and Belarbi in 2001 [37], Fang and Shiau in 2004 [38], and Peng and Wong in 2011 [39]. For RC hollow beams, the following studies were consulted: Hsu in 1968 [35], Lampert and Thürlimann in 1969 [40], Leonhardt and Schelling in 1974 [41], Bernardo and Lopes in 2009 [42], and Jeng in 2015 [26].

Table A1 in Appendix A summarizes the main properties for each reference beam. In Table 1, "P" and "H" stand for "plain" and "hollow" cross-section, respectively. For all the reference beams from Table A1, the experimental values of the cracking torque (M_{Tcr}^{exp}) and corresponding twist (θ_{cr}^{exp}) were obtained from the data or graphs given by the authors [26,35–42]. Such values are presented for each reference beam in Tables A2–A4 (see Appendix A).

Table 1. Comparative analysis.

Cross-Section		P		H		P + H	
Constitutive law		$\frac{M_{Tcr}^{exp}}{M_{Tcr}^{thli}}$	$\frac{\theta_{cr}^{exp}}{\theta_{cr}^{thli}}$	$\frac{M_{Tcr}^{exp}}{M_{Tcr}^{thli}}$	$\frac{\theta_{cr}^{exp}}{\theta_{cr}^{thli}}$	$\frac{M_{Tcr}^{exp}}{M_{Tcr}^{thli}}$	$\frac{\theta_{cr}^{exp}}{\theta_{cr}^{thli}}$
*l*1—Cervenka (1985) [28]	$\overline{x}$ =	1.02	1.16	1.29	1.71	1.05	1.23
	$cv(\%)$ =	12.13	25.19	21.47	35.22	21.29	38.54
*l*2—Vecchio and Collins (1986) [29]	$\overline{x}$ =	0.96	1.11	1.24	1.62	0.99	1.16
	$cv(\%)$ =	12.41	25.68	21.47	35.61	21.73	39.13
*l*3—Hsu (1991) [30]	$\overline{x}$ =	0.91	1.04	1.18	1.55	0.94	1.10
	$cv(\%)$ =	12.38	25.83	21.66	36.11	22.13	40.05
*l*4—Belarbi and Hsu (1994) [24]	$\overline{x}$ =	1.00	1.16	1.03	1.42	1.01	1.19
	$cv(\%)$ =	11.35	24.10	32.17	46.05	21.45	39.02
*l*5—Collins et al. (1996) [31]	$\overline{x}$ =	1.04	1.20	1.33	1.74	1.07	1.24
	$cv(\%)$ =	12.31	25.29	21.49	35.97	21.36	39.23
*l*6—Vecchio (2000) [32]	$\overline{x}$ =	0.96	1.08	1.18	1.50	1.00	1.15
	$cv(\%)$ =	11.82	26.20	19.22	37.88	18.56	37.43
*l*7—Bentz (2005) [33]	$\overline{x}$ =	0.94	1.08	1.26	1.68	0.99	1.16
	$cv(\%)$ =	12.24	25.91	21.23	34.90	22.79	40.35
*l*8—Stramandinoli and Rovere (2008) [34]	$\overline{x}$ =	0.86	0.98	1.13	1.46	0.89	1.06
	$cv(\%)$ =	12.84	26.75	22.11	36.09	22.72	39.36

The torsional response of all the reference beams was computed using the GSVATM, for each of the smeared σ—ε relationships for the tensile concrete presented in Section 3 (laws *l*1 to *l*8). From the obtained theoretical M_T—θ curves, the theoretical coordinates of the cracking point, i.e., the cracking torque (M_{Tcr}^{thli}, with $i = 1$ to 8) and corresponding twists, i.e., the cracking twists (θ_{cr}^{thli}, with $i = 1$ to 8), were obtained. Such values are also presented for each reference beam in Tables A2–A4 (see Appendix A). In addition, the ratios between the experimental to the theoretical values are also presented for each reference beam ($M_{Tcr}^{exp}/M_{Tcr}^{thli}$ and $\theta_{cr}^{exp}/\theta_{cr}^{thli}$, with $i = 1$ to 8).

Figure 7 presents, as an example, a graph with the experimental and theoretical M_T—θ curves, computed for each smeared constitutive law for tensile concrete, for reference beam N-20-20 [38]. Figure 7 confirms that the coordinates of the cracking point, namely the cracking torque, as well as the postcracking response, highly depends on the used smeared

constitutive law for the tensile concrete. The influence of the used smeared constitutive law is residual at the ultimate stage, namely for the maximum torque.

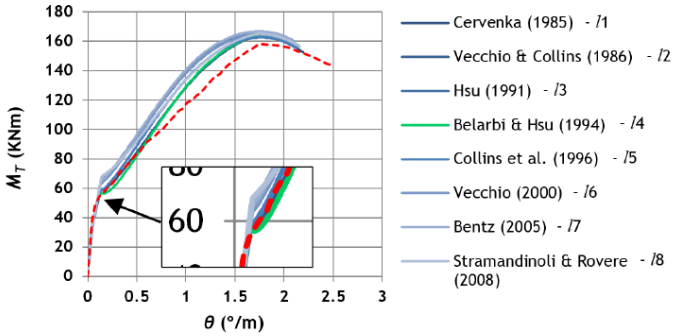

Figure 7. Example of M_T—θ curves for reference beam N-20-20.

Table 1 summarizes and compares the results from Tables A2–A4 (Appendix A) for the cracking torque (M_{Tcr}^{exp}) and corresponding twist (θ_{cr}^{exp}). For this, the following statistical parameters were computed for each ratio $M_{Tcr}^{exp}/M_{Tcr}^{thli}$ and $\theta_{cr}^{exp}/\theta_{cr}^{thli}$ ($i = 1$ to 8): the average value ($\overline{x}$) and the coefficient of variation ($cv(\%) = 100 \times s/\overline{x}$, with s being the sample standard deviation). Table 1 also presents separately the results for plain (P) and hollow (H) beams. This is because some studies showed that noticeable differences exist between the response of plain and hollow beams under torsion for the low loading stages, namely for the transition between the uncracked and the cracked stage [26].

Table 1 shows that, for the RC plain beams, the smeared constitutive laws *l*1, *l*2, *l*4, *l*5 and *l*6 allow us to predict the cracking torque M_{Tcr} (with $0.95 < \overline{x} < 1.05$) very well and with a very acceptable degree of dispersion ($cv < 13\%$). Among those models, the smeared constitutive law *l*4 from Belarbi and Hsu (1994) [24] is the best (with $\overline{x} = 1.00$ and $cv = 11.35\%$). For the RC hollow beams, this constitutive law gives the better average value $\overline{x} = 1.03$, although the degree of dispersion is high ($cv = 32.17\%$). The higher difficulty of reliably predicting the cracking torque for the RC hollow beams, when compared with the RC plain beams, was also observed and discussed in previous studies [18,26,27]. In particular, the RC hollow beams are more sensitive to the high variability of concrete tensile strength, which highly influences the cracking torque. When all beams are considered together, the smeared constitutive laws *l*2, *l*4, *l*6 and *l*7 give the best results with $\overline{x} \approx 1.00$, although the degree of dispersion is higher ($cv < 23\%$) due to the influence of the results for the RC hollow beams. In general, it can be stated that the smeared constitutive law *l*4 from Belarbi and Hsu (1994) [24] allows us to best predict the cracking torque, regardless of the cross-section type. This constitutive law has been widely used by authors in previous studies [9,16–19,23,26]. The results from Table 1 confirm the validity of such studies having chosen this smeared constitutive law for tensile concrete.

Regarding the twist corresponding to the cracking torque (θ_{cr}), Table 1 shows that, in general, there is a higher difficulty in obtaining a good prediction of this parameter. The constitutive laws *l*3 and *l*8 give the best average values for both the RC plain beams ($0.95 < \overline{x} < 1.05$) and also for all the RC beams together ($\overline{x} \leq 1.10$). However, the dispersion of these results is high ($cv > 25\%$). The results are the worst for the RC hollow beams, which was also reported in previous studies [17,18,25,27]. One possible explanation for this is that the experimental twists are very small until the end of the uncracked stage. Hence, experimental limitations related to the accurate measurement of the twists at this stage are expected. However, since the cracking twist is not very important for design, the previously reported worst results can also be considered not very important.

Figure 8 presents, for each smeared constitutive law (*l*1 to *l*8), scatter graphs showing the experimental versus the theoretical values for the cracking torque. Similar graphs are

not presented for the cracking twist because of the high dispersion of the results previously reported. In the graphs, different markers were used to distinguish the results regarding the cross-section type, namely "■" for RC plain beams and "□" for RC hollow beams.

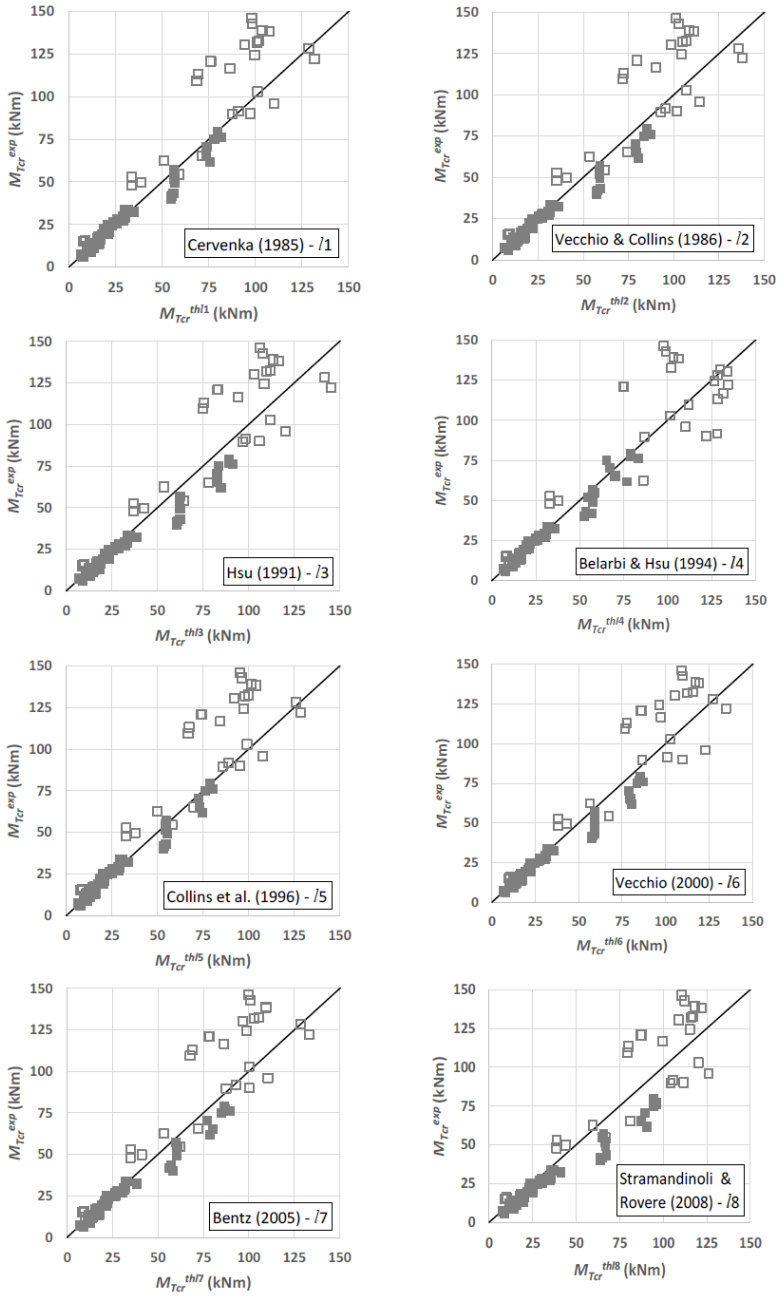

Figure 8. Experimental versos theoretical cracking torque.

Figure 8 visually confirms the observations previously stated from Table 1, namely the higher dispersion of the results for the RC hollow beams.

5. Conclusions

In this study, the GSVATM was used to check some proposed smeared constitutive laws for tensile concrete found in the literature in order to predict the response of the RC beams under torsion for the low loading stage; namely the transition from the uncracked stage to the cracked stage. As referred to in the introduction section, the smeared model GSVATM is simpler than the other, more complex models for the RC beams under torsion. In addition, it was also validated in several previous studies. Hence, the GSVATM was considered to be sufficiently simpler and reliable to evaluate the smeared constitutive laws for tensile concrete. From the obtained results, the following conclusions can be drawn:

(1) The different proposals for the smeared constitutive law for tensile concrete analyzed in this study lead to high differences in the shape of the postpeak descending branch of the corresponding smeared σ—ε curves;
(2) The obtained results confirm that the predicted response of the RC beams under torsion, for the transition from the uncracked stage to the cracked stage highly depends on the smeared constitutive law for tensile concrete incorporated into the model;
(3) The predictions for the cracking torque of the RC plain beams are better than the same ones for the RC hollow beams for which higher variability of the results is observed, as also reported in previous studies;
(4) Regardless of the used smeared constitutive law for tensile concrete, the cracking twist is not very well predicted. Namely, higher variability of the results is observed, as also reported in previous studies;
(5) Among the studied smeared constitutive laws for tensile concrete, the one proposed by Belarbi and Hsu in 1994 allows us to reliably predict the cracking torque of the RC beams under torsion, regardless of the cross-section type (plain or hollow). This result confirms the validity of several previous studies having incorporated this constitutive law in the used smeared truss models.

Finally, the authors consider that the results obtained in this study, using the smeared model GSVATM as reference model, can be extrapolated and could be useful to other smeared models for the RC beams under torsion. It must also be pointed out that additional solutions of experiments on the different failure mechanisms and related suitable approaches for the identification process for the parameters of relations of concrete are greatly needed and should be further studied, namely for the cracking of the RC beams under torsion.

Author Contributions: Conceptualization, L.B.; methodology, L.B.; validation, L.B.; formal analysis, M.T.; investigation, M.T.; data curation, M.T.; writing—original draft preparation, L.B.; writing—review and editing, L.B. and M.T.; supervision, L.B.; All authors have read and agreed to the published version of the manuscript.

Funding: No funding supported this work.

Institutional Review Board Statement: Not applicable.

Informed Consent Statement: Not applicable.

Data Availability Statement: Data is contained within the article.

Conflicts of Interest: The authors declare no conflict of interest.

Appendix A

Table A1. Properties of the reference beams.

Beam		x cm	y cm	t cm	x_1 cm	y_1 cm	A_{st}/s cm²/m	A_{sl} cm²	ρ_t %	ρ_l %	f_{ty} MPa	f_{ly} MPa	f'_c MPa	ε_o %
B3 [35]	P	25.4	38.1	-	21.6	34.3	10.16	11.36	1.17	1.17	320	328	28.1	0.20
B4 [35]	P	25.4	38.1	-	21.6	34.3	14.01	15.48	1.62	1.60	323	320	29.2	0.20
B5 [35]	P	25.4	38.1	-	21.6	34.3	18.47	20.39	2.13	2.11	321	332	30.6	0.20
B6 [35]	P	25.4	38.1	-	21.6	34.3	22.58	25.81	2.61	2.67	323	332	28.8	0.20
B7 [35]	P	25.4	38.1	-	21.6	34.3	10.16	5.16	1.17	0.53	319	320	26.0	0.19
B8 [35]	P	25.4	38.1	-	21.6	34.3	22.58	5.16	2.61	0.53	320	322	26.8	0.19
B9 [35]	P	25.4	38.1	-	21.6	34.3	4.66	11.36	0.54	1.17	343	319	28.8	0.20
C4 [35]	P	25.4	25.4	-	21.6	21.6	13.11	11.36	1.76	1.76	328	337	27.2	0.20
C5 [35]	P	25.4	25.4	-	21.6	21.6	17.67	15.48	2.37	2.40	329	328	27.2	0.20
C6 [35]	P	25.4	25.4	-	21.6	21.6	23.91	20.39	3.20	3.16	328	316	27.6	0.20
G3 [35]	P	25.4	50.8	-	21.6	47.0	8.29	11.36	0.88	0.88	328	339	26.8	0.19
G4 [35]	P	25.4	50.8	-	21.6	47.0	11.29	15.48	1.20	1.20	321	326	28.3	0.20
G5 [35]	P	25.4	50.8	-	21.6	47.0	15.05	20.39	1.60	1.58	328	331	26.9	0.19
G7 [35]	P	25.4	50.8	-	21.6	47.0	8.84	12.00	0.94	0.93	323	319	31.0	0.20
G8 [35]	P	25.4	50.8	-	21.6	47.0	12.32	17.03	1.31	1.32	329	322	28.3	0.20
I3 [35]	P	25.4	38.1	-	21.6	34.3	10.16	11.36	1.17	1.17	334	343	44.8	0.23
I4 [35]	P	25.4	38.1	-	21.6	34.3	14.01	15.48	1.62	1.60	326	315	45.0	0.23
I5 [35]	P	25.4	38.1	-	21.6	34.3	18.47	20.39	2.13	2.11	326	310	45.0	0.23
I6 [35]	P	25.4	38.1	-	21.6	34.3	22.58	25.81	2.61	2.67	329	326	45.8	0.23
J1 [35]	P	25.4	38.1	-	21.6	34.3	4.66	5.16	0.54	0.53	346	328	14.3	0.16
J2 [35]	P	25.4	38.1	-	21.6	34.3	7.21	8.00	0.83	0.83	341	320	14.6	0.16
J3 [35]	P	25.4	38.1	-	21.6	34.3	10.16	11.36	1.17	1.17	337	389	16.9	0.17
J4 [35]	P	25.4	38.1	-	21.6	34.3	14.01	15.48	1.62	1.60	332	324	16.8	0.17
K2 [35]	P	15.2	49.5	-	11.4	45.7	6.77	7.74	1.03	1.03	338	336	30.6	0.20
K3 [35]	P	15.2	49.5	-	11.4	45.7	10.42	12.00	1.58	1.59	321	316	29.0	0.20
K4 [35]	P	15.2	49.5	-	11.4	45.7	15.05	17.03	2.28	2.26	340	344	28.6	0.20
M1 [35]	P	25.4	38.1	-	21.6	34.3	4.76	8.00	0.55	0.83	353	326	29.9	0.20
M2 [35]	P	25.4	38.1	-	21.6	34.3	6.77	11.36	0.78	1.17	357	329	30.6	0.20
M3 [35]	P	25.4	38.1	-	21.6	34.3	9.24	15.48	1.07	1.60	326	322	26.8	0.29
M4 [35]	P	25.4	38.1	-	21.6	34.3	12.33	20.39	1.42	2.11	327	319	26.6	0.19
M5 [35]	P	25.4	38.1	-	21.6	34.3	15.63	25.81	1.81	2.67	331	335	28.0	0.20
M6 [35]	P	25.4	38.1	-	21.6	34.3	15.63	30.58	1.81	3.16	341	318	29.4	0.20
N1 [35]	P	15.2	30.5	-	13.0	28.3	3.50	2.84	0.62	0.61	341	352	29.5	0.20
N1a [35]	P	15.2	30.5	-	13.0	28.3	3.50	2.84	0.62	0.61	345	346	28.7	0.20
N2 [35]	P	15.2	30.5	-	13.0	28.3	6.35	5.16	1.13	1.11	338	331	30.4	0.20
N2a [35]	P	15.2	30.5	-	13.0	28.3	6.21	1.61	1.10	1.11	361	333	28.4	0.20
N3 [35]	P	15.2	30.5	-	13.0	28.3	5.08	4.26	0.90	0.92	352	352	27.3	0.20
N4 [35]	P	15.2	30.5	-	13.0	28.3	7.98	6.58	1.42	1.42	356	341	27.3	0.20
A2 [36]	P	25.4	25.4	-	22.2	22.2	7.82	5.16	1.08	0.80	285	380	38.2	0.22
A3 [36]	P	25.4	25.4	-	21.9	21.9	8.94	8.00	1.22	1.24	360	352	39.4	0.22
A4 [36]	P	25.4	25.4	-	21.9	21.9	12.42	11.36	1.69	1.76	360	351	39.2	0.22
B3 [36]	P	17.8	35.6	-	14.3	32.1	8.60	8.00	1.26	1.27	360	352	38.6	0.22
B4 [36]	P	17.8	35.6	-	14.3	32.1	11.76	11.36	1.73	1.80	360	351	38.5	0.22
B5UR1 [37]	P	20.3	30.5	-	16.5	26.7	6.56	5.16	0.92	0.83	373	386	39.6	0.20
B9UR1 [37]	P	20.3	30.5	-	16.5	26.7	6.56	5.16	0.92	0.83	373	386	75.0	0.27
B12UR1 [37]	P	20.3	30.5	-	16.5	26.7	6.56	5.16	0.92	0.83	399	386	80.6	0.27
B14UR1 [37]	P	20.3	30.5	-	16.5	26.7	6.56	5.16	0.92	0.83	386	386	93.9	0.29
B12UR2 [37]	P	20.3	30.5	-	16.5	26.7	6.95	5.16	0.97	0.83	386	386	76.2	0.27
B12UR3 [37]	P	20.3	30.5	-	16.5	26.7	7.46	6.58	1.04	1.06	386	380	72.9	0.26
B12UR4 [37]	P	20.3	30.5	-	16.5	26.7	7.88	7.74	1.10	1.25	386	373	75.9	0.27
B12UR5 [37]	P	20.3	30.5	-	16.5	26.7	10.13	8.00	1.41	1.29	386	380	76.7	0.27
H-06-12 [38]	P	35.0	50.0	-	30.0	45.0	7.10	20.65	0.61	1.18	440	410	78.5	0.27
H-07-10 [38]	P	35.0	50.0	-	30.0	45.0	7.89	17.03	0.68	0.97	420	500	68.4	0.26
H-07-16 [38]	P	35.0	50.0	-	30.0	45.0	7.89	28.39	0.68	1.62	420	500	68.4	0.26
H-12-12 [38]	P	35.0	50.0	-	30.0	45.0	14.19	20.65	1.22	1.18	440	410	78.5	0.27
H-12-16 [38]	P	35.0	50.0	-	30.0	45.0	14.19	28.39	1.22	1.62	440	520	78.5	0.27
H-14-10 [38]	P	35.0	50.0	-	30.0	45.0	16.13	17.03	1.38	0.97	360	500	68.4	0.26
H-20-20 [38]	P	35.0	50.0	-	30.0	45.0	23.46	34.06	2.01	1.95	440	560	78.5	0.27
N-06-06 [38]	P	35.0	50.0	-	30.0	45.0	7.10	12.00	0.61	0.69	440	440	35.5	0.21
N-06-12 [38]	P	35.0	50.0	-	30.0	45.0	7.10	20.65	0.61	1.18	440	410	35.5	0.21
N-07-10 [38]	P	35.0	50.0	-	30.0	45.0	7.89	17.03	0.68	0.97	420	500	33.5	0.21
N-07-16 [38]	P	35.0	50.0	-	30.0	45.0	7.89	28.39	0.68	1.62	420	500	33.5	0.21
N-12-12 [38]	P	35.0	50.0	-	30.0	45.0	14.19	20.65	1.22	1.18	440	410	35.5	0.21

Table A1. *Cont.*

Beam		x cm	y cm	t cm	x_1 cm	y_1 cm	A_{st}/s cm²/m	A_{sl} cm²	ρ_t %	ρ_l %	f_{ty} MPa	f_{ly} MPa	f'_c MPa	ε_o %
N-12-16 [38]	P	35.0	50.0	-	30.0	45.0	14.19	28.39	1.22	1.62	440	520	35.5	0.21
N-14-10 [38]	P	35.0	50.0	-	30.0	45.0	16.13	17.03	1.38	0.97	360	500	33.5	0.21
N-20-20 [38]	P	35.0	50.0	-	30.0	45.0	23.46	34.06	2.01	1.95	440	560	35.5	0.21
SW12-1 [39]	P	15.0	120.0	-	10.0	115.0	3.93	11.31	0.55	1.26	459	480	44.2	0.23
SW10-1 [39]	P	15.0	100.0	-	10.0	95.0	3.93	9.05	0.55	1.21	459	499	29.5	0.20
SW10-2 [39]	P	15.0	100.0	-	9.8	94.8	7.54	9.05	1.05	1.21	480	480	44.2	0.23
SW10-3 [39]	P	15.0	100.0	-	9.8	94.8	11.31	9.05	1.58	1.21	499	499	29.5	0.20
SW10-4 [39]	P	15.0	100.0	-	9.4	94.4	16.08	16.08	2.23	2.14	497	497	33.8	0.21
SW8-1 [39]	P	15.0	80.0	-	10.2	75.2	4.02	7.07	0.57	1.18	433	459	29.5	0.20
SW8-2 [39]	P	15.0	80.0	-	9.8	74.8	11.31	7.07	1.59	1.18	499	459	29.5	0.20
D3 [35]	H	25.4	38.1	6.4	21.6	34.3	10.16	11.36	1.17	1.17	333	341	28.4	0.20
D4 [35]	H	25.4	38.1	6.4	21.6	34.3	14.01	15.48	1.62	1.60	333	330	30.6	0.20
T0 [40]	H	50.0	50.0	8.0	43.0	43.0	10.28	32.16	0.71	1.29	357	345	45.1	0.23
T1 [40]	H	50.0	50.0	8.0	45.4	45.4	10.28	18.10	0.75	0.72	357	357	35.3	0.21
T2 [40]	H	50.0	50.0	8.0	43.0	43.0	10.28	18.10	0.71	0.72	357	357	35.3	0.21
T5 [40]	H	80.0	40.0	8.0	73.0	33.0	10.28	10.00	0.68	0.31	513	529	47.1	0.23
VH1 [41]	H	32.4	32.4	8.0	30.4	30.4	2.88	3.46	0.33	0.33	447	447	17.2	0.17
VH2 [41]	H	32.4	32.4	8.0	30.4	30.4	5.76	6.91	0.67	0.66	447	447	17.2	0.17
A2 [42]	H	60.0	60.0	10.7	53.8	53.1	6.28	13.95	0.37	0.39	696	672	47.3	0.23
A3 [42]	H	60.0	60.0	10.9	53.5	53.5	8.27	18.10	0.49	0.50	715	672	46.2	0.23
A4 [42]	H	60.0	60.0	10.4	52.0	52.5	11.22	23.75	0.65	0.66	715	724	54.8	0.24
A5 [42]	H	60.0	60.0	10.4	52.8	52.8	14.14	30.66	0.83	0.85	672	724	53.1	0.24
B2 [42]	H	60.0	60.0	10.8	53.3	53.4	6.70	14.58	0.40	0.41	696	672	69.8	0.26
B3 [42]	H	60.0	60.0	10.9	53.5	53.7	11.22	23.75	0.67	0.66	715	724	77.8	0.27
B4 [42]	H	60.0	60.0	11.2	52.3	53.6	15.08	32.17	0.89	0.89	672	724	79.8	0.27
B5 [42]	H	60.0	60.0	11.7	51.8	51.8	18.85	40.21	1.09	1.12	672	724	76.4	0.27
C2 [42]	H	60.0	60.0	10.0	53.2	53.3	6.28	13.95	0.37	0.39	696	672	94.8	0.28
C3 [42]	H	60.0	60.0	10.3	54.5	54.0	10.47	23.75	0.63	0.66	715	724	91.6	0.28
C4 [42]	H	60.0	60.0	10.3	54.6	54.5	14.14	30.66	0.86	0.85	672	724	91.4	0.28
C5 [42]	H	60.0	60.0	10.4	54.0	54.3	17.40	36.69	1.05	1.02	672	724	96.7	0.28
C6 [42]	H	60.0	60.0	10.4	53.3	52.9	22.62	48.25	1.34	1.34	672	724	87.5	0.28
A095c [26]	H	49.7	71.1	14.5	43.7	65.1	9.93	13.16	0.61	0.37	381	371	35.1	0.21
A120a [26]	H	50.2	71.9	18.4	44.2	65.9	7.59	20.00	0.46	0.55	380	464	27.6	0.20
B065b [26]	H	50.3	71.0	9.2	44.3	65.0	9.93	50.97	0.61	1.43	380	452	39.2	0.22
B080a [26]	H	50.0	72.1	11.2	44.0	66.1	12.90	28.39	0.79	0.79	392	454	46.5	0.23
B110a [26]	H	49.8	71.0	15.5	43.8	65.0	8.60	20.00	0.53	0.57	369	453	48.1	0.23
C065a [26]	H	49.5	78.1	8.5	43.5	72.1	9.93	20.00	0.59	0.52	376	338	78.8	0.27
C100a [26]	H	49.9	72.3	12.7	43.9	66.3	12.90	28.39	0.79	0.79	447	466	90.6	0.28
D075a [26]	H	49.8	73.4	8.7	43.8	67.4	12.90	28.39	0.79	0.78	381	469	94.9	0.29
D090a [26]	H	50.1	72.2	10.5	44.1	66.2	12.90	28.39	0.79	0.79	447	466	105.7	0.30

Table A2. Cracking torques and corresponding twists (smeared constitutive laws *l*1 to *l*3).

Beam	M_{Tcr}^{exp} kNm	θ_{cr}^{exp} °/m	M_{Tcr}^{thl1} kNm	$\frac{M_{Tcr}^{exp}}{M_{Tcr}^{thl1}}$	θ_{cr}^{thl1} °/m	$\frac{\theta_{cr}^{exp}}{\theta_{cr}^{thl1}}$	M_{Tcr}^{thl2} kNm	$\frac{M_{Tcr}^{exp}}{M_{Tcr}^{thl2}}$	θ_{cr}^{thl2} °/m	$\frac{\theta_{cr}^{exp}}{\theta_{cr}^{thl2}}$	M_{Tcr}^{thl3} kNm	$\frac{M_{Tcr}^{exp}}{M_{Tcr}^{thl3}}$	θ_{cr}^{thl3} °/m	$\frac{\theta_{cr}^{exp}}{\theta_{cr}^{thl3}}$
B3 [35]	20.1	0.12	20.9	0.96	0.10	1.21	22.0	0.91	0.11	1.15	23.2	0.87	0.11	1.09
B4 [35]	21.9	0.12	21.0	1.05	0.10	1.20	22.0	0.99	0.10	1.15	23.1	0.95	0.11	1.09
B5 [35]	22.6	0.14	21.4	1.05	0.10	1.42	22.2	1.02	0.10	1.36	23.4	0.97	0.11	1.30
B6 [35]	25.0	0.16	20.6	1.21	0.09	1.75	21.7	1.15	0.10	1.67	22.8	1.09	0.10	1.58
B7 [35]	20.2	0.11	20.0	1.01	0.10	1.07	21.0	0.96	0.11	1.02	22.1	0.91	0.11	0.97
B8 [35]	21.8	0.13	20.3	1.07	0.10	1.28	21.3	1.02	0.10	1.22	22.3	0.98	0.11	1.17
B9 [35]	19.6	0.11	20.8	0.94	0.10	1.04	22.0	0.89	0.11	0.99	23.2	0.85	0.11	0.94
C4 [35]	11.9	0.13	11.3	1.05	0.11	1.18	11.8	1.01	0.12	1.12	12.4	0.96	0.13	1.07
C5 [35]	14.0	0.17	11.2	1.25	0.11	1.51	11.9	1.17	0.12	1.41	12.5	1.12	0.12	1.35
C6 [35]	13.9	0.17	11.3	1.23	0.11	1.61	11.5	1.20	0.11	1.57	12.0	1.15	0.11	1.51
G3 [35]	27.1	0.10	29.5	0.92	0.09	1.05	31.0	0.87	0.10	1.00	32.7	0.83	0.10	0.95
G4 [35]	28.7	0.12	30.1	0.95	0.09	1.29	31.6	0.91	0.10	1.23	33.4	0.86	0.10	1.16
G5 [35]	29.5	0.11	29.2	1.01	0.09	1.30	30.7	0.96	0.09	1.24	32.3	0.91	0.10	1.17
G7 [35]	33.6	0.13	31.7	1.06	0.09	1.45	33.3	1.01	0.10	1.38	35.1	0.96	0.10	1.31
G8 [35]	33.6	0.12	30.1	1.12	0.09	1.37	31.6	1.06	0.09	1.30	33.4	1.01	0.10	1.23
I3 [35]	25.5	0.11	25.5	1.00	0.11	0.97	27.2	0.94	0.12	0.91	28.7	0.89	0.12	0.86
I4 [35]	28.0	0.12	25.7	1.09	0.11	1.15	27.3	1.03	0.11	1.08	28.8	0.97	0.12	1.02
I5 [35]	28.1	0.15	26.0	1.08	0.11	1.43	27.4	1.02	0.11	1.36	28.9	0.97	0.12	1.29
I6 [35]	27.5	0.13	26.2	1.05	0.10	1.22	27.7	0.99	0.11	1.15	29.2	0.94	0.12	1.09

Table A2. *Cont.*

Beam	M_{Tcr}^{exp} kNm	θ_{cr}^{exp} °/m	M_{Tcr}^{thl1} kNm	$\frac{M_{Tcr}^{exp}}{M_{Tcr}^{thl1}}$	θ_{cr}^{thl1} °/m	$\frac{\theta_{cr}^{exp}}{\theta_{cr}^{thl1}}$	M_{Tcr}^{thl2} kNm	$\frac{M_{Tcr}^{exp}}{M_{Tcr}^{thl2}}$	θ_{cr}^{thl2} °/m	$\frac{\theta_{cr}^{exp}}{\theta_{cr}^{thl2}}$	M_{Tcr}^{thl3} kNm	$\frac{M_{Tcr}^{exp}}{M_{Tcr}^{thl3}}$	θ_{cr}^{thl3} °/m	$\frac{\theta_{cr}^{exp}}{\theta_{cr}^{thl3}}$
J1 [35]	14.0	0.09	15.3	0.92	0.09	0.92	15.9	0.88	0.10	0.88	16.5	0.85	0.10	0.85
J2 [35]	17.1	0.12	15.1	1.13	0.09	1.38	15.7	1.09	0.09	1.32	16.5	1.03	0.10	1.26
J3 [35]	16.9	0.10	15.9	1.06	0.09	1.08	16.6	1.02	0.09	1.03	17.5	0.97	0.10	0.98
J4 [35]	18.0	0.11	15.6	1.15	0.09	1.28	16.3	1.10	0.09	1.23	17.1	1.05	0.09	1.17
K2 [35]	12.2	0.18	12.0	1.02	0.14	1.31	12.3	0.99	0.14	1.27	13.1	0.93	0.15	1.20
K3 [35]	12.4	0.19	11.5	1.08	0.13	1.49	11.9	1.05	0.13	1.45	12.6	0.98	0.14	1.37
K4 [35]	13.1	0.21	11.1	1.19	0.12	1.71	11.6	1.13	0.13	1.63	12.4	1.06	0.13	1.53
M1 [35]	19.2	0.11	21.2	0.90	0.10	1.03	22.5	0.85	0.11	0.97	23.6	0.81	0.12	0.92
M2 [35]	20.6	0.11	21.5	0.96	0.10	1.08	22.5	0.92	0.11	1.03	23.8	0.86	0.11	0.97
M3 [35]	20.7	0.12	20.0	1.03	0.10	1.24	21.0	0.98	0.10	1.18	22.2	0.93	0.11	1.12
M4 [35]	20.7	0.13	19.9	1.04	0.10	1.41	20.8	0.99	0.10	1.34	22.0	0.94	0.11	1.27
M5 [35]	21.7	0.12	20.2	1.07	0.09	1.30	21.3	1.02	0.10	1.23	22.4	0.97	0.10	1.17
M6 [35]	22.7	0.15	20.7	1.10	0.09	1.57	21.7	1.05	0.10	1.49	22.8	0.99	0.10	1.42
N1 [35]	7.6	0.13	6.7	1.14	0.16	0.81	7.0	1.08	0.17	0.77	7.4	1.02	0.18	0.73
N1a [35]	7.0	0.11	6.6	1.06	0.16	0.69	6.9	1.01	0.17	0.66	7.3	0.96	0.17	0.62
N2 [35]	7.4	0.22	6.8	1.10	0.15	1.40	7.1	1.05	0.16	1.34	7.5	0.99	0.17	1.27
N2a [35]	7.5	0.21	6.6	1.14	0.15	1.37	6.9	1.09	0.16	1.31	7.3	1.03	0.17	1.24
N3 [35]	7.4	0.21	6.4	1.15	0.15	1.39	6.7	1.10	0.16	1.33	7.1	1.04	0.17	1.25
N4 [35]	7.6	0.21	6.4	1.19	0.15	1.43	6.7	1.13	0.16	1.36	7.1	1.07	0.16	1.29
A2 [36]	11.3	0.12	13.4	0.84	0.13	0.94	14.0	0.81	0.13	0.89	14.8	0.76	0.14	0.84
A3 [36]	12.2	0.12	13.5	0.90	0.13	0.98	14.3	0.85	0.13	0.92	15.1	0.81	0.14	0.88
A4 [36]	12.5	0.15	13.5	0.93	0.12	1.20	14.3	0.88	0.13	1.14	15.1	0.83	0.14	1.08
B3 [36]	8.8	0.15	12.0	0.73	0.14	1.06	12.6	0.70	0.14	1.01	13.3	0.66	0.15	0.96
B4 [36]	10.2	0.15	12.0	0.85	0.13	1.09	12.6	0.81	0.14	1.04	13.3	0.77	0.15	0.98
B5UR1 [37]	11.6	0.09	12.4	0.94	0.14	0.63	13.1	0.89	0.14	0.60	13.8	0.84	0.15	0.57
B9UR1 [37]	13.0	0.13	16.2	0.80	0.15	0.91	17.3	0.75	0.16	0.86	18.2	0.71	0.17	0.81
B12UR1 [37]	16.2	0.09	16.7	0.97	0.15	0.61	17.8	0.91	0.16	0.57	18.8	0.86	0.17	0.55
B14UR1 [37]	19.3	0.12	17.7	1.09	0.15	0.78	18.9	1.02	0.16	0.73	19.9	0.97	0.17	0.69
B12UR2 [37]	17.8	0.11	16.4	1.09	0.15	0.75	17.4	1.02	0.16	0.71	18.4	0.97	0.17	0.67
B12UR3 [37]	16.0	0.10	16.1	1.00	0.15	0.70	17.3	0.93	0.16	0.65	18.0	0.89	0.16	0.62
B12UR4 [37]	16.9	0.14	16.4	1.03	0.15	0.96	17.5	0.96	0.16	0.89	18.4	0.92	0.16	0.85
B12UR5 [37]	13.6	0.04	16.7	0.81	0.15	0.24	17.8	0.76	0.16	0.23	18.6	0.73	0.16	0.22
H-06-12 [38]	75.0	0.09	78.0	0.96	0.09	1.00	83.5	0.90	0.09	0.93	83.5	0.90	0.09	0.93
H-07-10 [38]	70.5	0.09	73.9	0.95	0.09	1.08	79.0	0.89	0.09	1.01	82.9	0.85	0.10	0.96
H-07-16 [38]	65.3	0.09	73.5	0.89	0.08	1.03	79.2	0.82	0.09	0.95	83.1	0.79	0.09	0.91
H-12-12 [38]	77.1	0.07	79.7	0.97	0.09	0.85	85.0	0.91	0.09	0.80	89.5	0.86	0.10	0.76
H-12-16 [38]	79.3	0.09	79.7	1.00	0.09	1.06	85.3	0.93	0.09	0.99	89.4	0.89	0.10	0.95
H-14-10 [38]	61.8	0.09	75.7	0.82	0.09	1.00	80.6	0.77	0.09	0.94	84.9	0.73	0.10	0.89
H-20-20 [38]	76.0	0.09	81.8	0.93	0.09	1.05	87.1	0.87	0.09	0.99	91.6	0.83	0.10	0.94
N-06-06 [38]	43.2	0.08	56.1	0.77	0.08	1.02	59.3	0.73	0.08	0.96	62.5	0.69	0.09	0.91
N-06-12 [38]	51.8	0.11	56.1	0.92	0.08	1.47	59.1	0.88	0.08	1.39	62.4	0.83	0.09	1.32
N-07-10 [38]	41.6	0.11	54.7	0.76	0.08	1.40	57.6	0.72	0.08	1.33	60.7	0.68	0.09	1.26
N-07-16 [38]	40.0	0.11	54.7	0.73	0.08	1.43	57.5	0.70	0.08	1.36	60.6	0.66	0.08	1.29
N-12-12 [38]	49.3	0.09	56.7	0.87	0.08	1.18	59.2	0.83	0.08	1.13	62.5	0.79	0.09	1.07
N-12-16 [38]	57.1	0.12	56.3	1.02	0.08	1.58	59.2	0.96	0.08	1.50	62.5	0.91	0.08	1.42
N-14-10 [38]	41.8	0.12	55.2	0.76	0.08	1.56	57.9	0.72	0.08	1.49	61.1	0.68	0.09	1.41
N-20-20 [38]	55.0	0.13	56.6	0.97	0.08	1.68	58.9	0.93	0.08	1.61	62.4	0.88	0.08	1.52
SW12-1 [39]	32.3	0.15	34.6	0.93	0.13	1.16	36.4	0.89	0.14	1.11	38.8	0.83	0.15	1.03
SW10-1 [39]	24.6	0.13	23.2	1.06	0.13	1.00	24.7	1.00	0.14	0.93	25.8	0.95	0.14	0.90
SW10-2 [39]	29.6	0.20	29.1	1.02	0.14	1.47	31.1	0.95	0.15	1.37	32.0	0.92	0.15	1.36
SW10-3 [39]	26.6	0.15	23.9	1.11	0.13	1.16	25.3	1.05	0.14	1.10	26.7	1.00	0.15	1.04
SW10-4 [39]	27.7	0.16	25.7	1.08	0.13	1.24	27.1	1.02	0.14	1.17	28.8	0.96	0.15	1.10
SW8-1 [39]	19.7	0.16	18.6	1.06	0.14	1.13	20.0	0.98	0.15	1.03	21.0	0.94	0.16	0.99
SW8-2 [39]	22.5	0.14	18.9	1.19	0.14	1.06	20.1	1.12	0.15	0.98	21.2	1.06	0.15	0.94
D3 [35]	15.2	0.08	8.0	1.89	0.05	1.49	8.5	1.79	0.06	1.40	8.8	1.73	0.06	1.36
D4 [35]	15.8	0.12	8.9	1.78	0.06	2.05	9.3	1.70	0.06	1.96	9.7	1.63	0.06	1.88
T0 [40]	49.8	0.06	38.8	1.28	0.03	1.92	40.8	1.22	0.03	1.81	42.5	1.17	0.04	1.75
T1 [40]	48.0	0.04	33.7	1.43	0.03	1.35	35.3	1.36	0.03	1.27	36.8	1.31	0.03	1.23
T2 [40]	52.8	0.10	33.7	1.57	0.03	3.07	35.3	1.49	0.03	2.90	36.8	1.44	0.03	2.81
T5 [40]	62.5	0.06	50.8	1.23	0.03	2.07	53.7	1.16	0.03	1.89	53.6	1.17	0.03	2.10
VH1 [41]	12.0	0.12	9.8	1.22	0.07	1.65	10.4	1.15	0.08	1.55	10.9	1.10	0.08	1.48
VH2 [41]	11.5	0.07	10.4	1.10	0.08	0.90	11.1	1.03	0.08	0.85	11.7	0.99	0.09	0.81
A2 [42]	109.5	0.06	68.6	1.60	0.03	2.44	71.6	1.53	0.03	2.34	74.8	1.46	0.03	2.25
A3 [42]	113.3	0.06	69.2	1.64	0.03	2.18	72.3	1.57	0.03	2.09	75.5	1.50	0.03	2.02
A4 [42]	120.9	0.06	75.9	1.59	0.03	2.42	79.8	1.51	0.03	2.25	83.4	1.45	0.03	2.17
A5 [42]	120.9	0.04	76.1	1.59	0.03	1.66	79.4	1.52	0.03	1.59	82.9	1.46	0.03	1.53

Table A2. *Cont.*

Beam	M_{Tcr}^{exp} kNm	θ_{cr}^{exp} °/m	M_{Tcr}^{thl1} kNm	$\frac{M_{Tcr}^{exp}}{M_{Tcr}^{thl1}}$	θ_{cr}^{thl1} °/m	$\frac{\theta_{cr}^{exp}}{\theta_{cr}^{thl1}}$	M_{Tcr}^{thl2} kNm	$\frac{M_{Tcr}^{exp}}{M_{Tcr}^{thl2}}$	θ_{cr}^{thl2} °/m	$\frac{\theta_{cr}^{exp}}{\theta_{cr}^{thl2}}$	M_{Tcr}^{thl3} kNm	$\frac{M_{Tcr}^{exp}}{M_{Tcr}^{thl3}}$	θ_{cr}^{thl3} °/m	$\frac{\theta_{cr}^{exp}}{\theta_{cr}^{thl3}}$
B2 [42]	116.7	0.04	86.3	1.35	0.03	1.69	90.2	1.29	0.03	1.60	94.4	1.24	0.03	1.53
B3 [42]	130.5	0.05	94.2	1.39	0.03	1.74	98.4	1.33	0.03	1.65	103.1	1.26	0.03	1.57
B4 [42]	142.9	0.07	98.3	1.45	0.03	2.73	102.7	1.39	0.03	2.58	107.7	1.33	0.03	2.47
B5 [42]	146.3	0.06	98.0	1.49	0.03	2.44	101.4	1.44	0.03	2.38	106.3	1.38	0.03	2.28
C2 [42]	124.5	0.05	99.6	1.25	0.03	1.81	104.1	1.20	0.03	1.70	108.6	1.15	0.03	1.67
C3 [42]	131.9	0.06	100.8	1.31	0.03	2.35	104.7	1.26	0.03	2.29	109.9	1.20	0.03	2.18
C4 [42]	132.6	0.05	102.1	1.30	0.03	1.92	106.8	1.24	0.03	1.82	112.0	1.18	0.03	1.73
C5 [42]	138.3	0.05	107.4	1.29	0.03	1.91	111.3	1.24	0.03	1.85	116.9	1.18	0.03	1.76
C6 [42]	139.1	0.05	103.7	1.34	0.03	2.02	108.3	1.28	0.03	1.91	113.5	1.23	0.03	1.83
A095c [26]	102.9	0.03	101.0	1.02	0.04	0.82	106.9	0.96	0.04	0.77	112.0	0.92	0.05	0.74
A120a [26]	89.8	0.05	87.4	1.03	0.04	1.14	92.8	0.97	0.04	1.07	97.1	0.92	0.05	1.03
B065b [26]	54.4	0.03	59.1	0.92	0.03	1.23	62.1	0.88	0.03	1.16	64.7	0.84	0.03	1.12
B080a [26]	65.2	0.03	71.2	0.92	0.03	1.24	74.2	0.88	0.03	1.19	78.0	0.84	0.03	1.12
B110a [26]	128.3	0.04	128.6	1.00	0.04	0.99	135.8	0.94	0.04	0.93	141.8	0.90	0.05	0.90
C065a [26]	91.7	0.03	90.9	1.01	0.03	1.06	95.5	0.96	0.03	0.98	98.4	0.93	0.03	1.03
C100a [26]	122.2	0.03	131.6	0.93	0.03	0.85	137.8	0.89	0.04	0.81	145.3	0.84	0.04	0.76
D075a [26]	90.1	0.03	97.3	0.93	0.03	0.99	101.8	0.88	0.03	0.94	106.0	0.85	0.03	0.92
D090a [26]	96.1	0.03	110.0	0.87	0.03	1.08	114.3	0.84	0.03	1.05	120.2	0.80	0.03	0.99

Table A3. Cracking torques and corresponding twists (smeared constitutive laws *l*4 to *l*6).

Beam	M_{Tcr}^{exp} kNm	θ_{cr}^{exp} °/m	M_{Tcr}^{thl4} kNm	$\frac{M_{Tcr}^{exp}}{M_{Tcr}^{thl4}}$	θ_{cr}^{thl4} °/m	$\frac{\theta_{cr}^{exp}}{\theta_{cr}^{thl4}}$	M_{Tcr}^{thl5} kNm	$\frac{M_{Tcr}^{exp}}{M_{Tcr}^{thl5}}$	θ_{cr}^{thl5} °/m	$\frac{\theta_{cr}^{exp}}{\theta_{cr}^{thl5}}$	M_{Tcr}^{thl6} kNm	$\frac{M_{Tcr}^{exp}}{M_{Tcr}^{thl6}}$	θ_{cr}^{thl6} °/m	$\frac{\theta_{cr}^{exp}}{\theta_{cr}^{thl6}}$
B3 [35]	20.1	0.12	21.3	0.94	0.10	1.19	20.4	0.99	0.10	1.24	22.0	0.91	0.11	1.15
B4 [35]	21.9	0.12	21.5	1.02	0.10	1.17	20.4	1.07	0.10	1.24	22.0	0.99	0.10	1.15
B5 [35]	22.6	0.14	22.0	1.02	0.10	1.37	20.9	1.08	0.09	1.45	22.2	1.02	0.10	1.36
B6 [35]	25.0	0.16	20.9	1.19	0.09	1.73	20.1	1.24	0.09	1.80	21.7	1.15	0.10	1.67
B7 [35]	20.2	0.11	20.7	0.98	0.10	1.04	19.5	1.04	0.10	1.10	21.0	0.96	0.11	1.02
B8 [35]	21.8	0.13	20.8	1.05	0.10	1.25	19.7	1.10	0.10	1.32	21.3	1.02	0.10	1.22
B9 [35]	19.6	0.11	20.0	0.98	0.10	1.09	20.3	0.97	0.10	1.07	22.0	0.89	0.11	0.99
C4 [35]	11.9	0.13	11.6	1.02	0.12	1.15	11.0	1.08	0.11	1.21	11.8	1.01	0.12	1.12
C5 [35]	14.0	0.17	11.6	1.21	0.11	1.46	11.0	1.27	0.11	1.53	11.9	1.17	0.12	1.41
C6 [35]	13.9	0.17	11.4	1.21	0.11	1.58	10.9	1.27	0.10	1.65	12.0	1.16	0.11	1.51
G3 [35]	27.1	0.10	30.5	0.89	0.09	1.01	28.7	0.94	0.09	1.08	31.0	0.87	0.10	1.00
G4 [35]	28.7	0.12	31.0	0.93	0.09	1.25	29.4	0.98	0.09	1.32	31.6	0.91	0.10	1.23
G5 [35]	29.5	0.11	29.8	0.99	0.09	1.27	28.5	1.03	0.09	1.33	30.7	0.96	0.09	1.24
G7 [35]	33.6	0.13	32.8	1.02	0.10	1.40	30.9	1.09	0.09	1.49	33.3	1.01	0.10	1.38
G8 [35]	33.6	0.12	31.2	1.08	0.09	1.32	29.3	1.15	0.09	1.40	31.5	1.07	0.09	1.30
I3 [35]	25.5	0.11	26.3	0.97	0.11	0.94	25.1	1.02	0.11	0.99	27.2	0.94	0.12	0.91
I4 [35]	28.0	0.12	26.5	1.06	0.11	1.11	25.2	1.11	0.11	1.17	27.3	1.03	0.11	1.08
I5 [35]	28.1	0.15	26.8	1.05	0.11	1.39	25.4	1.11	0.10	1.46	27.4	1.02	0.11	1.36
I6 [35]	27.5	0.13	26.9	1.02	0.11	1.19	25.7	1.07	0.10	1.24	27.7	0.99	0.11	1.15
J1 [35]	14.0	0.09	15.2	0.92	0.09	0.92	14.8	0.95	0.09	0.95	15.9	0.88	0.10	0.88
J2 [35]	17.1	0.12	15.4	1.10	0.09	1.35	14.3	1.19	0.09	1.45	15.7	1.09	0.09	1.32
J3 [35]	16.9	0.10	16.5	1.03	0.09	1.04	15.4	1.10	0.09	1.11	16.6	1.02	0.09	1.03
J4 [35]	18.0	0.11	15.8	1.13	0.09	1.26	15.1	1.19	0.08	1.33	16.3	1.10	0.09	1.23
K2 [35]	12.2	0.18	12.7	0.96	0.14	1.24	11.8	1.04	0.13	1.33	12.7	0.96	0.14	1.24
K3 [35]	12.4	0.19	12.3	1.01	0.14	1.40	11.0	1.13	0.12	1.56	12.2	1.02	0.14	1.42
K4 [35]	13.1	0.21	12.1	1.08	0.13	1.56	10.8	1.21	0.12	1.75	12.0	1.09	0.13	1.58
M1 [35]	19.2	0.11	19.7	0.97	0.10	1.11	20.7	0.93	0.10	1.05	22.5	0.85	0.11	0.97
M2 [35]	20.6	0.11	21.5	0.96	0.10	1.08	20.9	0.98	0.10	1.10	22.5	0.92	0.11	1.03
M3 [35]	20.7	0.12	20.7	1.00	0.10	1.19	19.5	1.06	0.10	1.27	21.0	0.98	0.10	1.18
M4 [35]	20.7	0.13	20.1	1.03	0.10	1.39	19.3	1.07	0.09	1.45	20.8	0.99	0.10	1.34
M5 [35]	21.7	0.12	20.6	1.05	0.10	1.27	19.6	1.11	0.09	1.34	21.3	1.02	0.10	1.23
M6 [35]	22.7	0.15	21.0	1.08	0.09	1.54	20.0	1.13	0.09	1.62	21.7	1.05	0.10	1.49
N1 [35]	7.6	0.13	6.9	1.10	0.16	0.79	6.5	1.17	0.15	0.83	7.0	1.08	0.17	0.77
N1a [35]	7.0	0.11	6.4	1.11	0.15	0.72	6.4	1.10	0.15	0.71	6.9	1.01	0.17	0.66
N2 [35]	7.4	0.22	7.0	1.06	0.16	1.36	6.5	1.14	0.15	1.45	7.1	1.05	0.16	1.34
N2a [35]	7.5	0.21	6.7	1.12	0.16	1.35	6.4	1.17	0.15	1.41	6.9	1.09	0.16	1.31
N3 [35]	7.4	0.21	6.7	1.11	0.16	1.34	6.2	1.19	0.15	1.43	6.7	1.10	0.16	1.33
N4 [35]	7.6	0.21	6.6	1.16	0.15	1.39	6.2	1.22	0.14	1.46	6.7	1.13	0.16	1.36

Table A3. *Cont.*

Beam	M_{Tcr}^{exp} kNm	θ_{cr}^{exp} °/m	M_{Tcr}^{thl4} kNm	$\frac{M_{Tcr}^{exp}}{M_{Tcr}^{thl4}}$	θ_{cr}^{thl4} °/m	$\frac{\theta_{cr}^{exp}}{\theta_{cr}^{thl4}}$	M_{Tcr}^{thl5} kNm	$\frac{M_{Tcr}^{exp}}{M_{Tcr}^{thl5}}$	θ_{cr}^{thl5} °/m	$\frac{\theta_{cr}^{exp}}{\theta_{cr}^{thl5}}$	M_{Tcr}^{thl6} kNm	$\frac{M_{Tcr}^{exp}}{M_{Tcr}^{thl6}}$	θ_{cr}^{thl6} °/m	$\frac{\theta_{cr}^{exp}}{\theta_{cr}^{thl6}}$
A2 [36]	11.3	0.12	13.6	0.83	0.13	0.92	13.1	0.86	0.13	0.96	14.0	0.81	0.13	0.89
A3 [36]	12.2	0.12	13.9	0.87	0.13	0.95	13.2	0.92	0.12	1.00	14.3	0.85	0.13	0.92
A4 [36]	12.5	0.15	14.0	0.90	0.13	1.16	13.2	0.95	0.12	1.22	14.3	0.88	0.13	1.14
B3 [36]	8.8	0.15	12.2	0.72	0.14	1.05	11.6	0.76	0.13	1.10	12.6	0.70	0.14	1.01
B4 [36]	10.2	0.15	12.3	0.83	0.14	1.07	11.7	0.87	0.13	1.12	12.6	0.81	0.14	1.04
B5UR1 [37]	11.6	0.09	12.4	0.93	0.14	0.63	12.0	0.97	0.13	0.65	13.1	0.89	0.14	0.60
B9UR1 [37]	13.0	0.13	16.4	0.79	0.15	0.90	16.0	0.81	0.14	0.92	17.3	0.75	0.16	0.86
B12UR1 [37]	16.2	0.09	16.9	0.96	0.15	0.61	16.5	0.98	0.15	0.62	17.8	0.91	0.16	0.57
B14UR1 [37]	19.3	0.12	17.9	1.08	0.15	0.77	17.4	1.11	0.15	0.79	18.9	1.02	0.16	0.73
B12UR2 [37]	17.8	0.11	16.6	1.07	0.15	0.74	16.1	1.10	0.15	0.76	17.4	1.02	0.16	0.71
B12UR3 [37]	16.0	0.10	15.9	1.01	0.14	0.71	15.8	1.01	0.14	0.71	17.3	0.93	0.16	0.65
B12UR4 [37]	16.9	0.14	16.1	1.05	0.14	0.97	16.1	1.05	0.14	0.97	17.5	0.96	0.16	0.89
B12UR5 [37]	13.6	0.04	16.8	0.81	0.15	0.24	16.4	0.83	0.14	0.25	17.8	0.76	0.16	0.23
H-06-12 [38]	75.0	0.09	65.2	1.15	0.07	1.19	76.5	0.98	0.08	1.02	83.5	0.90	0.09	0.93
H-07-10 [38]	70.5	0.09	67.2	1.05	0.08	1.18	72.8	0.97	0.08	1.09	79.0	0.89	0.09	1.01
H-07-16 [38]	65.3	0.09	69.8	0.93	0.08	1.08	73.0	0.89	0.08	1.03	79.2	0.82	0.09	0.95
H-12-12 [38]	77.1	0.07	78.9	0.98	0.09	0.86	78.6	0.98	0.09	0.87	85.0	0.91	0.09	0.80
H-12-16 [38]	79.3	0.09	79.2	1.00	0.09	1.07	78.6	1.01	0.09	1.08	85.3	0.93	0.09	0.99
H-14-10 [38]	61.8	0.09	76.9	0.80	0.09	0.98	74.7	0.83	0.09	1.01	80.6	0.77	0.09	0.94
H-20-20 [38]	76.0	0.09	83.5	0.91	0.09	1.03	80.6	0.94	0.09	1.07	87.1	0.87	0.09	0.99
N-06-06 [38]	43.2	0.08	53.3	0.81	0.07	1.07	54.7	0.79	0.08	1.04	59.3	0.73	0.08	0.96
N-06-12 [38]	51.8	0.11	54.5	0.95	0.08	1.51	54.7	0.95	0.08	1.51	59.1	0.88	0.08	1.39
N-07-10 [38]	41.6	0.11	55.2	0.75	0.08	1.39	53.5	0.78	0.08	1.44	57.6	0.72	0.08	1.33
N-07-16 [38]	40.0	0.11	52.5	0.76	0.07	1.49	53.4	0.75	0.07	1.46	57.5	0.70	0.08	1.36
N-12-12 [38]	49.3	0.09	57.5	0.86	0.08	1.16	55.4	0.89	0.08	1.21	59.2	0.83	0.08	1.13
N-12-16 [38]	57.1	0.12	57.6	0.99	0.08	1.54	55.0	1.04	0.07	1.61	59.2	0.96	0.08	1.50
N-14-10 [38]	41.8	0.12	56.8	0.74	0.08	1.52	53.7	0.78	0.08	1.60	57.9	0.72	0.08	1.49
N-20-20 [38]	55.0	0.13	58.5	0.94	0.08	1.62	54.6	1.01	0.07	1.74	58.9	0.93	0.08	1.61
SW12-1 [39]	32.3	0.15	36.1	0.89	0.13	1.14	33.8	0.96	0.13	1.20	35.7	0.91	0.16	0.98
SW10-1 [39]	24.6	0.13	24.5	1.00	0.14	0.95	22.7	1.08	0.13	1.03	24.7	1.00	0.19	0.70
SW10-2 [39]	29.6	0.20	30.1	0.98	0.14	1.47	28.7	1.03	0.13	1.49	31.5	0.94	0.15	1.33
SW10-3 [39]	26.6	0.15	25.1	1.06	0.14	1.12	23.5	1.13	0.13	1.18	27.6	0.96	0.15	1.01
SW10-4 [39]	27.7	0.16	27.0	1.02	0.14	1.19	25.2	1.10	0.13	1.26	29.4	0.94	0.15	1.08
SW8-1 [39]	19.7	0.16	19.2	1.03	0.14	1.14	18.5	1.07	0.14	1.13	19.4	1.02	0.19	0.84
SW8-2 [39]	22.5	0.14	19.8	1.14	0.14	1.02	18.7	1.20	0.14	1.06	21.7	1.04	0.16	0.92
D3 [35]	15.2	0.08	7.9	1.92	0.05	1.55	7.9	1.92	0.05	1.50	9.3	1.62	0.06	1.27
D4 [35]	15.8	0.12	8.7	1.83	0.06	2.14	8.7	1.82	0.06	2.10	10.2	1.55	0.07	1.79
T0 [40]	49.8	0.06	38.1	1.31	0.03	2.09	37.9	1.32	0.03	1.99	43.2	1.15	0.03	1.79
T1 [40]	48.0	0.04	33.0	1.45	0.03	1.46	32.8	1.46	0.03	1.39	37.9	1.27	0.04	1.22
T2 [40]	52.8	0.10	33.0	1.60	0.03	3.32	32.8	1.61	0.03	3.16	37.9	1.39	0.04	2.78
T5 [40]	62.5	0.06	86.3	0.72	0.07	0.91	49.9	1.25	0.03	2.08	56.5	1.11	0.03	1.92
VH1 [41]	12.0	0.12	9.7	1.24	0.07	1.66	9.7	1.24	0.07	1.66	9.9	1.21	0.10	1.23
VH2 [41]	11.5	0.07	10.2	1.12	0.08	0.90	10.3	1.12	0.08	0.91	11.0	1.05	0.10	0.73
A2 [42]	109.5	0.06	112.0	0.98	0.06	1.13	66.9	1.64	0.03	2.54	76.6	1.43	0.03	2.27
A3 [42]	113.3	0.06	128.4	0.88	0.04	1.37	67.5	1.68	0.03	2.27	77.7	1.46	0.03	1.98
A4 [42]	120.9	0.06	75.2	1.61	0.02	2.60	74.5	1.62	0.03	2.44	86.2	1.40	0.03	2.14
A5 [42]	120.9	0.04	74.7	1.62	0.02	1.82	74.1	1.63	0.03	1.72	85.6	1.41	0.03	1.50
B2 [42]	116.7	0.04	131.8	0.89	0.04	1.25	84.5	1.38	0.03	1.70	97.5	1.20	0.03	1.49
B3 [42]	130.5	0.05	134.1	0.97	0.03	1.31	92.3	1.41	0.03	1.76	105.3	1.24	0.03	1.57
B4 [42]	142.9	0.07	99.0	1.44	0.03	2.76	96.4	1.48	0.03	2.76	109.9	1.30	0.03	2.46
B5 [42]	146.3	0.06	97.8	1.50	0.03	2.54	95.2	1.54	0.03	2.54	109.4	1.34	0.03	2.21
C2 [42]	124.5	0.05	126.5	0.98	0.03	1.49	97.4	1.28	0.03	1.83	96.3	1.29	0.04	1.38
C3 [42]	131.9	0.06	129.7	1.02	0.03	1.94	98.1	1.34	0.03	2.47	112.4	1.17	0.03	2.18
C4 [42]	132.6	0.05	102.1	1.30	0.03	2.02	100.1	1.32	0.03	1.95	116.0	1.14	0.03	1.69
C5 [42]	138.3	0.05	106.4	1.30	0.02	2.06	104.2	1.33	0.03	2.00	119.5	1.16	0.03	1.75
C6 [42]	139.1	0.05	103.4	1.34	0.03	2.10	101.7	1.37	0.03	2.04	117.0	1.19	0.03	1.78
A095c [26]	102.9	0.03	101.6	1.01	0.04	0.80	99.2	1.04	0.04	0.83	102.9	1.00	0.05	0.64
A120a [26]	89.8	0.05	86.8	1.03	0.04	1.15	85.7	1.05	0.04	1.18	86.4	1.04	0.04	1.11
B065b [26]	54.4	0.03	58.0	0.94	0.03	1.33	58.0	0.94	0.03	1.24	67.4	0.81	0.03	1.09
B080a [26]	65.2	0.03	70.3	0.93	0.02	1.32	69.9	0.93	0.03	1.26	79.7	0.82	0.03	1.13
B110a [26]	128.3	0.04	128.5	1.00	0.04	0.96	125.9	1.02	0.04	1.01	127.1	1.01	0.05	0.80
C065a [26]	91.7	0.03	128.2	0.72	0.03	0.83	89.0	1.03	0.03	1.07	101.0	0.91	0.03	0.99
C100a [26]	122.2	0.03	134.3	0.91	0.03	0.85	128.6	0.95	0.03	0.87	134.8	0.91	0.04	0.67
D075a [26]	90.1	0.03	121.9	0.74	0.03	0.84	95.3	0.95	0.03	1.00	109.8	0.82	0.03	0.90
D090a [26]	96.1	0.03	110.3	0.87	0.03	1.14	107.8	0.89	0.03	1.10	122.8	0.78	0.03	0.98

Table A4. Cracking torques and corresponding twists (smeared constitutive laws *l7* to *l8*).

Beam	M_{Tcr}^{exp} kNm	θ_{cr}^{exp} °/m	M_{Tcr}^{thl7} kNm	$\frac{M_{Tcr}^{exp}}{M_{Tcr}^{thl7}}$	θ_{cr}^{thl7} °/m	$\frac{\theta_{cr}^{exp}}{\theta_{cr}^{thl7}}$	M_{Tcr}^{thl8} kNm	$\frac{M_{Tcr}^{exp}}{M_{Tcr}^{thl8}}$	θ_{cr}^{thl8} kNm	$\frac{\theta_{cr}^{exp}}{\theta_{cr}^{thl8}}$
B3 [35]	20.1	0.12	21.5	0.94	0.11	1.18	24.6	0.82	0.12	1.03
B4 [35]	21.9	0.12	22.1	0.99	0.10	1.14	24.3	0.90	0.11	1.04
B5 [35]	22.6	0.14	22.8	0.99	0.10	1.33	24.7	0.91	0.11	1.23
B6 [35]	25.0	0.16	21.9	1.14	0.10	1.65	23.7	1.05	0.11	1.53
B7 [35]	20.2	0.11	20.2	1.00	0.10	1.06	23.9	0.84	0.12	0.90
B8 [35]	21.8	0.13	20.6	1.06	0.10	1.26	24.2	0.90	0.12	1.07
B9 [35]	19.6	0.11	21.9	0.90	0.11	0.99	24.7	0.79	0.12	0.88
C4 [35]	11.9	0.13	11.9	0.99	0.12	1.11	13.1	0.90	0.13	1.01
C5 [35]	14.0	0.17	11.8	1.18	0.12	1.42	12.8	1.10	0.13	1.32
C6 [35]	13.9	0.17	11.8	1.18	0.11	1.54	12.8	1.09	0.12	1.42
G3 [35]	27.1	0.10	30.5	0.89	0.09	1.02	35.0	0.77	0.11	0.88
G4 [35]	28.7	0.12	31.6	0.91	0.10	1.23	35.5	0.81	0.11	1.09
G5 [35]	29.5	0.11	30.9	0.95	0.09	1.23	34.2	0.86	0.10	1.11
G7 [35]	33.6	0.13	33.1	1.01	0.10	1.38	37.5	0.90	0.11	1.22
G8 [35]	33.6	0.12	32.1	1.05	0.10	1.28	35.3	0.95	0.11	1.16
I3 [35]	25.5	0.11	27.0	0.94	0.12	0.92	30.4	0.84	0.13	0.81
I4 [35]	28.0	0.12	27.4	1.02	0.11	1.08	30.3	0.92	0.13	0.97
I5 [35]	28.1	0.15	27.8	1.01	0.11	1.34	30.2	0.93	0.12	1.23
I6 [35]	27.5	0.13	28.3	0.97	0.11	1.13	29.9	0.92	0.12	1.07
J1 [35]	14.0	0.09	15.3	0.92	0.09	0.92	18.1	0.77	0.11	0.77
J2 [35]	17.1	0.12	15.3	1.11	0.09	1.36	17.6	0.97	0.11	1.18
J3 [35]	16.9	0.10	16.5	1.03	0.09	1.04	18.6	0.91	0.10	0.92
J4 [35]	18.0	0.11	16.4	1.09	0.09	1.22	18.1	0.99	0.10	1.10
K2 [35]	12.2	0.18	12.8	0.95	0.15	1.22	14.0	0.87	0.16	1.12
K3 [35]	12.4	0.19	12.4	1.01	0.14	1.40	13.1	0.95	0.15	1.32
K4 [35]	13.1	0.21	12.2	1.07	0.13	1.55	12.5	1.05	0.14	1.51
M1 [35]	19.2	0.11	21.9	0.88	0.11	0.99	25.4	0.76	0.12	0.86
M2 [35]	20.6	0.11	22.4	0.92	0.11	1.03	25.3	0.81	0.12	0.92
M3 [35]	20.7	0.12	21.1	0.98	0.10	1.17	23.4	0.88	0.11	1.06
M4 [35]	20.7	0.13	21.2	0.98	0.10	1.32	22.9	0.90	0.11	1.22
M5 [35]	21.7	0.12	22.0	0.99	0.10	1.19	23.1	0.94	0.11	1.13
M6 [35]	22.7	0.15	22.6	1.01	0.10	1.43	23.4	0.97	0.11	1.38
N1 [35]	7.6	0.13	7.1	1.07	0.17	0.77	8.0	0.95	0.19	0.68
N1a [35]	7.0	0.11	6.9	1.01	0.16	0.66	7.9	0.89	0.19	0.58
N2 [35]	7.4	0.22	7.3	1.02	0.17	1.30	8.0	0.93	0.18	1.19
N2a [35]	7.5	0.21	7.0	1.08	0.16	1.29	7.6	0.98	0.18	1.18
N3 [35]	7.4	0.21	7.0	1.06	0.17	1.28	7.6	0.97	0.18	1.18
N4 [35]	7.6	0.21	7.0	1.08	0.16	1.30	7.5	1.01	0.17	1.22
A2 [36]	11.3	0.12	13.8	0.82	0.13	0.91	15.9	0.71	0.15	0.79
A3 [36]	12.2	0.12	14.3	0.86	0.13	0.93	16.0	0.76	0.15	0.83
A4 [36]	12.5	0.15	14.4	0.87	0.13	1.13	15.8	0.79	0.15	1.03
B3 [36]	8.8	0.15	13.0	0.68	0.15	0.99	14.2	0.62	0.16	0.90
B4 [36]	10.2	0.15	13.0	0.78	0.15	1.01	14.0	0.73	0.16	0.93
B5UR1 [37]	11.6	0.09	13.0	0.89	0.14	0.60	14.8	0.79	0.16	0.53
B9UR1 [37]	13.0	0.13	17.2	0.76	0.16	0.86	19.7	0.66	0.18	0.75
B12UR1 [37]	16.2	0.09	17.8	0.91	0.16	0.58	20.2	0.80	0.18	0.51
B14UR1 [37]	19.3	0.12	18.8	1.02	0.16	0.73	21.5	0.90	0.18	0.64
B12UR2 [37]	17.8	0.11	17.4	1.03	0.16	0.71	19.9	0.89	0.18	0.62
B12UR3 [37]	16.0	0.10	17.5	0.91	0.16	0.64	19.5	0.82	0.18	0.58
B12UR4 [37]	16.9	0.14	18.0	0.94	0.16	0.87	19.7	0.86	0.18	0.80
B12UR5 [37]	13.6	0.04	18.0	0.75	0.16	0.22	20.0	0.68	0.18	0.20
H-06-12 [38]	75.0	0.09	85.0	0.88	0.09	0.92	94.2	0.80	0.10	0.83
H-07-10 [38]	70.5	0.09	77.1	0.91	0.09	1.03	89.5	0.79	0.10	0.89
H-07-16 [38]	65.3	0.09	80.3	0.81	0.09	0.94	87.5	0.75	0.10	0.86
H-12-12 [38]	77.1	0.07	87.0	0.89	0.10	0.78	96.3	0.80	0.11	0.71
H-12-16 [38]	79.3	0.09	86.5	0.92	0.09	0.98	94.6	0.84	0.10	0.89
H-14-10 [38]	61.8	0.09	78.8	0.78	0.09	0.96	90.5	0.68	0.10	0.83

Table A4. *Cont.*

Beam	M_{Tcr}^{exp} kNm	θ_{cr}^{exp} °/m	M_{Tcr}^{thl7} kNm	$\frac{M_{Tcr}^{exp}}{M_{Tcr}^{thl7}}$	θ_{cr}^{thl7} °/m	$\frac{\theta_{cr}^{exp}}{\theta_{cr}^{thl7}}$	M_{Tcr}^{thl8} kNm	$\frac{M_{Tcr}^{exp}}{M_{Tcr}^{thl8}}$	θ_{cr}^{thl8} kNm	$\frac{\theta_{cr}^{exp}}{\theta_{cr}^{thl8}}$
H-20-20 [38]	76.0	0.09	89.7	0.85	0.10	0.96	96.2	0.79	0.10	0.89
N-06-06 [38]	43.2	0.08	57.1	0.76	0.08	1.00	67.4	0.64	0.09	0.85
N-06-12 [38]	51.8	0.11	60.5	0.86	0.08	1.36	66.5	0.78	0.09	1.24
N-07-10 [38]	41.6	0.11	56.3	0.74	0.08	1.36	64.9	0.64	0.09	1.18
N-07-16 [38]	40.0	0.11	58.4	0.68	0.08	1.33	64.0	0.63	0.09	1.22
N-12-12 [38]	49.3	0.09	60.5	0.81	0.08	1.10	66.8	0.74	0.09	1.00
N-12-16 [38]	57.1	0.12	59.9	0.95	0.08	1.48	65.8	0.87	0.09	1.35
N-14-10 [38]	41.8	0.12	56.5	0.74	0.08	1.52	64.1	0.65	0.09	1.34
N-20-20 [38]	55.0	0.13	61.2	0.90	0.08	1.55	64.7	0.85	0.09	1.47
SW12-1 [39]	32.3	0.15	38.7	0.84	0.15	1.04	41.3	0.78	0.16	0.97
SW10-1 [39]	24.6	0.13	26.1	0.94	0.15	0.87	27.8	0.88	0.16	0.82
SW10-2 [39]	29.6	0.20	32.1	0.92	0.15	1.34	34.6	0.86	0.16	1.24
SW10-3 [39]	26.6	0.15	26.6	1.00	0.15	1.04	28.7	0.93	0.16	0.96
SW10-4 [39]	27.7	0.16	28.9	0.96	0.15	1.09	30.3	0.92	0.15	1.04
SW8-1 [39]	19.7	0.16	21.1	0.93	0.16	0.97	21.9	0.90	0.16	0.98
SW8-2 [39]	22.5	0.14	21.1	1.07	0.15	0.94	22.7	0.99	0.17	0.87
D3 [35]	15.2	0.08	8.4	1.81	0.06	1.42	9.1	1.67	0.06	1.32
D4 [35]	15.8	0.12	9.4	1.69	0.06	1.94	10.0	1.58	0.06	1.82
T0 [40]	49.8	0.06	41.2	1.21	0.03	1.78	44.1	1.13	0.04	1.68
T1 [40]	48.0	0.04	34.9	1.38	0.03	1.29	38.8	1.24	0.04	1.15
T2 [40]	52.8	0.10	34.9	1.51	0.03	2.93	38.8	1.36	0.04	2.63
T5 [40]	62.5	0.06	53.1	1.18	0.03	1.92	59.5	1.05	0.04	1.71
VH1 [41]	12.0	0.12	10.1	1.19	0.08	1.60	11.8	1.02	0.09	1.37
VH2 [41]	11.5	0.07	11.4	1.01	0.09	0.82	12.4	0.93	0.09	0.76
A2 [42]	109.5	0.06	67.7	1.62	0.03	2.49	79.5	1.38	0.03	2.09
A3 [42]	113.3	0.06	69.1	1.64	0.03	2.17	80.0	1.42	0.03	1.87
A4 [42]	120.9	0.06	77.9	1.55	0.03	2.34	87.7	1.38	0.03	2.05
A5 [42]	120.9	0.04	78.4	1.54	0.03	1.61	87.0	1.39	0.03	1.44
B2 [42]	116.7	0.04	86.4	1.35	0.03	1.69	99.8	1.17	0.03	1.44
B3 [42]	130.5	0.05	96.6	1.35	0.03	1.66	108.8	1.20	0.03	1.47
B4 [42]	142.9	0.07	100.7	1.42	0.03	2.60	112.4	1.27	0.03	2.36
B5 [42]	146.3	0.06	100.0	1.46	0.03	2.42	110.6	1.32	0.03	2.17
C2 [42]	124.5	0.05	99.0	1.26	0.03	1.79	115.2	1.08	0.03	1.56
C3 [42]	131.9	0.06	102.9	1.28	0.03	2.33	116.0	1.14	0.03	2.04
C4 [42]	132.6	0.05	105.4	1.26	0.03	1.86	117.1	1.13	0.03	1.66
C5 [42]	138.3	0.05	109.5	1.26	0.03	1.88	122.1	1.13	0.03	1.67
C6 [42]	139.1	0.05	109.5	1.27	0.03	1.87	118.1	1.18	0.03	1.75
A095c [26]	102.9	0.03	100.2	1.03	0.04	0.82	120.2	0.86	0.05	0.68
A120a [26]	89.8	0.05	87.6	1.03	0.04	1.15	104.2	0.86	0.05	0.95
B065b [26]	54.4	0.03	62.0	0.88	0.03	1.16	66.8	0.81	0.03	1.07
B080a [26]	65.2	0.03	72.0	0.91	0.03	1.22	81.3	0.80	0.03	1.09
B110a [26]	128.3	0.04	128.6	1.00	0.04	0.99	152.2	0.84	0.05	0.82
C065a [26]	91.7	0.03	92.8	0.99	0.03	1.01	105.7	0.87	0.03	0.88
C100a [26]	122.2	0.03	133.1	0.92	0.03	0.84	153.1	0.80	0.04	0.72
D075a [26]	90.1	0.03	100.1	0.90	0.03	0.95	111.8	0.81	0.03	0.85
D090a [26]	96.1	0.03	110.6	0.87	0.03	1.09	126.0	0.76	0.03	0.94

References

1. Hsu, T.T.C.; Mo, Y.L. *Unified Theory of Concrete Structures*; John Wiley Sons Ltd.: Chichester, UK, 2010; p. 500.
2. Bernardo, L.F.; Andrade, J.M. A unified softened truss model for RC and PC beams under torsion. *J. Build. Eng.* **2020**, *32*, 101467. [CrossRef]
3. Hsu, T.T.C.; Mo, Y.L. Softening of concrete in torsional members—Theory and tests. *J. Am. Concr. Inst.* **1985**, *82*, 290–303.
4. Hsu, T.; Belarbi, A.; Pang, X. A Universal panel tester. *J. Test. Eval.* **1995**, *23*, 41. [CrossRef]
5. Bernardo, L.F.A.; Lopes, S.M.R. Behavior of concrete beams under torsion—NSC plain and hollow beams. *Mater. Struct.* **2008**, *41*, 1143–1167. [CrossRef]
6. Bernardo, L.F.A.; Lopes, S.M.R. Theoretical behavior of HSC sections under torsion. *Eng. Struct.* **2011**, *33*, 3702–3714. [CrossRef]

7. Bairan Garcia, J.M.; Mari Bernat, A.R. Coupled model for the non-linear analysis of anisotropic sections subjected to general 3D loading. Part 1: Theoretical formulation. *Comput. Struct.* **2006**, *84*, 2254–2263. [CrossRef]
8. Bairan Garcia, J.M.; Mari Bernat, A.R. Coupled model for the nonlinear analysis of sections made of anisotropic materials, subjected to general 3D loading. Part 2: Implementation and validation. *Comput. Struct.* **2006**, *84*, 2264–2276. [CrossRef]
9. Jeng, C.-H.; Hsu, T.T. A softened membrane model for torsion in reinforced concrete members. *Eng. Struct.* **2009**, *31*, 1944–1954. [CrossRef]
10. Mostofinejad, D.; Behzad, T.S. Nonlinear modeling of RC beams subjected to torsion using smeared crack model. *Procedia Eng.* **2011**, *14*, 1447–1454. [CrossRef]
11. Valikhani, A.; Jahromi, A.J.; Mantawy, I.M.; Azizinamini, A. Numerical modelling of concrete-to-UHPC bond strength. *Materials* **2020**, *13*, 1379. [CrossRef]
12. Sucharda, O. Identification of fracture mechanic properties of concrete and analysis of shear capacity of reinforced concrete beams without transverse reinforcement. *Materials* **2020**, *13*, 2788. [CrossRef]
13. Hsu, T.T.C.; Mo, Y.L. Softening of concrete in torsional members—Prestressed concrete. *J. Am. Concr. Inst.* **1985**, *82*, 603–615.
14. Bernardo, L.F.; Taborda, C.S.; Andrade, J.M. Ultimate torsional behaviour of axially restrained RC beams. *Comput. Concr.* **2015**, *16*, 67–97. [CrossRef]
15. Taborda, C.S.B.; Bernardo, L.F.B.; Gama, J.M.R. Effective torsional strength of axially restricted RC beams. *Struct. Eng. Mech.* **2018**, *67*, 465–479.
16. Bernardo, L.F.A.; Andrade, J.M.A.; Nunes, N.C.G. Generalized softened variable angle truss-model for reinforced concrete beams under torsion. *Mater. Struct.* **2014**, *48*, 2169–2193. [CrossRef]
17. Bernardo, L.F.A.; Taborda, C.S.B.; Andrade, J.M.A. Generalized softened variable angle truss model for PC Beams under torsion. *Int. J. Concr. Struct. Mater.* **2018**, *12*, 62. [CrossRef]
18. Bernardo, L. Generalized softened variable angle truss model for RC hollow beams under torsion. *Materials* **2019**, *12*, 2209. [CrossRef] [PubMed]
19. Bernardo, L. Modeling the full behavior of reinforced concrete flanged beams under torsion. *Appl. Sci.* **2019**, *9*, 2730. [CrossRef]
20. Bernardo, L.; Andrade, J.; Lopes, S. Softened truss model for reinforced NSC and HSC beams under torsion: A comparative study. *Eng. Struct.* **2012**, *42*, 278–296. [CrossRef]
21. Teixeira, M.; Bernardo, L. Ductility of RC beams under torsion. *Eng. Struct.* **2018**, *168*, 759–769. [CrossRef]
22. Belarbi, A.; Hsu, T.T.C. Constitutive laws of softened concrete in biaxial tension—Compression. *Struct. J. Am. Concr. Inst.* **1995**, *92*, 562–573.
23. Zhang, L.X.; Hsu, T.C. Behaviour and analysis of 100 MPa concrete membrane elements. *J. Struct. Eng.* **1998**, *124*, 24–34. [CrossRef]
24. Belarbi, A.; Hsu, T.C. Constitutive laws of concrete in tension and reinforcing bars stiffened by concrete. *Struct. J. Am. Concr. Inst.* **1994**, *91*, 465–474.
25. Bernardo, L.F.A.; Andrade, J.M.A.; Oliveira, L.A.P. Reinforced and prestressed concrete hollow beams under torsion. *J. Civ. Eng. Manag.* **2013**, *19*, S141–S152. [CrossRef]
26. Jeng, C.H. Unified softened membrane model for torsion in hollow and solid reinforced concrete members: Modeling precracking and postcracking behavior. *J. Struct. Eng.* **2015**, *141*. [CrossRef]
27. Nobre, S.S. Evaluation of the Constitutive Law for Tensile Concrete for the Cracking of Reinforced Concrete Beams under Torsion. Master's Thesis, University of Beira Interior, Covilhã, Portugal, 2014; p. 150. (In Portuguese).
28. Cervenka, V. Constitutive model for cracked reinforced concrete. *J. Am. Concr. Inst.* **1985**, *82*, 877–882.
29. Vecchio, F.J.; Collins, M.P. The modified compression—Field theory for reinforced concrete elements subjected to shear. *J. Am. Concr. Inst.* **1986**, *83*, 219–231.
30. Hsu, T.T.C. Nonlinear analysis of concrete membrane elements. *Struct. J. Am. Concr. Inst.* **1991**, *88*, 552–561.
31. Collins, M.P.; Mitchell, D.; Adebar, P.; Vecchio, F.J. A General shear design method. *Am. Concr. Inst. Struct. J.* **1996**, *93*, 36–45.
32. Vecchio, F.J. Disturbed Stress field model for reinforced concrete: Formulation. *J. Struct. Eng.* **2000**, *126*, 1070–1077. [CrossRef]
33. Bentz, E.C. Explaining the riddle of tension stiffening models for shear panel experiments. *J. Struct. Eng.* **2005**, *131*, 1422–1425. [CrossRef]
34. Stramandinoli, R.S.B.; Rovere, H.L. An efficient tension-stiffening model for nonlinear analysis of reinforced concrete members. *Eng. Struct.* **2008**, *30*, 2069–2080. [CrossRef]
35. Hsu, T.T.C. *Torsion of Structural Concrete-Behavior of Reinforced Concrete Rectangular Members*; Torsion of Structural Concrete SP-18; American Concrete Institute: Detroit, MI, USA, 1968; pp. 261–306.
36. McMullen, A.E.; Rangan, B.V. Pure torsion in rectangular sections—A re-examination. *J. Am. Concr. Inst.* **1978**, *75*, 511–519.
37. Koutchoukali, N.E.; Belarbi, A. Torsion of high-strength reinforced concrete beams and minimum reinforcement requirement. *Am. Concr. Inst. Struct. J.* **2001**, *98*, 462–469.
38. Fang, I.K.; Shiau, J.K. Torsional behavior of normal and high-strength concrete beams. *Am. Concr. Inst. Struct. J.* **2004**, *101*, 304–313.
39. Peng, X.-N.; Wong, Y.-L. Behavior of reinforced concrete walls subjected to monotonic pure torsion—An experimental study. *Eng. Struct.* **2011**, *33*, 2495–2508. [CrossRef]

40. Lampert, P.; Thürlimann, B. Essais de Poutre en Béton Armé sous Torsion Simple et Flexion Combinées (Torsionsversuche und Torsions-Biege-Versuche an Stahlbetonbalken). *Comitée Européen du Béton B.I.* **1969**, *71*, 177–207.
41. Leonhardt, F.; Schelling, G. *Torsionsversuche na Stahlbetonbalken*; Bulletin No. 239; Deutscher Ausschuss für Stahlbeton: Berlin, Germany, 1974; 122p.
42. Bernardo, L.F.A.; Lopes, S.M.R. Torsion in HSC hollow beams: Strength and ductility analysis. *Am. Concr. Inst. Struct. J.* **2009**, *106*, 39–48.

Structures 26 (2020) 651–669

Contents lists available at ScienceDirect

Structures

journal homepage: www.elsevier.com/locate/structures

Refined softened-truss model with efficient solution procedure for reinforced concrete members under torsion combined with bending

L.F.A. Bernardo*, M.M. Teixeira

University of Beira Interior, C-MADE – Centre of Materials and Building Technologies, Covilhã, Portugal

ARTICLE INFO

Keywords:
Combined Action Softened Truss Model
Reinforced concrete members
Torsion
Bending
Efficient solution procedure
Stress–strain relationships

ABSTRACT

This article presents a refined version of the Combined Action Softened Truss Model (CA-STM) with efficient solution procedure to analyze reinforced concrete (RC) members under torsion combined with bending. To refine the model, a set of appropriate smeared stress–strain relationships for concrete and steel bars, to account for the softening and stiffening effects, are implemented. For solid sections, an alternative criterion to fix the maximum thickness for the panels constituting the walls of the equivalent hollow section is also considered. In addition, a simpler criterion is used to compute the equivalent longitudinal reinforcement for each panel. Instead of using the original algorithm to solve the CA-STM, which is based on a classical trial and error solution technique, an alternative one which lead to a more efficient solution procedure with higher numerical stability is implemented. These refinements allow the model to predict efficiently the response of RC members under torsion combined with bending. The results obtained from the refined efficient CA-STM procedure are compared with several experimental results found in the literature, where good agreement is observed.

1. Introduction

In many concrete structural systems, torsion can be one of the primary internal forces to be considered for the design of section members. As examples, long span curved bridges and complex building structures, under gravity and seismic loads, usually incorporates structural members under high torsion combined with other internal forces, such as girders or spandrel beams, and even columns [1–3]. For reinforced concrete (RC) members under such loading conditions, the internal stress state is not easy to be precisely characterized by simple analytical models, in particular after concrete cracking. For this reason, since the second half of the last century, several analytical models have been proposed to predict the effects of combined loading in RC members.

Most of the earliest models were based on the skew-bending approach which was firstly proposed by Hsu in [4] for RC members under pure torsion. This approach only considers the equilibrium at the ultimate stage and, for this reason, is only able to predict the strength capacity of the cross section. In addition, this model was mainly formulated and calibrated for small rectangular and solid RC members. In spite of this, it was further developed over more than two decades and had considerable influence in some important codes of practice, namely the ACI code until 1995. As examples, further developments to predict the capacity of RC members under combined loading (bending, torsion and shear) by using the skew-bending approach were proposed by McMullen and Warwaruk in [5], and also Elfgren et al. in [6].

From that same time period, several authors worked with a different approach, the space truss analogy (STA), and proposed refinements to the first 3D truss-based model from Rausch [7] in the beginning of last century. This happened because, when compared with the skew-bending theory, the STA is considered to be a more comprehensive analytical model, which allows to understand physically better how a cracked RC member behaves under torsion. The STA also allows to unify the formulation for both small and large cross sections with arbitrary geometry, as well as for RC and prestressed concrete (PC) members. When compared with the skew-bending approach, further developments of the STA also allowed to predict the envelope of the load-deformation response for RC members (not only the strength). Such models were developed for RC members under pure torsion (for instance, Mitchell and Collins in [8], Hsu and Mo in [9], Jeng and Hsu in [10], Bernardo et al. in [11]) and also under combined loading, namely for combined torsion and bending (Lampert and Thürlimann in [12]), for combined torsion and shear (Rahal and Collins in [13], Kothamuthyala et al. in [14]), for combined torsion, bending and axial load (Cocchi and Volpi in [15]), for combined torsion and axial force (Bernardo et al. in [16], Ganganagoudar et al. in [17]) and for more complex loading conditions (Rabbat and Collins in [18], Greene and

* Corresponding author at: University of Beira Interior, Department of Civil Engineering and Architecture, Edifício II das Engenharias, Calçada Fonte do Lameiro, 6201-001 Covilhã, Portugal.
E-mail address: lfb@ubi.pt (L.F.A. Bernardo).

https://doi.org/10.1016/j.istruc.2020.04.055
Received 21 December 2019; Received in revised form 26 March 2020; Accepted 29 April 2020

Belarbi in [19], Valipour and Foster in [20]). Further refinements of the models proposed in the previous studies also included PC members (Hsu and Mo in [21], Rahal and Collins in [22], Jeng et al. in [23], Bernardo et al. in [24]).

In spite of this, the accuracy of the previously referred models still needs to be checked and improved, namely for low loading stages and also for more general loading conditions. For this last case, the analysis naturally becomes more complex as a result of the internal stress states originated by each internal force and their interaction. For this reason, the work to develop refined STA based models for combined actions on RC members is still ongoing.

Among the more general models based on the STA, Greene and Belarbi in [19] proposed the so-called Combined Action Softened Truss Model (CA-STM). This model idealizes the real RC member under study as the association of 4 cracked RC panels under in-plane stresses, thus neglecting the concrete core in solid members. Each panel, is modeled with the Rotating Angle Softened Truss Model (RA-STM) from Pang and Hsu in [25], which is a softened truss-based model developed for two-dimensional (2D) RC members under in-plane stress states (membrane elements). The RA-STM is still widely used and has proven to be a reliable model to compute well the envelope of the load-deformation response for both RC and PC membrane elements [26–28]. The RA-STM is a simpler model which does not account for the shear in concrete in the struts, nor the Poisson's effect in the cracked stage, such as for the Softened Membrane Model (SMM) from Zhu and Hsu in [29] which constitutes a somewhat more complex analytical model. Nevertheless, the global theoretical predictions from the RA-STM are found to be in good agreement when compared with the experimental ones. Some differences are observed when the results from the RA-STM are compared with the predictions from the SMM [28]. These differences show that, in general, the post-peak behavior is better predicted by the SMM. However, this aspect is not very important for current design. In addition, the RA-STM is easier to be implemented in a computer with current programming languages because it involves less variables.

The aforementioned justify why the CA-STM uses the RA-STM to model each of the idealized cracked RC panels under in-plane stresses. It should be referred that improved SMM models for combined actions have been recently proposed with good results [14,17]. However, as for the RA-STM for RC and PC membrane elements, the CA-STM also showed to be able to predict well the response of RC members under torsion combined with bending, shear and axial force, namely a far as the torsional response of the members is concerned [30].

The original CA-STM has a somewhat complex calculation procedure due to the intrinsic nonlinear characteristic of the equations. Furthermore, as for the previously referred truss-based models, the calculation procedure is based on a trial-and-error technique which may require a large calculation effort. It can also lose numerical efficiency and stability due to the large number of initial estimates which are needed to start the calculations. For these reasons, alternative and efficient solution procedures are still required. Silva et al. in [31] studied a statically indeterminate RC beam under combined loading, namely the effects due to the decrease of the member's torsional stiffness after cracking. For this, the referred authors used a softened truss model based on the CA-STM and reformulated the calculation procedure as a system of nonlinear equations with constraints. This allowed to reduce the number of initial estimates. In addition, a new algorithm was proposed in which the nonlinear equations were solved using an optimization algorithm instead of using the original trial-and-error technique. This new calculation procedure showed to be numerically more efficient and stable, and also to require less computational calculation effort. In order to verify the effectiveness of the proposed calculation procedure, the predictions were compared with few experimental results related with RC beams under torsion and also under torsion combined with shear. Good agreement was observed, namely for the ultimate stage [31].

To complement the study from Silva et al. in [31], the proposed efficient calculation procedure for the CA-STM still needs to be checked based on a comparative analysis with a much more extensive experimental data. In particular, members under torsion combined with bending were not considered in the referred study to validate the proposed model. Furthermore, some numerical issues were reported, which are related with the used value to fix the maximum thickness for the walls of the equivalent hollow cross section, which have limited the number of studied members. Such numerical issues still need to be solved.

To fix the previously referred issues, a new refined version of the CA-STM is proposed in this article and used to compute the full response of RC members under torsion combined with bending. The results are checked against the experimental ones for several tested beams reported in the literature. This particular loading condition (torsion combined with bending) was chosen by the authors as the first one to be studied to check thoroughly the reliability of the proposed model, before other loading conditions are addressed.

To refine the CA-STM, some changes are proposed. Firstly, a set of appropriate smeared stress (σ) – strain (ε) relationships for concrete in compression and tensile steel bars embedded in concrete are implement to properly account for the softening and stiffening effects. The smeared relationships were chosen based on the conclusions of a previous study from Bernardo et al. in [32] where the authors tested several proposals for $\sigma - \varepsilon$ relationships found in the literature. The chosen relationships also proved to be appropriate for the RA-STM [26], which constitutes the base model for the CA-STM as previously referred. In addition, for solid cross sections an alternative criterion to fix the maximum thickness for the panels, which constitute the walls of the equivalent hollow cross section, is also proposed. The aim is to improve the numerical stability of the calculation procedure, as well as the estimates from the model for all loading stages, including the transition between the uncracked and cracked stage. To attain the previous goal, a simpler criterion is also used to compute the equivalent longitudinal reinforcement for each panel instead of using the original one for the CA-STM [19,30,31]. Finally, the original calculation procedure of the CA-STM is reviewed and reformulated according to some proposals from Silva et al. in [31] to improve the numerical efficiency and stability. The new version of the model is called here "refined efficient CA-STM procedure".

Based on a comparative analysis with several experimental results found in the literature, it is showed that the refined efficient CA-STM procedure predicts well the full behavior of RC members under torsion combined with bending.

2. Refined efficient CA-STM procedure

In this section, the refined efficient CA-STM procedure is presented with some detail and discussion. Although only RC members under torsion combined with bending will be studied latter to check the proposed new version of the model, for the sake of clarity the formulation for the general case of combined loading (Fig. 1) is described in the same way as performed in related previous studies [19,31]. More detailed information about the original CA-STM can be found in [19].

The CA-STM assumes that a RC member can be idealized as the association of 4 cracked RC panels to form a rectangular closed thin-walled member (Fig. 1), thus the concrete core is neglected in solid members. The internal forces applied in the cross section (see Fig. 1, which also shows the assumed positive directions for the axes, forces and moments) are transmitted to the RC panels through normal stresses for bending and axial force and/or shear stresses for torsion and shear force (Fig. 1). Classical theory for closed thin-walled members is assumed, which considers that the cross section resists to torsion through a constant shear stress flow acting along the perimeter of the panels. The CA-STM assumes this principle for both solid and hollow members, as well as for members under torsion combined with other internal forces. The thickness of each RC panel i ($t_{D,i}$, see Fig. 1) is considered to

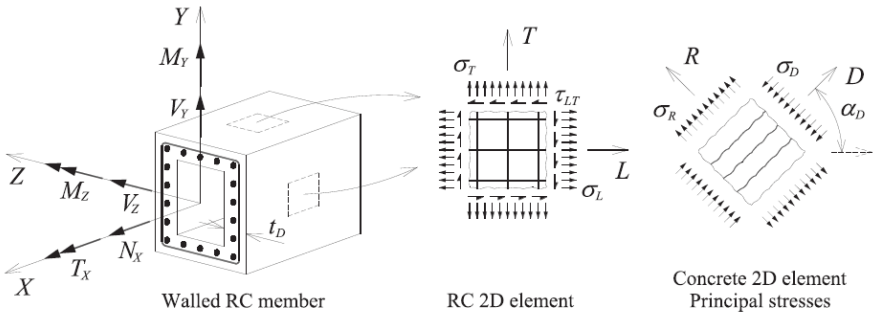

Fig. 1. Idealization of the RC member.

be equal to the effective thickness of the shear stress flow.

As previously referred, the assumed resistance mechanism for each RC panel is the RA-STM [25], which considers both longitudinal and transverse reinforcement in tension and diagonal concrete struts in compression (Fig. 1). As hypothesis, the dowel effect on the reinforcing bars is also neglected. In addition, perfect bond between reinforcing bars and concrete is assumed. The main coordinate system is referred to the principal stresses in the concrete 2D element (coordinate system $R-D$ in Fig. 1). In each RC panel, the angle $\alpha_{D,i}$ between axis D and the longitudinal axis L is allowed to vary so that the shear stress remains null in the main coordinate system ($R-D$). Finally, as will be presented latter, smeared constitutive relationships for the materials are assumed to characterize the relation between the stresses (σ) and strains (ε).

2.1. Idealization of the cross section and loading

As referred before, according to the CA-STM the real RC member is idealized as the association of 4 RC panels with some thickness. Then, the longitudinal and transverse reinforcement must be distributed by each RC panel. In addition, the in-plane stress state in each RC panel must be computed from the internal forces acting on the real cross section.

2.1.1. Cross section geometry

Fig. 2 illustrates how a real rectangular (with width b and height h) closed walled cross section (with real wall's thickness t_i, being i the number of the wall or panel) is transformed into the idealized cross section (with effective wall's thickness $t_{D,i}$). For rectangular solid cross sections, the walls' thickness t_i represents the maximum allowed thickness of each panel. Greene and Belarbi in [19] assumed t_i to be half the minimum outer dimension of the real cross section (usually the width b). However, as observed by Silva et al. in [31], such criterion sometimes leads to convergence problems during the calculation procedure, mainly for large solid cross sections. For this reason, the referred authors proposed to adopt a maximum thickness lesser than the one adopted by Greene and Belarbi in [19]. Furthermore, by applying the referred original criterion in this study, convergence problems were also observed for beams with high ratios of bending moment to torque and also for cross sections reinforced with highly asymmetrical longitudinal reinforcement between opposite panels. To solve these drawbacks, and since torsion is considered a primary internal force, in this study the maximum allowed thickness of each panel was assumed to be defined from torsional considerations, namely by using a normative condition. For this study, Eurocode 2 [33] was used as the standard code. For torsional design, this code prescribes the following effective thickness (t_{ef}) for the walls (with $A = A_{cp}$ the area limited by the outer perimeter of the cross section and $u = p_{cp}$ the referred perimeter):

$$t_{ef} = \frac{A}{u} = \frac{A_{cp}}{p_{cp}} \tag{1}$$

$$A_{cp} = bh \tag{2}$$

$$p_{cp} = 2b + 2h \tag{3}$$

After several simulations and comparisons with experimental results, it was found that the criterion from Eq. (1) to compute t_i generally led to good numerical stability and also good estimates.

The CA-STM assumes that the center line of the shear flow coincides with the axes of the RC panels in the cross section with effective wall's thickness $t_{D,i}$. The geometry of the center line of the shear flow is defined by the width b_0, the height h_0 and the area enclosed A_0 (see

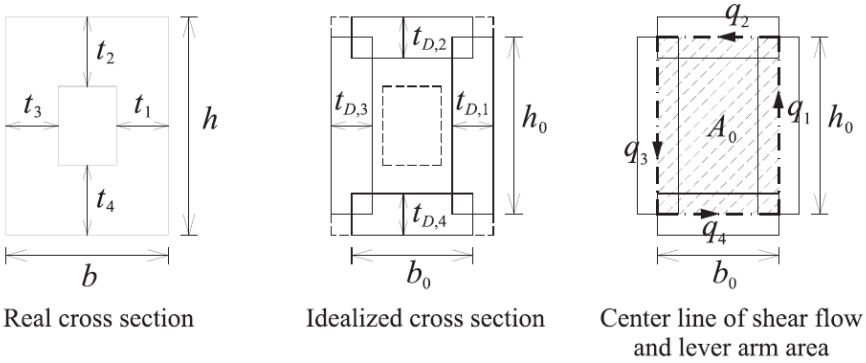

Fig. 2. Idealization of the cross section.

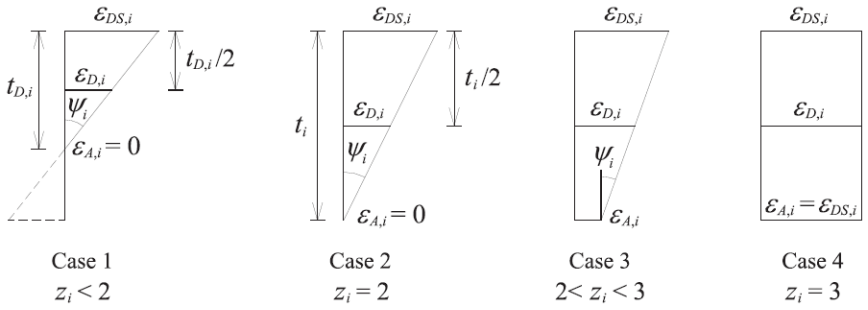

Fig. 3. Compressive strain diagrams in concrete struts.

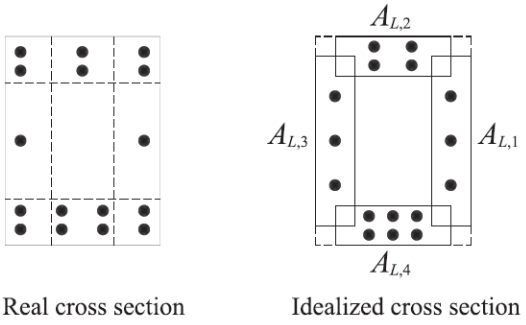

Fig. 4. Distribution of the longitudinal reinforcement (example).

Fig. 2):

$$b_0 = b - 0.5t_{D,1} - 0.5t_{D,3} \tag{4}$$

$$h_0 = h - 0.5t_{D,2} - 0.5t_{D,4} \tag{5}$$

$$A_0 = b_0 h_0 \tag{6}$$

2.1.2. Thickness of the shear flow

As firstly observed by Lampert and Thürlimann in [34] with experiments, as a RC member twists due to torsion the external faces become curved and assume a hyperbolic paraboloid shape. As a consequence, the concrete struts undergo bending in addition to compression. This effect is considered through a linear gradient of the principal compressive strains in the panels ($\varepsilon_{D,i}$). Fig. 3 shows the 4 possible shapes for the compressive strain diagrams along the thickness of the strut, where $\varepsilon_{DS,i}$ and $\varepsilon_{A,i}$ represent the strains at the exterior and interior faces of the concrete strut, respectively. According to Fig. 3, the average compressive strain $\varepsilon_{D,i}$ and the curvature of the strut ψ_i can be computed according to Eqs. (7) and (8), respectively.

$$\varepsilon_{D,i} = \frac{\varepsilon_{DS,i} + \varepsilon_{A,i}}{2} \tag{7}$$

$$\psi_i = -\frac{\varepsilon_{DS,i} - \varepsilon_{A,i}}{t_{D,i}} \tag{8}$$

In Fig. 3, z_i is a dimensionless parameter related to the shape of the strain diagram and ranging between the assumed values 0 and 3 [31]. This parameter allows to relate several variables, according to Eqs. (9) and (10), and is considered one of the primary variables in the efficient calculation procedure for the CA-STM.

$$\varepsilon_{A,i} = \begin{cases} 0 \text{ for } 0 < z_i \leqslant 2 \\ (z_i - 2)\varepsilon_{DS,i} \text{ for } 2 < z_i \leqslant 3 \end{cases} \tag{9}$$

$$t_{D,i} = \begin{cases} z_i t_i/2 \text{ for } 0 < z_i \leqslant 2 \\ t_i \text{ for } 2 < z_i \leqslant 3 \end{cases} \tag{10}$$

2.1.3. Equivalent steel areas for each panel

A detailed description of the criterion used in the original CA-STM to compute the equivalent steel areas for each panel, from the real cross section, can be found in [35]. This criterion was also used by Silva et al. in [31] to study RC beams under torsion and also under torsion combined with shear. However, for some of the RC beams under torsion combined with bending analyzed in the present study, the application of the original criterion sometimes led to inconsistencies, namely negative areas of longitudinal reinforcement for the panel opposite to the one where longitudinal tensile reinforcement for bending exists. This usually happened for beams with high asymmetrical longitudinal reinforcement between the opposite panels perpendicular to the bending plane. This inconsistency led to numerical problems and, for this reason, the original criterion was not applied in this study. Instead, the equivalent area of longitudinal steel area for each panel was simply considered to be the value corresponding to the influence area of each panel, as illustrated in Fig. 4 for a solid cross section as example. According to this criterion, half of the area of the longitudinal bar located at the corner is attributed to each adjacent panel. For the transverse reinforcement, since all analyzed beams were detailed with only one closed stirrup, the equivalent distributed steel area of transverse reinforcement is simply A_T/s, being A_T the area of one leg and s the longitudinal spacing of the stirrup.

2.1.4. Equivalent loading for each panel

The CA-STM assumes that the idealized cross section resists to shear forces (V_Y and V_Z) and torsion (T_X) through constant shear flows along the panels. For torsion, all panels contribute for the resistance with the shear flow computed from Bredt's theory for close thin walled tubes, while for shear force only the two panels parallel to the force contribute. The shear flow q_i is considered positive in the counter-clockwise direction (see Fig. 2). The interaction between torsion and shear in each panel is simply considered through the sum of each shear flow. Considering the positive direction for the internal forces in Fig. 1, the shear flow q_i in each panel is computed as follows (see Fig. 2 for the meaning of geometrical parameters):

$$q_1 = \frac{T_X}{2A_0} + \frac{V_Y}{2h_0} \tag{11}$$

$$q_2 = \frac{T_X}{2A_0} + \frac{V_z}{2b_0} \tag{12}$$

$$q_3 = \frac{T_X}{2A_0} - \frac{V_Y}{2h_0} \tag{13}$$

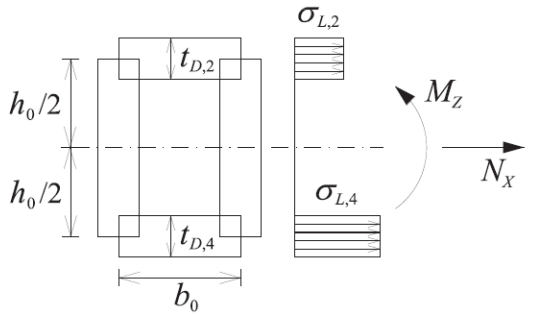

Fig. 5. Nomal stress distribution (example).

$$q_4 = \frac{T_X}{2A_0} - \frac{V_z}{2b_0} \tag{14}$$

The shear stress in each panel $\tau_{LT,i}$ is computed as follows:

$$\tau_{LT,i} = \frac{q_i}{t_{D,i}} \tag{15}$$

The CA-STM also assumes that the idealized cross section resists to bending moments (M_Y and M_Z) and axial force (N_X) through uniform normal stresses $\sigma_{L,i}$ in each panel, as illustrated in Fig. 5 for the loading case $M_Z + N_X$ as example. Based on this assumption, the following equations can be derived to relate the bending moments and the axial force to the normal stresses in the panels:

$$M_Y = (\sigma_{L,3}t_{D,3}h_0 - \sigma_{L,1}t_{D,1}h_0)\frac{b_0}{2} \tag{16}$$

$$M_Z = (\sigma_{L,4}t_{D,4}b_0 - \sigma_{L,2}t_{D,2}b_0)\frac{h_0}{2} \tag{17}$$

$$N_X = \sigma_{L,1}t_{D,1}h_0 + \sigma_{L,2}t_{D,2}b_0 + \sigma_{L,3}t_{D,3}h_0 + \sigma_{L,4}t_{D,4}b_0 \tag{18}$$

2.2. Equilibrium and compatibility equations

As stated before, the CA-STM assumes for the RC panels the same resistance mechanism as for the RA-STM [25,36], thus the equilibrium and compatibility equations for each panel are the same, although they must be rewritten for each panel i:

$$\sigma_{L,i} = \sigma_{D,i}\cos^2(\alpha_{D,i}) + \sigma_{R,i}\sin^2(\alpha_{D,i}) + f_{L,i}(A_{L,i}/(t_{D,i}w_{0,i})) \tag{19}$$

$$\sigma_{T,i} = \sigma_{R,i}\cos^2(\alpha_{D,i}) + \sigma_{D,i}\sin^2(\alpha_{D,i}) + f_{T,i}(A_T/(t_{D,i}s)) \tag{20}$$

$$\tau_{LT,i} = (\sigma_{R,i} - \sigma_{D,i})\sin(\alpha_{D,i})\cos(\alpha_{D,i})sign(q_i) \tag{21}$$

$$\gamma_{LT,i} = 2(\varepsilon_{R,i} - \varepsilon_{D,i})\sin(\alpha_{D,i})\cos(\alpha_{D,i})sign(q_i) \tag{22}$$

$$\varepsilon_{T,i} = \varepsilon_{R,i} + \varepsilon_{D,i} - \varepsilon_{L,i} \tag{23}$$

In the previous equations and for each panel i, the meaning of the new parameters are: $\sigma_{L,i}$ and $\sigma_{T,i}$ are the longitudinal and transverse stresses, respectively, $f_{L,i}$ and $f_{T,i}$ are the tensile stresses in the longitudinal and transverse reinforcement, respectively, $\sigma_{D,i}$ and $\sigma_{R,i}$ are the principal compressive and tensile stresses in concrete, respectively, $\tau_{LT,i}$ and $\gamma_{LT,i}$ are the shear stress and shear strain, respectively, $\alpha_{D,i}$ is the angle of concrete struts, $\varepsilon_{L,i}$ and $\varepsilon_{T,i}$ are the tensile strains in the longitudinal and transverse reinforcement, respectively, $\varepsilon_{D,i}$ and $\varepsilon_{R,i}$ are the principal compressive and tensile strains in concrete, respectively, and $w_{0,i}$ is the width of panel i (equal to b_0 for panels 2 and 4, and equal to h_0 for panels 1 and 3, see Fig. 2). The remaining parameters were already defined before. The terms $A_{L,i}/(t_{D,i}w_{0,i})$ and $A_T/(t_{D,i}s)$ represent the longitudinal ($\rho_{L,i}$) and transverse ($\rho_{T,i}$) reinforcement ratio for each panel i, respectively. Finally, term $sign(q_i)$ in Eq. (21) and (22) is a function to attribute the sign of the shear flow.

2.3. Constitutive laws for the materials

As referred in the introduction section and based on the conclusions of a previous study from Bernardo et al. in [32], appropriate smeared σ - ε relationships for the materials were chosen for this study. These relationships proved to be suitable for the RA-STM to model RC and PC panels [26–28] and will also be used here to refine the CA-STM.

As previously referred, the CA-STM idealizes the real RC member as the association of 4 cracked RC panels under in-plane stresses. Each panel is modeled with the RA-STM developed for 2D thin RC members under in-plane stresses (membrane elements). For this reason, the out-of-plane shear stress due to torsion and any influence of confinement are neglected, including for solid members for which the concrete core is disregarded. In fact, in the cracked stage and due to the location of the reinforcement, the torsional stresses are mainly supported by the outer shell of the cross section. For these reasons, smeared relationships for the materials calibrated from tests on thin RC panels subjected to in-plane shear were used in this study. This simplification is also considered in several previous studies which uses panels- or membrane-based models to simulate the behavior of RC members under torsion [8–11] and also RC members under torsion combined with other loadings [12–20]. From the results reported in such studies, the referred simplification proved to be valid.

2.3.1. Concrete in compression

For concrete in compression, the smeared and softened σ - ε relationship firstly proposed by Belarbi and Hsu in [37] and refined latter by Zhu et al. in [38] (Eq. (24), see Fig. 6) was adopted. The softening coefficient (ζ_i) was computed according to Zhang and Hsu in [39] (Eq. (25) to (27)).

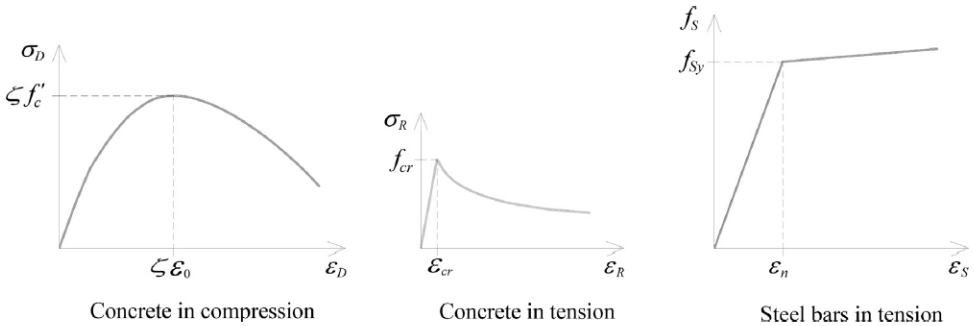

Fig. 6. Constitutive laws for the materials.

$$\sigma_{D,i} = \zeta_i f'_c \left[2\left(\frac{\varepsilon_{D,i}}{\zeta_i \varepsilon_0}\right) - \left(\frac{\varepsilon_{D,i}}{\zeta_i \varepsilon_0}\right)^2 \right] \text{ if } \varepsilon_{D,i} \leqslant \zeta_i \varepsilon_0 \quad (24a)$$

$$\sigma_{D,i} = \zeta_i f'_c \left[1 - \left(\frac{(\varepsilon_{D,i}/\zeta_i \varepsilon_0) - 1}{(4/\zeta_i) - 1} \right)^2 \right] \text{ if } \varepsilon_{D,i} > \zeta_i \varepsilon_0 \quad (24b)$$

$$\zeta_i = \left(\frac{5.8}{\sqrt{f'_c(\text{MPa})}} \leqslant 0.9 \right) \frac{1}{\sqrt{1 + \frac{400\varepsilon_{R,i}}{\eta'_i}}} \quad (25)$$

$$\eta_i = \frac{\rho_{T,i} f_{Ty} - \sigma_{T,i}}{\rho_{L,i} f_{Ly} - \sigma_{L,i}} \quad (26)$$

$$\begin{cases} \eta'_i = \eta_i \text{ if } \eta_i \leqslant 1 \\ \eta'_i = \frac{1}{\eta_i} \text{ if } \eta_i > 1 \end{cases} \quad (27)$$

In the previous equations, f'_c is the uniaxial compressive strength of concrete, ε_0 is the strain corresponding to the peak stress, f_{Ly} and f_{Ty} are the yielding stresses for the longitudinal and transverse reinforcement, respectively.

To simplify the calculation procedure, an equivalent uniform compressive stress is computed for the concrete struts from Eq. (28) and (29), where $k_{1D,i}$ is the ratio between the average compressive stress and the compressive peak stress ($\zeta_i f'_c$, see Fig. 6) in the concrete struts and is computed from integration of Eq. (24).

$$\sigma_{D,i} = k_{1D,i} \zeta_i f'_c \quad (28)$$

$$k_{1D,i} = \frac{\varepsilon_{DS,i}}{\zeta_i \varepsilon_0} - \frac{1}{3}\left(\frac{\varepsilon_{DS,i}}{\zeta_i \varepsilon_0}\right)^2 \text{ if } \varepsilon_{DS,i} \leqslant \zeta_i \varepsilon_0 \quad (29a)$$

$$k_{1D,i} = 1 - \frac{\zeta_i \varepsilon_0}{3\varepsilon_{DS,i}} - \frac{(\varepsilon_{DS,i} - \zeta_i \varepsilon_0)^3}{3\varepsilon_{DS,i}(4\varepsilon_0 - \zeta_i \varepsilon_0)^2} \text{ if } \varepsilon_{DS,i} > \zeta_i \varepsilon_0 \quad (29b)$$

2.3.2. Concrete in tension

For concrete in tension, the smeared σ - ε relationship firstly proposed by Belarbi and Hsu in [40] for shear elements and calibrated latter by Jeng and Hsu in [41] and Bernardo et al. in [42] for solid and hollow RC members under torsion, respectively, (Eq. (30) and (31), see Fig. 6) was adopted.

$$\sigma_{R,i} = E_c \varepsilon_{R,i} \text{ if } \varepsilon_{R,i} \leqslant \varepsilon_{cr} \quad (30a)$$

$$\sigma_{R,i} = f_{cr} \left(\frac{\varepsilon_{cr}}{\varepsilon_{R,i}} \right)^{0.4} \text{ if } \varepsilon_{R,i} > \varepsilon_{cr} \quad (30b)$$

$$f_{cr} = \frac{A_g}{2A_{cp}} \sqrt{f'_c} \quad (31)$$

In the previous equations, E_c is the Young's Modulus for concrete, ε_{cr} is the tensile strain corresponding to the peak stress f_{cr} (concrete tensile strength, see Fig. 6), A_g is the gross area of concrete (see Eq. (50)) and A_{cp} is the area limited by the outer perimeter of the cross section (Eq. (2)). Parameter ε_{cr} was set to be 0.000116 for solid cross sections [41] and 0.0000992 for hollow cross sections [42].

As for the concrete struts, an equivalent uniform tensile stress is computed for the concrete ties perpendicular to the struts from Eq. (32) and (33), where $k_{1R,i}$ is the ratio between the average tensile stress and the tensile peak stress (f_{cr}, see Fig. 6) in the concrete ties and is computed from integration of Eq. (30). In Eq. (33), $\varepsilon_{RS,i}$ is the tensile strain in the exterior of the concrete tie.

$$\sigma_{R,i} = k_{1R,i} f_{cr} \quad (32)$$

$$k_{1R,i} = \frac{\varepsilon_{RS,i}}{2\varepsilon_{cr}} \text{ if } \varepsilon_{RS,i} \leqslant \varepsilon_{cr} \quad (33a)$$

$$k_{1R,i} = \frac{\varepsilon_{cr}}{2\varepsilon_{RS,i}} + \frac{(\varepsilon_{cr})^{0.4}}{0.6\varepsilon_{RS,i}} [(\varepsilon_{RS,i})^{0.6} - (\varepsilon_{cr})^{0.6}] \text{ if } \varepsilon_{RS,i} > \varepsilon_{cr} \quad (33b)$$

2.3.3. Steel bars in tension

For steel bars in tension, the smeared and stiffened σ - ε relationship proposed by Jeng and Hsu in [41] (Eq. (34) to (36), see Fig. 6) was adopted. This bilinear σ - ε relationship constitutes a simplification of the nonlinear relationship proposed by Belarbi and Hsu in [40] and showed to give good results for the RA-STM and also to avoid numerical problems [26–28].

$$f_{S,i} = E_S \varepsilon_S \text{ if } \varepsilon_{S,i} \leqslant \varepsilon_{n,i} \quad (34a)$$

$$f_{S,i} = f_{Sy}[(0.91 - 2B_i) + (0.02 + 0,25B_i)\frac{\varepsilon_{S,i}}{\varepsilon_{Sy}}] \text{ if } \varepsilon_{S,i} > \varepsilon_{n,i} \quad (34b)$$

$$\varepsilon_{n,i} = (0,93 - 2B_i)\varepsilon_{Sy} \quad (35)$$

$$B_i = \frac{1}{\rho_i}\left(\frac{f_{cr}}{f_{Sy}}\right)^{1.5} \quad (36)$$

In the previous equations, for each reinforcement (longitudinal and transverse) and for each panel i, the meaning of the parameters are: $f_{S,i}$ and $\varepsilon_{S,i}$ are the average tensile stress and strain in the steel bars, respectively, f_{Sy} and ε_{Sy} are the yielding stress and yielding strain for steel (from Hooke's law $f_{Sy} = E_s \varepsilon_{Sy}$), respectively, E_S is the Young's Modulus for steel, and ρ_i is the reinforcement ratio (either longitudinal, $\rho_{L,i}$, or transversal, $\rho_{T,i}$).

2.4. Compatibility between panels

In addition to the equations presented in the previous sections, the CA-STM also requires additional conditions related with the compatibility between the deformations of the panels.

2.4.1. Longitudinal strains and longitudinal /transverse curvatures in the panels

The longitudinal and transverse strains in opposite panels can be related from the distance between the axis of panels (b_0 and h_0, see Fig. 7) and the corresponding longitudinal ($\phi_{L,13}$ and $\phi_{L,24}$) and transverse ($\phi_{T,13}$ and $\phi_{T,24}$) curvatures. From Fig. 7, the following equations can be stated:

$$\phi_{L,13} = \frac{\varepsilon_{L,1} - \varepsilon_{L,3}}{b_0} \quad (37)$$

$$\phi_{L,24} = \frac{\varepsilon_{L,2} - \varepsilon_{L,4}}{h_0} \quad (38)$$

$$\phi_{T,13} = \frac{\varepsilon_{T,1} - \varepsilon_{T,3}}{b_0} \quad (39)$$

$$\phi_{T,24} = \frac{\varepsilon_{T,2} - \varepsilon_{T,4}}{h_0} \quad (40)$$

The CA-STM assumes that the longitudinal strains in the 4 panels are related together based on a linear gradient. As a consequence, the longitudinal strain in each panel ($\varepsilon_{L,i}$) can be related with the longitudinal strain at the longitudinal axis (ε_{CL}, see Fig. 7) and the longitudinal curvatures. In the original CA-STM calculation procedure [19,35], and based on this assumption, 4 equations were stated to compute the longitudinal strain for each panel. According to Silva et al. in [31] for their proposed efficient calculation procedure, the number of independent variables can be reduced. As a consequence, a unique equation can be stated to relate all the longitudinal strains in the panels (see Fig. 7):

$$\varepsilon_{CL} = \frac{\varepsilon_{L,1} + \varepsilon_{L,3}}{2} = \frac{\varepsilon_{L,2} + \varepsilon_{L,4}}{2} \Rightarrow \varepsilon_{L,1} + \varepsilon_{L,3} = \varepsilon_{L,2} + \varepsilon_{L,4} \quad (41)$$

Eq. (41) will also be used in this study.

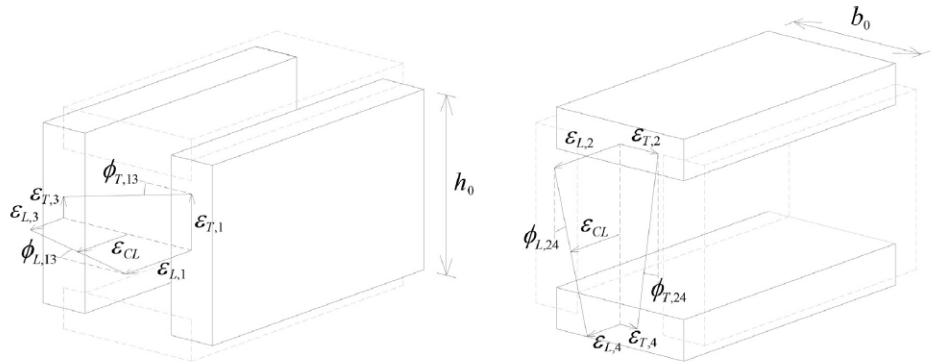

Fig. 7. Longitudinal and transverse curvatures.

2.4.2. Curvature in the concrete struts

As referred in Section 2.1.2, as a RC member twists due to torsion the concrete struts undergo bending in addition to compression. As a consequence, the concrete struts in each panel undergo a curvature ψ_i, which can be computed from the twist θ as follows [12]:

$$\psi_i = \theta \sin(2\alpha_{D,i}) \tag{42}$$

Since the CA-STM allows to consider torsion combined with other internal forces, the additional longitudinal and transverse curvatures in panels ($\phi_{L,13}$, $\phi_{L,24}$, $\phi_{T,13}$, and $\phi_{T,24}$, see Fig. 7) must be considered. This can be done from the following equations proposed by Osongo in [43]:

$$\psi_i = \theta \sin(2\alpha_{D,i}) + \begin{bmatrix} -\phi_{L,13} \\ -\phi_{L,24} \\ \phi_{L,13} \\ \phi_{L,24} \end{bmatrix} \cos^2(\alpha_{D,i}) + \begin{bmatrix} -\phi_{T,13} \\ -\phi_{T,24} \\ \phi_{T,13} \\ \phi_{T,24} \end{bmatrix} \sin^2(\alpha_{D,i}) \tag{43}$$

The curvatures computed from Eq. (43) must agree with the same ones computed from Eq. (8).

2.4.3. Twist of the member

Based on the classical Bredt's theory for thin walled tubes under torsion, the twist θ can be computed from the shear strain γ_{LT} as follows:

$$\theta = \frac{p_0}{2A_0}\gamma_{LT} \tag{44}$$

For the typical members under study (with the rectangular cross section idealized as the association of 4 RC panels), and accounting for the contribution of each panel to compute the perimeter of the shear flow p_0, Eq. (44) is rewritten as:

$$\theta = [(\gamma_{LT,1} + \gamma_{LT,3})h_0 + (\gamma_{LT,2} + \gamma_{LT,4})b_0]\frac{1}{2A_0} \tag{45}$$

3. Efficient solution procedure

3.1. Additional equations

3.1.1. Variable angle as function of the strains

By using trigonometric identities together with the compatibility equations (Eqs. (22) and (23)), the angle of the concrete struts in each panel $\alpha_{D,i}$ can be written as function of the principal ($\varepsilon_{D,i}$ and $\varepsilon_{R,i}$), longitudinal ($\varepsilon_{L,i}$) and transverse ($\varepsilon_{T,i}$) strains through Eq. (46) or Eq. (47). Multiplying these two equations by each other gives Eq. (48). Combining Eq. (46) and Eq. (47) allows to write Eq. (49).

$$\sin^2(\alpha_{D,i}) = \frac{\varepsilon_{L,i} - \varepsilon_{D,i}}{\varepsilon_{R,i} - \varepsilon_{D,i}} = \frac{\varepsilon_{R,i} - \varepsilon_{T,i}}{\varepsilon_{R,i} - \varepsilon_{D,i}} \tag{46}$$

$$\cos^2(\alpha_{D,i}) = \frac{\varepsilon_{R,i} - \varepsilon_{L,i}}{\varepsilon_{R,i} - \varepsilon_{D,i}} = \frac{\varepsilon_{T,i} - \varepsilon_{D,i}}{\varepsilon_{R,i} - \varepsilon_{D,i}} \tag{47}$$

$$\cos(\alpha_{D,i})\sin(\alpha_{D,i}) = \frac{\sqrt{\varepsilon_{R,i} - \varepsilon_{L,i}}\sqrt{\varepsilon_{L,i} - \varepsilon_{D,i}}}{\varepsilon_{R,i} - \varepsilon_{D,i}} \tag{48}$$

$$\alpha_{D,i} = \arctan\left(\sqrt{\frac{\varepsilon_{L,i} - \varepsilon_{D,i}}{\varepsilon_{T,i} - \varepsilon_{D,i}}}\right) sign(q_i) \tag{49}$$

The previous equation allows to eliminate the angle $\alpha_{D,i}$ in the system of nonlinear equations to be solved, providing numerical efficiency and stability.

3.1.2. Geometrical parameters

In the calculation procedure, some geometrical parameters (both for the real and idealized cross section) are needed, namely the following ones which were previously defined: A_{cp} (Eq. (2)), p_{cp} (Eq. (3)), b_0 (Eq. (4)), h_0 (Eq. (5)) and A_0 (Eq. (6)). In addition, the gross area of concrete $A_g$can be defined from Fig. 2:

$$A_g = (b - t_1)t_4 + (h - t_2)t_1 + (b - t_3)t_2 + (h - t_4)t_3 \tag{50}$$

3.2. Selected primary variables and initial estimates

According to the RA-STM and for a cracked RC panel under in-plane stresses, 3 primary variables are needed to compute the behavior of the member for each loading increment [26], namely: the concrete principal strains (ε_D and ε_R) and the angle of the direction of the principal compressive stress (direction of the concrete struts) to the longitudinal axis (α_D). If the panel undergoes bending, then the effect of the curvature (ψ) must also be accounted and 4 primary variables are needed. Since the CA-STM idealizes the cross section as the combination of 4 panels with curvature, it can be concluded that 16 primary variables (unknowns) are needed to compute the behavior of the full cross section, namely: $\varepsilon_{D,i}$, $\varepsilon_{R,i}$, $\alpha_{D,i}$ and ψ_i, with $i = 1, 2, 3, 4$. However, in order to improve the numerical efficiency, and following Silva et al. in [31], some of the initial primary variables can be substituted by other equivalent ones. The proposed 16 primary variables (unknowns) are: $\varepsilon_{DS,i}$, $\varepsilon_{R,i}$, $\varepsilon_{L,i}$ and z_i, with $i = 1, 2, 3, 4$. In addition, instead of setting values for the internal forces acting on the real cross section, these are normalized with respect to the torsional moment and constant values are assumed for the following ratios: N_X/T_X, V_Y/T_X, V_Z/T_X, M_Y/T_X and M_Z/T_X. Thus, the internal forces vary proportionally as T_X increases. This allows to consider T_X as a primary variable and it substitutes $\varepsilon_{DS,1}$

for which an initial value is assumed. The aforementioned implies that the calculation procedure is mainly fitted for RC beams for which torsion is a primary internal force when compared to the other ones, since very high ratios can originate divergences and convergence problems. The final selected 16 primary variables (unknowns) are: T_X, $\varepsilon_{DS,j}$, $\varepsilon_{R,i}$, $\varepsilon_{L,i}$ and z_i, with $i = 1, 2, 3, 4$ and $j = 2, 3, 4$ (this last index does not start at 1 because the value for $\varepsilon_{DS,1}$ will be assumed, as explain latter).

Since T_X is considered as an unknown, it is scaled by dividing it by the cracking torque T_{cr} of the cross section, which was computed with Eq. (51) from ACI 318 [44], where τ_{cr} is the cracking shear stress (Eurocode 2 [33] does not incorporate an explicit equation to compute the cracking torque).

$$T_{cr} = \tau_{cr}\frac{{A_{cp}}^2}{p_{cp}} = 0.33\sqrt{f'_c\ (\text{MPa})}\frac{{A_{cp}}^2}{p_{cp}} \tag{51}$$

To estimate the primary variables to compute the first solution point, a linear elastic model for a plain concrete panel under pure shear is initially assumed for each panel. The initial values for the primary variables are assumed to be equal for the 4 panels of the idealized cross section. The initial estimates are set as follows:

- the initial value for the compressive strain in the exterior of the concrete strut of each panel, ${\varepsilon^0}_{DS,i}$, is considered to be equal to the initial value assumed for $\varepsilon_{DS,1}$:

$${\varepsilon^0}_{DS,i} = \varepsilon_{DS,1} \tag{52}$$

- The initial value for the tensile strain in the concrete tie of each panel, ${\varepsilon^0}_{R,i}$, is assumed to be equal to half of $\varepsilon_{DS,1}$ with changed sign:

$${\varepsilon^0}_{R,i} = -\varepsilon_{DS,1}/2 \tag{53}$$

- The initial value for the longitudinal strain in each panel, ${\varepsilon^0}_{L,i}$, is null since an elastic plain concrete panel under pure shear is initially assumed:

$${\varepsilon^0}_{L,i} = 0 \tag{54}$$

- The initial value for the torsional moment, ${T^0}_X$, is assumed to be the cracking torque from Eq. (51). Since an elastic plain concrete panel under pure shear is assumed, $\tau_{cr} = {\sigma^0}_{R,i}$ (from the Mohr's circle for stresses) and by using Eq. (53) and Hooke's law, Eq. (51) can be written as follows:

$${T^0}_X = \varepsilon_{DS,1}\frac{E_c}{2}\frac{{A_{cp}}^2}{p_{cp}} \tag{55}$$

- From the range of values allowed for the dimensionless parameter related to the shape of the strain diagram in the concrete struts, z_i ($0 \leqslant z_i \leqslant 3$), an intermediate one is assumed for the initial value, ${z^0}_i$, for each panel:

$${z^0}_i = 1 \tag{56}$$

3.3. Nonlinear equations and solution procedure

The 16 equations constituting the system of nonlinear equations, which need to be solved to compute the behavior of the RC member according to the refined efficient CA-STM procedure, can be divided into 5 groups of equations. These equations are stated in terms of the so-called residual functions $F_{CA-STM}(i)$ which are solved for the primary variables in order to be minimized.

Based on Eq. (20), and since CA-STM neglects the transmission of transverse stresses between panels ($\sigma_{T,i} = 0$), the following 4 equations can be stated ($i = 1, 2, 3, 4$):

$$F_{CA-STM}(i) = \sigma_{R,i}\cos^2(\alpha_{D,i}) + \sigma_{D,i}\sin^2(\alpha_{D,i}) + f_{T,i}(A_T/(t_{D,i}s)) = 0 \tag{57}$$

The second group of 4 equations are based on the assumption that the curvatures of the panels (ψ_i) computed from Eq. (8) must agree with the same ones from Eq. (43) ($i = 1, 2, 3, 4$):

$$F_{CA-STM}(4+i) = \theta\sin(2\alpha_{D,i}) + \begin{bmatrix} -\phi_{L,13} \\ -\phi_{L,24} \\ \phi_{L,13} \\ \phi_{L,24} \end{bmatrix}\cos^2(\alpha_{D,i}) + \begin{bmatrix} -\phi_{T,13} \\ -\phi_{T,24} \\ \phi_{T,13} \\ \phi_{T,24} \end{bmatrix}\sin^2(\alpha_{D,i}) + \frac{\varepsilon_{DS,i} - \varepsilon_{A,i}}{t_{D,i}} = 0 \tag{58}$$

Similarly, the third group of 4 equations are based on the assumption that the shear stresses in the panels ($\tau_{LT,i}$), computed from Eq. (21), must agree with the same ones from Eq. (15) ($i = 1, 2, 3, 4$):

$$F_{CA-STM}(8+i) = (\sigma_{R,i} - \sigma_{D,i})\sin(\alpha_{D,i})\cos(\alpha_{D,i})sign(q_i) - \frac{q_i}{t_{D,i}} = 0 \tag{59}$$

Eq. (16) to (18) allow to write 3 additional equilibrium equations which state the balance between stresses and internal forces:

$$F_{CA-STM}(13) = (\sigma_{L,3}t_{D,3}h_0 - \sigma_{L,1}t_{D,1}h_0)\frac{b_0}{2} - M_Y = 0 \tag{60}$$

$$F_{CA-STM}(14) = (\sigma_{L,4}t_{D,4}b_0 - \sigma_{L,2}t_{D,2}b_0)\frac{h_0}{2} - M_Z = 0 \tag{61}$$

$$F_{CA-STM}(15) = \sigma_{L,1}t_{D,1}h_0 + \sigma_{L,2}t_{D,2}b_0 + \sigma_{L,3}t_{D,3}h_0 + \sigma_{L,4}t_{D,4}b_0 - N_X = 0 \tag{62}$$

Finally, the last equation comes from Eq. (41) which states the compatibility between longitudinal strains:

$$F_{CA-STM}(16) = \varepsilon_{L,1} - \varepsilon_{L,2} + \varepsilon_{L,3} - \varepsilon_{L,4} = 0 \tag{63}$$

Based on the aforementioned, the solution procedure can be summarized as follows: knowing the geometry of the real cross section (b, h and t_i), the longitudinal ($A_{L,i}$) and transverse ($A_{T,i}/s$) reinforcement in each panel, the mechanical properties of concrete (f'_c, E_c, ε_0 and ε_{cr}) and steel (f_{Ly}, f_{Ty} and E_s), the ratios of internal forces (N_X/T_X, V_Y/T_X, V_Z/T_X, M_Y/T_X and M_Z/T_X) and the assumed initial strain $\varepsilon_{DS,1}$, determine the variables T_X, $\varepsilon_{DS,j}$, $\varepsilon_{R,i}$, $\varepsilon_{L,i}$ and z_i ($i = 1, 2, 3, 4$ and $j = 2, 3, 4$) which are the solutions for the system of 16 nonlinear equations $F_{CA-STM} = 0$ (Eq. (57) to Eq. (63)), i.e., which minimize the residual functions F_{CA-STM} within a given tolerance and under the constraints $0 \leqslant z_i \leqslant 3$ ($i = 1, 2, 3, 4$). This numerical procedure aims to solve the system of 16 nonlinear equations by minimizing the norm $\|F_{CA-STM}\|$ under the referred constraints. The problem is formulated as a constrained nonlinear least-squares problem, where the 16 defined residual functions must be driven to zero.

Fig. 8 presents a simplified flowchart for the algorithm used to implement the refined efficient CA-STM procedure. Some initial data must be given to start the calculation procedure. In addition to the initial data related with the geometry of the cross section, material properties and loading condition, the chosen path's increment $\Delta\varepsilon_{DS,1}$ for the strain $\varepsilon_{DS,1}$ and the maximum value $\varepsilon_{DS,MAX}$ must also be given. After some preliminary calculations, the simplified model, i.e., the linear elastic model for a plain concrete panel under pure shear, is used and the initial estimates (${T^0}_X$, ${\varepsilon^0}_{L,i}$, ${\varepsilon^0}_{R,i}$, ${\varepsilon^0}_{DS,i}$, ${z^0}_i$, with $i = 1, 2, 3, 4$) are obtained to compute the first solution point (with index $k = 1$). After this, all the remaining solution points are computed from the refined efficient CA-STM procedure. For this, the strain $\varepsilon_{DS,1}$ is incremented by $\Delta\varepsilon_{DS,1}$ for each step (${\varepsilon^{k+1}}_{DS,1} = {\varepsilon^k}_{DS,1} + \Delta\varepsilon_{DS,1}$) and the variables to compute the behavior of the cross section (T_X, $\varepsilon_{DS,j}$, $\varepsilon_{R,i}$, $\varepsilon_{L,i}$, z_i, with $i = 1, 2, 3, 4$ and $j = 2, 3, 4$) are calculated by solving Eq. (57) to (63). For each step, the initial point is defined as the solution point from the previous one. The calculation procedure holds until the conventional ultimate (failure) value specified for concrete in compression ($\varepsilon_{cu} = \varepsilon_{DS,MAX}$) is reached (${\varepsilon^{k+1}}_{DS,1} \geqslant \varepsilon_{cu}$). In this study, Eurocode 2 [33] was used to compute ε_{cu} by correlation with f'_c.

For this study, the algorithm for the refined efficient CA-STM procedure was implemented in MATLAB [45] and the function *lsqnonlin*

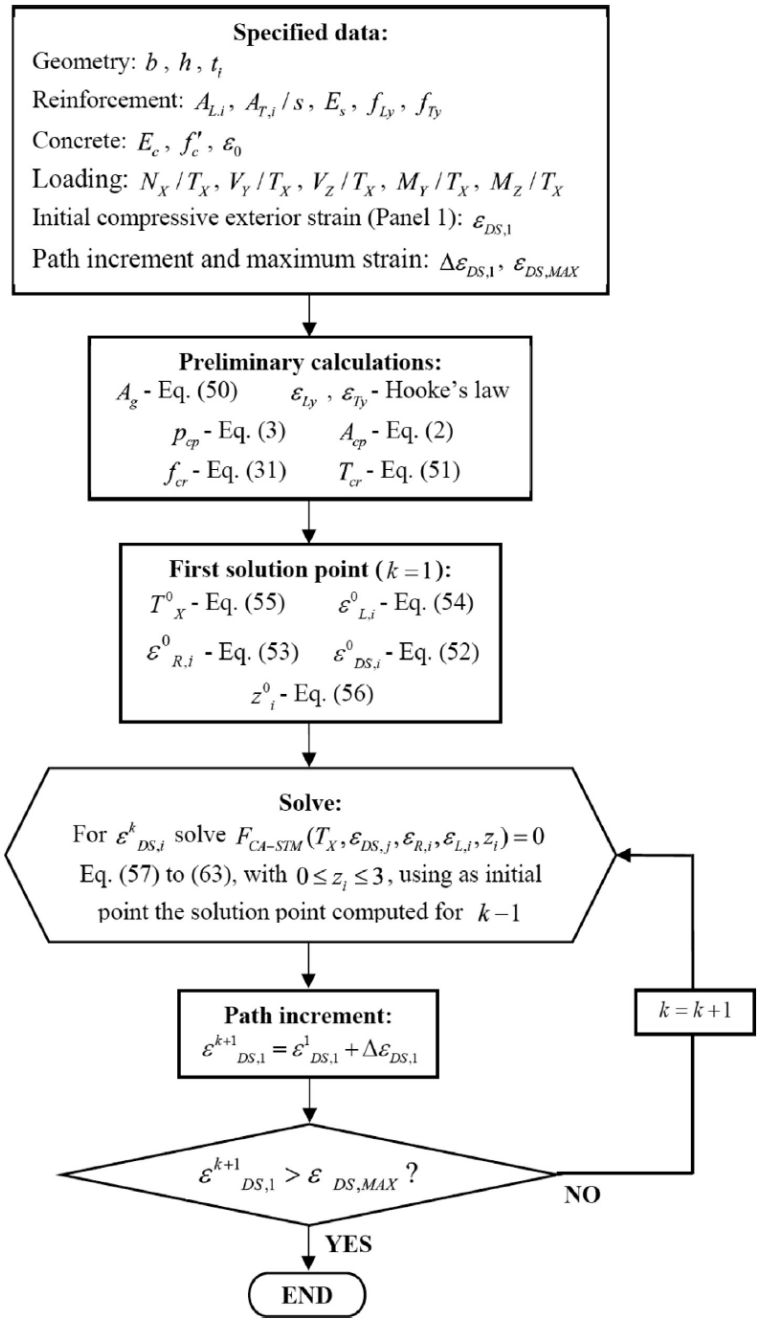

Fig. 8. Flowchart.

was used to solve the constrained nonlinear least-squares problem.

4. Comparison with experimental results

To check the proposed refined efficient CA-STM procedure for RC beams under torsion combined with bending, the theoretical predictions are compared with several experimental results found in the literature. Such results were reported from the testing of the following beams: 19 beams from McMullen and Warwaruk in [46] (series 1, 2, 3 and 4), 7 beams from Lampert and Thürlimann in [47] (series TB), 10 beams from Pandit and Warwaruk in [48] (series B, C, D and E), 16 beams from Goode and Helmy in [49] (series III, IV, V and VI), 14

Table 1
Characteristics of the reference RC beams.

Beam	*	$b$cm	$h$cm	$t_1$cm	$t_2$cm	$t_3$cm	$t_4$cm	f'_cMPa	$A_{L,1}$cm^2	$A_{L,2}$cm^2	$A_{L,3}$cm^2	$A_{L,4}$cm^2	A_T/scm^2/m	f_{Ly}MPa	f_{Ty}MPa	M_Z/T_X
1–2 [46]	S	15	30	–	–	–	–	30.6	1.78	0.71	1.78	2.84	8.55	344	379	0.34
1–3 [46]	S	15	30	–	–	–	–	34.9	1.78	0.71	1.78	2.84	8.55	344	379	0.50
1–4 [46]	S	15	30	–	–	–	–	34.3	1.78	0.71	1.78	2.84	8.55	344	379	1.00
1–5 [46]	S	15	30	–	–	–	–	33.2	1.78	0.71	1.78	2.84	8.55	344	379	2.00
1–6 [46]	S	15	30	–	–	–	–	38.2	1.78	0.71	1.78	2.84	8.55	344	379	4.00
2–2 [46]	S	15	30	–	–	–	–	34.6	2.84	2.84	2.84	2.84	8.55	323	370	0.50
2–3 [46]	S	15	30	–	–	–	–	37.9	2.84	2.84	2.84	2.84	8.55	323	370	1.00
2–4 [46]	S	15	30	–	–	–	–	36.0	2.84	2.84	2.84	2.84	8.55	323	370	2.00
2–5 [46]	S	15	30	–	–	–	–	36.6	2.84	2.84	2.84	2.84	8.55	323	370	4.00
3–2 [46]	S	15	30	–	–	–	–	36.7	1.36	0.71	1.36	2.00	6.23	351	379	0.95
3–3 [46]	S	15	30	–	–	–	–	37.6	1.36	0.71	1.36	2.00	6.23	351	379	0.93
3–4 [46]	S	15	30	–	–	–	–	37.6	1.36	0.71	1.36	2.00	6.23	351	379	1.64
3–5 [46]	S	15	30	–	–	–	–	40.1	1.36	0.71	1.36	2.00	6.23	351	379	3.57
4–1 [46]	S	15	30	–	–	–	–	37.1	1.36	0.71	1.36	2.00	9.34	351	370	1.67
4–2 [46]	S	15	30	–	–	–	–	39.3	1.36	0.71	1.36	2.00	4.67	351	370	1.64
4–3 [46]	S	15	30	–	–	–	–	40.3	1.36	0.71	1.36	2.00	3.72	351	370	1.64
4–4 [46]	S	15	30	–	–	–	–	39.1	1.36	0.71	1.36	2.00	3.10	351	370	1.72
4–5 [46]	S	15	30	–	–	–	–	38.4	1.36	0.71	1.36	2.00	3.99	351	370	2.00
4–6 [46]	S	15	30	–	–	–	–	43.3	1.00	0.71	1.00	1.29	3.99	351	370	2.00
TB0 [47]	H	50	50	8	8	8	8	28.6	4.53	4.53	4.53	4.53	10.27	390	390	1.00
TB1 [47]	H	50	50	8	8	8	8	27.9	2.26	2.26	2.26	11.31	10.27	390	390	1.00
TB2 [47]	H	50	50	8	8	8	8	27.9	2.26	2.26	2.26	11.31	10.27	390	390	2.00
TB3 [47]	H	50	50	8	8	8	8	28.6	2.26	2.26	2.26	11.31	10.27	390	390	3.70
TB4 [47]	S	50	50	–	–	–	–	31.4	2.26	2.26	2.26	11.31	10.27	390	390	1.00
TB5 [47]	H	50	50	8	8	8	8	26.5	2.26	2.26	2.26	11.31	4.55	384	396	1.00
TB6 [47]	H	50	50	8	8	8	8	26.7	2.26	2.26	2.26	11.31	4.55	384	396	1.00
B-2 [48]	S	15.8	31	–	–	–	–	32.0	1.00	0.71	1.00	1.29	4.66	399	395	2.71
B-3 [48]	S	15.4	31	–	–	–	–	32.3	1.00	0.71	1.00	1.29	4.66	399	395	1.16
C-1 [48]	S	15.2	31	–	–	–	–	34.3	1.36	0.71	1.36	2.00	6.21	368	395	3.59
C-2 [48]	S	15.6	31	–	–	–	–	33.2	1.36	0.71	1.36	2.00	6.21	368	395	1.86
C-3 [48]	S	15.5	31	–	–	–	–	36.8	1.36	0.71	1.36	2.00	6.21	368	395	1.10
D-1 [48]	S	15.8	31	–	–	–	–	33.7	3.84	2.00	3.84	5.68	6.21	348	395	6.43
D-2 [48]	S	15.8	31	–	–	–	–	35.2	3.84	2.00	3.84	5.68	6.21	348	395	2.23
D-3 [48]	S	15.8	31	–	–	–	–	32.1	3.84	2.00	3.84	5.68	6.21	348	395	1.25
E-1 [48]	S	15.8	31	–	–	–	–	33.9	1.29	1.29	1.29	1.29	6.21	402	395	2.44
E-2 [48]	S	15.8	31	–	–	–	–	35.2	1.29	1.29	1.29	1.29	6.21	402	395	1.09
III.1 [49]	S	10.2	20.3	–	–	–	–	25.4	1.51	0.18	1.51	2.84	2.52	403	324	0.20
III.2 [49]	S	10.2	20.3	–	–	–	–	30.9	1.51	0.18	1.51	2.84	2.52	403	324	1.91
III.3 [49]	S	10.2	20.3	–	–	–	–	29.5	1.51	0.18	1.51	2.84	2.52	403	324	1.20
III.4 [49]	S	10.2	20.3	–	–	–	–	29.3	1.51	0.18	1.51	2.84	2.52	403	324	4.89
IV.1 [49]	S	10.2	20.3	–	–	–	–	29.4	1.51	0.18	1.51	2.84	5.04	403	324	0.14
IV.2 [49]	S	10.2	20.3	–	–	–	–	27.5	1.51	0.18	1.51	2.84	5.04	403	324	0.94
IV.3 [49]	S	10.2	20.3	–	–	–	–	26.9	1.51	0.18	1.51	2.84	5.04	403	324	1.64
IV.4 [49]	S	10.2	20.3	–	–	–	–	25.5	1.51	0.18	1.51	2.84	5.04	403	324	4.24
V.1 [49]	S	10.2	20.3	–	–	–	–	31.9	0.73	0.18	0.73	1.29	2.52	397	324	0.19
V.2 [49]	S	10.2	20.3	–	–	–	–	25.6	0.73	0.18	0.73	1.29	2.52	397	324	0.98
V.3 [49]	S	10.2	20.3	–	–	–	–	25.9	0.73	0.18	0.73	1.29	2.52	397	324	1.43
V.4 [49]	S	10.2	20.3	–	–	–	–	28.7	0.73	0.18	0.73	1.29	2.52	397	324	3.87

Beam	*	$b$cm	$h$cm	$t_1$cm	$t_2$cm	$t_3$cm	$t_4$cm	f'_cMPa	$A_{L,1}$cm^2	$A_{L,2}$cm^2	$A_{L,3}$cm^2	$A_{L,4}$cm^2	A_T/scm^2/m	f_{Ly}MPa	f_{Ty}MPa	M_Z/T_X
VI.1 [49]	S	10.2	20.3	–	–	–	–	26.5	0.73	0.18	0.73	1.29	5.04	397	324	0.18
VI.2 [49]	S	10.2	20.3	–	–	–	–	28.6	0.73	0.18	0.73	1.29	5.04	397	324	0.75
VI.3 [49]	S	10.2	20.3	–	–	–	–	25.4	0.73	0.18	0.73	1.29	5.04	397	324	3.71
VI.4 [49]	S	10.2	20.3	–	–	–	–	27.4	0.73	0.18	0.73	1.29	5.04	397	324	1.13
RE1 [50]	S	16.5	25.4	–	–	–	–	31.7	1.29	1.29	1.29	1.29	9.32	307	338	0.08
RE2 [50]	S	16.5	25.4	–	–	–	–	31.7	1.29	1.29	1.29	1.29	9.32	307	338	0.38
RE3 [50]	S	16.5	25.4	–	–	–	–	31.7	1.29	1.29	1.29	1.29	9.32	307	338	0.56
RE4 [50]	S	16.5	25.4	–	–	–	–	31.7	1.29	1.29	1.29	1.29	9.32	307	338	1.14
RE5 [50]	S	16.5	25.4	–	–	–	–	31.7	1.29	1.29	1.29	1.29	9.32	307	338	1.64
RE4* [50]	S	16.5	25.4	–	–	–	–	31.7	1.29	1.29	1.29	1.29	9.32	307	338	3.57
RU1 [50]	S	16.5	25.4	–	–	–	–	25.4	1.78	0.71	1.78	2.84	6.99	330	338	0.09
RU2** [50]	S	16.5	25.4	–	–	–	–	25.4	1.78	0.71	1.78	2.84	6.99	330	338	0.60
RU3** [50]	S	16.5	25.4	–	–	–	–	24.9	1.78	0.71	1.78	2.84	6.99	330	338	0.80
RU3A** [50]	S	16.5	25.4	–	–	–	–	31.9	1.78	0.71	1.78	2.84	6.99	330	338	1.59
RU4 [50]	S	16.5	25.4	–	–	–	–	25.4	1.78	0.71	1.78	2.84	6.99	330	338	1.69
RU5 [50]	S	16.5	25.4	–	–	–	–	25.4	1.78	0.71	1.78	2.84	6.99	330	338	3.33
RU5A [50]	S	16.5	25.4	–	–	–	–	30.3	1.78	0.71	1.78	2.84	6.99	330	338	4.00
RU6 [50]	S	16.5	25.4	–	–	–	–	24.9	1.78	0.71	1.78	2.84	6.99	330	338	4.76
BT2 [51]	S	15.2	30.5	–	–	–	–	38.0	1.29	1.29	1.29	1.29	4.20	324	248	6.43
BT3 [51]	S	15.2	30.5	–	–	–	–	38.0	1.29	1.29	1.29	1.29	4.20	324	248	2.80
BT4 [51]	S	15.2	30.5	–	–	–	–	37.4	1.29	1.29	1.29	1.29	4.20	324	248	1.25
BT5 [51]	S	15.2	30.5	–	–	–	–	29.9	1.29	1.29	1.29	1.29	4.20	324	248	0.66
BBT3 [51]	S	15.2	30.5	–	–	–	–	41.2	2.84	2.84	2.84	2.84	6.21	361	245	5.91

(*continued on next page*)

Table 1 (*continued*)

Beam	*	$b$cm	$h$cm	$t_1$cm	$t_2$cm	$t_3$cm	$t_4$cm	f'_cMPa	$A_{L,1}$cm^2	$A_{L,2}$cm^2	$A_{L,3}$cm^2	$A_{L,4}$cm^2	A_T/scm^2/m	f_{Ly}MPa	f_{Ty}MPa	M_Z/T_X
BBT4 [51]	S	15.2	30.5	–	–	–	–	41.2	2.84	2.84	2.84	2.84	6.21	361	245	5.54
BBT6 [51]	S	15.2	30.5	–	–	–	–	34.8	2.84	2.84	2.84	2.84	6.21	361	245	1.12
V1 [52]	S	12.7	20.3	–	–	–	–	45.9	1.29	1.29	1.29	2.58	4.20	345	345	1.34
V2 [52]	S	12.7	20.3	–	–	–	–	39.7	1.29	1.29	1.29	2.58	4.20	345	345	3.36
V3 [52]	S	12.7	20.3	–	–	–	–	33.9	1.29	1.29	1.29	2.58	4.20	345	345	5.59
V5 [52]	S	12.7	20.3	–	–	–	–	37.2	1.29	1.29	1.29	2.58	4.20	345	345	3.64
V6 [52]	S	12.7	20.3	–	–	–	–	34.8	1.29	1.29	1.29	2.58	4.20	345	345	1.53
S1II [52]	S	12.7	20.3	–	–	–	–	33.8	0.81	1.29	0.81	1.03	3.15	345	345	6.41
S2I [52]	S	12.7	20.3	–	–	–	–	37.2	0.81	1.29	0.81	1.03	3.15	345	345	9.62
S2II [52]	S	12.7	20.3	–	–	–	–	37.2	0.81	1.29	0.81	1.03	3.15	345	345	4.20
S3 [52]	S	12.7	20.3	–	–	–	–	33.1	0.81	1.29	0.81	1.03	3.15	345	345	1.07
S4I [52]	S	12.7	20.3	–	–	–	–	38.6	0.81	1.29	0.81	1.03	3.15	345	345	12.35
S4II [52]	S	12.7	20.3	–	–	–	–	38.6	0.81	1.29	0.81	1.03	3.15	345	345	4.26
S5I [52]	S	12.7	20.3	–	–	–	–	36.2	0.81	1.29	0.81	1.03	3.15	345	345	7.41
S5II [52]	S	12.7	20.3	–	–	–	–	36.2	0.81	1.29	0.81	1.03	3.15	345	345	4.72
L1-2II [52]	S	12.7	20.3	–	–	–	–	28.7	1.65	1.29	1.65	2.00	3.15	345	345	1.87
L2-1II [52]	S	12.7	20.3	–	–	–	–	39.5	1.65	1.29	1.65	2.00	3.15	345	345	2.18
L3-1I [52]	S	12.7	20.3	–	–	–	–	29.2	1.65	1.29	1.65	2.00	3.15	345	345	8.13
L3-1II [52]	S	12.7	20.3	–	–	–	–	29.2	1.65	1.29	1.65	2.00	3.15	345	345	3.50
L4-1 [52]	S	12.7	20.3	–	–	–	–	32.1	1.65	1.29	1.65	2.00	3.15	345	345	2.83
L4-2 [52]	S	12.7	20.3	–	–	–	–	26.2	1.65	1.29	1.65	2.00	3.15	345	345	1.26
L5-2 [52]	S	12.7	20.3	–	–	–	–	25.2	1.65	1.29	1.65	2.00	3.15	345	345	2.0
L6-2I [52]	S	12.7	20.3	–	–	–	–	27.9	1.65	1.29	1.65	2.00	3.15	345	345	7.09

*S = Solid; H = Hollow.

beams from Collins et al. in [50] (series RE and RU), 7 beams from Kemp in [51] (series BT and BBT) and 21 beams from Iyengar and Rangan in [52] (series V, S and L). Hence, a total of 94 reference RC beams under torsion (T_X) combined with bending in the vertical plane (M_Z) were used.

In the referred series, RC beams predominantly tested under bending were disregarded. For such beams, the ratio M_Z/T_X is very high and the calculation procedure lead to convergence problems. As referred in Section 2.1.1, the maximum allowed thickness for each panel was fixed from normative considerations for torsion (Eq. (1)). This limiting condition is probably too restrictive for bending, for which inner concrete layers are also effective, mainly in the compression zone of the cross section due to bending.

Also, in the referred series, some RC beams were tested under pure torsion or pure bending. The reported experimental values for the ultimate torque and ultimate bending moment of such beams were only used to draw interaction curves, as presented latter.

For the referred series, RC beams with atypical detailing for the reinforcement (for instance, some beams were only detailed with longitudinal reinforcement) were not considered because the corresponding experimental behavioral curves showed to be atypical. Also, some duplicate beams which showed similar experimental results were disregarded.

It should be also pointed out that the results of 12 beams tested by Osongo in [43] (series TBS, TBO and TBU) were not considered in this study. For such beams, the theoretical behavioral curves computed from the refined efficient CA-STM procedure showed to be very different from the experimental ones. This problem was also reported by Cerquido in [53] by using both the original and the efficient calculation procedure for the CA-STM (without the refinements incorporated in this study). It should be also noted that Green and Belarbi in [30] did not use the experimental results from Osongo [43] to validate the original CA-STM. No explanation was found for the referred problem. For this reason, the experimental results from Osongo in [43] were not considered in this study.

Table 1 summarizes the properties of the reference RC beams used in this study to validate the refined efficient CA-STM procedure. Most of the presented parameters were defined in the previous sections (for the geometrical parameters see Fig. 2 and for the area of longitudinal reinforcement in each panel see Fig. 4). For concrete, the strain ε_0 corresponding to the peak stress f'_c was computed from Eurocode 2 [33] by correlation with f'_c. Young's Modulus for steel was set equal to 210 GPa for beams of TB series (the value was given by the authors [47]) and equal to 200 GPa for the remaining beams. For a given beam, when the cross section incorporates longitudinal rebars with different yielding stresses, an average value was assumed for all the longitudinal reinforcement. Also, for beams for which the ratio M_Z/T_X was not kept constant during the tests, the corresponding value computed from the ultimate (maximum) internal forces given by the authors ($T_{X,ult}$ and $M_{Z,ult}$) was considered.

The theoretical response of each of the 94 reference RC beams from Table 1 was computed using the refined efficient CA-STM procedure presented in the previous sections. The results are compared with the experimental ones reported by the authors [46–52]. For each reference beam, Table 2 presents the experimental and theoretical values for some key parameters considered important for design, namely: the cracking torque ($T^{exp}_{X,cr}$ and $T^{th}_{X,cr}$), the cracking bending moment ($M^{exp}_{Z,cr}$ and $M^{th}_{Z,cr}$), the ultimate (maximum) torque ($T^{exp}_{X,ult}$ and $T^{th}_{X,ult}$) and the ultimate (maximum) bending moment ($M^{exp}_{Z,ult}$ and $M^{th}_{Z,ult}$). The ratios of the experimental to the theoretical values are also presented ($T^{exp}_{X,cr}/T^{ult}_{X,cr}$, $M^{exp}_{Z,cr}/M^{th}_{Z,cr}$, $T^{exp}_{X,ult}/T^{th}_{X,ult}$ and $M^{exp}_{Z,ult}/M^{th}_{Z,ult}$), as well as the corresponding computed values for the mean ($\bar{x}$), standard deviation (s) and coefficient of variation (cv). The values for the cracking torque and cracking bending moment are only presented for the reference beams tested under proportional loading and for which the experimental values were given by the authors. For the remaining beams, nether such experimental values nor experimental curves were given.

For some reference beams tested under no proportional loading, the authors gave the experimental values for the cracking points (for instance in [49]), or indicated them in the plots of some experimental behavioral curves (for instance in [48,49]). However, in such beams the bending moment was initially applied and increased with no torque, until a prescribed value less that the estimated ultimate bending moment was reached. Next, the bending moment was kept constant and the torque was applied and increased until the beam's failure. The beams were already in the cracked stage before the torque was applied. This was confirmed from the analysis of the experimental behavioral curves for torsion, in which a cracking point is not clearly observed. In such beams, the given experimental values for the cracking points were not considered to be reliable for comparison with the theoretical predictions because the model assumes proportional loading.

The results in Table 2 show that the refined efficient CA-STM

Table 2
Comparative analysis.

Beam	$T^{exp}_{X,cr}$kNm	$T^{th}_{X,cr}$kNm	$\frac{T^{exp}_{X,cr}}{T^{th}_{X,cr}}$	$T^{exp}_{X,ult}$kNm	$T^{th}_{X,ult}$kNm	$\frac{T^{exp}_{X,ult}}{T^{th}_{X,ult}}$	$M^{exp}_{Z,cr}$kNm	$M^{th}_{Z,cr}$kNm	$\frac{M^{exp}_{Z,cr}}{M^{th}_{Z,cr}}$	$M^{exp}_{Z,ult}$kNm	$M^{th}_{Z,ult}$kNm	$\frac{M^{exp}_{Z,ult}}{M^{th}_{Z,ult}}$
1–2 [46]	5.54	4.09	1.35	15.60	15.17	1.03	2.71	1.39	1.95	5.31	5.16	1.03
1–3 [46]	5.42	4.37	1.24	15.80	16.72	0.94	2.71	2.18	1.24	7.91	8.36	0.95
1–4 [46]	4.29	3.93	1.09	18.00	15.68	1.15	4.29	3.93	1.09	17.91	15.68	1.14
1–5 [46]	4.41	4.00	1.10	14.80	11.92	1.24	8.81	8.00	1.10	30.17	23.84	1.27
1–6 [46]	3.28	2.83	1.16	10.20	10.08	1.01	13.45	11.32	1.19	40.91	40.33	1.01
2–2 [46]	5.42	4.59	1.18	19.40	17.46	1.11	2.71	2.30	1.18	8.81	8.73	1.01
2–3 [46]	4.29	4.38	0.98	18.80	17.17	1.09	4.29	4.38	0.98	17.96	17.17	1.05
2–4 [46]	4.29	3.57	1.20	15.10	12.40	1.22	8.81	7.86	1.12	28.70	27.28	1.05
2–5 [46]	3.39	2.81	1.21	10.20	8.56	1.19	8.81	10.20	0.86	36.27	34.23	1.06
3–2 [46]	5.08	3.98	1.28	13.20	13.55	0.97	–	–	–	12.59	12.87	0.98
3–3 [46]	4.86	4.06	1.20	13.60	13.68	0.99	–	–	–	12.59	12.72	0.99
3–4 [46]	6.10	4.41	1.38	13.00	12.19	1.07	–	–	–	21.26	15.00	1.42
3–5 [46]	4.86	4.64	1.05	8.20	8.03	1.02	–	–	–	29.93	28.67	1.04
4–1 [46]	4.40	4.17	1.06	13.60	11.78	1.15	7.34	7.00	1.05	21.01	21.34	0.98
4–2 [46]	4.41	4.00	1.10	11.40	10.30	1.11	7.34	6.88	1.07	17.96	17.73	1.01
4–3 [46]	4.41	4.28	1.03	10.50	9.91	1.06	7.34	7.03	1.04	17.29	16.25	1.06
4–4 [46]	4.52	4.06	1.11	9.60	8.99	1.07	7.34	6.98	1.05	14.91	15.47	0.96
4–5 [46]	3.62	3.73	0.97	11.60	9.60	1.21	9.60	7.45	1.29	22.60	19.20	1.18
4–6 [46]	3.62	3.60	1.01	7.50	6.99	1.07	7.34	7.20	1.02	14.24	13.97	1.02
TB0 [47]	25.50	18.84	1.35	88.78	81.47	1.09	26.50	18.84	1.41	107.91	81.47	1.32
TB1 [47]	25.50	20.49	1.24	115.27	114.03	1.01	36.00	19.41	1.85	134.40	112.76	1.19
TB2 [47]	22.78	20.36	1.12	86.82	85.89	1.01	38.00	40.15	0.95	189.82	182.53	1.04
TB3 [47]	20.00	19.69	1.02	57.88	69.23	0.84	39.00	62.65	0.62	227.59	256.15	0.89
TB4 [47]	35.50	36.20	0.98	113.80	119.70	0.95	53.50	36.91	1.45	145.68	119.70	1.22
TB5 [47]	25.00	21.71	1.15	94.18	93.84	1.00	35.50	32.63	1.09	113.31	117.91	0.96
TB6 [47]	39.00	36.85	1.06	96.14	94.17	1.02	26.50	28.54	0.93	114.78	118.45	0.97
B-2 [48]	–	–	–	8.14	9.29	0.88	–	–	–	22.04	25.17	0.88
B-3 [48]	–	–	–	10.74	10.73	1.00	–	–	–	12.43	12.05	1.03
C-1 [48]	–	–	–	8.81	9.01	0.98	–	–	–	31.64	32.34	0.98
C-2 [48]	–	–	–	11.87	11.72	1.01	–	–	–	22.04	21.80	1.01
C-3 [48]	–	–	–	12.54	14.33	0.88	–	–	–	12.43	15.77	0.79
D-1 [48]	–	–	–	11.19	12.04	0.93	–	–	–	71.98	77.44	0.93
D-2 [48]	–	–	–	18.53	16.27	1.14	–	–	–	41.25	36.28	1.14
D-3 [48]	–	–	–	17.63	15.37	1.15	–	–	–	22.04	19.21	1.15
E-1 [48]	–	–	–	8.59	10.07	0.85	–	–	–	22.04	25.89	0.85
E-2 [48]	–	–	–	11.41	13.62	0.84	–	–	–	12.43	14.85	0.84
III.1 [49]	–	–	–	2.77	2.68	1.03	–	–	–	0.54	0.54	1.00
III.2 [49]	–	–	–	4.46	3.61	1.24	–	–	–	8.52	6.90	1.23
III.3 [49]	–	–	–	3.84	3.46	1.11	–	–	–	4.60	4.16	1.11
III.4 [49]	–	–	–	4.16	3.54	1.18	–	–	–	20.34	17.32	1.17
IV.1 [49]	–	–	–	3.88	3.88	1.00	–	–	–	0.54	0.54	1.00
IV.2 [49]	–	–	–	4.92	4.70	1.05	–	–	–	4.60	4.41	1.04
IV.3 [49]	–	–	–	5.20	4.58	1.14	–	–	–	8.52	7.51	1.13
IV.4 [49]	–	–	–	4.80	4.54	1.06	–	–	–	20.34	19.25	1.06
V.1 [49]	–	–	–	2.88	3.10	0.93	–	–	–	0.54	0.59	0.92
V.2 [49]	–	–	–	2.71	2.93	0.92	–	–	–	2.64	2.87	0.92
V.3 [49]	–	–	–	3.22	2.92	1.10	–	–	–	4.60	4.17	1.10
V.4 [49]	–	–	–	2.71	2.99	0.91	–	–	–	10.49	11.58	0.91

Beam	$T^{exp}_{X,cr}$kNm	$T^{th}_{X,cr}$kNm	$\frac{T^{exp}_{X,cr}}{T^{th}_{X,cr}}$	$T^{exp}_{X,ult}$kNm	$T^{th}_{X,ult}$kNm	$\frac{T^{exp}_{X,ult}}{T^{th}_{X,ult}}$	$M^{exp}_{Z,cr}$kNm	$M^{th}_{Z,cr}$kNm	$\frac{M^{exp}_{Z,cr}}{M^{th}_{Z,cr}}$	$M^{exp}_{Z,ult}$kNm	$M^{th}_{Z,ult}$kNm	$\frac{M^{exp}_{Z,ult}}{M^{th}_{Z,ult}}$
VI.1 [49]	–	–	–	3.05	3.97	0.77	–	–	–	0.54	0.71	0.76
VI.2 [49]	–	–	–	3.54	4.26	0.83	–	–	–	2.64	3.20	0.83
VI.3 [49]	–	–	–	2.83	3.51	0.81	–	–	–	10.49	13.03	0.81
VI.4 [49]	–	–	–	4.07	4.10	0.99	–	–	–	4.60	4.63	0.99
RE1 [50]	–	–	–	9.20	12.13	0.76	–	–	–	0.71	0.95	0.75
RE2 [50]	–	–	–	9.42	11.15	0.84	–	–	–	3.62	4.24	0.85
RE3 [50]	–	–	–	9.21	10.59	0.87	–	–	–	5.12	5.93	0.86
RE4 [50]	–	–	–	8.43	9.83	0.86	–	–	–	9.54	11.21	0.85
RE5 [50]	–	–	–	7.46	8.22	0.91	–	–	–	12.23	13.48	0.91
RE4* [50]	–	–	–	4.29	5.10	0.84	–	–	–	15.14	18.19	0.83
RU1 [50]	–	–	–	8.28	10.48	0.79	–	–	–	0.71	0.90	0.79
RU2** [50]	–	–	–	9.59	10.52	0.91	–	–	–	5.77	6.31	0.91
RU3** [50]	–	–	–	11.87	10.35	1.15	–	–	–	9.49	8.28	1.15
RU3A**[50]	–	–	–	10.10	9.83	1.03	–	–	–	15.97	15.63	1.02
RU4 [50]	–	–	–	9.66	8.58	1.13	–	–	–	16.39	14.50	1.13
RU5 [50]	–	–	–	8.52	7.38	1.15	–	–	–	28.20	24.56	1.15
RU5A [50]	–	–	–	7.72	7.28	1.06	–	–	–	30.15	29.11	1.04
RU6 [50]	–	–	–	6.68	6.82	0.98	–	–	–	31.78	32.48	0.98
BT2 [51]	–	–	–	4.43	6.08	0.73	–	–	–	28.48	39.12	0.73
BT3 [51]	–	–	–	6.92	7.47	0.93	–	–	–	19.39	20.91	0.93

(*continued on next page*)

Table 2 (*continued*)

Beam	$T^{exp}_{X,cr}$kNm	$T^{th}_{X,cr}$kNm	$\frac{T^{exp}_{X,cr}}{T^{th}_{X,cr}}$	$T^{exp}_{X,ult}$kNm	$T^{th}_{X,ult}$kNm	$\frac{T^{exp}_{X,ult}}{T^{th}_{X,ult}}$	$M^{exp}_{Z,cr}$kNm	$M^{th}_{Z,cr}$kNm	$\frac{M^{exp}_{Z,cr}}{M^{th}_{Z,cr}}$	$M^{exp}_{Z,ult}$kNm	$M^{th}_{Z,ult}$kNm	$\frac{M^{exp}_{Z,ult}}{M^{th}_{Z,ult}}$
BT4 [51]	–	–	–	8.85	8.58	1.03	–	–	–	11.10	10.73	1.03
BT5 [51]	–	–	–	9.69	9.06	1.07	–	–	–	6.39	5.98	1.07
BBT3 [51]	–	–	–	7.92	10.50	0.75	–	–	–	46.78	62.04	0.75
BBT4 [51]	–	–	–	8.20	10.42	0.79	–	–	–	45.43	57.74	0.79
BBT6 [51]	–	–	–	15.59	12.61	1.24	–	–	–	17.45	14.12	1.24
V1 [52]	–	–	–	4.63	5.66	0.82	–	–	–	6.22	7.58	0.82
V2 [52]	–	–	–	4.07	5.00	0.81	–	–	–	13.67	16.81	0.81
V3 [52]	–	–	–	2.88	4.07	0.71	–	–	–	15.82	22.75	0.70
V5 [52]	–	–	–	4.41	5.04	0.88	–	–	–	16.05	18.33	0.88
V6 [52]	–	–	–	3.84	5.03	0.76	–	–	–	5.88	7.70	0.76
S1II [52]	–	–	–	2.71	3.02	0.90	–	–	–	17.40	19.45	0.89
S2I [52]	–	–	–	1.81	1.90	0.95	–	–	–	17.40	18.23	0.95
S2II [52]	–	–	–	3.50	3.63	0.96	–	–	–	14.69	15.25	0.96
S3 [52]	–	–	–	3.28	4.12	0.80	–	–	–	3.62	4.41	0.82
S4I [52]	–	–	–	1.36	2.16	0.63	–	–	–	16.72	26.71	0.63
S4II [52]	–	–	–	3.50	3.66	0.96	–	–	–	14.92	15.60	0.96
S5I [52]	–	–	–	2.26	2.61	0.87	–	–	–	16.72	19.38	0.86
S5II [52]	–	–	–	3.16	3.60	0.88	–	–	–	14.20	17.00	0.84
L1-2II [52]	–	–	–	3.62	3.93	0.92	–	–	–	6.78	7.34	0.92
L2-1II [52]	–	–	–	3.73	4.54	0.82	–	–	–	8.14	9.89	0.82
L3-1I [52]	–	–	–	2.26	2.94	0.77	–	–	–	18.42	23.91	0.77
L3-1II [52]	–	–	–	3.39	3.59	0.94	–	–	–	11.87	12.56	0.95
L4-1 [52]	–	–	–	3.39	3.98	0.85	–	–	–	9.61	11.27	0.85
L4-2 [52]	–	–	–	3.05	3.73	0.82	–	–	–	3.84	4.70	0.82
L5-2 [52]	–	–	–	3.28	3.57	0.92	–	–	–	6.55	7.13	0.92
L6-2I [52]	–	–	–	2.49	3.12	0.80	–	–	–	17.63	13.44	1.31
		$\bar{x}$	1.14		$\bar{x}$	0.97		$\bar{x}$	1.16		$\bar{x}$	0.97
		s	0.12		s	0.14		s	0.30		s	0.15
		cv	10.51%		cv	14.34%		cv	25.68%		cv	15.55%

procedure seems slightly to overestimate both the cracking torque $T_{X.cr}$ ($\bar{x}$ = 1.14) and the cracking bending moment $M_{Z.cr}$ ($\bar{x}$ = 1.16), with an acceptable degree of dispersion for the first one (cv = 10.51%) but with much higher dispersion for the second one (cv = 25.68%). Nevertheless, the results can be considered not bad if one considers that the high variability of the tensile concrete strength and the interaction between internal forces make it difficult to estimate accurately the cracking points by using a truss-based model. The higher degree of dispersion for the cracking bending moment can probably be explained because the model neglects the concrete core (most of the analyzed beams for the cracking points were solid). It is expected that the concrete core influences the response of the beams in the early loading stages.

From Table 2, it can also be stated that the model predicts similarly and very well both the ultimate torque $T_{X.ult}$ and the ultimate bending moment $M_{Z.ult}$ ($\bar{x}$ = 0.97 for both), and with acceptable degrees of dispersion (cv = 14.34% and cv = 15.55%, respectively).

As referred in the introduction section, to validate the CA-STM with the original calculation procedure, Green and Belarbi in [30] used some experimental results, namely the following 18 reference RC beams under torsion combined with bending: beams 1–3 to 1–5 [46], beams 2–2 to 2–4 [46], beams 4–1 to 4–6 [46] and beams TB1, TB2 and TB4 to TB6 [47]. For such beams, and from the comparative analyzes performed by Green and Belarbi [30], only the results for the ultimate torque are available to be used here for comparison. From their results, the following statistical parameters were obtained for the ratio $T^{exp}_{X,ult}/T^{th}_{X,ult}$: $\bar{x}$ = 1.13 and cv = 5.88%. These results can be considered good and validate the original CA-STM to predict the ultimate torque. The results obtained in the present study, using 94 reference beams (which constitute a much larger database), show that the refined efficient CA-STM procedure remains reliable to predict the ultimate torque. Furthermore, the model shows to also predict well the ultimate bending moment and the cracking values for both the internal forces. In addition, the refined efficient CA-STM procedure provides higher numerical efficiency and stability.

Figs. 9 to 12 present selected behavioral curves for some of the reference RC beams or series of beams. It should be referred that for most of the reference beams used in this study, the experimental curves were not provided by the authors. Figs. 9 to 11 also incorporates sectional details of the specimens. In the drawings, dimensions and spacing of the stirrups are in centimeters. Diameters "ϕ" of the rebars are in millimeters and "#" refers to imperial rebar size (as used by the authors).

Fig. 9 presents experimental and theoretical torque (T_X) – twist (θ) curves. For some beams, two theoretical curves are presented for comparison, one computed with the refined efficient CA-STM procedure (called "Eff. CA-STM" in the graphs) and another one drawn from the results presented by Green and Belarbi in [30] by using the original CA-STM procedure (called "CA-STM" in the graphs). It should be referred that for some beams from Pandit and Warwaruk in [48], the reported ultimate torque by the authors is somewhat higher when compared to the same one visualized in the experimental curves (for instance, see the curves for Beam C-1 in Fig. 9 and the experimental ultimate torque given in Table 2). For such beams, it seems that the presented experimental curves are not complete.

Fig. 10 presents the experimental and theoretical bending moment (M_Z) – twist (θ) curves for some of the beams from McMullen and Warwaruk in [46]. Fig. 11 presents the experimental and theoretical bending moment (M_Z) – longitudinal curvature ($\phi_{L,24}$) curves for some of the beams from Lampert and Thürlimann in [47] (only these authors presented the referred experimental curves for some of their beams).

Figs. 9 to 11 show that, in general, the global response of the reference RC beams under torsion combined with bending is well captured by the refined efficient CA-STM procedure. For both the torsional and bending global response of the beams, Figs. 9 and 10 show that all the behavioral stages (uncracked, cracked and ultimate stages) are predicted, as well as the transitions between them. In particular, both the ultimate loadings and the transition from the uncracked to the cracked stage are predicted with reasonable accuracy, corroborating the results obtained in Table 2. In addition, the almost bilinear shape observed in the experimental $M_Z - \phi_{L,24}$ curves in Fig. 11 is also well predicted by the refined efficient CA-STM procedure, as well as the yielding point and the post-yielding behavior. When compared with the

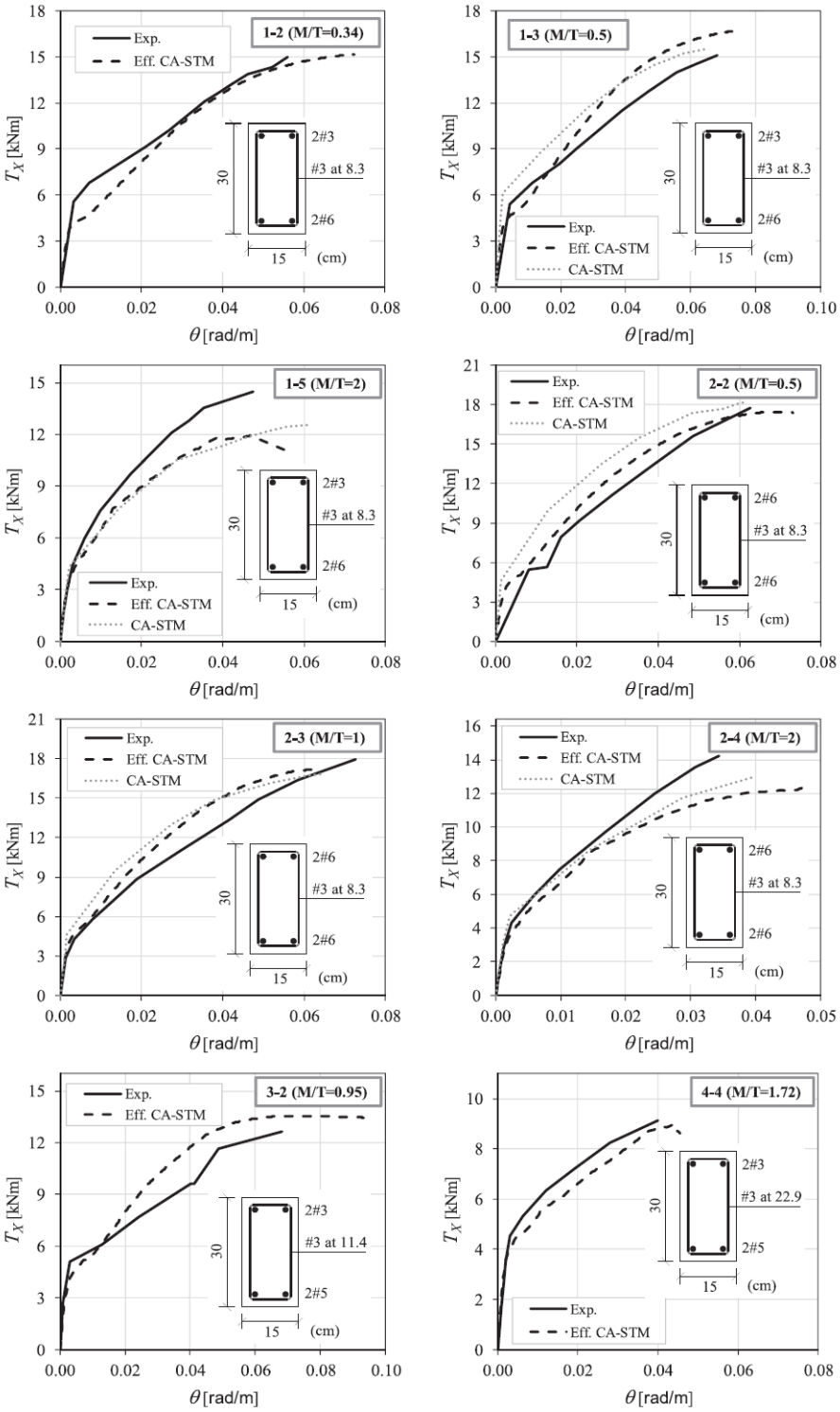

Fig. 9. $T_X - \theta$ curves for selected beams.

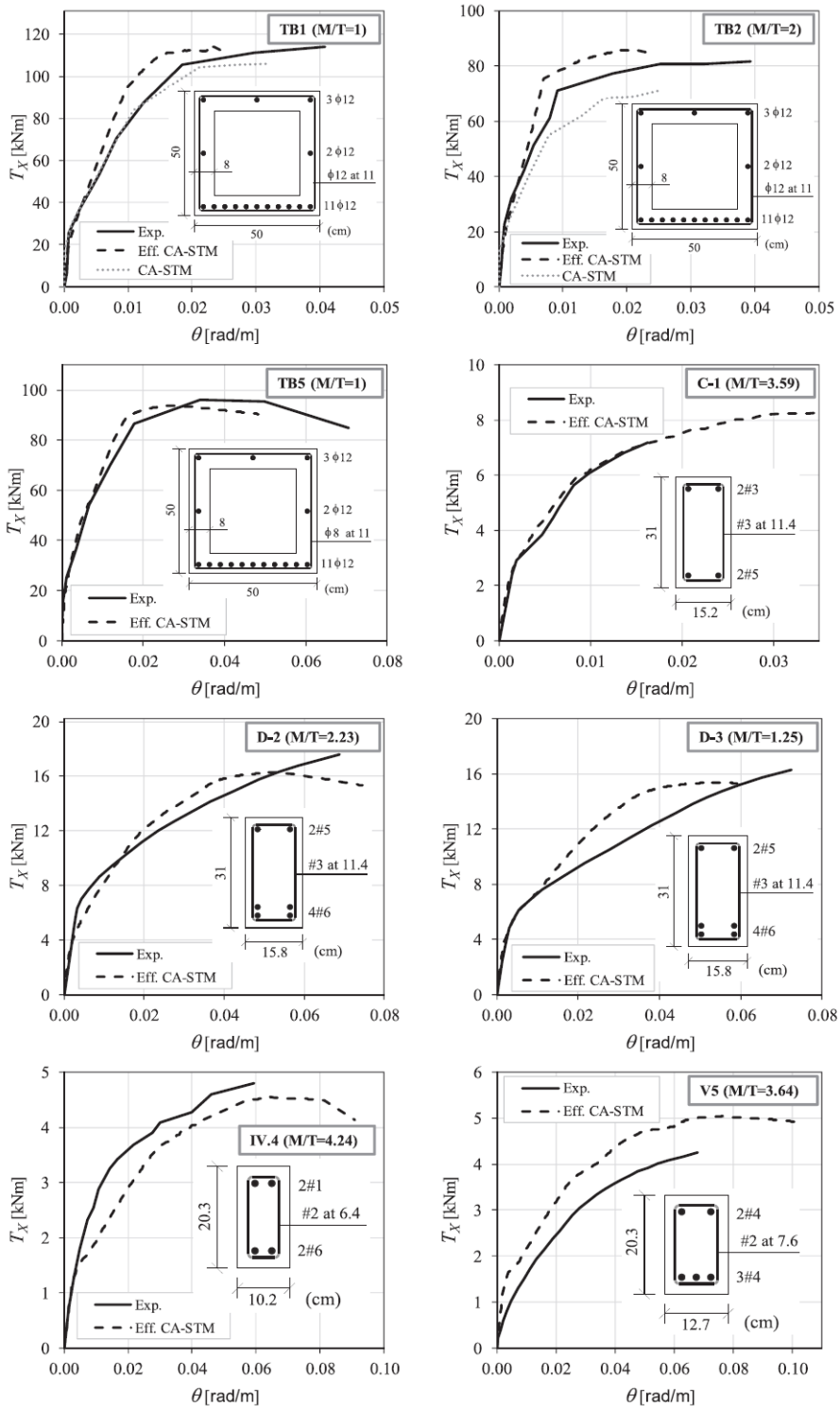

Fig. 9. (*continued*)

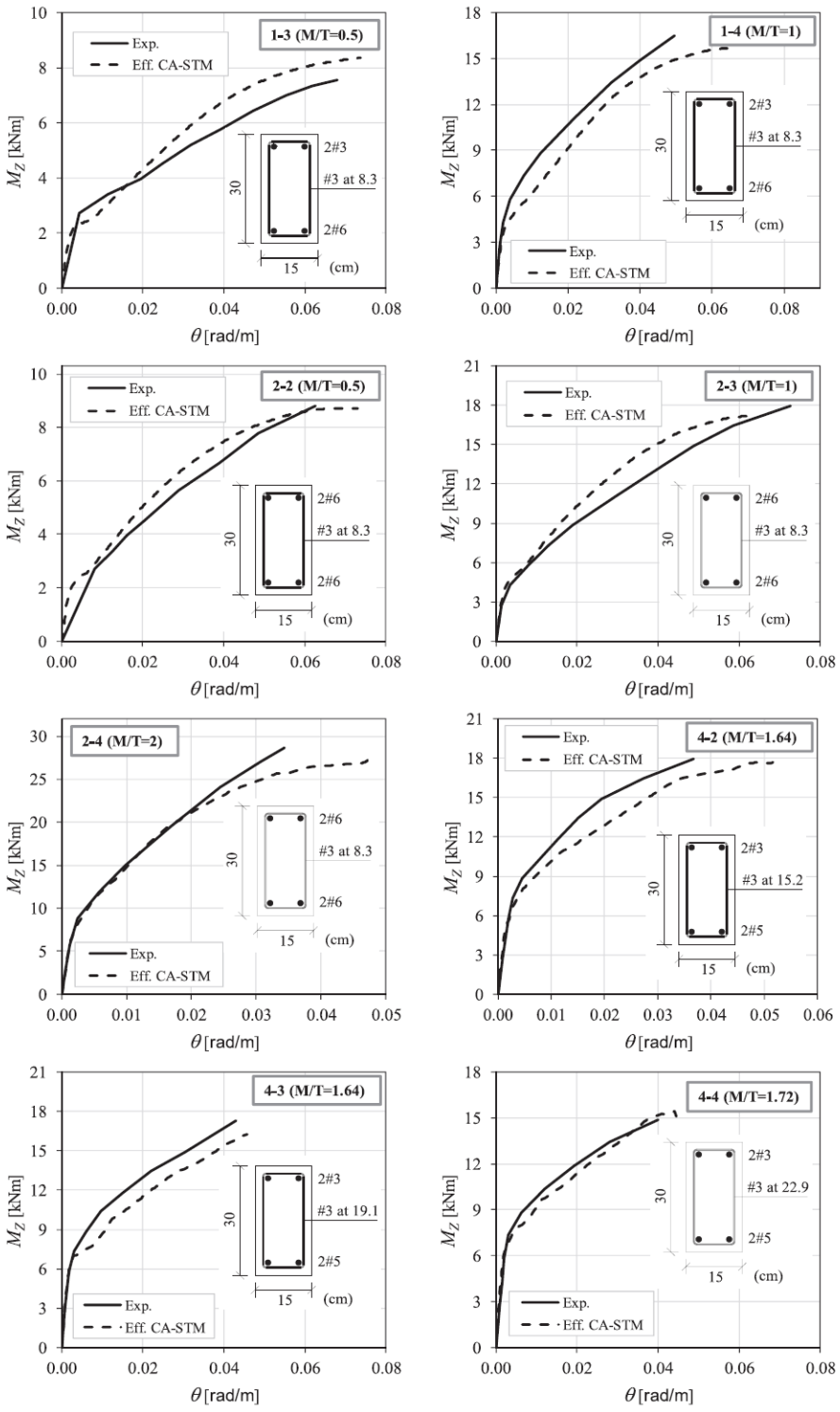

Fig. 10. $M_Z - \theta$ curves for selected beams.

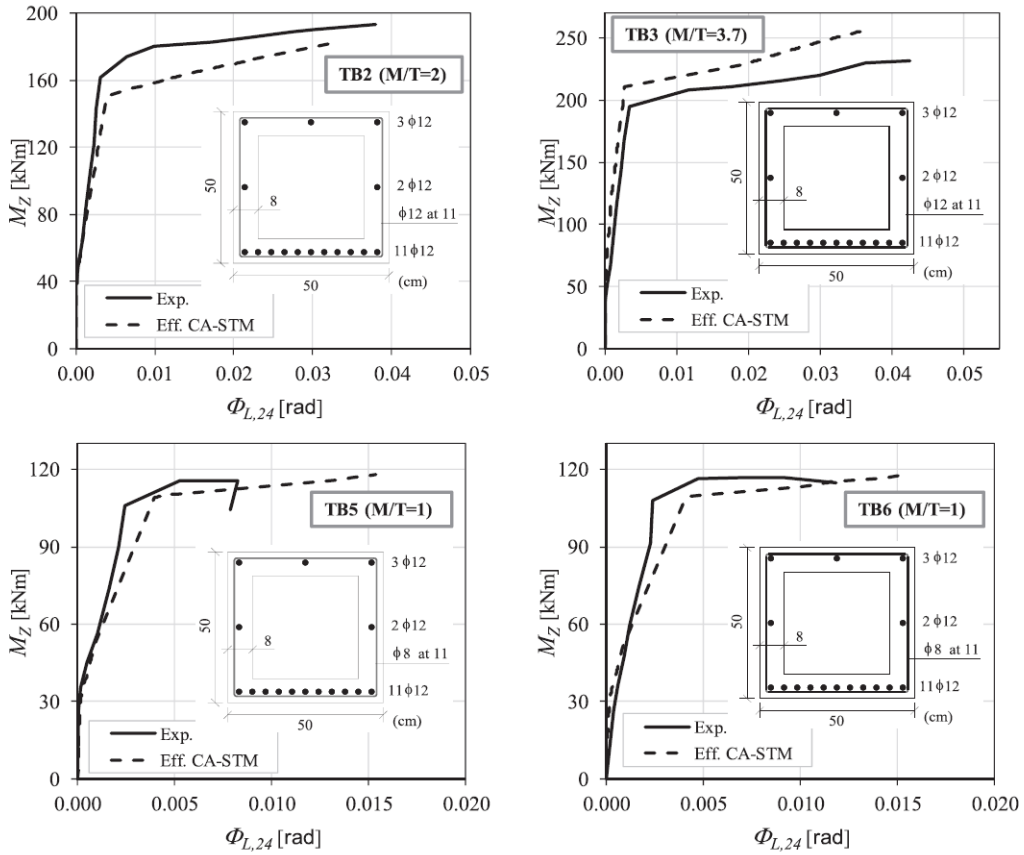

Fig. 11. $M_Z - \phi_{L,24}$ curves for selected beams.

original CA-STM from Green and Belarbi [30] in Fig. 9, the predictions from the refined efficient CA-STM procedure show some differences, which can be attributed to the different used constitutive laws for the materials and also to the different geometrical criteria used in this study.

Finally, Fig. 12 presents some experimental versus theoretical interaction ($T_X - M_Z$) curves for selected beams' series (with equal beams but different ratios M_Z/T_X). When available or when possible to be computed, the experimental and theoretical results of beams under pure torsion or pure bending where added to complete the interaction curves.

Fig. 12 shows that the shape on the experimental interaction curves agree reasonably well with the theoretical ones. In addition, both the experimental and theoretical curves are also relatively close. These observations allow to state that the refined efficient CA-STM procedure is able to predict with reasonable accuracy the interaction between the torque and bending at failure, as well as the dominant failure mode of the analyzed reference beams. This last one strongly depends on the torque to the bending ratio, as experimentally observed by authors from the measurement of the strains in the reinforcements [46–50].

5. Conclusions

In this article, a refined version of the CA-STM with an efficient solution procedure was presented. This new version of the model, called refined efficient CA-STM procedure was used to calculate the full response of several reference RC beams under torsion combined with bending, which experimental results were found in the literature. From the results obtained throughout this study, the following conclusions can be drawn:

- The refinements of the CA-STM calculation procedure proposed in this study, namely by incorporating a set of appropriate smeared stress–strain relationships for the materials and a simpler criterion to compute the equivalent longitudinal reinforcement, have proven to be adequate to model with reasonable accuracy the response of RC beams under torsion combined with bending for all loading levels, including the transition from the uncracked to the cracked stage;
- The additional proposed refinements of the CA-STM calculation procedure leading to an alternative algorithm, in order to avoid using the original trial-and-error solution technique, and the definition of a new criterion to fix the maximum thickness for the panels in solid members, led to a more efficient calculation procedure with higher numerical stability. The numerical results were obtained in very acceptable amounts of time. The average processing time for the analyzed reference RC beams was approximately 30 s per beam (although with some variation between beams) by using a normal computer (intel(R) Core(TM) i7-4700MQ CPU @ 2.40 GHz);
- When compared with several experimental results of tested RC

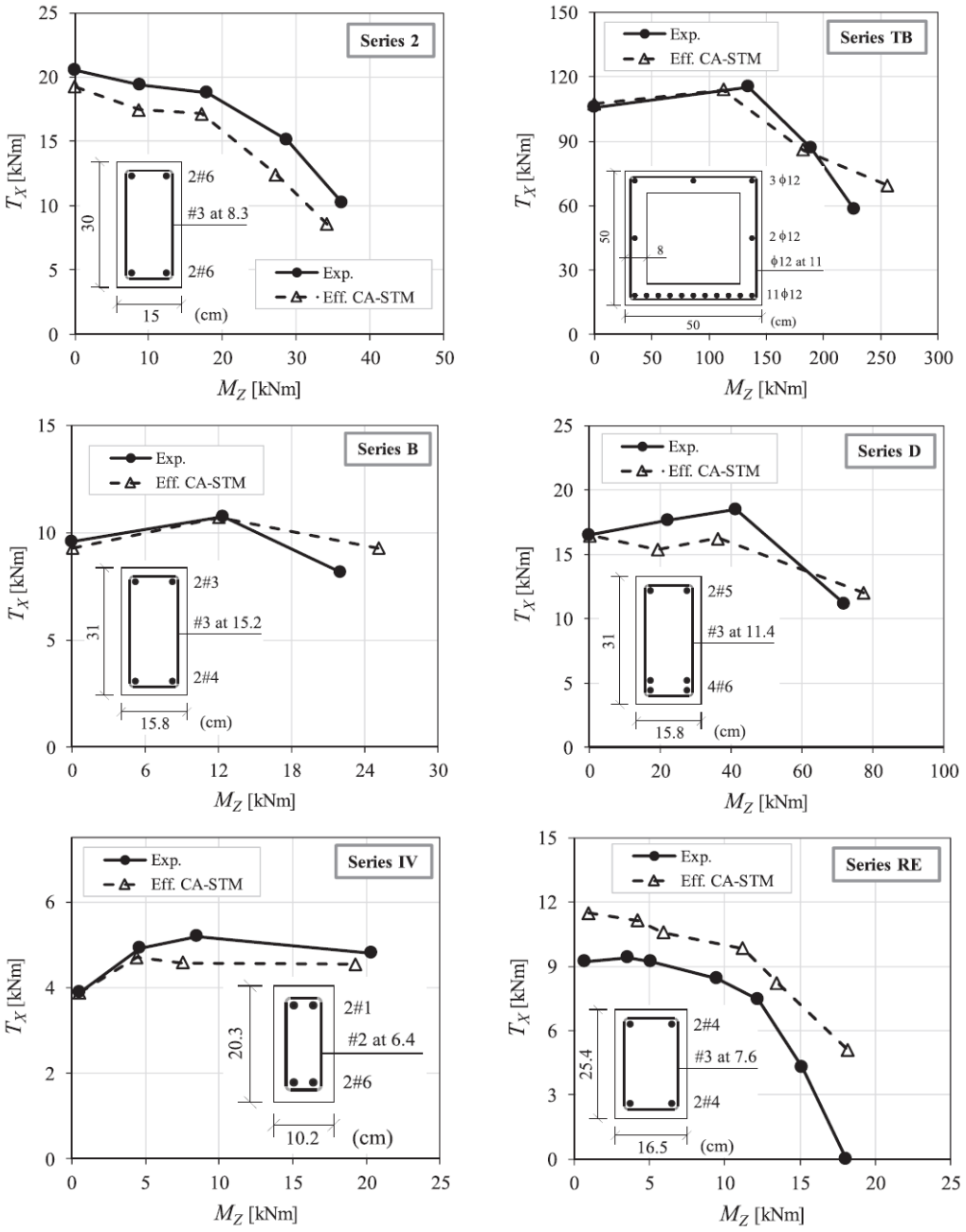

Fig. 12. Interaction curves for selected series.

beams under torsion combined with bending, the refined efficient CA-STM procedure proved to be a reliable truss-based model to predict the full behavior of such members, namely the cracking and ultimate key points.

- The refined efficient CA-STM procedure showed to be a simple and reliable truss-based model for RC members and can constitutes an alternative analytical model to more complicated ones. It can easily be used to build simple computational tools which can be very useful to optimize and help to design RC members.

The work should proceed in order to check the reliability of the refined efficient CA-STM procedure for other more general and current

loading combinations.

Declaration of Competing Interest

The authors declare that they have no known competing financial interests or personal relationships that could have appeared to influence the work reported in this paper.

References

[1] Mondal TG, Prakash SS (2016) Nonlinear Finite Element Analysis of RC Bridge Columns under Torsion with and without Axial Compression, J Bridge Eng, 21(2), pp. 13. DOI. 10.1061/ (ASCE) BE.1943-5592.0000798.

[2] Prakash SS, Li Q, Belarbi A. Behavior of Circular and Square Reinforced Concrete Bridge Columns under Combined Loading Including Torsion. ACI Struct J 2013;109(3):317–28.

[3] Prakash S, Belarbi A, You Y-M. Seismic performance of circular RC columns subjected to axial force, bending, and torsion with low and moderate shear. Eng Struct 2010;32(1):46–59.

[4] Hsu TTC. Torsion of Structural Concrete – Behaviour of Reinforced Concrete Rectangular Members, Torsion of Structural Concrete. SP-18. American Concrete Institute; 1968. p. 261–306.

[5] McMullen AE, Warwaruk J. Concrete Beams in Bending, Torsion and Shear. J Struct Division 1970;96(5):885–903.

[6] Elfgren L, Karlsson I, Losberg A. Torsion-Bending-Shear Interaction for Concrete Beams. J Struct Division 1974;100(8):1657–76.

[7] Rausch E (1929) Berechnung des Eisenbetons gegen Verdrehung (Design of Reinforced Concrete in torsion), Ph.D. Thesis, Berlin, 53pp. (in German).

[8] Mitchell D, Collins MP. Diagonal Compression Field Theory – A Rational Model for Structural Concrete in Pure Torsion. ACI J 1974;71(8):396–408.

[9] Hsu TTC, Mo YL. Softening of Concrete in Torsional Members – Theory and Tests. J Am Concr Institute 1985;82(3):290–303.

[10] Jeng C_H, Hsu TTC. A Softened Membrane Model for Torsion in Reinforced Concrete Members. Eng Struct 2009;31:1944–54.

[11] Bernardo LFA, Andrade JMA, Nunes NCG. Generalized softened variable angle truss-model for reinforcement concrete beams under torsion. Mater Struct 2015;48(7):2169–93.

[12] Lampert P, Thürlimann B. Ultimate Strength and Design of Reinforced Concrete Beams in Torsion and Bending. Institut für Baustatik und Konstruktion, vol 42. 1972; Birkhäuser, Basel: 107-131.

[13] Rahal KN, Collins MP. Analysis of Sections Subjected to Combined Shear and Torsion – A Theoretical Model. ACI Struct J 1995;92(4):459–69.

[14] Kothamuthyala SR, Thammishetti N, Prakash SS, Vyasarayani CP. Optimization-Based Improved Softened Membrane Model for Rectangular Reinforced Concrete Members under Combined Shear and Torsion. J Struct Eng 2019;145(2). https://doi.org/10.1061/(ASCE)ST.1943-541X.0002228.

[15] Cocchi GM, Volpi M. Inelastic Analysis of Reinforced Concrete Beams subjected to Combined Torsion, Flexural and Axial Loads. Comput Struct 1996;61(3):479–94.

[16] Bernardo LFA, Taborda CSB, Andrade JMA. Ultimate torsional behaviour of axially restrained RC beams. Comput Concr 2015;16(1):67–97.

[17] Ganganagoudar A, Mondal TG, Prakash SS. Improved Softened Membrane Model for Reinforced Concrete Circular Bridge Columns under Torsion. J Bridge Eng 2016;21(7):1–12. https://doi.org/10.1061/(ASCE)BE.1943-5592.0000907.

[18] Rabbat BG, Collins MP. A Variable Angle Space Truss Model for Structural Concrete Members Subjected to Complex Loading. SP 55. American Concrete Institute; 1978. p. 547–87.

[19] Greene GG, Belarbi A (2009) Model for Reinforced Concrete Members under Torsion, Bending, and Shear. I: Theory. J Eng Mechan, 135(9): 961–969.

[20] Valipour HR, Foster SJ. Nonlinear reinforced concrete frame element with torsion. Eng Struct 2010;32:988–1002.

[21] Hsu TTC, Mo YL. Softening of Concrete in Torsional Members – Prestressed Concrete. J Am Concr Institute 1985;82(5):603–15.

[22] Rahal KN, Collins MP. Combined Torsion and Bending in Reinforced and Prestressed Concrete Beams. ACI Struct J 2003;10(2):157–65.

[23] Jeng C_H, Chiu HJ, Chen CS. Modelling the Initial Stresses in Prestressed Concrete Members under Torsion. ASCE Confer Proceed 2010;369(162):1773–81.

[24] Bernardo LFA, Taborda CSB, Andrade JMA. Generalized Softened Variable Angle Truss Model for PC Beams Under Torsion. Int J Concr Struct Mater 2018;12: 62:15.

[25] Pang XB, Hsu TTC. Behavior of Reinforced Concrete Membrane Elements in Shear. Struct J Am Concr Institute 1995;92(6):665–79.

[26] Bernardo LFA, Cerquido BMD, Silva JRB, Horowitz B. Efficient Refined Rotating-Angle Softened Truss Model Procedure to Analyze Reinforced Concrete Membrane Elements. Struct Concr 2018;19(6):1971–82.

[27] Bernardo LFA, Lyrio ARB, Silva JRB, Horowitz B. Refined Softened Truss Model with Efficient Solution Procedure for Prestressed Concrete Membranes. J Struct Eng 2018;144(6):04018045.

[28] Bernardo LFA, Filho BMVC, Horowitz B. Predicting the behavior of prestressed concrete membrane elements by refined rotating-angle softened-truss model with efficient solution procedure. Struct Concr 2020;1–15. https://doi.org/10.1002/suco.201900481.

[29] Hsu TTC, Zhu RRH. Softened Membrane Model for Reinforced Concrete Elements in Shear. Struct J Am Concr Institute 2002;99(4):460–9.

[30] Greene GG, Belarbi A (2009) Model for Reinforced Concrete Members under Torsion, Bending, and Shear. II: Model Application and Validation. J Eng Mechan, 135(9): 970–977.

[31] Silva J, Horowitz B, Bernardo L. Efficient Analysis of Beam Sections Using Softened Truss Model. ACI Struct J 2017;114(3):765–74.

[32] Bernardo LFA, Andrade JMA, Lopes SMR. Softened Truss Model for Reinforced NSC and HSC Beams under Torsion: a Comparative Study. Eng Struct 2012;42:278–96.

[33] NP EN 1992-1-1, Eurocode 2: Design of Concrete Structures - Part 1: General Rules and Rules for Buildings; March 2010.

[34] Lampert P, Thürlimann B Torsionsversuche an Stahlbetonbalken (Torsion tests on reinforced concrete beams), Institut für Baustatik, ETH Zürich, 101 pp (in German); 1968.

[35] Greene GGJr. Behavior of reinforced concrete girders under cyclic torsion and torsion combined with shear: experimental investigation and analytical models, Ph. D Thesis. 2006; University of Missouri-Rolla: USA.

[36] Hsu TTC, Mo YL. Unified Theory of Concrete Structures. Wiley; 2010.

[37] Belarbi A, Hsu TTC. Constitutive Laws of Softened Concrete in Biaxial Tension-Compression. Struct J Am Concr Institute 1995;92(5):562–73.

[38] Zhu RRH, Hsu TTC, Lee JY. Rational Shear Modulus for Smeared-Crack Analysis of Reinforced Concrete. Struct J Am Concr Institute 2001;98(4):443–50.

[39] Zhang LX, Hsu TTC. Behavior and Analysis of 100 MPa Concrete Membrane Elements. J Struct Eng 1998;124(1):24–34.

[40] Belarbi A, Hsu TTC. Constitutive Laws of Concrete in Tension and Reinforcing Bars Stiffened by Concrete. Struct J Am Concr Institute 1994;91(4):465–74.

[41] Jeng CH, Hsu TTC. A softened membrane model for torsion in reinforced concrete members. Eng Struct 2009;31(9):1944–54.

[42] Bernardo LFA, Andrade JMA, Oliveira LAP. Reinforced And Prestressed Concrete Hollow Beams Under Torsion, J Civil Eng Manage 2013: 19 (1) S141-S152.36.

[43] Onsongo WM. The Diagonal Compression Field Theory for Reinforced Concrete Beams Subjected to Combined Torsion, Flexure and Axial Loads Ph.D. Thesis Canada: University of Toronto; 1978.

[44] ACI Committee 318. Building Code Requirements for Structural Concrete (ACI 318-14) and Commentary (ACI 318R-14), American Concrete Institute. 2014; Farmington Hills, MI: pp. 519.

[45] MathWorks. MATLAB_R2018a; 2018.

[46] McMullen AE, Warwaruk J. The Torsional Strength of Rectangular Reinforced Concrete Beams Subjected to Combined Loading, Report No. 2. 1967; Department of Civil Engineering: University of Alberta, Edmonton, July, pp. 162.

[47] Lampert P, Thürlimann B. Torsions-Biege-versuche an Stahlbetonbalken (Torsion tests on reinforced concrete beams under torsion and bending). 1969; Institut für Baustatik: ETH Zürich, pp. 116 (in German).

[48] Pandit GS, Warwaruk J. Reinforced Concrete Beams in Combined Bending and Torsion. Am Concr Institute Special Publication, SP- 1968;18:133–64.

[49] Goode CD, Helmy MA. Ultimate Strength of Reinforced Concrete Beams in Combined Bending and Torsion. American Concrete Institute Special Publication, SP- 1968;18:357–78.

[50] Collins MP, Walsh PF, Archer FE, Hall AS. Ultimate Strength of Concrete Beams Subjected to Combined Torsion and Bending. American Concrete Institute Special Publication, SP- 1968;18:379–402.

[51] Kemp EL. Behavior of Concrete Members Subject to Torsion and to Combined Torsion, Bending and Shear. American Concrete Institute Special Publication, SP-1968;18:179–202.

[52] Iyengar KTSR, Rangan BV. Strength and Stiffness of Reinforced Concrete Beams Under Combined Bending and Torsion. American Concrete Institute Special Publication 1968;SP-18:403–40.

[53] Cerquido BMD. Analysis of reinforced concrete sections with the softened truss model. Master Thesis 150. Covilhã, Portugal: Department of Civil Engineering and Architecture, University of Beira Interior; 2017. pp.150 (in Portuguese).

Capítulo 3

Estudo do comportamento último das secções críticas de vigas de betão armado sujeitas à torção pura

Neste capítulo são apresentados dois artigos científicos, um publicado em revista internacional e outro publicado em congresso internacional, no âmbito do comportamento último de vigas de betão armado sujeitas à torção pura. Apresenta-se lista de artigos que integram o presente capítulo:

Teixeira, M. M. and Bernardo, L. F. A. (2018). Ductility of RC beams under torsion. *Engineering Structures*. **168**: 759-769. https://doi.org/10.1016/j.engstruct.2018.05.021

Teixeira, M. M. and Bernardo, L. F. A. (2021). Torsional strength of reinforced concrete beams – Evaluation of some codes of practice. *Concrete structures: New trends for eco-efficiency and performance*. Lisbon, June 2021. Fib Symposium. 2035-2046 pp.

Engineering Structures 168 (2018) 759–769

Contents lists available at ScienceDirect

Engineering Structures

journal homepage: www.elsevier.com/locate/engstruct

Ductility of RC beams under torsion

M.M. Teixeira, L.F.A. Bernardo*

University of Beira Interior, C-MADE – Centre of Materials and Building Technologies, Covilhã, Portugal

ARTICLE INFO

Keywords:
Reinforced concrete
Beams
Torsion
Ductility
Codes of practice

ABSTRACT

In this article, the torsional ductility of reinforced concrete (RC) beams with rectangular cross section is studied. For this, the experimental results of several RC beams found in the literature were compiled and analyzed. A torsional ductility index was used to characterize the torsional ductility of the studied beams. The following variables study were considered: compressive concrete strength, torsional reinforcement ratio and cross section type (plain or hollow). The influence of each variable study on the torsional ductility is studied and important findings are pointed out which could help for the design of RC beams under torsion. An additional comparative analysis with the rules from some codes of practice in use is also performed. It is shown that, in general, the codes are too much restrictive as far as the maximum torsional reinforcement is concerned. As a consequence, this can leads to the unacceptance of several beams with ductile behavior.

1. Introduction

Nowadays, it is well known that plastic deformation capacity constitutes an important requirement to ensure the redistribution capacity of internal forces in structures, in order to prevent a sudden and progressive structural collapse. This property, which depends on the ductility of the critical sections of reinforced concrete (RC) members, is important because it is related with the structural safety for the ultimate limit states.

Over the last decades, many experimental studies have shown that the critical cross sections of RC members, namely beams, can provide sufficient ductility after the yielding of the reinforcement to ensure the redistribution capacity of the internal forces for the ultimate state. This is particularly accepted for RC beams under bending, including high-strength concrete beams [1–3]. For RC members under shear force, doubts about the ductile behavior may still exist. However, experimental researches show that RC members under shear, including high-strength concrete panels, can also present good levels of ductility [4,5]. This is because the softening effect (influence of diagonal cracking on the strength and deformation capacity of concrete in compression) leads to internal energy dissipation through appreciable levels of plastic shear deformation.

The above considerations about RC members under shear can also be extended to RC beams under torsion, due to the prevalence of an internal shear stress state imposed by the external torsional moments. Few previous researches on RC beams under torsion have shown that these structural elements can also present appreciable ductility and plastic twist capacity in their critical sections [6,7]. These studies also show that, as for bending and shear force, some requirements are need to ensure torsional ductility in RC beams. For instance, a minimum and maximum amount of torsional reinforcement must be provided, in order to avoid a brittle and premature failure due to the yielding of the reinforcement right after cracking or a brittle failure due to compressive concrete crushing. When compared with the bending case, these studies seems to show that the range for the amount of torsional reinforcement compatible with ductility is much narrower. Additionally, special care must also be given to the detailing of the torsional reinforcement. For instance, spacing between steel bars cannot be exaggerated so that cracks are always intersected by bars.

Older experimental studies also show that RC hollow beams are less ductile when compared to similar RC plain beams [8]. Since hollow beams are commonly used, this observation becomes very important.

In order to provide sufficient ductility in structural members, structural engineers usually follow the rules from codes of practice. For RC beams under bending and shear forces, codes of practice in use provide sufficient information. However, for torsion specific rules to ensure ductility are much scarcer. For instance, in some codes the minimum amount of torsional reinforcement, which can be considered a basic requirement, is still inexistent. Additionally, the maximum torsional reinforcement can indirectly be satisfied by checking the maximum compressive stress allowed in the concrete struts. This limit is usually given in the codes. However, some codes continue to refer to some ductility rules for bending and shear forces, as far as longitudinal and transverse torsional reinforcement is concerned.

* Corresponding author at: University of Beira Interior, Department of Civil Engineering and Architecture, Edifício II das Engenharias, Calçada Fonte do Lameiro, 6201-001 Covilhã, Portugal.
E-mail address: lfb@ubi.pt (L.F.A. Bernardo).

https://doi.org/10.1016/j.engstruct.2018.05.021
Received 16 December 2017; Received in revised form 13 April 2018; Accepted 7 May 2018

Table 1
Properties of reference beams.

Beam	[a]	x cm	y cm	t cm	x_1 cm	y_1 cm	A_{sl} cm^2	A_{st}/s cm^2/m	ρ_l %	ρ_t %	f_{ly} MPa	f_{ty} MPa	m_b	f_c MPa	ε_{c3} ‰	$\theta_{y,th}$ °/m	$\theta_{u,th}$ °/m	$\mu_{\theta,th}$	$\theta_{y,exp}$ °/m	$\theta_{u,exp}$ °/m	$\mu_{\theta,exp}$
B3 [8]	P	25.4	38.1	–	21.6	34.3	11.36	10.16	1.17	1.17	328	320	1.02	28.1	1.75	2.14	3.60	1.69	2.37	3.86	1.63
B4 [8]	P	25.4	38.1	–	21.6	34.3	15.48	14.01	1.60	1.62	320	323	0.98	29.2	1.75	1.91	3.37	1.77	2.56	4.63	1.81
B5 [8]	P	25.4	38.1	–	21.6	34.3	20.39	18.47	2.11	2.13	332	321	1.02	30.6	1.75	1.76	3.22	1.83	2.85	5.10	1.79
B6 [8]	P	25.4	38.1	–	21.6	34.3	25.81	22.58	2.67	2.61	332	323	1.05	28.8	1.75	1.63	2.99	1.83	3.05	4.41	1.44
B9 [8]	P	25.4	38.1	–	21.6	34.3	11.36	4.66	1.17	0.54	319	343	2.03	28.8	1.75	1.58	3.94	2.50	1.73	4.34	2.51
C4 [8]	P	25.4	25.4	–	21.6	21.6	11.36	13.11	1.76	1.76	337	328	1.03	27.2	1.75	2.12	3.74	1.76	3.68	5.91	1.61
C5 [8]	P	25.4	25.4	–	21.6	21.6	15.48	17.67	2.40	2.37	328	329	1.01	27.2	1.75	1.95	3.52	1.80	3.98	8.83	2.22
C6 [8]	P	25.4	25.4	–	21.6	21.6	20.39	23.91	3.16	3.20	316	328	0.95	27.6	1.75	1.81	3.35	1.85	4.43	7.30	1.65
G3 [8]	P	25.4	50.8	–	21.6	47.0	11.36	8.29	0.88	0.88	339	328	1.03	26.8	1.75	1.85	3.50	1.89	2.03	3.89	1.91
G4 [8]	P	25.4	50.8	–	21.6	47.0	15.48	11.29	1.20	1.20	326	321	1.01	28.3	1.75	1.95	3.31	1.70	2.47	3.82	1.55
G5 [8]	P	25.4	50.8	–	21.6	47.0	20.39	15.05	1.58	1.60	331	328	1.00	26.9	1.75	1.70	2.99	1.76	2.53	4.49	1.78
G7 [8]	P	25.4	50.8	–	21.6	47.0	12.00	8.84	0.93	0.94	319	323	0.98	31.0	1.75	1.77	3.83	2.17	1.67	3.96	2.38
G8 [8]	P	25.4	50.8	–	21.6	47.0	17.03	12.32	1.32	1.31	322	329	0.99	28.3	1.75	1.87	3.23	1.72	2.26	4.42	1.96
I3 [8]	P	25.4	38.1	–	21.6	34.3	11.36	10.16	1.17	1.17	343	334	1.03	44.8	1.75	1.98	4.71	2.38	1.62	5.01	3.09
I4 [8]	P	25.4	38.1	–	21.6	34.3	15.48	14.01	1.60	1.62	315	326	0.96	45.0	1.75	2.12	4.18	1.97	1.61	2.68	1.67
I5 [8]	P	25.4	38.1	–	21.6	34.3	20.39	18.47	2.11	2.13	310	326	0.94	45.0	1.75	1.99	3.84	1.93	2.24	5.20	2.32
I6 [8]	P	25.4	38.1	–	21.6	34.3	25.81	22.58	2.67	2.61	326	329	1.01	45.8	1.75	1.83	3.64	1.99	2.35	5.16	2.19
J1 [8]	P	25.4	38.1	–	21.6	34.3	5.16	4.66	0.53	0.54	328	346	0.94	14.3	1.75	2.21	3.12	1.41	2.38	5.20	2.19
J2 [8]	P	25.4	38.1	–	21.6	34.3	8.00	7.21	0.83	0.83	320	341	0.93	14.6	1.75	1.88	2.82	1.50	2.62	5.20	1.98
J4 [8]	P	25.4	38.1	–	21.6	34.3	15.48	14.01	1.60	1.62	324	332	0.97	16.8	1.75	1.61	2.61	1.62	3.15	5.21	1.66
K2 [8]	P	15.2	49.5	–	11.4	45.7	7.74	6.77	1.03	1.03	336	338	0.99	30.6	1.75	2.91	5.41	1.86	2.30	3.55	1.54
K3 [8]	P	15.2	49.5	–	11.4	45.7	12.00	10.42	1.59	1.58	316	321	0.99	29.0	1.75	2.61	4.69	1.80	3.39	5.88	1.73
K4 [8]	P	15.2	49.5	–	11.4	45.7	17.03	15.05	2.26	2.28	344	340	1.00	28.6	1.75	2.32	4.28	1.85	3.92	8.66	2.21
M2 [8]	P	25.4	38.1	–	21.6	34.3	11.36	6.77	1.17	0.78	329	357	1.38	30.6	1.75	1.95	3.89	2.00	2.05	3.71	1.81
N1 [8]	P	15.2	30.5	–	13.0	28.3	2.84	3.50	0.61	0.62	352	341	1.01	29.5	1.75	2.85	7.53	2.64	2.48	10.64	4.29
N1a [8]	P	15.2	30.5	–	13.0	28.3	2.84	3.50	0.61	0.62	346	345	0.98	28.7	1.75	2.87	7.33	2.56	2.53	10.63	4.21
N2 [8]	P	15.2	30.5	–	13.0	28.3	5.16	6.35	1.11	1.13	331	338	0.96	30.4	1.75	3.41	5.80	1.70	3.89	8.18	2.10
N2a [8]	P	15.2	30.5	–	13.0	28.3	1.61	6.21	1.11	1.10	333	361	0.93	28.4	1.75	3.29	5.58	1.69	3.84	10.40	2.71
N3 [8]	P	15.2	30.5	–	13.0	28.3	4.26	5.08	0.92	0.90	352	352	1.02	27.3	1.75	3.43	5.81	1.69	3.60	9.75	2.71
N4 [8]	P	15.2	30.5	–	13.0	28.3	6.58	7.98	1.42	1.42	341	356	0.96	27.3	1.75	2.94	5.13	1.74	4.12	9.33	2.26
VB2 [10]	P	44.0	24.0	–	42.0	22.0	7.01	5.84	0.66	0.71	541	541	0.94	26.4	1.75	2.37	3.85	1.63	3.42	4.18	1.22
VB3 [10]	P	44.0	24.0	–	42.0	22.0	7.01	5.84	0.66	0.71	541	541	0.94	39.1	1.75	2.77	4.71	1.70	3.20	4.50	1.40
VB4 [10]	P	44.0	24.0	–	42.0	22.0	7.01	5.84	0.66	0.71	541	541	0.94	49.8	1.75	2.93	5.29	1.81	2.93	4.24	1.45
VM2 [10]	P	44.0	24.0	–	42.0	22.0	6.60	5.32	0.63	0.65	432	436	0.96	36.1	1.75	2.31	5.03	2.18	2.18	3.43	1.57
VM3 [10]	P	58.7	32.0	–	56.1	29.4	12.84	7.14	0.68	0.65	461	442	1.10	40.0	1.75	1.71	3.91	2.29	1.82	3.66	2.02
VQ1 [10]	P	32.4	32.4	–	30.4	30.4	3.46	2.88	0.33	0.33	557	557	0.99	19.0	1.75	2.69	3.78	1.41	2.68	3.24	1.21
VQ3 [10]	P	58.0	18.6	–	56.0	16.6	4.27	3.05	0.40	0.41	433	433	0.96	17.6	1.75	2.89	4.23	1.46	2.52	2.98	1.18
VQ9 [10]	P	80.6	14.0	–	78.6	12.0	5.08	2.82	0.45	0.45	441	441	0.99	19.5	1.75	3.56	5.31	1.49	3.82	4.59	1.20
VS2-VQ2 [10]	P	44.0	24.0	–	42.0	22.0	3.66	3.05	0.35	0.37	433	433	0.94	19.0	1.75	2.33	4.12	1.77	1.77	2.70	1.52
VS3 [10]	P	44.0	24.0	–	42.0	22.0	5.49	4.55	0.52	0.55	433	433	0.94	19.5	1.75	2.42	3.59	1.48	3.70	3.97	1.08
VS4-VQ5 [10]	P	44.0	24.0	–	42.0	22.0	7.32	6.10	0.69	0.74	433	433	0.94	19.0	1.75	2.11	3.28	1.55	3.46	3.99	1.15
VS9 [10]	P	44.0	24.0	–	42.0	22.0	3.48	2.90	0.33	0.35	571	571	0.94	17.6	1.75	2.66	3.77	1.42	2.97	3.74	1.26
VS10-VB1 [10]	P	44.0	24.0	–	42.0	22.0	6.96	5.80	0.66	0.70	571	571	0.94	19.0	1.75	2.12	3.29	1.55	3.37	3.86	1.14
A2 [11]	P	25.4	25.4	–	22.2	22.2	5.16	7.82	0.80	1.08	380	285	0.99	38.2	1.75	2.11	5.87	2.78	2.12	4.17	1.96
A3 [11]	P	25.4	25.4	–	21.9	21.9	8.00	8.94	1.24	1.22	352	360	1.00	39.4	1.75	2.75	4.99	1.81	2.36	7.49	3.17
A4 [11]	P	25.4	25.4	–	21.9	21.9	11.36	12.42	1.76	1.69	351	360	1.02	39.2	1.75	2.42	4.50	1.86	2.98	4.34	1.46
B3 [11]	P	17.8	35.6	–	14.3	32.1	8.00	8.60	1.27	1.26	352	360	0.98	38.6	1.75	3.01	5.40	1.79	3.61	7.32	2.03
B4 [11]	P	17.8	35.6	–	14.3	32.1	11.36	11.76	1.80	1.73	351	360	1.02	38.5	1.75	2.59	4.89	1.89	3.50	6.54	1.87
B5UR1 [12]	P	20.3	30.5	–	16.5	26.7	5.16	6.56	0.83	0.92	386	373	0.94	39.6	1.75	2.65	5.97	2.25	1.33	3.75	2.82
B7UR1 [12]	P	20.3	30.5	–	16.5	26.7	5.16	6.56	0.83	0.92	386	399	0.88	64.6	1.84	2.42	7.49	3.10	0.58	2.35	4.06
B9UR1 [12]	P	20.3	30.5	–	16.5	26.7	5.16	6.56	0.83	0.92	386	373	0.94	75.0	1.98	2.38	8.42	3.53	1.87	3.93	2.10
B12UR1 [12]	P	20.3	30.5	–	16.5	26.7	5.16	6.56	0.83	0.92	386	399	0.88	80.6	2.06	2.35	8.39	3.57	0.52	1.80	3.48
B12UR2 [12]	P	20.3	30.5	–	16.5	26.7	5.16	6.95	0.83	0.97	386	386	0.86	76.2	2.00	2.33	8.03	3.45	0.31	2.07	6.58
B12UR3 [12]	P	20.3	30.5	–	16.5	26.7	6.58	7.46	1.06	1.04	380	386	1.00	72.9	1.95	2.52	7.40	2.94	1.05	3.31	3.14
B12UR4 [12]	P	20.3	30.5	–	16.5	26.7	7.74	7.88	1.25	1.10	373	386	1.10	75.9	2.00	2.64	7.12	2.70	1.09	3.06	2.81
B12UR5 [12]	P	20.3	30.5	–	16.5	26.7	8.00	10.13	1.29	1.41	380	386	0.90	76.7	2.01	2.64	6.53	2.47	1.54	3.85	2.51
B14UR1 [12]	P	20.3	30.5	–	16.5	26.7	5.16	6.56	0.83	0.92	386	386	0.91	93.9	2.24	2.29	9.13	3.99	0.04	2.99	70.45
H-12–12 [13]	P	35.0	50.0	–	30.0	45.0	20.65	14.19	1.18	1.22	410	440	0.90	78.5	2.03	1.68	4.01	2.39	1.30	4.43	3.40
H-14–10 [13]	P	35.0	50.0	–	30.0	45.0	17.03	16.13	0.97	1.38	500	360	0.98	68.4	1.89	1.65	3.91	2.37	1.29	4.90	3.80
N-12–12 [13]	P	35.0	50.0	–	30.0	45.0	20.65	14.19	1.18	1.22	410	440	0.90	35.5	1.75	1.62	2.88	1.78	2.09	6.51	3.11
N-14–10 [13]	P	35.0	50.0	–	30.0	45.0	17.03	16.13	0.97	1.38	500	360	0.98	33.5	1.75	1.60	2.84	1.77	2.61	5.95	2.27
NBS-43–44 [14]	P	35.0	50.0	–	30.0	45.0	7.60	5.09	0.43	0.44	400	385	1.03	35.0	1.75	1.45	4.86	3.34	0.91	4.17	4.59
D3 [8]	H	25.4	38.1	6.4	21.6	34.3	11.36	10.16	1.17	1.17	341	333	1.02	28.4	1.75	2.02	3.57	1.77	2.22	3.44	1.55
D4 [8]	H	25.4	38.1	6.4	21.6	34.3	15.48	14.01	1.60	1.62	330	333	0.98	30.6	1.75	1.91	3.38	1.77	2.27	3.27	1.44
T1 [9]	H	50.0	50.0	8.0	45.4	45.4	18.10	10.28	0.72	0.75	357	357	0.97	35.3	1.75	1.22	3.13	2.56	1.53	2.32	1.51
T2 [9]	H	50.0	50.0	8.0	43.0	43.0	18.10	10.28	0.72	0.71	357	357	1.02	35.3	1.75	1.22	3.14	2.57	1.71	4.00	2.34
VH1 [10]	H	32.4	32.4	8.0	30.4	30.4	3.46	2.88	0.33	0.33	447	447	0.99	17.2	1.75	2.46	3.48	1.41	2.36	2.86	1.21
VH2 [10]	H	32.4	32.4	8.0	30.4	30.4	6.91	5.76	0.66	0.67	447	447	0.99	17.2	1.75	1.88	2.91	1.55	1.89	3.67	1.94
A1 [6]	H	60.0	60.0	9.8	53.7	54.7	6.53	3.14	0.18	0.19	696	637	1.05	48.4	1.75	1.44	5.30	3.68	0.78	2.69	3.45
A2 [6]	H	60.0	60.0	10.7	53.8	53.1	13.95	6.28	0.39	0.37	672	696	1.00	47.3	1.75	1.68	3.33	1.99	1.69	3.74	2.22
A3 [6]	H	60.0	60.0	10.9	53.5	53.5	18.10	8.27	0.50	0.49	672	715	0.96	46.2	1.75	1.66	2.79	1.68	1.46	2.14	1.47
A4 [6]	H	60.0	60.0	10.4	52.0	52.5	23.75	11.22	0.66	0.65	724	715	1.03	54.8	1.75	1.54	2.79	1.82	1.58	2.42	1.53
A5 [6]	H	60.0	60.0	10.4	52.8	52.8	30.66	14.14	0.85	0.83	724	672	1.11	53.1	1.75	1.38	2.44	1.77	1.52	2.20	1.45

(continued on next page)

Table 1 (*continued*)

Beam	[a]	x cm	y cm	t cm	x_1 cm	y_1 cm	A_{sl} cm^2	A_{st}/s cm^2/m	ρ_l %	ρ_t %	f_{ly} MPa	f_{ty} MPa	m_b	f_c MPa	ε_{c3} ‰	$\theta_{y,th}$ °/m	$\theta_{u,th}$ °/m	$\mu_{\theta,th}$	$\theta_{y,exp}$ °/m	$\theta_{u,exp}$ °/m	$\mu_{\theta,exp}$
B2 [6]	H	60.0	60.0	10.8	53.3	53.4	14.58	6.70	0.41	0.40	672	696	0.99	69.8	1.91	1.61	3.02	1.88	1.68	2.89	1.73
B3 [6]	H	60.0	60.0	10.9	53.5	53.7	23.75	11.22	0.66	0.67	724	715	1.00	77.8	2.02	1.76	3.10	1.76	1.42	1.98	1.39
B4 [6]	H	60.0	60.0	11.2	52.3	53.6	32.17	15.08	0.89	0.89	724	672	1.09	79.8	2.05	1.67	2.79	1.67	1.25	1.66	1.32
B5 [6]	H	60.0	60.0	11.7	51.8	51.8	40.21	18.85	1.12	1.09	724	672	1.11	76.4	2.00	1.48	2.57	1.73	1.15	1.56	1.36
C1 [6]	H	60.0	60.0	9.7	54.0	54.9	6.53	3.14	0.18	0.19	696	637	1.04	91.7	2.21	1.43	7.28	5.09	1.13	2.03	1.80
C2 [6]	H	60.0	60.0	10.0	53.2	53.3	13.95	6.28	0.39	0.37	672	696	1.01	94.8	2.26	1.58	2.77	1.75	1.41	2.18	1.55
C3 [6]	H	60.0	60.0	10.3	54.5	54.0	23.75	10.47	0.66	0.63	724	715	1.06	91.6	2.21	1.91	3.32	1.73	1.37	1.63	1.19
C4 [6]	H	60.0	60.0	10.3	54.6	54.5	30.66	14.14	0.85	0.86	724	672	1.07	91.4	2.21	1.88	2.96	1.58	1.47	1.77	1.21
C5 [6]	H	60.0	60.0	10.4	54.0	54.3	36.69	17.40	1.02	1.05	724	672	1.05	96.7	2.28	1.79	2.82	1.57	1.35	1.63	1.20
C6 [6]	H	60.0	60.0	10.4	53.3	52.9	48.25	22.62	1.34	1.34	724	672	1.08	87.5	2.16	1.51	2.57	1.71	1.13	1.47	1.30
C065a [16]	H	49.5	78.1	8.5	43.5	72.1	20.00	9.93	0.52	0.59	338	376	0.78	78.8	2.04	0.76	4.63	6.08	0.13	0.86	6.59
C100a [16]	H	49.9	72.3	12.7	43.9	66.3	28.39	12.90	0.79	0.79	466	447	1.04	90.6	2.20	1.16	3.79	3.26	0.96	2.23	2.31
D090a [16]	H	50.1	72.2	10.5	44.1	66.2	28.39	12.90	0.79	0.79	466	447	1.04	105.7	2.41	1.11	3.96	3.58	0.73	2.06	2.81

[a] P – Plain section; H – Hollow section.

In this article, the torsional ductility of RC beams with rectangular cross section is studied. For this, several experimental results of RC beams tested under pure torsion and collected from literature are used. A torsional ductility index is used to characterize the ductility of the studied beams under torsion. The influence of the following variables study is evaluated: compressive concrete strength, torsional reinforcement ratio and cross section type (plain or hollow). Additionally, a comparative analysis with the rules from some codes of practice in use is also performed, in order to check their adequacy to guarantee the ductility of RC beams under torsion.

It should be referred that in real structures torsion is usually combined with other internal forces (bending moments, shear and axial forces) in the critical sections. However, in current structures torsion can be one of the primary internal forces for the design. Moreover, as usually required by the codes of practice, the design for combined loading requires to design the cross section separately for each internal force and, eventually, complement the analysis with interaction requirements. From this point of view, the study of RC beams under pure torsion can be considered important.

2. Research significance

Specific studies on the torsional ductility of RC beams are very scarce [6,7]. Moreover, these studies only focused RC hollow beams. In the literature, no additional studies were found on the torsional ductility of RC plain beams, neither comparative analyses between similar plain and hollow RC beams. In [7] it was shown, from numerical analyses with continuous and curved RC beams, that the redistribution capacity of torsional moments is as much important as for bending. This requires that sufficient torsional ductility must be ensured in the critical sections.

The lack of specific studies on this subject is reflected in the limited rules for most of codes of practice in use. For instance, when compared with the ductility rules for bending, the number of ductility rules directly related with torsion is much lesser or even inexistent.

For these reasons, a specific study on the torsional ductility of RC beams can be considered important.

3. Reference beams

From the literature, several RC beams with rectangular cross section and tested under torsion were collected for this study. These beams come from the following studies: Hsu in 1968 [8], Lampert and Thurlimann in 1969 [9], Leonhardt and Schelling in 1974 [10], McMullen and Rangan in 1978 [11], Koutchkali and Belarbi in 2001 [12], Fang and Shiau in 2004 [13], Chiu et al. in 2007 [14], Bernardo and Lopes in 2009 [6], Peng and Wong in 2011 [15] and Jeng in 2015 [16]. Beams from other studies found in literature and some of the beams belonging to the all set from the previous studies were discarded because of the applied criteria. The criteria to select the beams for this study were the following;

- The complete experimental curve Torque (T) – Twist (θ) should be given for the beam. This is because the torsional ductility is characterized from this curve (Section 4);
- The beam should have a typical behavior under torsion. To check this, the experimental T–θ curve was qualitatively analyzed. This curve should show a typical shape with all the behavioral stages until failure, such as described in [8];
- In addition to the previous criterion, basic and current requirements were also checked by using ACI Code [17]. This code was used because it constitutes one of the codes in use with higher number of specific rules for torsion, in order to impose a good behavior for a RC beam under torsion. These requirements included: proper detailing and proper solution for the torsional reinforcement, maximum spacing between bars, minimum diameter for the bars and minimum size for the walls (hollow beams). Some beams that do not respected requirements related with the minimum and maximum amount of torsional reinforcement were considered because they are of interest for this study (Section 6);
- The beam should have a minimum ductile failure. This was checked by visualizing qualitatively the experimental T–θ curve in the ultimate stage. This one should show inelastic deformations for the peak load and eventually also a post-peak descending branch. This shape indicates that the test was carried out with sufficient control to register the experimental inelastic deformations in the ultimate stage. In general, such behavior occurs when the torsional reinforcement yields before the maximum torque is reached. However, ductile behavior was also observed for some beams for which this condition did not occurred. This will be discussed in the next section.

Table 1 presents some of the geometrical and mechanical properties for the reference beams that were effectively used in this study, namely: the width (x) and the height (y) of the cross section, the thickness of the walls for hollow sections (t), the total area of longitudinal reinforcement (A_{sl}), the distributed area of the transverse reinforcement (A_{st}/s, with A_{st} the area for one bar of the hoop and s the longitudinal spacing between hoops), the longitudinal reinforcement ratio ($\rho_l = A_{sl}/xy$), the transverse reinforcement ratio ($\rho_t = A_{st}u/A_c s$, with $u = 2(x_1 + y_1)$ and $A_c = xy$, being x_1 and y_1 the average width and height of the transverse reinforcement), the average yielding stress for the longitudinal and transverse reinforcement (f_{ly} and f_{ty}, respectively), the effective balance between longitudinal and transverse reinforcement for the ultimate state ($m_b = (\rho_l f_{ly})/(\rho_t f_{ty}) = [A_{sl}s/(A_t 2(x_1 + y_1))]/(f_{ly}/f_{ty})$) and the average compressive strength for concrete (f_c). Parameter m_b represents the

ratio between the mechanical ratios of the longitudinal reinforcement to the transverse reinforcement. The other parameters presented in Table 1 will be explained later. Some of the properties for the materials are usually not given by the authors, namely the average Young's Modulus for steel and concrete (E_s and E_c, respectively). For concrete, the Young's Modulus was computed from the European code EC 2 [18] by correlation with f_c. For steel bars, the Young's Modulus was considered to be 200 GPa [18].

Some of the properties presented in Table 1 are related with the variables study to be analyzed (Section 5) and are also need to compute both the experimental and theoretical ductility indexes (Section 4).

4. Torsional ductility index

In this study, the same torsional ductility index μ_θ defined and used by Bernardo and Lopes in 2015 [6] was used. This index, based on the angular deformation per unit meter (twist), is defined as follows:

$$\mu_\theta = \frac{\theta_u}{\theta_y} \quad (1)$$

where

θ_u = ultimate twist (corresponding to the ultimate torque T_u);
θ_y = yielding twist (corresponding to the yielding torque T_y).

In this study, the experimental and theoretical values for μ_θ are computed for the reference beams. The experimental values are obtained from the experimental $T-\theta$ curves. The theoretical values are obtained from the theoretical $T-\theta$ curves computed from the Generalized Softened Variable Angle Truss Model (GSVATM). This analytical model was chosen because it provides good predictions for the behavior of RC beams under torsion [19].

The yielding twist θ_y is defined from the key point of the $T-\theta$ curve corresponding to the yielding of the torsional reinforcement (point with coordinates $(\theta_y;T_y)$). For beams with balanced torsional reinforcement ($m_b \approx 1$), both longitudinal and transverse reinforcements generally yield at the same time (or almost). In this situation, only one yielding point is defined in the $T-\theta$ curve. If two closely yielding points are identified (one for each torsional reinforcement), then an average point is defined. This situation is exemplified in Fig. 1 for Beam G4 [8]. For beams with unbalanced torsional reinforcement, longitudinal and transverse reinforcement do not yield at the same time. In this case two yielding points far apart exist in the $T-\theta$ curve (or even only one if the reinforcements are highly unbalanced). In this case, the chosen criterion was defined from the observation of the shape of the $T-\theta$ curve immediately after the first yielding point. If a pronounced nonlinear shape starts to develop right after this point (deformation rate starts to increase when compared with torque rate), then the effective yielding point is attributed to the first yielding point (or to the unique one if only one of the torsional reinforcement yielded). These situations are exemplified in Fig. 1 for Beams B9 and M2 [8]. If the nonlinear shape starts only after the second yielding point, either this second point is considered the effective yielding point, either an average point is defined if the two yielding points are not too far apart.

It should be referred that the theoretical $T-\theta$ curve was sometimes used to check the location of the yielding key point for the reference beams for which the authors did not provide sufficient data to identify clearly this point. This can be done because it is known that the GSVATM provides good predictions, including for the cracking and maximum torque [19]. For such beams, the location of the experimental yielding point was obtained from an interpolation between the cracking and maximum torque in the experimental $T-\theta$ curve, by knowing the relative location of this point between the cracking and maximum torque in the theoretical $T-\theta$ curve. In the end, the location of the yielding point in the experimental $T-\theta$ curve was confirmed from a qualitative analysis of the shape of the curve right after this point. In Fig. 1, it can be seen that this procedure is quite acceptable from comparison between the experimental and theoretical $T-\theta$ curves, namely for the torque levels and the relative location of the yielding point between the cracking and maximum torque (see Beams G4 and B9 in Fig. 1).

Still related with the yielding point of the $T-\theta$ curve, it was observed that for some reference beams a ductile behavior (inelastic deformations) rises before the yielding of the torsional reinforcement. This situation is exemplified in Fig. 1 for Beams I5 and K3 [8]. For this last one, the torsional reinforcement did not yielded. This occurs particularly in beams with normal strength concrete and with moderate or high torsional reinforcement ratio. This behavior is not new and can be explained due to the nonlinear behavior of the compressive concrete before the peak stress due to the initiation of the crushing phenomena.

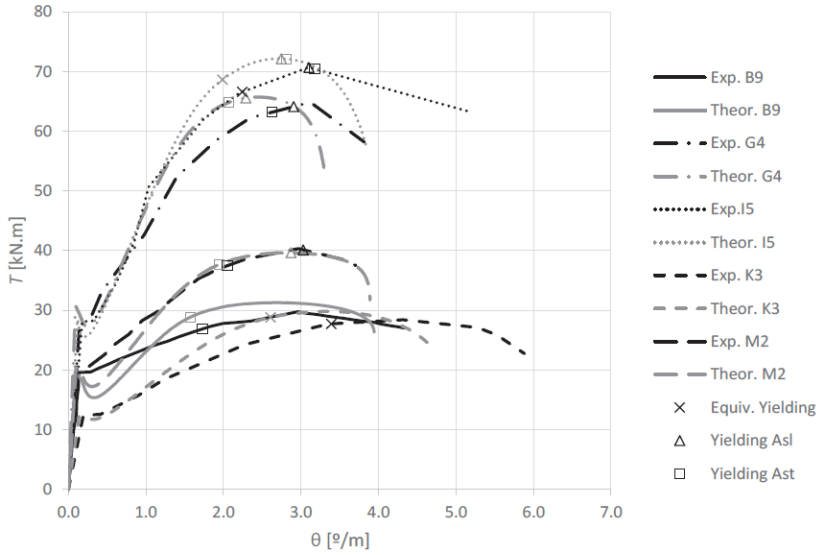

Fig. 1. Experimental and theoretical $T-\theta$ curves for some reference beams.

In current situations with over-reinforced sections in bending, an appropriate design based on the strain control for the reinforcement can maximize this favorable behavior of the compressive concrete [20]. For the reference beams that show this behavior, this ductile behavior must be considered and a criterion is need to define an equivalent yielding point in the $T-\theta$ curve. The chosen criterion was to attribute for the equivalent yielding point, the point in the $T-\theta$ curve for which the strain in the concrete in compression reaches the strain corresponding to the peak stress. This was done with the help of the theoretical results from the GSVATM, since experimental data for the strain in the compressive concrete in the principal direction of stresses are not usually provided in the studies. To compute a reference value for the strain corresponding to the peak stress for the concrete in compression, three values from EC 2 [18] were tested: ε_{c1} from a nonlinear stress (σ) – strain (ε) relationship, ε_{c2} from a parabola-rectangle $\sigma-\varepsilon$ relationship and ε_{c3} from a bilinear $\sigma-\varepsilon$ relationship. After the calculations and a comparative analysis between the concerned referred beams, it was found that ε_{c3} from a bilinear $\sigma-\varepsilon$ relationship is more realistic to estimate the equivalent yielding point in the $T-\theta$ curve. Table 1 presents the values for ε_{c3} computed from EC 2 [18] for the reference beams. For all the remaining reference beams, it was checked that the equivalent yielding point (concrete) is located to the right of the yielding point (torsional reinforcement) in the $T-\theta$ curves.

The location and verification of the key point corresponding to ε_{c3} in the experimental $T-\theta$ curve was obtained in a similar way as previously explained for the yielding point. The location of the equivalent yielding point is exemplified in Fig. 1 for Beams I5 and K3 [8].

From the referred above, and by knowing the location of the yielding point (or equivalent yielding point), the value for θ_y was obtained for both the theoretical and experimental $T-\theta$ curves ($\theta_{y,th}$ and $\theta_{y,exp}$, respectively). These values are presented in Table 1.

The ultimate twist θ_u is defined from the key point of the $T-\theta$ curve, in the post-peak descending branch, for which the beam no longer resists high torques. For this study, the same criterion discussed and used by Bernardo and Lopes in 2009 [6] is adopted. This criterion assumes that the ultimate twist corresponds to the key point with 80% of the maximum torque. This situation applies to Beam G4 [8] illustrated in Fig. 1. For the beams for which the last point of the $T-\theta$ curve corresponds to a torque higher than 80% of the maximum torque, the key point to define the ultimate twist is assumed to be the last point of the $T-\theta$ curve (point with maximum twist). For instance, this situation applies for Beam B9 illustrated in Fig. 1.

From the referred above, and by knowing the location of the key point to define the ultimate twist, the value for θ_u was obtained for both the theoretical and experimental $T-\theta$ curves ($\theta_{u,th}$ and $\theta_{u,exp}$, respectively). These values are presented in Table 1.

Table 1 also presents, for each reference beam, the theoretical and experimental torsional ductility index, $\mu_{\theta,th}$ and $\mu_{\theta,exp}$ respectively, computed from Eq. (1). From Table 1, it should be noted that appreciable differences exist between $\mu_{\theta,th}$ and $\mu_{\theta,exp}$ for some of the reference beams. This is because the theoretical and experimental $T-\theta$ curves usually show different shapes in the ending. This occur because GSVATM incorporates criteria to stop the calculations, namely conventional limits for the strains in the materials. For this reason, in this study the theoretical values for the torsional ductility index are only used to validate the experimental trends observed with the same experimental values (Section 5), which are expected to present higher dispersion. Since the theoretical $T-\theta$ curves are computed with the same stopping criteria for all the reference beams, it is assumed that the obtained theoretical trends are valid to check the experimental ones.

5. Analysis of the torsional ductility index

The aim of this section is to analyze qualitatively, with scatter graphs, the evolution of the torsional ductility index as function of some variables study related with the characteristics of the reference beams. The analysis of the results from previous experimental researches carried out over the last decades allow to state that the ultimate behavior of RC beams under torsion, with rectangular cross section, is influenced by the following variables [7,8,10,21]:

- concrete compressive strength (f_c);
- total ratio of torsional reinforcement ρ_{tot} (beams with balanced reinforcement);
- section type (plain or hollow);
- unbalance of torsional reinforcement (characterized with parameter m_b);
- height to width ratio (y/x) of the rectangular cross section.

Among these variables, the first three are those that show notable influence in the ultimate behavior of the beams, namely for the ultimate deformations, provided that m_b and y/x are not very far from unity (common situation for beams in pure torsion). This is also true for the torsional ductility.

The aim of this study is to investigate the influence of each of the previously referred variables study on the torsional ductility of the reference beams. For this and from Table 1, groups of beams are created according to the chosen variable to be studied. In each group, the variable study to be analyzed varies while the other variables are kept constant (or approximately). To study the influence of the variables f_c, ρ_{tot}, m_b and y/x on the torsional ductility index, the reference beams were also separated into two groups: plain and hollow cross section.

For each group of beams, a minimum number of beams must exist to provide a sufficient number of points in the graphs to show reliable trends. This condition somewhat limited the number of analysis that could be performed.

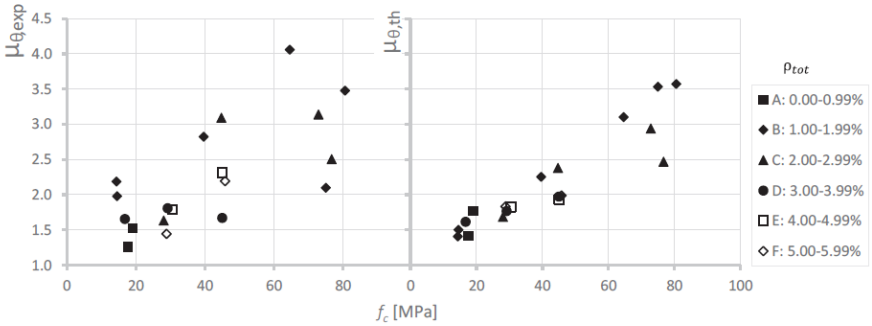

Fig. 2. Influence of f_c in μ_θ for groups of RC beams with similar ρ_{tot} (plain beams).

5.1. Concrete compressive strength

Fig. 2 shows the influence of the concrete compressive strength, f_c, in the torsional ductility index μ_θ for some groups with plain beams having equal or similar total reinforcement ratio, ρ_{tot}. A range of 1% for ρ_{tot} was considered to provide a sufficient number of beams for each group. As previously referred, variables m_b and y/x show to have a small effect in the ultimate stage, namely in the torsional ductility, provided that they are not very far from unity. For this reason, and to provide a sufficient number of beams and groups for the analysis, these variables were allowed to vary in the following ranges: $0.90 \leqslant m_b \leqslant 1.10$ and $0.50 \leqslant y/x \leqslant 2.00$. The studied groups include the following beams: Group A – VS9 and VS2-VQ2 [10]; Group B – J1 and J2 [8] + B5UR1, B7UR1, B9UR1 and B12UR1 [12]; Group C: B3 and I3 [8] + B12UR3 and B12UR5 [12]; Group D: J4, B4 and I4 [8]; Group E: B5 and I5 [8]; Group F: B6 and I6 [8]. Fig. 2 presents both the experimental and theoretical torsional ductility indexes for the same reference beams ($\mu_{\theta,exp}$ and $\mu_{\theta,th}$, respectively).

As expected, Fig. 2 shows larger dispersion of the results for the experimental torsional ductility indexes, when compared to the theoretical ones. Some dispersion is also observed for the theoretical results. This is probably related with the size of the interval that was considered for the torsional reinforcement ratio, ρ_{tot}, for each group. Fig. 2 also shows that, for a given range of ρ_{tot}, torsional ductility tends to increase as the concrete compressive strength f_c increases, regardless of being normal or high strength concrete. For this latter, this constitutes a positive observation. This trend is observed for both the experimental and theoretical torsional ductility indexes. For this reason, the observed experimental trend can be considered reliable.

Fig. 3 presents the same graphs as in Fig. 2, but now for RC hollow beams. The groups include the following beams: Group A – A2, A3, B2 and C2 [6]; Group B – A4, A5, B3, B4, C3 and C4 [6]; Group C – B5, C5 and C6 [6]. Fig. 3 shows a different trend for hollow beams, that is, the torsional ductility (both experimentally and theoretically) tends to decrease as the concrete compressive strength increases. This result was already observed by Bernardo and Lopes 2009 [6] with the same hollow beams and is reproduced here for comparison with the result for plain beams.

From Figs. 2 and 3, it is observed that, for a given range of ρ_{tot}, plain beams present higher torsional ductility when compared to hollow beams. This observation confirms an important point previously discussed in Section 1. In fact, from the $T-\theta$ curves, it is observed that for hollow beams the torque capacity decreases faster after the peak torque, comparatively to plain beams. From the previous results, it seems also that, with regard to torsional ductility, high strength concrete is favorable for plain beams and unfavorable for hollow beams.

These observations are probably related to the influence of the concrete core in plain beams for the ultimate stage, namely for the deformation capacity. In such beams, concrete core allows for higher capacity to redistribute the shear stresses (from the external to the center of the cross section). This allow plain beams to sustain high torques during a larger range for the deformations at the ultimate stage. In hollow beams, the lowest capacity do redistribute shear stresses leads to a faster degradation of the cross section and to a faster loss of the torque capacity. As a consequence, hollow beams show lower torsional ductility.

The results of this section show that, although it is accepted that, for similar plain and hollow beams, the concrete core has negligible influence on the torsional resistance (as observed in previous studies, for instance [8]), this is no longer true as far as torsional ductility is concerned.

5.2. Torsional reinforcement ratio

Fig. 4 shows the influence of the total reinforcement ratio ρ_{tot} in the torsional ductility index μ_θ (for both the experimental and theoretical values) for some groups with plain beams having equal or similar concrete compressive strength, f_c. A range of 10 MPa for f_c was considered for each group. Again, the following ranges were considered: $0.90 \leqslant m_b \leqslant 1.10$ and $0.50 \leqslant y/x \leqslant 2.00$. The groups include the following beams: Group A – N1a, G3, N3, N2a, G4, G8, N4 and G5 [8]; Group B – A2, A3 and A4 [11]; Group C: I3, I4, I5 and I6 [8]; Group D: B9UR1, B12UR3 and B12UR5 [12].

From Fig. 4, it can be observed that, for a given range of the concrete compressive strength, the torsional ductility indexes, both experimentally (although with higher dispersion) and theoretically, decreases notably as the total torsional reinforcement ratio increases, up to a certain limit. This one seems to be in the range 2.0–3.0%. After this limit, few beams continue to show a torsional ductility index greater than unity (this one corresponds to non-ductility). This can be due to the influence of the nonlinear concrete behavior under compression, as discussed in Section 4. According to the theoretical results (with less dispersion), the value of the referred limit seems to depend on the level of concrete strength. This limit seems to increase, within the previously referred range (2.0–3.0%), as the concrete strength increases.

Fig. 5 presents the same graphs as in Fig. 4, but now for RC beams with hollow cross section. The groups include the following beams: Group A – A1, A2 and A3 [6]; Group B – B3 and B4 [6]; Group C – C1, C2, C3, C4 and C5 [6]. For hollow beams, Fig. 5 shows a similar trend as the one previously observed for plain beams, and also similar to the trend observed in a previous study with the same beams [6]. However, the limit of ρ_{tot} for which the torsional ductility starts to stabilize (with a small value) seems to be less, in the range 1.0–1.5%. As for plain beams, this limit seems to increase, within this range, as the concrete strength increases.

From Figs. 4 and 5, it seems also that the range for ρ_{tot} compatible with a notable ductile behavior is much larger for plain beams, when compared with hollow beams. Again, this observation can be explained

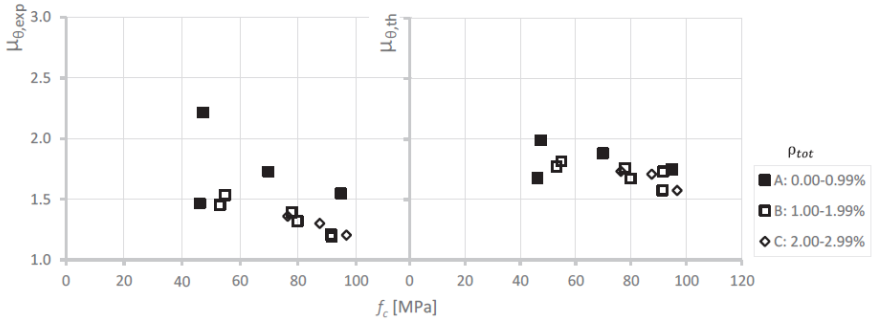

Fig. 3. Influence of f_c in μ_θ for groups of RC beams with similar ρ_{tot} (hollow beams).

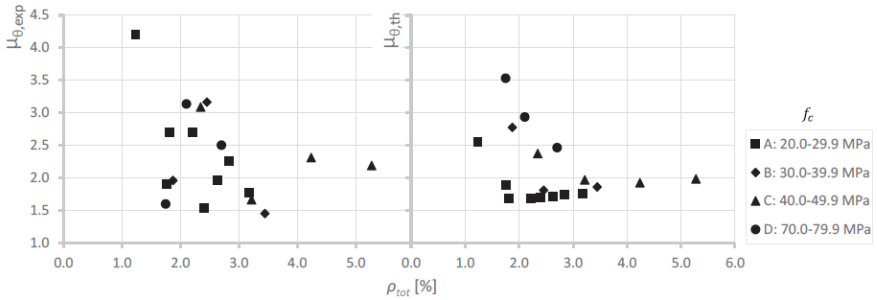

Fig. 4. Influence of ρ_{tot} in μ_θ for groups of RC beams with similar f_c (plain beams).

due to the influence of the concrete core, as previously discussed (Section 5.1).

Finally, when compared with the results in Section 5.1, it can be stated that the total reinforcement ratio, ρ_{tot}, shows higher influence on the torsional ductility, when compared to the concrete compressive strength, f_c.

5.3. Cross section type

To visualize better the influence of the concrete core in the torsional ductility, Fig. 6 shows the influence of the section type (plain or hollow) in the torsional ductility index μ_θ (for both the experimental and theoretical values) for beams with $m_b \approx 1$ and $y/x = 1$ (no values different from unity were found for hollow beams under torsion, see Table 1). In the previous section it was observed that the total reinforcement ratio ρ_{tot} shows higher influence on the torsional ductility, when compared to the concrete compressive strength f_c. For this reason, the results in Fig. 6 are presented in terms of ρ_{tot} .The graphs include the following beams: Plain beams – C4, C5 and C6 [8] + A2, A3 and A4 [11]; Hollow beams – T1 and T2 [9] + VH1 and VH2 [10] + A1, A2, A3, A4, A5, B2, B3, B4. C1, C2, C3, C4, C5 and C6 [6].

In general, Fig. 6 confirms the conclusions stated in the previous Sections 5.1 and 5.2. A notable decrease of the torsional ductility is observed for low torsional reinforcements until a limit is reached, which is in the following range: 1.0–1.5% (for hollow beams) and 2.0–3.0% (for plain beams). From this limit, some beams continue to show some ductility (with μ_θ in the range 1.5–2.0). The experimental results follow this trend for hollow beams. For plain beams, the tendency is not so clear due to the dispersion of the points.

In general, it can be confirmed that, for a given reinforcement ratio, torsional ductility is higher for plain beams.

5.4. Other variables study

For the remaining variables study, m_b and y/x, it was not possible to form groups with a sufficient number of beams, such that the variable to be study varied and the other ones were kept constant (or approximately). For this reason, no clear tendencies were observed, neither theoretically nor experimentally. Moreover, high dispersion were observed with only few points in the graphs, for both experimental and theoretical results. The authors believe that the observed high dispersion can be explained because the influence of the variables m_b and y/x in the torsional ductility is very small. It should be negligible when compared with the influence of the variables previously studied. For these reasons, no dispersion charts are presented in this section. It should be referred that this point also contributed to reduce even more the number of reference beams effectively used in this study (see Table 1), when compared to the initial set of reference beams collected from literature (around 120).

6. Comparative analysis with codes of practice

This section presents a comparative analysis between the maximum and minimum values of the torsional reinforcement ratio that are proposed by the codes of practice, with the effective torsional reinforcement ratio of the reference beams, in light of their torsional ductility indexes μ_θ. Since it was previously observed (Section 5) that the experimental trends are reliable (they matched with the theoretical ones), then only the experimental torsional ductility indexes are used here. The aim is to check the suitability of the code's rules to ensure the torsional ductility for RC beams, in order to avoid premature or brittle torsional failures due to insufficient or excessive torsional reinforcement.

The following reference codes of practice are considered: American code ACI 318R-14 [17], European Codes MC 10 [22] and EC 2 [18], and Canadian Standard CAN3-A23.3-14 [23].

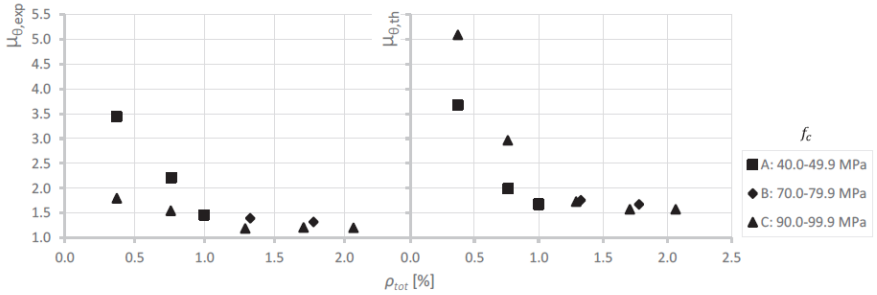

Fig. 5. Influence of ρ_{tot} in μ_θ for groups of RC beams with similar f_c (hollow beams).

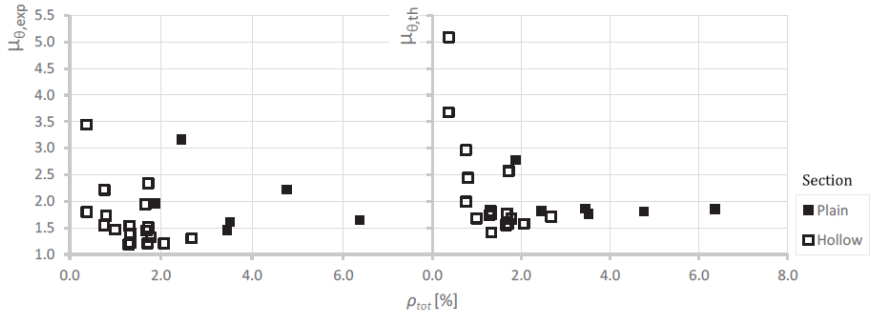

Fig. 6. Influence of the section type in μ_θ.

RC beams with a brittle and premature torsional failure due to insufficient reinforcement should not be accepted by codes of practice. This should be guaranteed through the imposition of a minimum limit for the torsional reinforcement. From the studied codes, only the ACI code explicitly imposes a minimum amount for the torsional longitudinal reinforcement. Both ACI and Canadian codes impose a minimum amount for the torsional transverse reinforcement. The other ones (European codes) refer in general to the minimum amount of reinforcement for bending (longitudinal reinforcement) and shear (transverse reinforcement).

RC beams with a brittle failure due to crushing of the compressive concrete in the struts should also not be accepted by codes of practice. This should be guaranteed through the imposition of a maximum limit for the torsional reinforcement. This requirement can be directly or indirectly imposed. In general, codes of practice impose a maximum limit for the stress in the compressive concrete in the struts. This limit can be used to compute the maximum torsional reinforcement to guarantee this requirement.

In this study and for the aim of the present section, only beams with approximately balanced reinforcement condition are considered: $0.90 \leqslant m_b \leqslant 1.10$ (the same ones considered in Sections 5.1 and 5.2). Moreover, the limits for the torsional reinforcement are applied only for transverse reinforcement.

In RC beams mainly under torsion the torsional reinforcement is usually balanced, i.e. $m_b = 1$. For such beams, both longitudinal and transverse reinforcements participate equally for the torsional behavior of the beams. For example as referred in Section 4, both reinforcements will yield at the same time (before or after the concrete crushing in the struts). If too much transverse reinforcement exists, which can lead to a brittle failure, then too much longitudinal reinforcement also exist. Then, for beams with balanced reinforcement, either longitudinal or transverse torsional reinforcement can be used as a key parameter to analyze the torsional ductility. In RC beams under torsion the shear effect is relevant and it seems to be more logical to relate its behavior with the transverse reinforcement. These reasons justify partially why the transverse torsional reinforcement was chosen for this section.

In addition to the previous justifications, for this section the minimum and maximum normative values for the allowed quantity of reinforcement are need. As far as specific rules for torsion are concerned, the majority of them are defined only for the transverse reinforcement. For instance, for the torsional longitudinal reinforcement, ACI code only specifies the minimum quantity. The other analyzed codes don't specify specific rules for the torsional longitudinal reinforcement. From the aforementioned, one can conclude that it is not possible to perform complete comparative analyzes based only on the torsional longitudinal reinforcement.

Table 2 presents, for each reference beam and for each code of practice, the minimum and maximum transverse reinforcement ratio ($\rho_{t,min}$ and $\rho_{t,max}$). These are computed from the minimum and maximum distributed area for the transverse reinforcement. Table 2 also presents the effective transverse reinforcement ratio (ρ_t) and the experimental ductility index ($\mu_{\theta,exp}$). From Table 2 it is observed that, except for CAN3-A23.3-14 and ACI 318R-14, the codes of practice did not predicted a brittle and premature failure due to insufficient reinforcement for any of the reference beams. This is consistent with the real failure of the reference beams used in this study. For few beams, CAN3-A23.3-14 and ACI 318R-14 (only for one beam) failed because it predicted such a failure. For all the codes of practice, some reference beams with real ductile behavior are expected to have a brittle failure due to concrete crushing. For these beams, the codes failed their predictions.

For each code, the results from Table 2 are analyzed below with the help of graphs.

Figs. 7–10 present, for each of the analyzed codes of practice and regardless of the concrete strength, the experimental torsional ductility index, $\mu_{\theta,exp}$, with the transverse reinforcement ratio, ρ_t. Graphs of Figs. 7–10 also show, for each range of values for $\rho_{t,min}$ and $\rho_{t,max}$ computed from the codes' rules, the average (vertical lines) and the width of the range with the maximum and minimum boundaries values. Since the range for the values of $\rho_{t,max}$ is large when all the reference beams are included, the beams are grouped according to some chosen range. This option allow to visualize better how many beams don't comply with the upper code's limit ($\rho_{t,max}$). The range of values for $\rho_{t,min}$ is narrow, regardless of the used code. For this reason, a single range is presented for $\rho_{t,min}$. Additionally, in Figs. 7–10 plain and hollow beams are distinguished by using "plain and hollow markers".

Fig. 7 shows that the interval defined by the maximum and the minimum transverse reinforcement ratio computed from ACI 318R-14 is very restrictive, mainly for $\rho_{t,max}$ and for plain beams. Several plain beams (almost regardless of $\rho_{t,max}$) and some hollow beams do not comply with the maximum limit from the code. In both cases, these beams show a ductile behavior (mainly for plain sections). These observations contradict the code, for which a brittle failure due to concrete crushing should be expected.

For MC 10, Fig. 8 shows similar results as the ones previously reported from Fig. 7, namely that several plain beams and some hollow beams do not comply with $\rho_{t,max}$ computed from the code. It is observed that the interval defined by $\rho_{t,min}$ and $\rho_{t,max}$ found by MC 10 is also very restrictive, mainly for $\rho_{t,max}$ and for plain beams. When compared with ACI 318R-14, MC 10 slightly restricts less $\rho_{t,min}$.

Fig. 9 shows that, when compared to MC 10 and ACI 318R-14, EC 2 restricts less the transverse reinforcement ratio, mainly the maximum limit ($\rho_{t,max}$). As a result, more reference beams comply with the limits imposed by the code. Only few plain beams, with some ductile behavior, do not comply with $\rho_{t,max}$. All hollow beams with ductile behavior comply with the code's limits. From this perspective, EC 2 is better.

Finally, Fig. 10 shows that, for CAN3-A23.3-14, the results are similar to the ones observed for EC 2, although it is more restrictive for $\rho_{t,max}$ and less ductile beams comply when compared to EC2. Again, some plain beams and some hollow beams do not comply with $\rho_{t,max}$

Table 2
Transverse reinforcement ratios from codes of practice.

Beam	$\mu_{\theta,exp}$	ρ_t %	m_b	ACI 318R-14		MC 10		EC 2		CAN3-A23.3–14	
				$\rho_{t,min}$ %	$\rho_{t,max}$ %	$\rho_{t,min}$ %	$\rho_{t,max}$ %	$\rho_{t,min}$ %	$\rho_{t,max}$ %	$\rho_{t,min}$ %	$\rho_{t,max}$ %
B3 [8]	1.63	1.17	1.02	1.33	7.10[b]	0.63	3.83[b]	0.83	16.69	2.46	9.41[b]
B4 [8]	1.81	1.62	0.98	1.37	7.45[b]	0.66	4.11[b]	0.88	17.78	2.57	10.06[b]
B5 [8]	1.79	2.13	1.02	1.31	7.35[b]	0.65	4.15[b]	0.87	17.83[b]	2.53	10.15[b]
B6 [8]	1.44	2.61	1.05	1.32	7.03[b]	0.63	3.82[b]	0.84	16.67[b]	2.47	9.43[b]
C4 [8]	1.61	1.76	1.03	1.30	5.53[b]	0.59	3.07[b]	0.66	13.29	2.36	7.21[b]
C5 [8]	2.22	2.37	1.01	1.33	5.65[b]	0.61	3.12[b]	0.68	13.57[b]	2.42	7.37[b]
C6 [8]	1.65	3.20	0.95	1.38	5.99[b]	0.64	3.36[b]	0.71	14.47[b]	2.53	7.86[b]
G3 [8]	1.91	0.88	1.03	1.29	7.51[b]	0.59	3.86[b]	0.87	17.27	2.33	9.72
G4 [8]	1.55	1.20	1.01	1.34	8.01[b]	0.63	4.22[b]	0.94	18.79	2.49	10.65[b]
G5 [8]	1.78	1.60	1.00	1.32	7.73[b]	0.60	3.99[b]	0.89	17.80	2.39	10.02[b]
G7 [8]	2.38	0.94	0.98	1.38	8.59[b]	0.69	4.75[b]	1.02	20.85	2.66	11.94
G8 [8]	1.96	1.31	0.99	1.36	8.07[b]	0.64	4.25[b]	0.95	18.95	2.52	10.74[b]
I3 [8]	3.09	1.17	1.03	1.54	8.55[b]	0.81	5.45[b]	1.08	23.55	2.97	14.31
I4 [8]	1.67	1.62	0.96	1.68	9.40[b]	0.88	6.00[b]	1.18	25.91	3.24	15.75
I5 [8]	2.32	2.13	0.94	1.71	9.56[b]	0.90	6.11[b]	1.20	26.36	3.30	16.03[b]
I6 [8]	2.19	2.61	1.01	1.64	9.03[b]	0.86	5.73[b]	1.15	24.99	3.17	15.27[b]
J1 [8]	2.19	0.54	0.94	1.33	5.10	0.35	1.97[b]	0.47	9.09	1.76	4.83
J2 [8]	1.98	0.83	0.93	1.37	5.26[b]	0.37	2.05[b]	0.49	9.42	1.82	5.01[b]
J4 [8]	1.66	1.62	0.97	1.35	5.58[b]	0.42	2.33[b]	0.56	10.63[b]	1.92	5.71[b]
K2 [8]	1.54	1.03	0.99	0.78	5.00[b]	0.65	4.96[b]	0.66	13.97	1.51	6.91
K3 [8]	1.73	1.58	0.99	0.83	5.15[b]	0.66	4.98[b]	0.68	14.12	1.56	6.94[b]
K4 [8]	2.21	2.28	1.00	0.76	4.74[b]	0.60	4.56[b]	0.62	12.92[b]	1.42	6.33[b]
N1 [8]	4.29	0.62	1.01	0.74	4.61	0.35	2.40[b]	0.53	10.91	1.41	6.25
N1a [8]	4.21	0.62	0.98	0.76	4.62	0.35	2.37[b]	0.53	10.84	1.41	6.19
N2 [8]	2.10	1.13	0.96	0.79	4.97[b]	0.38	2.62[b]	0.58	11.91	1.52	6.85
N2a [8]	2.71	1.10	0.93	0.79	8.45	0.36	4.92[b]	0.55	17.50	1.46	11.25
N3 [8]	2.71	0.90	1.02	0.75	4.36[b]	0.33	2.17[b]	0.51	10.03	1.36	5.70
N4 [8]	2.26	1.42	0.96	0.77	4.54[b]	0.34	2.26[b]	0.52	10.44	1.40	5.93[b]
VB2 [10]	1.22	0.71	0.94	1.40	4.69[b]	0.29	1.86[b]	0.49	9.82	2.51	6.02
VB3 [10]	1.40	0.71	0.94	1.58	5.71[b]	0.37	2.73[b]	0.64	13.74	3.05	8.92
VB4 [10]	1.45	0.71	0.94	1.78	6.44	0.43	3.15[b]	0.74	16.65	3.44	11.36
VM2 [10]	1.57	0.65	0.96	1.90	6.77	0.44	3.12[b]	0.76	15.85	3.68	10.17
VM3 [10]	2.02	0.65	1.10	2.50	8.56	0.59	3.96[b]	1.02	20.58	4.83	13.53
VQ1 [10]	1.21	0.33	0.99	1.00	3.97	0.29	1.32[b]	0.39	7.09	1.52	4.32
VQ3 [10]	1.18	0.41	0.96	2.31	4.19	0.20	1.35[b]	0.40	7.80	3.38[c]	4.40
VQ9 [10]	1.20	0.45	0.99	3.14[c]	3.46	0.18	1.34[b]	0.37	7.22	4.84[c]	3.82
VS2-VQ2 [10]	1.52	0.37	0.94	1.75	4.98	0.28	1.68[b]	0.48	9.13	2.66	5.43
VS3 [10]	1.08	0.55	0.94	1.75	5.03	0.28	1.72[b]	0.49	9.32	2.70	5.56
VS4-VQ5 [10]	1.15	0.74	0.94	1.75	4.98[b]	0.28	1.68[b]	0.48	9.13	2.66	5.43[b]
VS9 [10]	1.26	0.35	0.94	1.33	3.63	0.20	1.18[b]	0.34	6.44	1.94	3.81
VS10-VB1 [10]	1.14	0.70	0.94	1.33	3.77[b]	0.21	1.27[b]	0.36	6.92	2.02	4.11[b]
A2 [11]	1.96	1.08	0.99	1.28	6.94[b]	0.56	4.04[b]	0.73	18.05	2.48	10.73
A3 [11]	3.17	1.22	1.00	1.41	6.41[b]	0.66	3.77[b]	0.81	17.13	2.71	10.05
A4 [11]	1.46	1.69	1.02	1.41	6.35[b]	0.66	3.71[b]	0.81	16.92	2.72	9.93[b]
B3 [11]	2.03	1.26	0.98	0.97	5.77[b]	0.66	4.86[b]	0.74	16.12	1.88	8.97
B4 [11]	1.87	1.73	1.02	0.98	5.68[b]	0.66	4.73[b]	0.75	15.83	1.89	8.81[b]
B5UR1 [12]	2.82	0.92	0.94	1.03	5.78[b]	0.66	4.86[b]	0.71	16.24	1.99	9.09
B9UR1 [12]	2.10	0.92	0.94	1.42	7.95	0.97	7.16	1.03	25.77	2.73	17.21
B12UR3 [12]	3.14	1.04	1.00	1.42	7.53	0.97	6.56[b]	1.03	24.28	2.74	16.07
B12UR4 [12]	2.81	1.10	1.10	1.47	7.40[b]	1.01	6.29[b]	1.08	23.85	2.84	16.12
B12UR5 [12]	2.51	1.41	0.90	1.45	8.15[b]	0.99	7.35[b]	1.06	26.46	2.81	17.84
H-12–12 [13]	3.40	1.22	0.90	2.35	13.10[b]	1.23	8.51[b]	1.69	39.89	4.54	29.01
H-14–10 [13]	3.80	1.38	0.98	1.80	11.76[b]	0.93	8.09[b]	1.28	35.21	3.47	24.32
N-12–12 [13]	3.11	1.22	0.90	1.58	8.81[b]	0.77	5.12[b]	1.05	22.36	3.05	13.12[b]
N-14–10 [13]	2.27	1.38	0.98	1.26	8.23[b]	0.61	5.00[b]	0.83	20.42	2.43	11.91[b]
NBS-43–44 [14]	4.59	0.44	1.03	1.61	8.85	0.78	5.07[b]	1.07	22.33	3.11	13.08
D3 [8]	1.55	1.17	1.02	1.28	6.09[b]	1.01	4.22[b]	0.81	11.15	2.38	6.90
D4 [8]	1.44	1.62	0.98	1.32	8.34[b]	1.10	6.97[b]	0.88	16.15	2.55	9.81[b]
T1 [9]	1.51	0.75	0.97	2.59	10.55	1.41	8.11[b]	1.46	21.48	5.00	13.32
T2 [9]	2.34	0.71	1.02	2.59	9.33	1.41	6.65[b]	1.46	18.89	4.99	11.78
VH1 [10]	1.21	0.33	0.99	1.25	5.82	0.65	3.10	0.44	8.93	1.80	4.87
VH2 [10]	1.94	0.67	0.99	1.25	11.64	0.65	7.73[b]	0.44	14.23[b]	1.80	9.73[b]
A1 [6]	3.45	0.19	1.05	2.04	8.12[b]	1.18	6.50	1.20	18.22	3.94[c]	12.01
A2 [6]	2.22	0.37	1.00	1.84	8.19	1.15	6.55	1.08	18.27	3.56	11.98
A3 [6]	1.47	0.49	0.96	1.77	8.28[b]	1.13	6.73[b]	1.04	18.33	3.42	11.95
A4 [6]	1.53	0.65	1.03	1.93	8.34[b]	1.20	6.81[b]	1.15	19.30	3.73	13.12
A5 [6]	1.45	0.83	1.11	2.02	8.37[b]	1.25	6.61[b]	1.20	19.19	3.90	12.95[b]
B2 [6]	1.73	0.40	0.99	2.24	10.16	1.46	8.59	1.36	24.58	4.32	18.03
B3 [6]	1.39	0.67	1.00	2.30	10.52[b]	1.53	9.01[b]	1.40	25.73	4.44	19.73
B4 [6]	1.32	0.89	1.09	2.48	11.17[b]	1.70	9.41[b]	1.51	27.32	4.78	21.19
C1 [6]	1.80	0.19	1.04	2.81	11.08	1.67	9.57	1.72	27.13	5.42[c]	22.54

(*continued on next page*)

Table 2 (*continued*)

Beam	$\mu_{\theta,exp}$	ρ_t %	m_b	ACI 318R-14		MC 10		EC 2		CAN3-A23.3–14	
				$\rho_{t,min}$ %	$\rho_{t,max}$ %	$\rho_{t,min}$ %	$\rho_{t,max}$ %	$\rho_{t,min}$ %	$\rho_{t,max}$ %	$\rho_{t,min}$ %	$\rho_{t,max}$ %
C2 [6]	1.55	0.37	1.01	2.61	10.89	1.61	9.51	1.61	26.62	5.04	22.53
C3 [6]	1.19	0.63	1.06	2.50	10.43[b]	1.57	8.92[b]	1.53	25.56	4.82	21.21
C4 [6]	1.21	0.86	1.07	2.65	11.03[b]	1.68	9.40[b]	1.63	27.00	5.12	22.39
C5 [6]	1.20	1.05	1.05	2.73	11.56[b]	1.74	10.03[b]	1.68	28.20	5.26	24.15
C6 [6]	1.30	1.34	1.08	2.41	10.43[b]	1.53	9.00[b]	1.48	25.60	4.65	20.74[b]
C100a [16]	2.31	0.79	1.04	3.17	20.25	2.97	20.39	2.30	49.64	6.12	40.95
D090a [16]	2.81	0.79	1.04	3.44	18.09	2.67	18.58	2.51	43.58	6.63	39.52

[b] Brittle failure due to concrete crushing expected in these beams.
[c] Brittle and premature failure due to insufficient reinforcement expected in these beams.

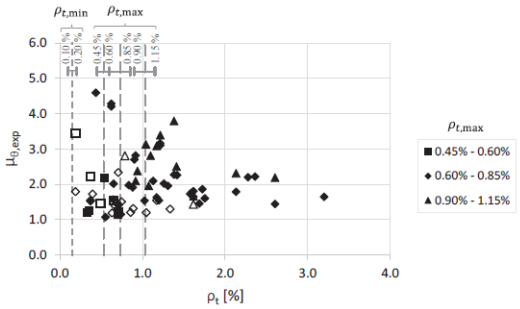

Fig. 7. Transverse reinforcement ratios versus ductility (ACI 318R-14 [17]).

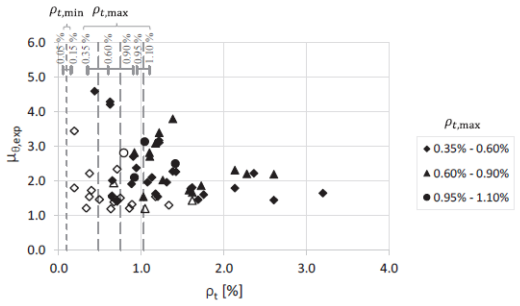

Fig. 8. Transverse reinforcement ratios versus ductility (MC 10 [22]).

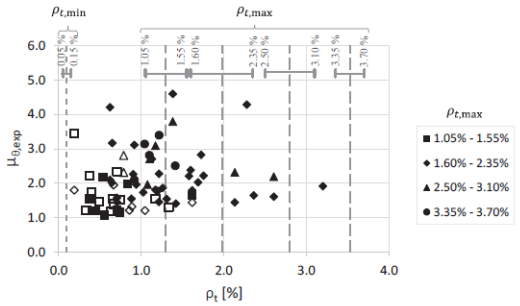

Fig. 9. Transverse reinforcement ratios versus ductility (EC 2 [18]).

computed from the code, but in a small number when compared to ACI 318R-14 and MC 10. When compared with all the other codes, CAN3-A23.3-14 is more restrictive as far as $\rho_{t,min}$ is concerned. Few beams

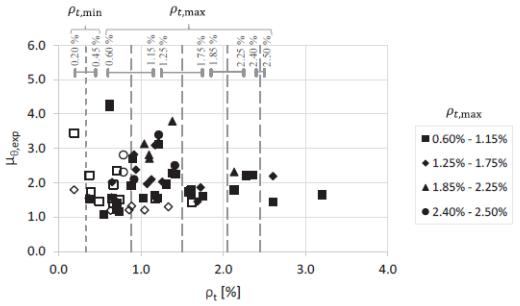

Fig. 10. Transverse reinforcement ratios versus ductility (CAN3-A23.3-14 [23]).

don't comply with $\rho_{t,min}$ computed from the code. However, as referred before, these beams did not show a brittle and premature failure due to insufficient reinforcement.

For the studied codes, it was observed that they all failed to predict brittle failure due to concrete crushing for several reference beams, mainly for ACI 318R-14, MC 10 and CAN3-A23.3-14. This can be explained because some of these beams, mainly beams with higher ρ_t, show a ductile behavior prior to the yielding of the torsional reinforcement. This is probably due to the nonlinear behavior of the compressive concrete before the peak load, due to the initiation of the crushing phenomena (as discussed in Section 4). This phenomenon seems not be properly incorporated by the codes through the upper limit for the torsional reinforcement, in order to avoid brittle failure due to excessive reinforcement. As previously stated, this limit is computed indirectly from the maximum stress allowed for the compressive concrete in the struts. For most of the studied codes, this limit seems to be too conservative because it don't cover the full range of RC beams with torsional ductility.

7. Conclusions

In this article the torsional ductility of RC beams with rectangular cross section was studied. From the results obtained through this study, the following conclusions are drawn:

- The torsional ductility index used in this study proved to be adequate to characterize the torsional ductility of RC beams and to perform comparative analysis between the beams;
- For plain RC beams, torsional ductility increases as the compressive strength increases, while the opposite tendency is observed for hollow RC beams;
- The torsional ductility decreases notably as the total torsional reinforcement ratio increases. This is true until a limit is reached and

from which a residual ductile behavior seems to be observed (which is higher for plain beams). This limit seems to increase as the concrete strength increases and has a value in the range 2.0–3.0% for plain beams and 1.0–1.5% for hollow beams;
- Similar RC beams with plain and hollow cross sections show different level of torsional ductility due to the influence of the concrete core. For a given reinforcement ratio, plain beams are more ductile than hollow beams. Plain beams also show a ductile behavior for a larger range of the torsional reinforcement ratio;
- The total reinforcement ratio shows higher influence on the torsional ductility when compared to the concrete compressive strength;
- For ACI 318R-14, MC 10 and EC2, it was observed that the rule to define the minimum torsional transverse reinforcement for RC beams with approximately balanced reinforcement, in order to avoid brittle and premature failure due to insufficient reinforcement, is adequate. For CAN3-A23.3–14, this limit seems to be slightly excessive;
- ACI 318R-14 and MC 10, as well as CAN3-A23.3–14 although to a less lesser extent, are excessively restrictive with respect to the maximum torsional transverse reinforcement and lead to the unacceptance of RC beams with ductile behavior under torsion. This is mainly true for plain beams, again with approximately balanced reinforcement. From the studied codes, EC 2 is the one that has shown to be the better with regard to the maximum torsional transverse reinforcement. For the other studied codes, the value for the maximum stress allowed for the compressive concrete in the struts seems to be too conservative and should be reviewed.

References

[1] Bernardo LFA, Lopes SMR. Plastic analysis of HSC beams in flexure. Mater Struct 2009;42(1):51–69.
[2] Carmo RNF, Lopes SMR. Ductility and linear analysis with moment redistribution in reinforced high strength concrete beams. Can J Civ Eng 2005;32(1):194–203.
[3] Pecce M, Fabbrocino G. Plastic rotation capacity of beams in normal and high-performance concrete. ACI Struct J 1999;96(2):290–6.
[4] Pang XB, Hsu TTC. Behavior of reinforced concrete membrane elements in shear. ACI Struct J 1995;92(6):665–79.
[5] Zhang LX, Hsu TTC. Behavior and analysis of 100 MPa concrete membrane elements. J Struct Eng 1998;124(1):24–34.
[6] Bernardo LFA, Lopes SMR. Torsion in HSC hollow beams: strength and ductility analysis. ACI Struct J 2009;106(1):39–48.
[7] Lopes SMR, Bernardo LFA. Twist behavior of high-strength concrete hollow beams – formation of plastic hinges along the length. Eng Struct 2009;31(1):138–49.
[8] Hsu TTC. Torsion of structural concrete – behavior of reinforced concrete rectangular members. Torsion of structural concrete, SP-18. American Concrete Institute; 1968. p. 261–306.
[9] Lampert P, Thürlimann B. Essais de Poutre en Béton Armé sous Torsion Simple et Flexion Combinées (Torsionsversuche und Torsions-Biege-Versuche an Stahlbetonbalken). Comitée Européen du Béton, B.I. no 71; 1969. p. 177–207.
[10] Leonhardt F, Schelling G. Torsionsversuche na Stahlbetonbalken. Bulletin No. 239. Deutscher Ausschuss für Stahlbeton; 1974. 122 pp.
[11] McMullen AE, Rangan BV. Pure torsion in rectangular sections – a re-examination. J Am Concrete Inst 1978;75(10):511–9.
[12] Koutchoukali N-E, Belarbi A. Torsion of high-strength reinforced concrete beams and minimum reinforcement requirement. ACI Struct J 2001;98(4):462–9.
[13] Fang IK, Shiau JK. Torsional behavior of normal- and high-strength concrete beams. ACI Struct J 2004;101(3):304–13.
[14] Chiu H-J, Fang I-K, Young W-T, Shiau J-K. Behavior of reinforced concrete beams with minimum torsional reinforcement. Eng Struct 2007;29:2193–205.
[15] Peng X-N, Wong Y-L. Behavior of reinforced concrete walls subjected to monotonic pure torsion – an experimental study. Eng Struct 2011;33:2495–508.
[16] Jeng CH. Unified softened membrane model for torsion in hollow and solid reinforced concrete members modeling the entire pre- and post-cracking behavior. J Struct Eng 2015;141(10).
[17] ACI Committee 318. Building code requirements for reinforced concrete (ACI 318-14) and commentary (ACI 318R-14). Detroit (MI): American Concrete Institute; 2014.
[18] NP EN 1992-1-1. Eurocode 2: design of concrete structures – Part 1: general rules and rules for buildings; 2010.
[19] Bernardo LFA, Andrade JMA, Nunes NCG. Generalized softened variable angle truss-model for reinforcement concrete beams under torsion. Mater Struct 2015;48:2169–93.
[20] Pilakoutas K, Neocleous K, Guadagnini M. Design philosophy issues of fiber reinforced polymer reinforced concrete structures. J Compos Constr 2002;6(3):154–61.
[21] Teixeira MM. Ductility of reinforced concrete beams under torsion. Master thesis. Covilhã (Portugal): Department of Civil Engineering and Architecture, University of Beira Interior; 2015 [in Portuguese].
[22] CEB-FIP MODEL CODE. Suisse: Comité Euro-International du Béton; 2010.
[23] CSA Standard. Design of concrete structures – A23.3-14. Missisauga: Canadian Standards Association; 2014.

Torsional Strength of Reinforced Concrete Beams – Evaluation of some Codes of Practice

M. M. Teixeira[1, *], L.F.A. Bernardo [2]

1. PhD Student, Department of Civil Engineering and Architecture, University of Beira Interior, C-MADE – Centre of Materials and Building Technologies, Covilhã, Portugal
2. Assistant Professor with Aggregation, Department of Civil Engineering and Architecture, University of Beira Interior, C-MADE – Centre of Materials and Building Technologies, Covilhã, Portugal

[*]Corresponding author email: mafalda.m.teixeira@ubi.pt (M.M. Teixeira)

Abstract

In this article, a comparative analysis between experimental results of several reinforced concrete (RC) beams, with rectangular cross section, and the predictions for the torsional strength from some codes of practice is presented. The following codes were analyzed: ACI codes ACI 318R-89 and ACI 318R-14, European codes MC90, MC10 and EC2, and Canadian code CSA A23.3-04.

In the first stage, the chosen beams to be studied are checked in light of the codes of practice. The purpose of this verification was to neglect the beams that don´t meet minimum basic requirements from the codes and, because of this, would show atypical behaviours.

In the second stage, the torsional strength of each beam predicted from the codes of practice are compared with the experimental ones. It is shown that, for some beams´ series and for some codes of practice, high differences still exist between the normative and experimental values of the torsional strength.

Keywords: *reinforced concrete beams, torsional strength, codes.*

1. Introduction

Going back almost a century of investigation, the study of the resistance of concrete structural elements subjects to torsion was developed based on two types of mechanical models: the Space Truss Model (Rausch 1930) and the Skew-Bending Theory (Lessig, Cowan, Elfgren, etc., since 1958).

The Space Truss Model (STM) combined with the classic Bredt's thin tube theory (Bredt 1896) served as the basis to the development of all subsequent models and refinements to predict the plastic behaviour of reinforced concrete (RC) elements subject to torsion. After the fundamental results of Lampert and Thurlimann (1969), Elfgren (1972), Collins (1973), Hsu and Mo (1985a, 1985b), etc., the Variable Angle Truss Model (VATM) become used and dominates European codes (MC 90 1990 e EC 2 2002), American codes (ACI 318R-14 2014) and Canadian code (CSA A23.3-04 2004). Each code introduced some simplifications focused on shear flow midline's position and/or on the effective wall's thickness in a plain or hollow cross section.

The Skew-Bending Theory (SBT), based on a spatial failure surface model, has been satisfactorily proven by many theoretical and experimental studies. The model is directly related to empirical observations and is essentially applicable to elements with small rectangular section. However, because this model is applied to three-dimensional elements, its use is not practical in complex structures. The STM, on the other hand, is applicable to any type of cross section, by decomposing the section into simpler parts (walls), allowing a uniform treatment to several load cases and avoiding some scientific imperfections of the SBT (Muller 1976). The torsion design's guideline of American codes (such as ACI 318R-89 1989) and Russians codes adopted the SBT until 1995, where, from then on, the STM was integrated into American codes.

The national and regulations codes currently have a character of law in some countries and a character of recommendation in other countries. In Europe, some countries are replacing their regulations (e.g.: Model Codes) with European standards (e.g.: Eurocodes). In the United States of America, on the other hand, each state of the union has its own law and the ACI regulations stand out.

The present study's purpose is to verify the reliability of some codes and regulations of practices, which are based on the theoretical models previously mentioned, for the prediction of the torsional moment resistance of RC beams with rectangular (plain and hollow) cross section. For this and from the literature consulted, the information about many experimental tests of RC beams under pure torsion was compiled, namely the experimental ultimate torque observed in laboratory, and compared with the respective value computed with each code under study.

The selected codes for this study were the American codes ACI 318R-89 and ACI 318R-14, the European codes MC90, MC10 and EC2 and the Canadian code CSA A23.3-04. The choice of these documents took into account the type of theoretical model on which their guidelines are based, their character (normative or regulate) in the country in which they are applied and their territorial scope.

2. Codes' equations

The code ACI 318R-89 bases its guidelines on the SBT, while the remaining codes under study base their guidelines on the STM combined with the classic Bredt's thin tube theory.

The ACI 318R-89 code is the only one which has specific guidelines to design the transverse and longitudinal torsion reinforcement. ACI 318R-14 and CSA A23.3-04 codes have specific guidelines to design only transverse torsion reinforcement. On the other hand, European codes and regulations send to specific guidelines for shear reinforcement's design to be used for the design of torsional reinforcement.

This section summarizes and adapts the equations, presented in each codes under study, to compute the torsional moment resistance of RC beams, with rectangular (plain and hollow) cross section, under pure torsion. For all equations presented below, the symbology was adapted (uniformized) to the same and they are identified in the following nomenclature table.

Nomenclature

A_k	area enclosed within centerline of wall's thickness	f_{yt}	average yield strength of transversal reinforcement
A_l	total area of longitudinal reinforcement	p_h	perimeter of the centerline of hoop
A_o	area enclosed within circular shear flow	s	longitudinal spacing between hoops
A_{oh}	area enclosed within centerline of hoops	t	thickness of the hollow section's wall or equivalent
A_t	area for one bar of the hoop	u_k	perimeter of the area A_k
T	torsional moment applied	x	smaller dimension of cross section
T_c	torsional moment resisted by concrete	x_1	shortest distance of closed stirrups
T_R	torsional moment resistance	y	larger dimension of cross section
T_s	torsional moment resisted by torsion's reinforcement	y_1	greater distance of closed stirrups
V	shear strength applied	θ	inclination of diagonal stresses
V_R	shear strength resistance	ρ_l	ratio of longitudinal reinforcement
f_c	average compression strength of concrete	ρ_t	ratio of transverse reinforcement
f_{ck}	characteristic value of the concrete's compression strength after 28 days	ρ_{tot}	ratio of total reinforcement
f_{yl}	average yield strength of longitudinal reinforcement		

2.1. ACI 318R-89 code

For the design of rectangular cross sections of RC beams subjected to pure torsion, the clause 11.6.5 of the code requires that the following safety condition must be verified:

$$T \leq \phi T_R \tag{1}$$

For the present study, the resistance reduction factor ϕ was considered unitary. T_R is given by:

$$T_R = T_c + T_s \tag{2}$$

Combining the equations defined in clauses 11.6.6.1 and 11.6.9.1, to calculate T_c and T_s, respectively, and for plain and hollow cross section's beams with a wall's thickness greater than $x/4$, T_R can be determined through the following equation:

$$T_R = \frac{x^2 y}{3}\left(2{,}4\sqrt{f_c}\right) + \alpha_t \frac{x_1 y_1 A_t f_{yt}}{s} \tag{3}$$

For hollow cross section's beams with a thickness between $x/10$ and $x/4$, the clause 11.6.1.2 requires the application of a reduction factor equal to $4t/x$ appended to T_c, being thus T_R determined by:

$$T_R = \left(\frac{4t}{x}\right)\frac{x^2 y}{3}\left(2{,}4\sqrt{f_c}\right) + \alpha_t \frac{x_1 y_1 A_t f_{yt}}{s} \tag{4}$$

In both equations (3) and (4), the efficiency coefficient α_t is equal to $0{,}66 + 0{,}33(y_1/x_1)$ and equal or less than 1.5.

According to clause 11.6.9.4, for beams whose predicted a theoretical brittle failure, T_R should be calculated for the maximum limit stress allowed for concrete under compression, a stress equal to $4T_c$. Thus, for this beams, in equation (2), T_s is equal to $4T_c$.

2.2. ACI 318R-14 code

As for the previous code, for the design of rectangular cross sections of RC beams subjected to pure torsion, the clause R22.7.6 of the code requires that the safety condition presented in equation (1) must be verified. However, when calculating T_R, the code assumes that this must be checked only by the torsional reinforcement, neglecting any contribution from the concrete ($T_c = 0$). Thus, the clause 22.7.6.1 defines that T_R is the smallest value from equation (5) and (6):

$$T_R = \frac{2A_o A_t f_{yt}}{s}\cot\theta \tag{5}$$

$$T_R = \frac{2A_o A_l f_{yl}}{p_h}\cot\theta \tag{6}$$

Where A_o is equal to $0{,}85A_{oh}$ (defined by the clause 22.7.6.1.1) and the angle θ (being through 30º and 60º) is calculated by combining equation (5) with the calculation of the longitudinal resistant force due to torsion, N, obtained by $V\cot\theta$ (defined by the clause 22.7.6.1):

$$cot^2\theta = \frac{A_l f_{yl} s}{A_t f_{yt} p_h} \tag{7}$$

The clause 22.7.7.1 determines that, for rectangular beams for which it is expected a theoretical brittle failure, T should be calculated for the maximum limit stress allowed for concrete under compression, where this stress is given by the following relation:

$$\frac{T p_h}{1{,}7A_{oh}^2} \leq \phi 8\sqrt{f_c} \tag{8}$$

For the present study, the resistance reduction factor ϕ was considered unitary.

In the case of beams with hollow cross sections, the clause 22.7.7.1.2 defines that, if the wall thickness, t, is less than A_{oh}/p_h, then the first term of equation (8) should be replaced by $T/(1{,}7A_{oh}t)$.

2.3. MC90 code

According to the clause 6.3.5.2 of the code, for rectangular beams subjected to pure torsion, the calculation of T_R is obtained by the circular shear force applied on an equivalent tubular section. This shear force is given by the following equation:

$$V_R = \frac{T_R u_k}{2A_k \delta} \tag{9}$$

Where the correction coefficient, δ, is given by $1{,}0 - 0{,}25(x/y)$.

The verification condition imposed by this code to determine T_R is the lowest value of the torsional moment resistance conferred by the longitudinal force, F_{Sdi}, by the resistant compression force applied on the concrete struts, F_{Rcwi}, and by the shear force resistance applied on the transverse reinforcement, F_{Rtwi}. The shear strength given by the referred forces are calculated by the following equations:

$$V_{Sdi} = \left(A_l f_{yl}\right)/\cot\theta \tag{10}$$

$$V_{Rcwi} = f_{cd2} t u_k \cos\theta \sin\theta \tag{11}$$

where f_{cd2} is the average value of the compressive strength of cracked concrete, given by $0{,}60(1 - f_{ck}/250)\, f_c$ (determined by the clause 6.2.2.2);

$$V_{Rtwi} = A_t f_{yt} \cot\theta \frac{u_k}{s} \tag{12}$$

In equations (10), (11) and (12), θ can be calculated by combining equations (10) and (12), with the following expression:

$$tan^2\theta = \frac{A_t f_{yt} u_k}{A_l f_{yl} s} \tag{13}$$

Note that, when determining the minimum value of the resistances obtained from F_{Sdi}, F_{Rcwi} and F_{Rtwi}, the theoretical separation between beams with ductile failure and with brittle failure is implicit.

2.4. MC10 code

As for the MC90 code, the clause 7.3.4.1 of the MC10 code determines that for rectangular beams subjected to pure torsion, the calculation of T_R is obtained by the circular shear force applied on an equivalent tubular section. This shear force is now given by the following equation:

$$V_R = \frac{T_R}{2A_k} u_k \tag{14}$$

In this code, the correction coefficient, δ is taken from the original expression (9).

The code distinguishes three levels of approximation for the calculating model of the shear strength resistance resulting from the torsional moment, V_R. The level II approximation is based on the variable angle stress model, applicable to elements composed of a minimum stirrup reinforcement. At this level of approach, the shear resistance conferred by the concrete is neglected. Thus, the clause 7.3.3.3 determines that V_R. is equal to the shear stress balanced by the shear reinforcement in the yield stress, $V_{Rd,s}$, given by the following equation:

$$V_{Rd,s} = \frac{A_t}{s} u_k f_{yt} (\cot\theta + \cot\alpha) \sin\alpha \tag{15}$$

Where α is the angle between the stirrups and the element's horizontal axis.

The clause determines that the shear strength resistance in an equivalent tubular section must be less than the maximum shear allowed by the code, $V_{Rd,máx}$, determined by:

$$V_{Rd,máx} = k_c \frac{f_{ck}}{\gamma_c} t u_k \frac{\cot\theta - \cot\alpha}{1 + cot^2\theta} \tag{16}$$

For the level II approximation of the model, the concrete reduction factor k_c is equal to $0.55(30/f_{ck})^{1/3}$ and less than 0.55. The cracked concrete partial safety factor γ_c is equal to 1.5.

In equations (15) and (16), θ can be deduced by the combination of equation (15) and the calculation of the additional longitudinal force due to the torsion, F_{td}, obtained by $(V/2)(\cot\theta - \cot\alpha)$. Thus, for the calculation of T_R, θ is determinate by:

$$cot^2\theta = \frac{2A_l f_{yl} s}{A_t f_{yt} u_k} \tag{17}$$

2.5. EC2 code

To ensure that an element subject to pure torsion doesn't suffer a brittle failure due to the compression of the concrete struts, the clause 6.3.2 (4) requires that the following condition must be verified:

$$T/T_{Rd,máx} \leq 1{,}0 \tag{18}$$

The maximum torsional moment allowed by the code, $T_{Rd,máx}$, is determined by:

$$T_{Rd,máx} = 2\nu\alpha_{cw} f_c A_k t \sin\theta \cos\theta \tag{19}$$

Where the coefficient of reduction of the cracked concrete strength ν is obtained by $0{,}6[1 - (f_{ck}/250)]$ (defined in the clause 6.2.2. (6)); and for non-prestressed structures, the coefficient α_{cw} is unitary.

As the previous European codes and according to the clause 6.3.2 (1), T can be obtained through the shear force applied on an equivalent tubular section, through the following equation:

$$V = \frac{T}{2A_k} u_k \tag{20}$$

Thus, according to the clause 6.2.3 (3) and for RC beams with vertical stirrups and rectangular cross section, V_R is given by:

$$V_R = \frac{A_t}{s} u_k f_{yt} \cot\theta \tag{21}$$

The value of θ can be deduced combining equation (21) with the calculation of the longitudinal torsional reinforcement's cross section area (determinate by the clauses 6.3.2 (3)). Thus, θ is calculated by:

$$tan^2\theta = \frac{A_t f_{yt} u_k}{A_l f_{yl} s} \tag{22}$$

Note that, when determining the minimum value between T and $T_{Rd,máx}$, the theoretical separation between beams with ductile failure and with brittle failure is implicit.

2.6. CSA A23.3-04 code

The clause 11.3.10.2 of the code determinate that, in the design of rectangular cross sections beams under pure torsion, the following safety condition must be respected:

$$T \leq T_R \tag{23}$$

According to the clause 11.3.10.3, T_R is calculated using the following equation:

$$T_R = 2A_o \frac{\phi_s A_t f_{yt}}{s} \cot\theta \tag{24}$$

Where A_o is equal to $0{,}85A_{oh}$ and, for the present study, the reinforcement resistance factor ϕ_s was considered unitary.

Through equation (24) and the calculation of the force developed in the longitudinal reinforcement in beams subjected to pure torsion (determined by the clause 11.3.9.2, combined with the clause 11.3.10.6), it is possible to determinate the value of θ, through the following equation:

$$tan^2\theta = \frac{0{,}45 p_h \phi_s A_t f_{yt}}{A_l f_{yl} s} \tag{25}$$

For rectangular beams for which a theoretical brittle failure is expected, the clause 11.3.10.4 determines that T should be calculated for the maximum limit stress allowed for concrete under compression, given by the following relation:

$$\frac{T p_h}{1{,}7A_{oh}^2} \leq 0{,}25\phi_c f_c \tag{26}$$

For the present study, the concrete strength factor ϕ_c was considered unitary.

For hollow cross section beams with a thickness' wall less than A_{oh}/p_h, the term on the left side of equation (26) should be replaced by $T/(1{,}7A_{oh}t)$.

3. Reference beams

From the literature consulted, a total of 116 pure torsion teste results on RC beams with rectangular cross section (plain and hollow section) were compiled. These beams were collected from the following studies: Hsu (1968), Lampert and Thurlimann (1969), Leonhardt and Schelling (1974), McMullen and Rangan (1978), Rasmussen and Baker (1995), Koutchkali and Belarbi (2001), Fang and Shiau (2004), Chiu et al. (2007), Bernardo and Lopes (2009), Peng and Wong (2011) and Jeng (2014).

The beam selection criteria for the present study took into account the record of the experimental curve Torsion (T) - Rotation (θ_T) until the ultimate torque, the observation of a typical behaviour of beams under torsion (Hsu 1968) and the minimum design requirements stipulated by the ACI 318R-14 code (chosen code because it constitutes one of the codes in use with a greater number of specific rules for torsion). A detailed discussion on such applied criteria can be found in Teixeira and Bernardo (2018).

Table A1 in Appendix A presents the main characteristics of the reference beams (geometric and material properties), necessary for the calculation of T_R according to the codes' guidelines.

4. Results

Table A1 in Appendix A presents also the values of the ultimate torque recorded by the authors in the many tests performed, $T_{R,exp}$, and the ration between $T_{R,exp}$ and the theoretical value of the torsional moment resistance calculated according to the codes' guidelines presented in section 2, $T_{R,th}$.

Table 1 summarizes and compares the values presented in Table A1, showing their average value, $\bar{x}$, and their coefficient of variation, cv (where $cv(\%) = 100(s/\bar{x})$, with s being the sample standard deviation). Table 1 also presents separately the results for plain (P) and hollow (H) beams.

Figure 1 presents, for each code under study, scatter graphs showing the experimental versus theoretical values for the ultimate torque. In the graphs, different markers were used to distinguish the results regarding the cross-section type, namely "■" for RC plain beams and "□" for RC hollow beams. These graphs allow to view the results described in Tables 1.

Table 1 – Comparative analyses.

Cross section		P	H	P+H
		$T_{R,exp}/T_{R,th}$	$T_{R,exp}/T_{R,th}$	$T_{R,exp}/T_{R,th}$
ACI 318R-89 [13]	$\bar{x}=$	1.18	1.26	1.19
	$cv(\%)=$	19%	22%	20%
ACI 318R-14 [10]	$\bar{x}=$	1.45	1.43	1.45
	$cv(\%)=$	27%	15%	25%
MC 90 [8]	$\bar{x}=$	1.21	1.34	1.24
	$cv(\%)=$	23%	23%	23%
MC 10 [14]	$\bar{x}=$	1.61	1.09	1.50
	$cv(\%)=$	39%	33%	41%
EC2 [9]	$\bar{x}=$	1.03	1.03	1.03
	$cv(\%)=$	24%	24%	24%
CSA 23.3-04 [11]	$\bar{x}=$	0.93	1.05	0.95
	$cv(\%)=$	27%	29%	28%

5. Comparative analysis

All the observations and conclusions described below should be considered with some reservation, as the dispersion of results, translated by the percentage of cv, is higher than the consensual maximum reference limit usually accepted by the scientific community (maximum $cv = 10\%$).
Table 1 shows that ACI 318R-89 is the code that better predicts the T_R of RC beams with plain cross section ($cv = 19\%$) and the ACI 318R-14 code is the best predictor of the T_R of RC beams with hollow cross section ($cv = 15\%$)). Both show an average $T_{R,exp}/T_{R,th}^{i}$ ratio greater than the unit ($\bar{x}_{ACI89} = 1.19$ and $\bar{x}_{ACI14} = 1.45$), which means that the design of the beams under the American codes' guidelines is done on the safety side. This conclusion can be confirmed in Figure 1. The influence of f_c and ρ_{tot} in the prediction of the T_R is well known. American codes tend to underestimate beams with normal resistance ($f_c \leq 50MPa$) and get closer to the $T_{R,exp}$ as f_c increases, regardless of the type of section. The influence of the ρ_{tot} in the prediction of the T_R is verified for each type of section. For beams with plain section, the ACI 318R-89 code tends to underestimate the T_R of the beams as the ρ_{tot} increases, while for beams with hollow section the influence of the ρ_{tot} is the opposite. For both types of section, the ACI 318R-14 code tends to underestimate the T_R as the ρ_{tot} increases. Note that these two codes are based on different mechanical models (matter discussed in section 2).

In general, the European regulations MC90 and MC10 are on the safety side ($\bar{x}_{MC90} = 1.24$ and $\bar{x}_{MC10} = 1.49$), with MC10 being the code that most deviates from the $T_{R,exp}$ of the beams (with $cv = 41\%$). According to the results, the influence of f_c and ρ_{tot} in the prediction of the T_R calculated by these European regulations is different. For the MC90 code, the ρ_{tot} has much more influence on T_R than the f_c. The code tends to underestimate the T_R for beams with low ρ_{tot}, approaching to the $T_{R,exp}$ as the ρ_{tot} increases (in particular for beams with plain cross section). The influence of f_c in the prediction of the T_R calculated by the MC10 is more evident than the ρ_{tot}. The MC10 tends to underestimate T_R for beams with normal strength concrete, approaching to the $T_{R,exp}$ as the f_c increases, however, overestimating the T_R of beams made of high-strength concrete ($f_c > 50MPa$), particularly for beams with hollow cross section. Although these two regulatory standards are based on the same mechanical model, the observations described are related to the T_R limitation defined to each regulation. The MC90 limits the T_R by the lowest value of the resistance provided by the longitudinal and the transverse reinforcement and by the strength of the concrete. The MC10, on the other hand, limits the T_R only by the strength of the concrete.

According to Table 1, EC2 shows to be the code that most closely matches with the $T_{R,exp}$ of the tested beams ($\bar{x}_{EC2} = 1.03$) without variation in the dispersion of the results by section ($cv = 24\%$). On the other hand, CSA A23.3-04 is the code that presents the worst results, one can conclude that the design of beams by the guidelines of this code is not done on the safety side ($\bar{x}_{CSA} < 1.00$), particularly the design of plain cross section beams ($\bar{x}_{CSA} = 0.93$). Although the method to design cross section beams under torsion is different in each code, the influence of the material characteristics in the prediction to the T_R is similar. Both EC2 and CSA A23.3-04 code underestimate the T_R of beams with low ρ_{tot} and

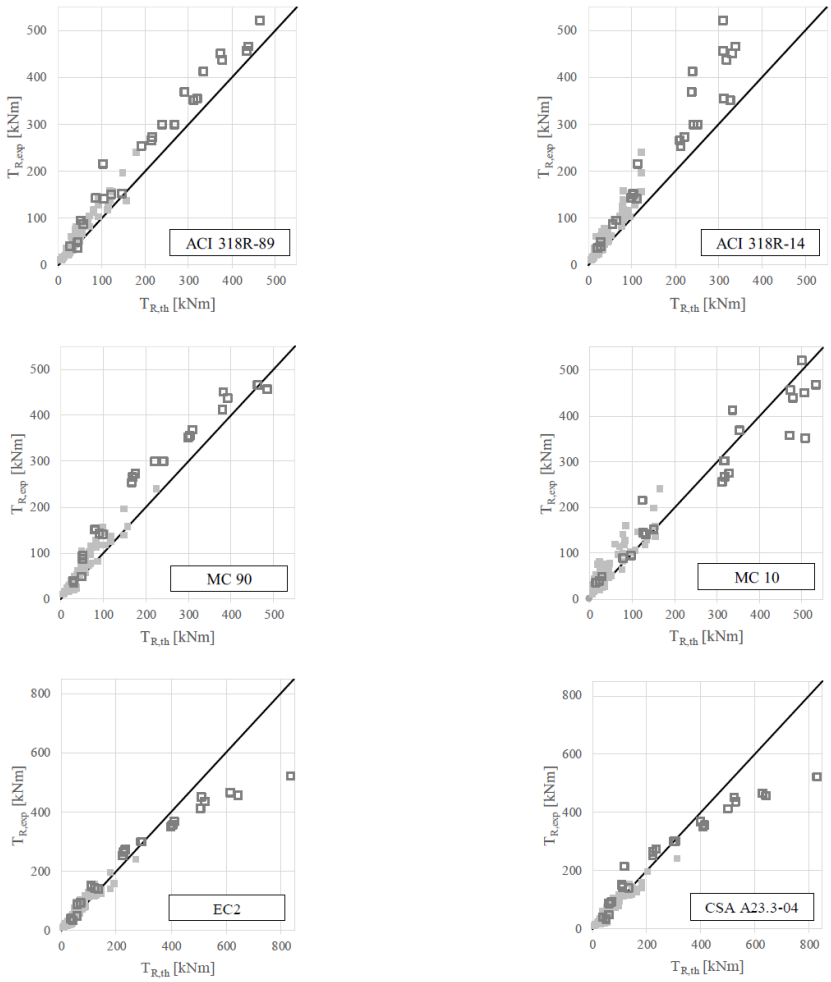

Figure 1 – Experimental versus theoretical ultimate torque.

overestimate T_R as the ρ_{tot} increases. However, the influence of the f_c is not as clear as the influence of the ρ_{tot}, due to the dispersion of the results.

6. Conclusions

In this paper, a comparative analysis was presented between the values of the ultimate torque of RC beams with rectangular cross section (plain and hollow) tested under pure torsion and the values of the normative torsional moment resistance calculated according to the some codes. From the obtained results, it is possible to conclude the following:

- The type of the beams' section, as well as f_c and ρ_{tot} have direct influence on the prediction of the beams' resistance capacity to pure torsion and, consequently, on their designs;

- The American codes tend to overestimate the T_R of plain cross section beams with low ρ_{tot}, assuming a theoretical brittle failure due to insufficient reinforcement. The limit of the minimum torsion reinforcement stipulated by these codes needs to be revised;

- The MC90 code tends to overestimate the T_R of beams with high and/or unbalanced ρ_{tot}, regardless of the type of section or f_c. These beams foresee a theoretical brittle failure due to compression strength in concrete struts or insufficient longitudinal reinforcement (in the case of the Rasmussen and Baker

beams (1995)). For this, it is necessary to review the reinforcement maximum limit, in order to avoid high stresses in the concrete struts and to review the minimum limit of longitudinal reinforcement, to guarantee the resistance of the beams to the additional longitudinal force caused by the torsional moment;

- The MC10 code tends to overestimate the T_R of beams with high-strength concrete, regardless of the type of section. The stress limit on the concrete struts should be revised to avoid brittle failure by compression in the concrete struts;

- The EC2 and CSA A23.3-04 codes tend to overestimate the T_R of beams with high ρ_{tot}, regardless of the type of section or f_c. The stress limit on the concrete struts must be revised to avoid brittle failure by compression in the concrete struts;

- In general, in the design of rectangular RC beams subject to pure torsion, the code that proved to be more on the safety side was the American code ACI 318R-14, while the code that demonstrated to be less on the security side was the Canadian code CSA A23.3-04. The code that showed to be closer to the real behaviour of the beams and on the safety side was the code ACI 318R-89, while the code EC2 showed average results very close to the unit.

This studied showed in particular that the EC2 stress limit values need to be revised to estimate better the torsional strength of RC beams. Additional studies on this subject are still need in order to refine the EC2 formulation.

References

ACI Committee 318, Building code Requirements for Reinforced concrete, (ACI 318-89) and Commentary (ACI 318R-89), American concrete Institute, Detroit, MI, 1989.

ACI Committee 318, Building code Requirements for Reinforced concrete, (ACI 318-14) and Commentary (ACI 318R-14), American concrete Institute, Detroit, MI, 2014.

Bernardo, L.F.A. and Lopes, S.M.R. (2009). Torsion in HSC Hollow Beams: Strength and Ductility Analysis. ACI Structural Journal, 106(1): 39-48.

Bredt, R. (1896). Kritische Bemerkungen zur Drehungselastizitat (Critical remarks on torsional elasticity). Zeitschrift des Vereines Deutscher Ingenieure. Band 40, No. 28, pp. 785-790; No. 29, pp. 813-817 (in German).

CEB-FIP MODEL CODE 1990, Comité euro-International du Béton, Suisse, 1990.

CEB-FIP MODEL CODE 2010, Comité Euro-International du Béton, Suisse, 2010.

CEN prEN 1992-1-1, "Eurocode 2: Design of concrete structures – Part 1: general Rules and Rules for Buildings", April 2002.

Chiu H-J., Fang I-K., Young W-T. and Shiau J-K. (2007). Behaviour of reinforced concrete beams with minimum torsional reinforcement. Engineering Structures, vol. 29, pp. 2193-2205, Taiwan.

Collins, M. P. (1973). Torque-Twist Characteristics of Reinforced Concrete Beams. Inelasticity and Non-Linearity in Structural Concrete, Study No. 8, pp. 211-232, University of Waterloo Press, Waterloo, Ontario, Canada.

CSA Standard, design of concrete structures (A23.3-04), Canadian Standards Association, Mississauga, 2004.

Elfgren, L. (2004). Reinforced Concrete Beams Loaded in Combined Torsion, Bending and Shear. Publication 71:3, Division of Concrete Structures, 1972, 249 pp, Chalmers University of Technology, Goteborg, Sweden.

Fang, I.K. and Shiau, J.K. (2004). Torsional Behaviour of Normal – and High-Strength Concrete Beams. ACI Structural Journal, 101(3), pp. 304-313.

Hsu, T.T.C. (1968). Torsion of Structural Concrete – Behaviour of Reinforced Concrete Rectangular Members. Torsion of Structural Concrete, SP-18, pp. 261-306, American Concrete Institute, Detroit.

Hsu, T.T.C. and Mo, Y.L. (1985a). Softening of Concrete in Torsional Members – Theory and Tests. Journal of the American Concrete Institute, Proc., Vol. 82, No. 3, pp. 290-303.

Hsu, T.T.C. and Mo, Y.L. (1985b). Softening of Concrete in Torsional Members – Design recommendations. Journal of the American Concrete Institute, Proc., Vol. 82, No. 4, pp. 443-452.

Jeng, C.H. (2014). Unified Softened Membrane Model for Torsion in Hollow and Solid reinforced concrete Members Modeling the Entire Pre- and Post- cracking Behaviour. Journal of Structural Engineering.

Lampert, P. und Thurlimann, B. (1969a). Torsionsversuche an Stahlbetonbalken (Torsion Test of reinforced Concrete Beams). Bericht, Nr. 6506-2, Institut fur Baustatik, ETH, Zurich, 101 pp. (in German).

Lampert, P., and Thurlimann, B. (1969b). Essais de Poutre en Béton Armé sous Torsion Simple et Flexion Combinées (Test on Reinforced Concrete Beam Under Pure Torsion and Combined Bending). TestsComitée Européen du Béton, B.I. nº 71, pp 177-207 (in French).

Leonhardt, Fritz, and Schelling, Günther (1974). Torsionsversuche an Stahlbetonbalken (Torsion Tests on Reinforced Concrete Beams). Bulletin No. 239, Deutscher Ausschuss für Stahlbeton, Berlin, 122 pp (in German).

Koutchoukali N-E. and Belarbi A. (2001). Torsion of High-Strength Reinforced Concrete Beams and Minimum Reinforcement Requirement. ACI Structural Journal, 98(4): 462-9.

McMullen, A. E. and Rangan, B. V. (1978). Pure Torsion in Rectangular Sections – A Re-Examination. Journal of the American Concrete Institute, 75(10), pp. 511-519.

Muller, P. (1976). Failure Mechanisms for Reinforced Concrete Beams in Torsion and Bending. Publication No. 36-II, IABSE.

Peng X-N. and Wong Y-L. (2011). Behaviour of reinforced concrete walls subjected to monotonic pure torsion-An experimental study. Engineering Structures, vol. 33, pp. 2495-2508, China.

Rasmussen LJ and Baker G. (1995). Torsion in reinforced normal and high-strength concrete beams – Part 1: Experimental test series. ACI Struct J;92(1):56–62.

Rausch, E. (1929). Berechnung des Eisenbetons gegen Verdrehung (Design of Reinforcerd Concrete in torsion). Ph.D. thesis. Berlin, 53 pp. (in German).

Teixeira, M.M. and Bernardo, L.F.A (2018). Ductility of RC Beams under Torsion. Engineering Structures, 168: 759–769.

Appendix A: Table A1 – Properties of reference beams and ratio between the experimental and theoretical ultimate torque.

Beam	*	x	y	t	x_1	y_1	A_t/s	A_l	ρ_t	ρ_l	f_{yt}	f_{yl}	f_c	$T_{R,exp}$	$T_{R,exp}/T_{R,th}$					
		cm	cm	cm	cm	cm	cm²/m	cm²	%	%	MPa	MPa	MPa	kNm	ACI89	ACI14	MC90	MC10	EC22	CSA04
B3 [15]	Plain	25.4	38.1	-	21.6	34.3	10.16	11.36	1.17	1.17	320	328	28.1	20.1	0.99	1.28	1.16	1.38	0.97	0.85
B4 [15]	Plain	25.4	38.1	-	21.6	34.3	14.01	15.48	1.62	1.60	323	320	29.2	21.9	1.07	1.58	1.09	1.62	0.91	0.80
B5 [15]	Plain	25.4	38.1	-	21.6	34.3	18.47	20.39	2.13	2.11	321	332	30.6	22.6	1.24	1.83	0.98	1.79	0.82	0.88
B6 [15]	Plain	25.4	38.1	-	21.6	34.3	22.58	25.81	2.61	2.67	323	332	28.8	25.0	1.41	2.07	1.12	2.12	0.93	1.03
C4 [15]	Plain	25.4	25.4	-	21.6	21.6	13.11	11.36	1.76	1.76	328	337	27.2	11.9	0.97	1.71	1.04	1.66	0.78	0.87
C5 [15]	Plain	25.4	25.4	-	21.6	21.6	17.67	15.48	2.37	2.40	329	328	27.2	14.0	1.04	2.00	1.10	1.93	0.83	1.02
C6 [15]	Plain	25.4	25.4	-	21.6	21.6	23.91	20.39	3.20	3.16	328	316	27.6	13.9	1.20	2.29	1.25	2.17	0.93	1.16
G3 [15]	Plain	25.4	50.8	-	21.6	47.0	8.29	11.36	0.88	0.88	328	339	26.8	27.1	0.98	1.13	1.31	1.37	1.15	0.97
G4 [15]	Plain	25.4	50.8	-	21.6	47.0	11.29	15.48	1.20	1.20	321	326	28.3	28.7	1.12	1.44	1.31	1.64	1.14	0.97
G5 [15]	Plain	25.4	50.8	-	21.6	47.0	15.05	20.39	1.60	1.58	328	331	26.9	29.5	1.27	1.64	1.08	1.92	0.94	0.84
G7 [15]	Plain	25.4	50.8	-	21.6	47.0	8.84	12.00	0.94	0.93	323	319	31.0	33.6	1.02	1.12	1.39	1.22	1.22	1.03
G8 [15]	Plain	25.4	50.8	-	21.6	47.0	12.32	17.03	1.31	1.32	329	322	28.3	33.6	1.27	1.63	1.37	1.89	1.19	1.01
I3 [15]	Plain	25.4	38.1	-	21.6	34.3	10.16	11.36	1.17	1.17	334	343	44.8	25.5	1.10	1.23	1.35	0.98	1.12	0.99
I4 [15]	Plain	25.4	38.1	-	21.6	34.3	14.01	15.48	1.62	1.60	326	315	45.0	28.0	1.17	1.56	1.36	1.22	1.13	1.00
I5 [15]	Plain	25.4	38.1	-	21.6	34.3	18.47	20.39	2.13	2.11	326	310	45.0	28.1	1.29	1.90	1.28	1.47	1.06	0.94
I6 [15]	Plain	25.4	38.1	-	21.6	34.3	22.58	25.81	2.61	2.67	329	326	45.8	27.5	1.39	2.04	1.08	1.57	0.90	0.80
J2 [15]	Plain	25.4	38.1	-	21.6	34.3	7.21	8.00	0.83	0.83	341	320	14.6	17.1	1.10	1.38	1.30	3.40	1.09	0.96
J3 [15]	Plain	25.4	38.1	-	21.6	34.3	10.16	11.36	1.17	1.17	337	389	16.9	16.9	1.05	1.55	1.05	2.92	0.87	1.00
J4 [15]	Plain	25.4	38.1	-	21.6	34.3	14.01	15.48	1.62	1.60	332	324	16.8	18.0	1.22	1.79	1.22	3.37	1.02	1.16
K2 [15]	Plain	15.2	49.5	-	11.4	45.7	6.77	7.74	1.03	1.03	338	336	30.6	12.2	1.12	1.59	1.35	1.27	1.25	1.11
K3 [15]	Plain	15.2	49.5	-	11.4	45.7	10.42	12.00	1.58	1.59	321	316	29.0	12.4	1.38	1.96	1.20	1.63	1.11	0.97
K4 [15]	Plain	15.2	49.5	-	11.4	45.7	15.05	17.03	2.28	2.26	340	344	28.6	13.1	1.71	2.42	0.99	2.04	0.91	1.20
M2 [15]	Plain	25.4	38.1	-	21.6	34.3	6.77	11.36	0.78	1.17	357	329	30.6	20.6	1.42	1.32	1.53	1.48	1.27	1.12
M3 [15]	Plain	25.4	38.1	-	21.6	34.3	9.24	15.48	1.07	1.60	326	322	26.8	20.7	1.27	1.53	1.24	1.87	1.03	0.91
M4 [15]	Plain	25.4	38.1	-	21.6	34.3	12.33	20.39	1.42	2.11	327	319	26.6	20.7	1.18	1.74	1.07	2.11	0.89	0.90
M5 [15]	Plain	25.4	38.1	-	21.6	34.3	15.63	25.81	1.81	2.67	331	335	28.0	21.7	1.29	1.90	1.07	2.18	0.89	0.95
M6 [15]	Plain	25.4	38.1	-	21.6	34.3	15.63	30.58	1.81	3.16	341	318	29.4	22.7	1.36	2.00	1.15	2.33	0.96	0.98
N1 [15]	Plain	15.2	30.5	-	13.0	28.3	3.50	2.84	0.62	0.61	341	352	29.5	7.6	1.03	1.21	1.53	1.06	1.34	1.13
N1a [15]	Plain	15.2	30.5	-	13.0	28.3	3.50	2.84	0.62	0.61	345	346	28.7	7.0	1.04	1.22	1.54	1.09	1.34	1.13
N2 [15]	Plain	15.2	30.5	-	13.0	28.3	6.35	5.16	1.13	1.11	338	331	30.4	7.4	1.11	1.41	1.42	1.57	1.25	1.05
N3 [15]	Plain	15.2	30.5	-	13.0	28.3	5.08	4.26	0.90	0.92	352	352	27.3	7.4	1.06	1.26	1.39	1.60	1.22	1.03
N4 [15]	Plain	15.2	30.5	-	13.0	28.3	7.98	6.58	1.42	1.42	356	341	27.3	7.6	1.28	1.62	1.19	1.92	1.04	0.87
VB2 [17]	Plain	44.0	24.0	-	42.0	22.0	5.84	7.01	0.71	0.66	541	541	26.4	26.4	0.97	1.09	1.23	1.71	1.06	0.83
VB4 [17]	Plain	44.0	24.0	-	42.0	22.0	5.84	7.01	0.71	0.66	541	541	49.8	49.8	0.98	1.08	1.41	0.97	1.22	0.96
VM1 [17]	Plain	29.4	16.0	-	28.0	14.6	3.63	3.00	0.66	0.64	442	442	39.1	39.1	1.20	1.30	1.76	1.14	1.52	1.20
VM2 [17]	Plain	44.0	24.0	-	42.0	22.0	5.32	6.60	0.65	0.63	432	432	36.1	36.1	1.04	1.14	1.54	1.05	1.33	1.05
VM3 [17]	Plain	58.7	32.0	-	56.1	29.4	7.14	12.84	0.65	0.68	461	461	40.0	40.0	1.06	1.06	1.49	1.03	1.29	1.01
VQ1 [17]	Plain	32.4	32.4	-	30.4	30.4	2.88	3.46	0.33	0.33	557	557	19.0	19.0	0.86	0.85	1.34	1.72	1.00	0.80
VQ3 [17]	Plain	58.0	18.6	-	56.0	16.6	3.05	4.27	0.41	0.40	433	433	17.6	17.6	0.83	1.01	1.32	1.47	1.21	0.93
VQ9 [17]	Plain	80.6	14.0	-	78.6	12.0	2.82	5.08	0.45	0.45	441	441	19.5	19.5	0.98	1.11	1.47	2.04	1.41	1.04
VS3 [17]	Plain	44.0	24.0	-	42.0	22.0	4.55	5.49	0.55	0.52	433	433	19.5	19.5	0.92	1.01	1.33	1.85	1.15	0.90
VS4-VQ5 [17]	Plain	44.0	24.0	-	42.0	22.0	6.10	7.32	0.74	0.69	433	433	19.0	19.0	0.94	1.05	1.20	2.33	1.03	0.81
VS9 [17]	Plain	44.0	24.0	-	42.0	22.0	2.90	3.48	0.35	0.33	571	571	17.6	17.6	0.80	0.91	1.20	1.67	1.04	0.81
VS10-VB1[17]	Plain	44.0	24.0	-	42.0	22.0	5.80	6.96	0.70	0.66	571	571	19.0	19.0	0.91	1.01	0.93	2.26	0.80	0.63
VU2 [17]	Plain	44.0	24.0	-	42.0	22.0	5.60	5.04	0.68	0.48	441	441	19.5	19.5	0.82	1.33	1.31	1.89	1.13	0.88
VU3 [17]	Plain	44.0	24.0	-	42.0	22.0	4.18	6.72	0.51	0.64	441	441	18.5	18.5	1.06	0.96	1.34	2.34	1.16	0.91
A2 [18]	Plain	25.4	25.4	-	22.2	22.2	7.82	5.16	1.08	0.80	285	380	38.2	11.3	1.06	1.42	1.50	1.00	1.12	1.00
A3 [18]	Plain	25.4	25.4	-	21.9	21.9	8.94	8.00	1.22	1.24	360	352	39.4	12.2	1.27	1.49	1.49	1.18	1.12	1.01
A4 [18]	Plain	25.4	25.4	-	21.9	21.9	12.42	11.36	1.69	1.76	360	351	39.2	12.5	1.25	1.85	1.32	1.45	0.99	0.90
B3 [18]	Plain	17.8	35.6	-	14.3	32.1	8.60	8.00	1.26	1.27	360	352	38.6	8.8	1.09	1.59	1.29	1.18	1.13	1.01
B4 [18]	Plain	17.8	35.6	-	14.3	32.1	11.76	11.36	1.73	1.80	360	351	38.5	10.2	1.37	2.00	1.20	1.47	1.05	0.92
B30.1 [19]	Plain	16.0	27.5	-	14.0	25.5	8.78	15.27	0.03	1.57	665	620	41.7	41.7	1.10	1.29	0.80	1.57	0.68	0.53
B30.2 [19]	Plain	16.0	27.5	-	14.0	25.5	8.78	15.27	0.03	1.57	669	638	38.2	38.2	1.06	1.25	0.79	1.56	0.68	0.54
B30.3 [19]	Plain	16.0	27.5	-	14.0	25.5	8.78	15.27	0.03	1.57	672	605	36.3	36.3	1.08	1.28	0.81	1.63	0.69	0.56
B50.1 [19]	Plain	16.0	27.5	-	14.0	25.5	8.78	15.27	0.03	1.57	665	612	61.8	61.8	1.09	1.28	0.71	1.37	0.61	0.43
B50.2 [19]	Plain	16.0	27.5	-	14.0	25.5	8.78	15.27	0.03	1.57	665	614	57.1	57.1	1.04	1.23	0.69	1.35	0.59	0.43
B50.3 [19]	Plain	16.0	27.5	-	14.0	25.5	8.78	15.27	0.03	1.57	665	612	61.7	61.7	1.04	1.23	0.68	1.32	0.58	0.42
B70.1 [19]	Plain	16.0	27.5	-	14.0	25.5	8.78	15.27	0.03	1.57	658	617	77.3	77.3	0.98	1.15	0.62	1.17	0.53	0.36
B70.2 [19]	Plain	16.0	27.5	-	14.0	25.5	8.78	15.27	0.03	1.57	656	614	76.9	76.9	1.01	1.19	0.64	1.22	0.55	0.38
B70.3 [19]	Plain	16.0	27.5	-	14.0	25.5	8.78	15.27	0.03	1.57	663	617	76.2	76.2	1.03	1.21	0.65	1.24	0.56	0.38

Beam	*	x	y	t	x_1	y_1	A_t/s	A_l	ρ_t	ρ_l	f_{yt}	f_{yl}	f_c	$T_{R,exp}$	$T_{R,exp}/T_{R,th}$					
		cm	cm	cm	cm	cm	cm²/m	cm²	%	%	MPa	MPa	MPa	kNm	ACI89	ACI14	MC90	MC10	EC2	CSA04
B110.1 [19]	Plain	16.0	27.5	-	14.0	25.5	8.78	15.27	0.03	1.57	655	618	109.8	109.8	1.01	1.19	0.66	1.12	0.56	0.45
B110.2 [19]	Plain	16.0	27.5	-	14.0	25.5	8.78	15.27	0.03	1.57	660	634	105.0	105.0	0.99	1.16	0.64	1.11	0.55	0.42
B110.3 [19]	Plain	16.0	27.5	-	14.0	25.5	8.78	15.27	0.03	1.57	655	629	105.1	105.1	1.03	1.22	0.67	1.17	0.57	0.44
B7UR1 [20]	Plain	20.3	30.5	-	16.5	26.7	6.56	5.16	0.92	0.83	386	386	64.6	64.6	0.94	1.15	1.28	0.75	1.07	0.99
B12UR3 [20]	Plain	20.3	30.5	-	16.5	26.7	7.46	6.58	1.04	1.06	386	380	72.9	16.0	1.02	1.05	1.29	0.75	1.07	1.00
B12UR4 [20]	Plain	20.3	30.5	-	16.5	26.7	7.88	7.74	1.10	1.25	386	373	75.9	16.9	1.04	1.07	1.24	0.72	1.03	0.96
B12UR5[20]	Plain	20.3	30.5	-	16.5	26.7	10.13	8.00	1.41	1.29	386	380	76.7	13.6	0.87	1.08	1.09	0.64	0.91	0.83
H-06-12 [21]	Plain	35.0	50.0	-	30.0	45.0	7.10	20.65	0.61	1.18	440	410	78.5	75.0	1.41	1.24	1.63	0.87	1.34	1.17
H-07-10 [21]	Plain	35.0	50.0	-	30.0	45.0	7.89	17.03	0.68	0.97	420	500	68.4	70.5	1.33	1.17	1.53	0.94	1.26	1.11
H-07-16 [21]	Plain	35.0	50.0	-	30.0	45.0	7.89	28.39	0.68	1.62	420	500	68.4	65.3	1.52	1.27	1.35	1.25	1.12	0.98
H-12-12 [21]	Plain	35.0	50.0	-	30.0	45.0	14.19	20.65	1.22	1.18	440	410	78.5	77.1	1.22	1.28	1.55	0.99	1.28	1.12
H-12-16 [21]	Plain	35.0	50.0	-	30.0	45.0	14.19	28.39	1.22	1.62	440	520	78.5	79.3	1.30	1.61	1.32	1.28	1.09	0.95
H-14-10 [21]	Plain	35.0	50.0	-	30.0	45.0	16.13	17.03	1.38	0.97	360	500	68.4	61.8	0.85	1.24	1.14	0.86	0.94	0.83
H-20-20 [21]	Plain	35.0	50.0	-	30.0	45.0	23.46	34.06	2.01	1.95	440	560	78.5	76.0	1.33	1.97	1.06	1.44	0.87	0.76
N-06-06 [21]	Plain	35.0	50.0	-	30.0	45.0	7.10	12.00	0.61	0.69	440	440	35.5	43.2	1.09	1.05	1.38	0.99	1.14	0.99
N-06-12 [21]	Plain	35.0	50.0	-	30.0	45.0	7.10	20.65	0.61	1.18	440	410	35.5	51.8	1.37	1.16	1.34	1.39	1.11	0.97
N-07-10 [21]	Plain	35.0	50.0	-	30.0	45.0	7.89	17.03	0.68	0.97	420	500	33.5	41.6	1.31	1.41	1.35	1.55	1.11	0.98
N-07-16 [21]	Plain	35.0	50.0	-	30.0	45.0	7.89	28.39	0.68	1.62	420	500	33.5	40.0	1.38	1.48	1.10	1.90	0.91	0.79
N-12-12 [21]	Plain	35.0	50.0	-	30.0	45.0	14.19	20.65	1.22	1.18	440	410	35.5	49.3	1.02	1.43	1.17	1.44	0.96	0.84
N-12-16 [21]	Plain	35.0	50.0	-	30.0	45.0	14.19	28.39	1.22	1.62	440	520	35.5	57.1	1.14	1.69	0.93	1.74	0.76	0.75
N-14-10 [21]	Plain	35.0	50.0	-	30.0	45.0	16.13	17.03	1.38	0.97	360	500	33.5	41.8	1.06	1.57	1.06	1.49	0.87	0.76
N-20-20 [21]	Plain	35.0	50.0	-	30.0	45.0	23.46	34.06	2.01	1.95	440	560	35.5	55.0	1.30	1.93	1.00	1.83	0.83	0.86
HAS-90-50[22]	Plain	42.0	42.0	-	37.0	37.0	5.94	15.89	0.50	0.90	385	400	78.0	78.0	1.40	1.43	2.06	0.96	1.55	1.36
HBS-74-17[22]	Plain	35.0	50.0	-	30.0	30.0	2.02	12.89	0.17	0.74	600	505	67.0	67.0	1.19	1.18	1.55	0.79	1.28	1.12
HCS-91-50[22]	Plain	25.0	70.0	-	20.0	20.0	5.09	15.89	0.50	0.91	385	400	78.0	78.0	1.50	1.60	1.92	1.20	1.75	1.52
SW12-1 [24]	Plain	15.0	120	-	10.0	115.0	3.93	11.31	0.55	1.26	459	480	44.2	32.3	1.71	1.86	1.52	2.87	1.47	1.28
SW10-1 [24]	Plain	15.0	100	-	10.0	95.0	3.93	9.05	0.55	1.21	459	499	29.5	24.6	1.49	1.92	1.28	3.26	1.23	1.07
SW10-2 [24]	Plain	15.0	100	-	9.8	94.8	7.54	9.05	1.05	1.21	480	480	44.2	29.6	1.37	2.19	1.30	2.62	1.25	1.05
SW10-3 [24]	Plain	15.0	100	-	9.8	94.8	11.31	9.05	1.58	1.21	499	499	29.5	26.6	1.83	2.31	1.14	3.57	1.10	1.44
SW10-4 [24]	Plain	15.0	100	-	9.4	94.4	16.08	16.08	2.23	2.14	497	497	33.8	27.7	1.85	2.63	0.93	3.34	0.89	1.48
SW8-1 [24]	Plain	15.0	80.0	-	10.2	75.2	4.02	7.07	0.57	1.18	433	459	29.5	19.7	1.53	2.99	1.28	2.00	1.22	1.12
SW8-2 [24]	Plain	15.0	80.0	-	9.8	74.8	11.31	7.07	1.59	1.18	499	459	29.5	22.5	1.85	3.08	1.16	2.24	1.11	1.51
D3 [15]	Hollow	25.4	38.1	6.4	21.6	34.3	10.16	11.36	1.17	1.17	333	341	28.4	15.2	1.42	1.38	1.35	1.64	1.13	1.08
D4 [15]	Hollow	25.4	38.1	6.4	21.6	34.3	14.01	15.48	1.62	1.60	333	330	30.6	15.8	1.06	1.63	0.98	1.62	0.82	0.78
T1 [16]	Hollow	50.0	50.0	8.0	45.4	45.4	10.28	18.10	0.75	0.72	357	357	35.3	48.0	1.32	1.27	1.41	1.06	1.06	1.05
T2 [16]	Hollow	50.0	50.0	8.0	43.0	43.0	10.28	18.10	0.71	0.72	357	357	35.3	11.5	1.64	1.44	1.58	1.12	1.19	1.28
VH2 [17]	Hollow	32.4	32.4	8.0	30.4	30.4	5.76	6.91	0.67	0.66	447	447	17.2	34.5	0.75	1.74	1.15	2.22	0.86	0.67
A1 [23]	Hollow	60.0	60.0	9.8	53.7	54.7	3.11	6.53	0.19	0.18	637	696	48.4	150.8	1.22	1.48	1.88	1.00	1.41	1.41
A2 [23]	Hollow	60.0	60.0	10.7	53.8	53.1	6.28	13.95	0.37	0.39	696	672	47.3	109.5	1.32	1.20	1.53	0.81	1.15	1.14
A3 [23]	Hollow	60.0	60.0	10.9	53.5	53.5	8.27	18.10	0.49	0.50	715	672	46.2	113.3	1.25	1.24	1.37	0.94	1.02	1.00
A4 [23]	Hollow	60.0	60.0	10.4	52.0	52.5	11.22	23.75	0.65	0.66	715	724	54.8	120.9	1.26	1.55	1.19	1.04	0.90	0.92
A5 [23]	Hollow	60.0	60.0	10.4	52.8	52.8	14.14	30.66	0.83	0.85	672	724	53.1	120.9	1.23	1.73	1.08	1.22	0.81	0.83
B2 [23]	Hollow	60.0	60.0	10.8	53.3	53.4	6.70	14.58	0.40	0.41	696	672	69.8	116.7	1.26	1.24	1.57	0.83	1.17	1.16
B3 [23]	Hollow	60.0	60.0	10.9	53.5	53.7	11.22	23.75	0.67	0.66	715	724	77.8	130.5	1.11	1.14	1.17	0.75	0.88	0.86
B4 [23]	Hollow	60.0	60.0	11.2	52.3	53.6	15.08	32.17	0.89	0.89	672	724	79.8	142.9	1.16	1.38	1.12	0.91	0.84	0.83
B5 [23]	Hollow	60.0	60.0	11.7	51.8	51.8	18.85	40.21	1.09	1.12	672	724	76.4	146.3	1.05	1.48	0.94	0.96	0.71	0.71
C1 [23]	Hollow	60.0	60.0	9.7	54.0	54.9	3.11	6.53	0.19	0.18	637	696	91.7	151.8	1.03	1.48	1.89	1.00	1.42	1.40
C2 [23]	Hollow	60.0	60.0	10.0	53.2	53.3	6.28	13.95	0.37	0.39	696	672	94.8	124.5	1.23	1.26	1.57	0.83	1.18	1.20
C3 [23]	Hollow	60.0	60.0	10.3	54.5	54.0	10.47	23.75	0.63	0.66	715	724	91.6	131.9	1.12	1.08	1.17	0.69	0.88	0.86
C4 [23]	Hollow	60.0	60.0	10.3	54.6	54.5	14.14	30.66	0.86	0.85	672	724	91.4	132.6	1.20	1.36	1.18	0.89	0.88	0.86
C5 [23]	Hollow	60.0	60.0	10.4	54.0	54.3	17.40	36.69	1.05	1.02	672	724	96.7	138.3	1.07	1.38	1.01	0.88	0.76	0.74
C6 [23]	Hollow	49.7	60.0	10.4	53.3	52.9	22.62	48.25	1.34	1.34	672	724	87.5	139.1	1.12	1.69	0.83	1.04	0.62	0.63
HAH-81-35[22]	Hollow	42.0	42.0	7.5	37.0	37.0	4.19	14.31	0.35	0.81	385	493	78.0	94.3	1.78	1.46	1.84	0.97	1.38	1.39
HCH-91-42[22]	Hollow	25.0	70.0	7.5	20.0	65.0	4.30	15.89	0.42	0.91	385	400	78.0	87.5	1.51	1.59	1.71	1.10	1.56	1.51
A120a [25]	Hollow	50.2	71.9	18.4	44.2	65.9	7.59	20.00	0.46	0.55	380	464	27.6	89.8	2.07	1.92	1.46	1.74	1.25	1.82
B080a [25]	Hollow	50.0	72.1	11.2	44.0	66.1	12.90	28.39	0.79	0.79	392	454	46.5	65.2	1.11	1.20	1.25	0.94	1.03	0.99

Capítulo 4

Estudo experimental de vigas de secção vazada com betões de alta resistência e pré-esforço longitudinal ensaiadas à torção pura

Neste capítulo é apresentado um artigo científico, publicado em revista internacional, onde são apresentados e discutidos os resultados de um estudo experimental envolvendo vigas de secção vazada sujeitas à torção construídas com betões de alta resistência e incorporando pré-esforço longitudinal.

Bernardo, L. F. A., Lopes, S. M. R. and Teixeira, M. M. (2020). Experimental Study on the Torsional Behaviour of Prestressed HSC Hollow Beams. *Applied Science*. **10**(2): 642. https://doi.org/10.3390/app10020642

applied sciences

MDPI

Article

Experimental Study on the Torsional Behaviour of Prestressed HSC Hollow Beams

Luís Bernardo [1,*], Sérgio Lopes [2] and Mafalda Teixeira [1]

[1] Department of Civil Engineering and Architecture, Centre of Materials and Building Technologies (C-MADE), University of Beira Interior, 6201-001 Covilhã, Portugal; mafalda.m.teixeira@ubi.pt
[2] Department of Civil Engineering, Center for Mechanical Engineering, Materials and Processes (CEMMPRE), University of Coimbra, 3030-788 Coimbra, Portugal; sergio@dec.uc.pt
* Correspondence: lfb@ubi.pt

Received: 23 December 2019; Accepted: 13 January 2020; Published: 16 January 2020

check for updates

Abstract: This article describes an experimental program developed to study the influence of longitudinal prestress on the behaviour of high-strength concrete hollow beams under pure torsion. The pre-cracking, the post-cracking and the ultimate behaviour are analysed. Three tests were carried out on large hollow high-strength concrete beams with similar concrete strength. The variable studied was the level of longitudinal uniform prestress. Some important conclusions on different aspects of the beams' behaviour are presented. These conclusions, considered important for the design of box bridges, include the influence of the level of prestress in the cracking and ultimate behaviour.

Keywords: concrete structures; beams & girders; torsion; high-strength concrete; prestressing

1. Introduction

Pure torsion does not really occur too often in concrete structures; it usually occurs together with other internal forces such as shear, bending and axial forces. However, in some structures, such as the case of curved box bridges, the torsional action can be very important for design.

The application of prestress usually increases the cracking and ultimate resistances of concrete structures. Prestress is particularly important in High-Strength Concrete (HSC) structures. In general, HSC structures are expected to be more flexible than Normal-Strength Concrete (NSC) structures because of the smaller cross-section area of members. This high flexibility could be problematic for the serviceability limit states. The use of the prestress technique can also help to solve such problems associated with high flexibility.

The application of longitudinal prestress in members under high torsional loads is a common situation, as for instance in curved bridges. Many of such structures are also built with HSC and use hollow cross-sections for the girders (Figure 1) because they present some advantages when compared to solid cross-sections. In large cross-sections under high torsion, the internal shear flow is mainly absorbed by the outer concrete shell. Thus, the concrete at the centre zone of the cross-section is redundant and can be removed. As a consequence, hollow cross-sections allow for a high reduction in weight and concrete consumption, without compromising the torsional strength.

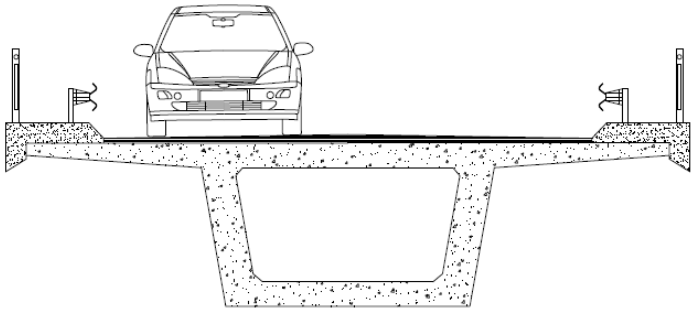

Figure 1. Example of a hollow (box) cross-section for the girder of a bridge deck.

Since the end of the last century, it is well known that the uniaxial stress-strain curve for HSC is quite different from that for NSC [1]. Therefore, it is not obvious that the computing and design models for HSC members can be directly extrapolated from NSC. Nowadays, many codes of practice already include HSC range. However, some aspects of the structural behaviour of HSC members still need to be studied in order to check if the physical models accepted for NSC can be adopted for HSC. The response of HSC beams to torsional loads constitutes an example of such cases.

There are still few experimental studies on hollow beams under pure torsion reported in the literature and most of them involve only a small number of NSC beams [2–5]. Only some few recent works report new results for both NSC and HSC hollow beams [6,7]. When compared with NSC beams, such studies demonstrate some of the advantages of HSC, namely, to increase the cracking and ultimate torsional strengths, as well as the torsional stiffness of the beams. However, some disadvantages of using HSC are also pointed out, in particular related to the torsional ductility which constitutes an important property to be considered for design. By using the experimental results reported in the previously referred experimental studies and also by using numerical models, other recent studies show that some ductility can be observed in NSC beams under torsion, namely for a certain range of the torsional reinforcement. However, almost no torsional ductility in HSC beams under torsion is observed [8–10]. Such studies also show that the level of the observed torsional ductility is normally low when compared with flexural ductility [11,12].

Few previous studies leading with testing of prestressed concrete rectangular beams under torsion can be found in the literature, namely—Mitchell and Collins in 1974 [4], El-Degwy and McMullen in 1985 [13], Hsu and Mo in 1985 [14] and Wafa et al. in 1995 [15]. Among the beams tested in the referred studies (twenty-seven beams), only three where hollow and built with NSC. This is because building hollow beams for testing is more complicated when compared with solid beams. Furthermore, due to the complexity of the experimental program, only a constant longitudinal prestressing was considered in all the referred studies. The authors did not find any previous study on the experimental behaviour of HSC prestressed hollow beams under torsion.

From the foregoing, experimental studies on the behaviour of prestressed hollow beams under torsion are needed, in particular for HSC beams. This article presents an experimental study on the global behaviour of HSC hollow beams with uniform longitudinal prestress. The beams were loaded under pure torsion and tested up to failure. As for the previous referred studies, a uniform longitudinal prestress was applied. This was considered to be sufficient to give some indications on the influence of prestress on the behaviour of HSC hollow beams under torsion.

2. Experimental Program

2.1. Test Specimens

For this study, three hollow beams were tested up to failure. The beams had a squared cross-section and were 5.90 m long. During testing, the beams had an extremity fixed to the strong floor of the laboratory and the load was applied to the other extremity by an electromechanical actuator. In this

extremity, a special device transformed the linear point load applied by the actuator into a torque applied to the beam extremity. The dimensions of the test models are presented in Figure 2. The geometry and dimensions of the adopted cross-section are in line with some of the works previously referred and leading with hollow beams.

External prestressing was applied through four 0.6'' wires (0.6 inches or 1.52 cm diameter) centred in the cross-section (Figure 2). The torsional reinforcement ratio was kept constant for the three beams and it corresponds to an average value which was defined accounting for the range of values that were used in a previous experimental work on similar beams with no prestressing [6]. The concrete strength was approximately constant, varying between 77.8 and 80.8 MPa. The average level of stress in concrete induced by prestress (f_{cp}) varied between 0 MPa (beam with no prestress) and 3.08 MPa, after short term losses. The maximum value is not very high because the losses were somewhat important. This is because the effect of anchorage slip becomes important when the length of the wires is relatively small.

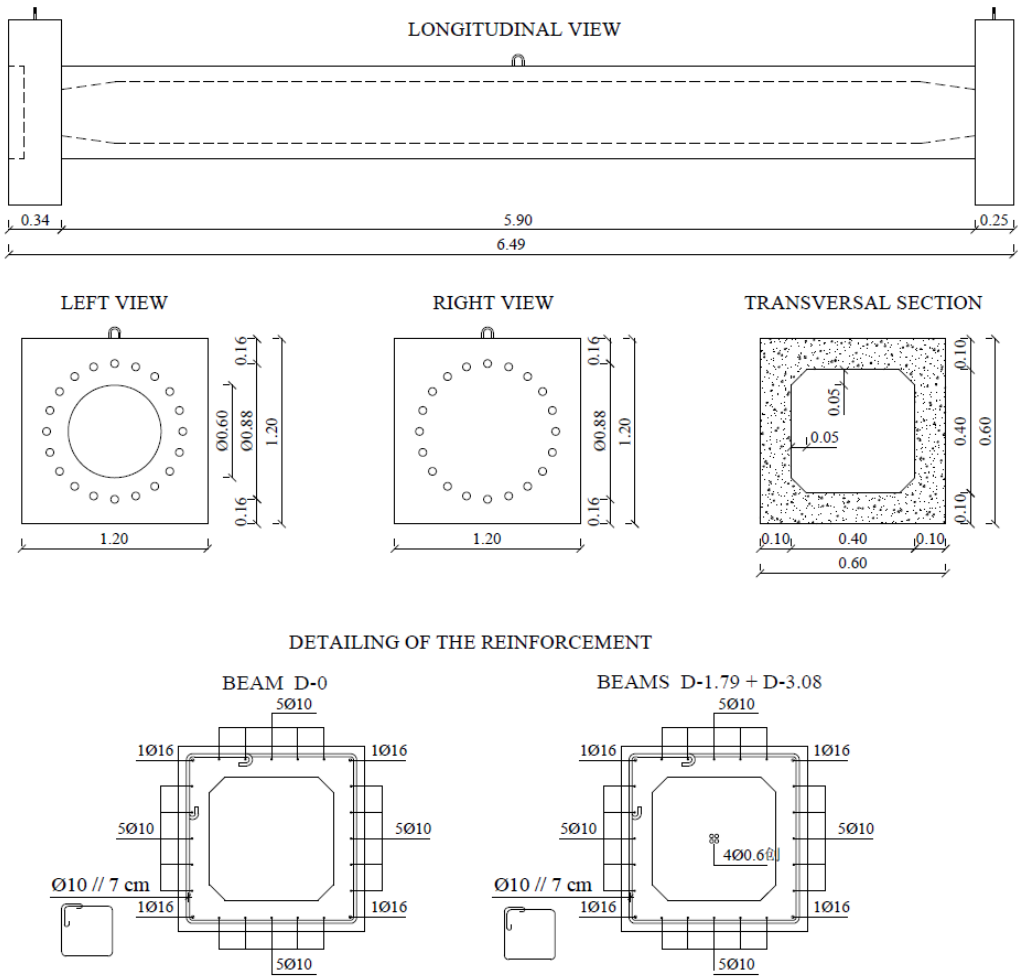

Figure 2. Geometry and detailing of test beams.

Table 1 summarizes the characteristics of each test beam, namely—the real thickness of the walls of the cross-section (t), the distance between parallel branches of stirrups, x_1 and y_1, the total area of ordinary longitudinal reinforcement (A_{sl}), the area of one branch of the transverse reinforcement (A_{st}), the longitudinal spacing of the stirrups (s), the total area of prestress longitudinal reinforcement (A_{sp}), the ratios of longitudinal reinforcement ($\rho_l = A_{sl}/A_c$, where $A_c = xy$ and $x = y = 60$ cm) and transverse reinforcement ($\rho_t = A_{st}u/A_cs$, where $u = 2(x_1 + y_1)$), the total ratio of reinforcement

($\rho_{tot} = \rho_l + \rho_t$), the balanced ratio of the longitudinal to transverse reinforcement ($m_b = A_{sl}s/A_{st}u$) and the average values for the compressive concrete strength obtained from cylindrical specimens (f_c).

The beams are named according to the series to which they belong (series D) and to the average stress (in MPa) in concrete induced by prestress, f_{cp}, after short term losses.

Table 1. Properties of test beams.

Beam.	t cm	x_1 cm	y_1 cm	A_{sl} cm^2	A_{st} cm^2	A_{sp} cm^2	s cm	ρ_l %	ρ_t %	ρ_{tot} %	m_b	f_c MPa	f_{ctm} MPa	E_c GPa
D-0	10.9	53.5	53.7	23.75	0.79	0	7.0	0.66	0.67	1.33	0.99	77.8	4.33	40.7
D-1.79	11.4	54.3	54.2	23.75	0.79	5.60	7.0	0.66	0.68	1.34	0.97	80.8	4.43	41.1
D-3.08	11.5	55.0	54.6	23.75	0.79	5.60	7.0	0.66	0.68	1.34	0.96	78.8	3.66	37.4

2.2. Materials Properties

The average value of the compressive concrete strength used in each tested beam was obtained from 5 cube specimens, casted and tested at the same time of the corresponding beam. The equivalent cylindrical values were computed by following the indications from Eurocode 2 [16]. Table 2 presents the concrete mix design used to produce the concrete.

Table 1 also presents, for each tested beam, the average values for the tensile concrete strength (f_{ctm}) and for the concrete Young's Modulus (E_c). These two parameters were computed from f_c also following the indications from Eurocode 2 [16].

As example, Figure 3 illustrates a stress (σ)–strain (ε) curve recorded during the test of one of the concrete samples. The initial part of the graph shows the influence of the adjustment due to the existent gap between the loading plates of the test machine and the concrete specimen.

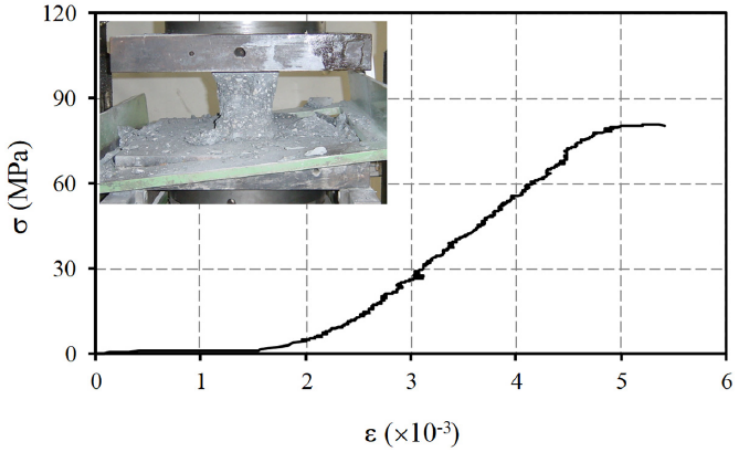

Figure 3. Uniaxial σ–ε curve for concrete.

Table 2. Concrete mix design (contents per m^3).

Components	Dosage
Thin sand	164 kg
Thick sand	908 kg
Crushed Granit 5–11 mm	734 kg
Normal Portland Cement (C): Type I/42.5R	375 kg
Admixture—Rheobuild 1000	4.8 ℓ
Silica Fume (Sikacrete HD)	41 kg
Water (A)	145 ℓ
A/(C + Additions)	0.35

The ordinary reinforcement used in the beams consisted of hot rolled ribbed steel bars (with 10 and 16 mm diameters) sold commercially as Class A500. In order to know the average values of the yield stress and corresponding strain of the bars (f_y and ε_y, respectively), tensile tests on steel samples were carried out (6 samples of each of the diameters that were used in the beams). The following average values were obtained—$f_y = 686$ MPa and $\varepsilon_y = 3.43 \times 10^{-3}$. For the steel Young´s Modulus, the typical value set in codes of practice was assumed, $E_s = 200$ GPa [16].

As example, Figure 4a illustrates some σ–ε curves recorded during the tensile tests of steel specimens (ordinary reinforcement).

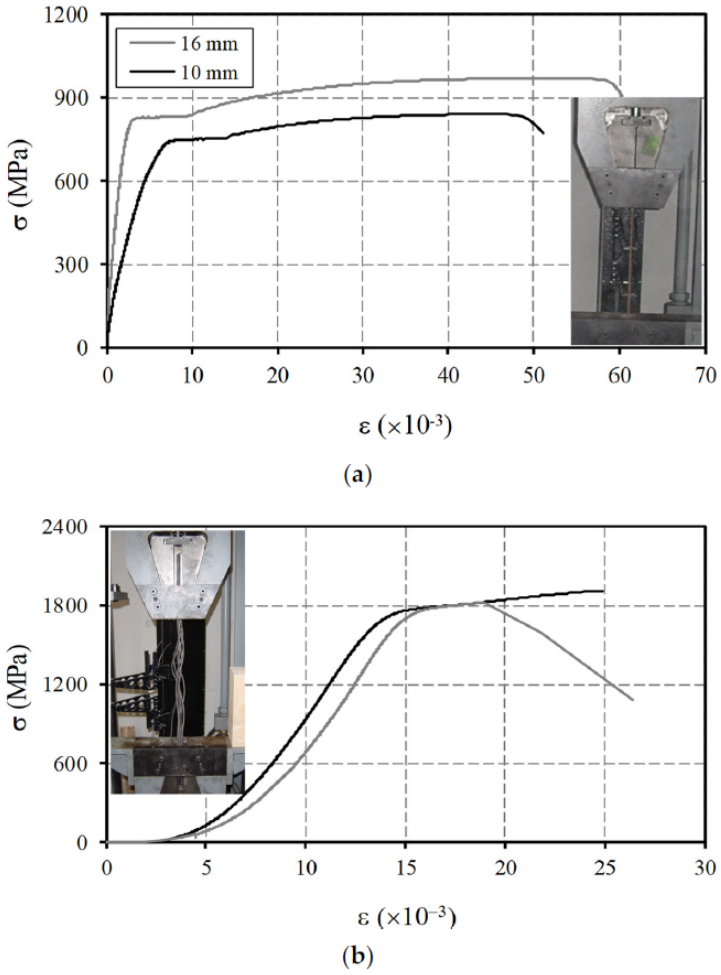

Figure 4. Uniaxial σ–ε curves for reinforcement: (**a**) ordinary and (**b**) prestress.

The prestress reinforcement used in Beams D-1.79 and D-3.08 consisted of four 0.6″ wires (0.6 inches or 1.52 cm diameter) belonging to Class S1670/1860. Tests on 6 prestress wire specimens were also carried out and the average values of the 0.1% limit proportional stress ($f_{p0.1\%}$) and the ultimate stress (f_{pu}) of the wires were obtained—$f_{p0.1\%} = 1670.5$ MPa and $f_{pu} = 1867.1$ MPa, respectively. The corresponding strain at 0.1% was computed by assuming a linear relationship between strains and stresses, which led to $\varepsilon_{p0.1\%} = 8.567 \times 10^{-3}$. The Young's Modulus was assumed to be the one indicated by the supplier, $E_p = 195$ GPa.

As example, Figure 4b illustrates σ–ε curves recorded during the tensile test of two prestress steel specimens (with 4 × 0.6 inches wires each).

It should be referred that some slip was observed between the steel specimens and the claws of the test machine. This explains the apparent different initial stiffness between the curves for 10

and 16 mm bars in Figure 4a and also the initial part of the curves in Figure 4b. This problem had no implication to the previously presented strain values at the end of the elastic stage. The strains were computed from Hooke's law by knowing the stresses and assuming the Young's Modulus.

2.3. Testing Procedure

The test device is made of three main components:

- a test frame where the mechanical actuator is fixed;
- a device that receives the load from the mechanical actuator and applies a torsional moment in one end of the test beams;
- a device that fixes the test beam at the other end, restricting its transversal rotation (twist) and allowing its longitudinal deformation (elongation).

Figure 5 illustrates the global test device with a beam in its test position.

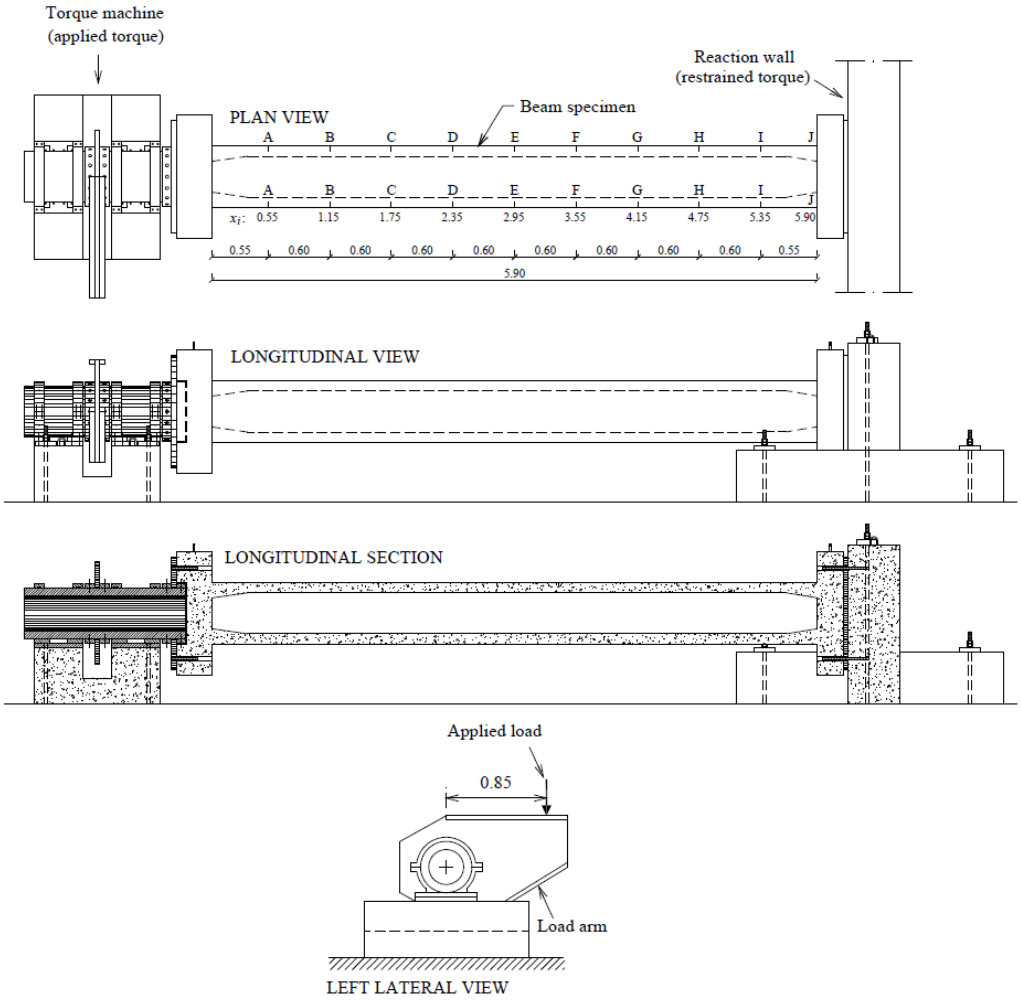

Figure 5. Test setup.

The load was applied by imposing a low deformation rate with an electromechanical actuator. Several load cells were placed in different points of the global test device in order to record at any time the general loading state of the beams.

The transversal rotations (twists) were read in 10 sections uniformly spaced along the length of the beams (Sections A-A to J-J), as illustrated in Figure 5. For this, 10 pairs of displacement transducers

were placed at the top face of the beam (they were fixed to an external anchored referential). Special care was taken to allow free horizontal relative movements between the beams and the LVDT arms. Because of this, the horizontal projection of the distance between pairs of transducers remained constant during the test and the rotation angles at each section could be easily computed from the transducers' readings.

The torsional reinforcement bars were instrumented in three selected sections at quarters of the beams' length. Resistance strain gauges were stuck on the 4 longitudinal corner bars and on the 4 branches of one stirrup.

For Beams D-1.79 and D-3.08, in order to evaluate the effective longitudinal prestressing force after losses and also the changes in this force due to the application of increasing torque, a load cell was placed between the head of the beam and the head of anchorage. Figure 6 illustrates longitudinal cuts at the ends of the prestressed beams and shows the technical solutions adopted to prestress the beams and to read the prestress force during the tests.

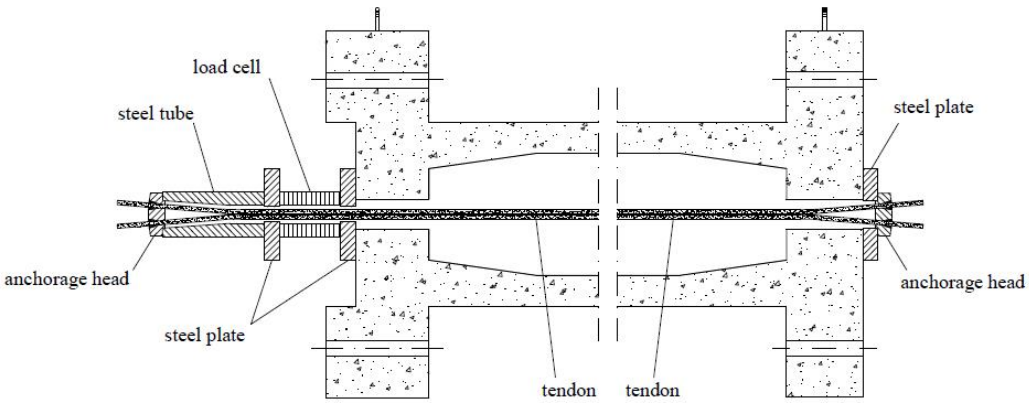

Figure 6. Anchorage zones at both ends of the prestressed beams.

A Data Logger was used to record all the readings. Figure 7 shows general views of a beam in its position with the instrumentation ready for testing.

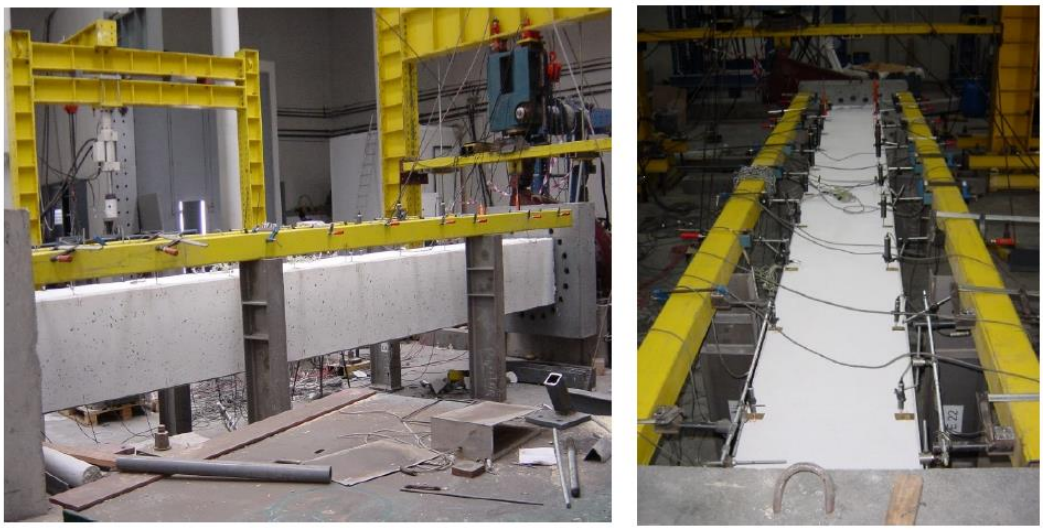

Figure 7. Beam specimen in test position.

3. Global Analysis of the Experimental Results

3.1. Torsional Moments vs. Twists

Figure 8 presents the graphs of torque (T) *versus* the average twists (θ_m) for the tested beams. The torque, T, was obtained multiplying the load applied by the actuator by the horizontal projection of the level arm, 0.85 m, which remained constant (see Figure 5). The average twist, θ_m, was obtained by dividing the experimental angle measured in Section A-A to the distance between Sections A-A and J-J, 5.35 m (Figure 5). In each T–θ_m curve, identification marks were used to highlight the points corresponding to cracking () and to yielding of the transverse (□) and longitudinal (△) reinforcement. The yielding points were calculated from the experimental values of the strains recorded by the strain gauges stuck to the reinforcement bars.

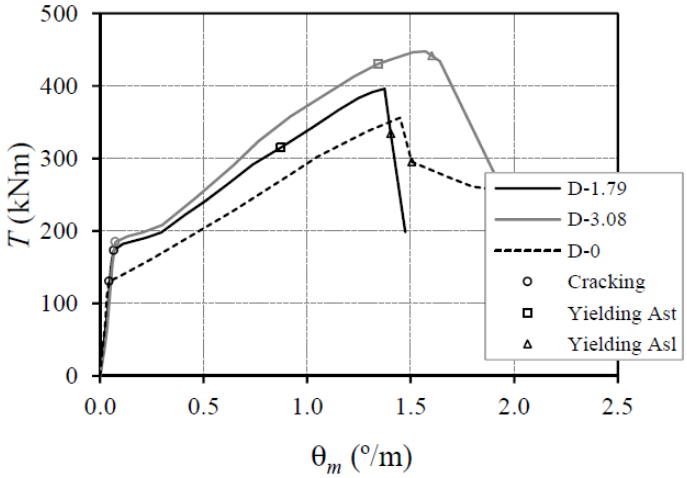

Figure 8. T–θ_m curves.

As expected, Figure 8 shows the high influence of prestress in the cracking torque. It is known that prestress delays the formation of cracking. For a moderate concrete stress (induced by prestress) of 1.79 MPa (Beam D-1.79) an increase of approximately 32.5% on the cracking torque is observed, when compared with the beam without prestress (Beam D-0). This shows the efficiency of uniform longitudinal prestress to delay the cracking in beams under torsion. This high influence of prestress can be explained because in torsion the concrete is under a lower and more uniform level of tensile stresses (in the whole section) when compared with the bending situation. Therefore, even for low levels of prestress, the cracking stage is delayed. It is also observed that, in State I (non-cracked state), the steel bars, including the prestressed wires, generally have little influence on the stiffness of the beams. In fact, the T–θ_m curves are almost coincident at this state.

In State II (cracked state), the T–θ_m curves are almost parallel to each other. This shows that the contribution of the longitudinal prestress for the stiffness of the beams is small at this state. This is due to the adopted prestressing technique (external longitudinal and centred prestress).

As expected, Figure 8 also shows that the use of prestress increases the resistant torque, T_r, of the beams. However, there is not a clear tendency with respect to the associated twist at the ultimate torque, θ_{T_r}. In fact, since prestress induces a compressive stress state in concrete, it would be expected that the deformation capacity of concrete in the compressed areas of the beam (namely in the struts) would decrease as the level of prestress increases. As a consequence, the twist corresponding to the ultimate torque should decrease as the stress induced by prestress increases. This is not the case for Beam D-3.08, which has the highest level of prestress and reaches a twist θ_{T_r} that exceeds the same one of the other beams. However, this observation can be explained due to the type of failure of Beams D-0 and D-1.79, which was fragile and somehow premature (failure by pull off of the concrete corners).

This subject will be discussed later. This aspect also justifies the different shape of the descending branches of T–θ_m curves that is observed and the absence of yielding points before the peak torque is reached for Beam D-0.

T–θ_m curves of Figure 8 also show that, before the peak torque is reached, the prestressed beams only present points corresponding to yielding of the transverse reinforcement. It is observed that the yielding of longitudinal reinforcement only occurs after the peak torque. After cracking, the longitudinal prestress reinforcement starts working as ordinary reinforcement under the torsional loading. Consequently, the beams with balanced longitudinal to transverse reinforcement ratios will lose this balance because of the influence of the prestress wires. Hence, the calculation of the balanced ratio of the longitudinal to transverse reinforcements should account for the area of the prestressed steel ($m_{b,tot} = (A_{sl} + nA_{sp})s/A_{st}u$ with $n = E_p/E_s$), which leads to an excess of longitudinal reinforcement of about 20%. Therefore, the transverse reinforcement should yield before the longitudinal reinforcement, as observed in Figure 8.

Table 3 presents, for each tested beam, the main properties of T–θ_m curves, namely—the cracking torque and correspondent twist (T_{cr} and θ_{cr}), the torsional stiffness in State I ($(GC)^{\mathrm{I}}$), the torsional stiffness in State II ($(GC)^{\mathrm{II}}$), the torque corresponding to the yielding of the transverse reinforcement and correspondent twist (T_{ty} and θ_{ty}), the resistant torque (peak torque) and correspondent twist (T_r and θ_{T_r}). Since the yielding of the longitudinal reinforcement occurs after the peak torque, the corresponding values are not presented.

Table 3. Properties of T–θ_m curves.

Beam	T_{cr} kNm	θ_{cr} °/m	$(GC)^{\mathrm{I}}$ kNm²	$T^{\mathrm{II}}=a\theta^{\mathrm{II}}+b$	$(GC)^{\mathrm{II}}$ kNm²	T_{ty} kNm	θ_{ty} °/m	T_r kNm	θ_{T_r} °/m
D-0	130.5	0.04	172,940	a = 170.87; b = 119.43	9790	-	-	355.9	1.45
D-1.79	172.9	0.07	152,188	a = 194.73; b = 142.95	11,157	314.9	0.87	396.0	1.38
D-3.08	184.7	0.08	141,823	a = 148.05; b = 132.34	14,212	430.0	1.34	447.7	1.57

The torsional stiffness in State I was calculated dividing T_{cr} by θ_{cr} (with θ_{cr} in radians unit). Prior to the calculation of the torsional stiffness in State II, the equation of the line of T–θ_m curve in the linear elastic stage was previously calculated from linear interpolation. For this calculation, the points of the T–θ_m curves located in the zone that can be identified as belonging to State II were selected. Only the zone of the curves that is approximately a straight line was considered. After the calculation of the equation, $T = a\theta + b$ (see Table 3), the stiffness $(GC)^{\mathrm{II}}$ is equal to the slope a of the line (with twists converted to radian units).

The analysis of the values displayed in Table 3 confirms the trends observed in the T–θ_m curves from Figure 8 and previously discussed.

3.2. Force in the Prestress Reinforcement vs. Twists

Figure 9 presents the graphs of the force in the longitudinal prestress reinforcement (F_{ps}) *versus* the average twist (θ_m). The force F_{ps} was obtained directly from the load cell placed in the anchorage zone of the prestressed wires. The evolution of the recorded values starts from the initial value of the applied prestress force (after short-term losses).

The curves of Figure 9 show the existence of a small horizontal zone where the force in the prestress reinforcement is almost constant and equal to the force due to initial prestress. This zone ends as the first crack appears in the beam. After this zone, the force in the prestressed wires increases gradually. In fact, before cracking, the internal reinforcement steel bars are also under very low levels of stress. The strains in the beam during the pre-cracking state are very small, as confirmed by the readings of the strains in the reinforcement bars (recorded from the strain gauges). Decompression of concrete takes place at a certain point of this initial horizontal zone (before this point, concrete is only in compression).

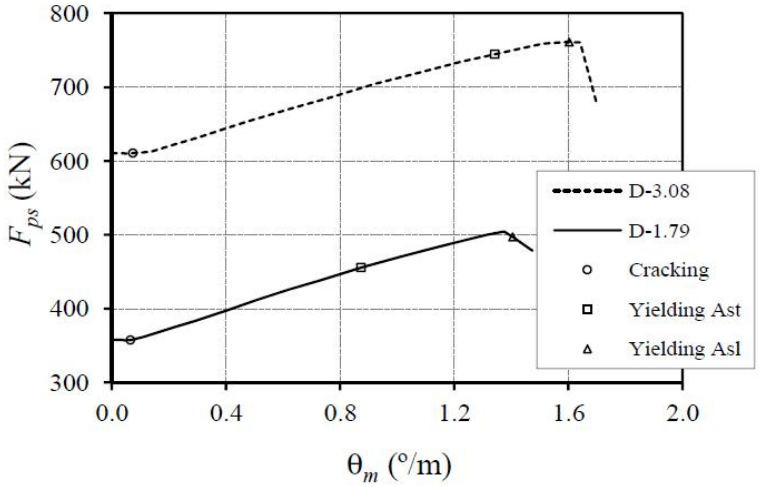

Figure 9. F_{ps}–θ_m curves.

After cracking, the torsional longitudinal reinforcement bars become effective and the tensile stress in the bars increases as the longitudinal deformation of the beam increases. The elongation of the beams also causes the increasing of the initial force in the prestressed reinforcement. This increasing occurs up to the failure of the beams.

4. Failure Modes and Cracking Patterns

Figures 10 and 11 show some photographic records of the failure zone of the tested beams. From these photos and from the analysis of the T–θ_m graphs at their final part it is possible to distinguish two failure modes.

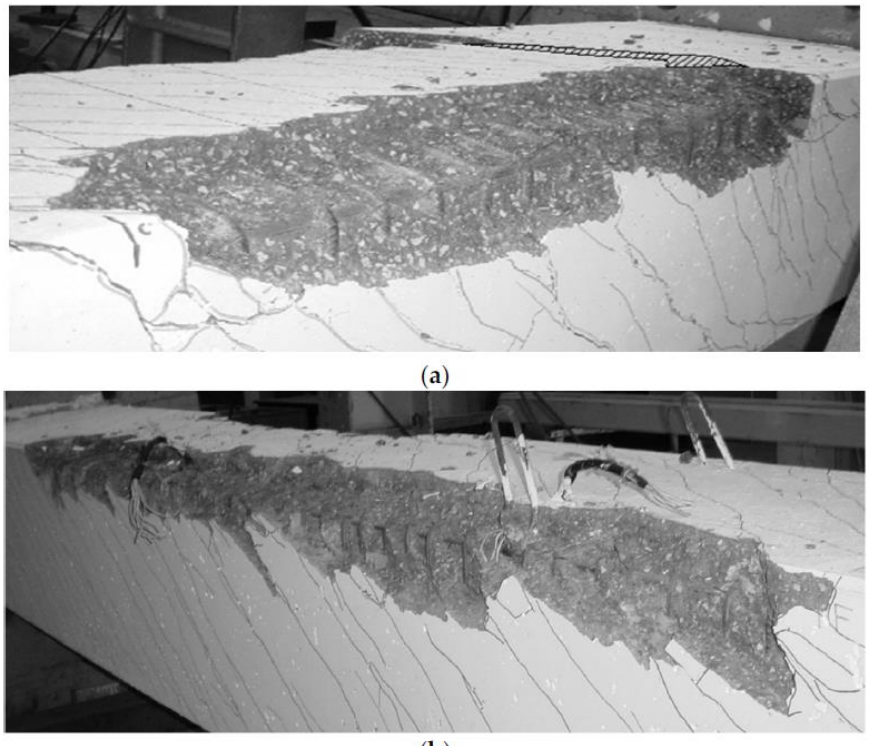

(**a**)

(**b**)

Figure 10. Fragile failure by concrete break off at the corners: (**a**) Beam D-0 and (**b**) Beam D-1.79.

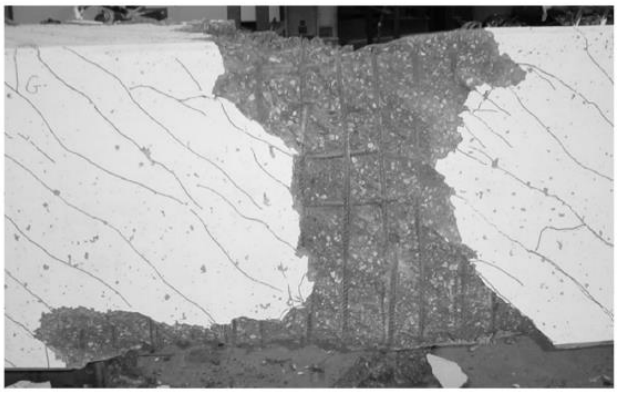

Figure 11. Fragile failure by crushing of concrete: Beam D-3.08.

With a low level of prestress (1.79 MPa), Beam D-1.79 had the same failure mode as Beam D-0 (with no prestress), characterized by concrete break off at the corners (Figure 10). It should be mentioned that this particular fragile failure mode, somehow frequent in hollow beams, was observed and reported in previous studies [6,10]. For a moderate prestress level (3.08 MPa), Beam D-3.08 clearly shows a fragile failure by crushing of concrete in the struts due to compression. This failure mode was particularly destructive and explosive (Figure 11). These results seem to show that the prestress level influences the failure mode. The results seem to indicate that, as the initial prestress increases, the failure becomes more fragile. This reveals an unfavourable effect of the prestress, which is observed for moderate levels of prestress.

To analyse the cracking pattern of the tested beams, photographs were taken and posterior graphic tools were used to produce graphic type images for the three visible faces (lateral faces and top face) for all the beams. Such illustrations are presented in Figures 12–14.

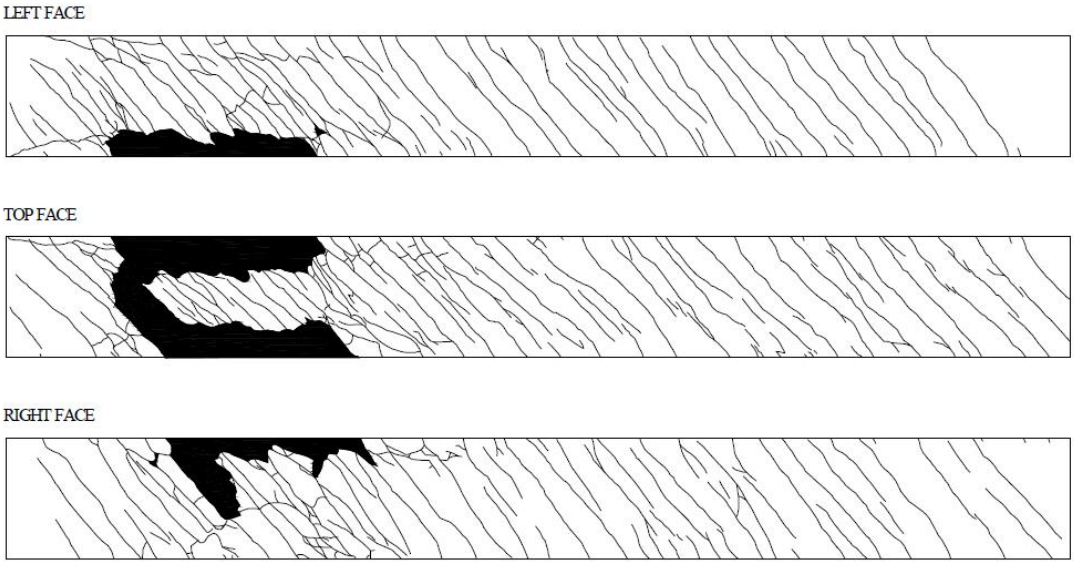

Figure 12. Cracking pattern: Beam D-0.

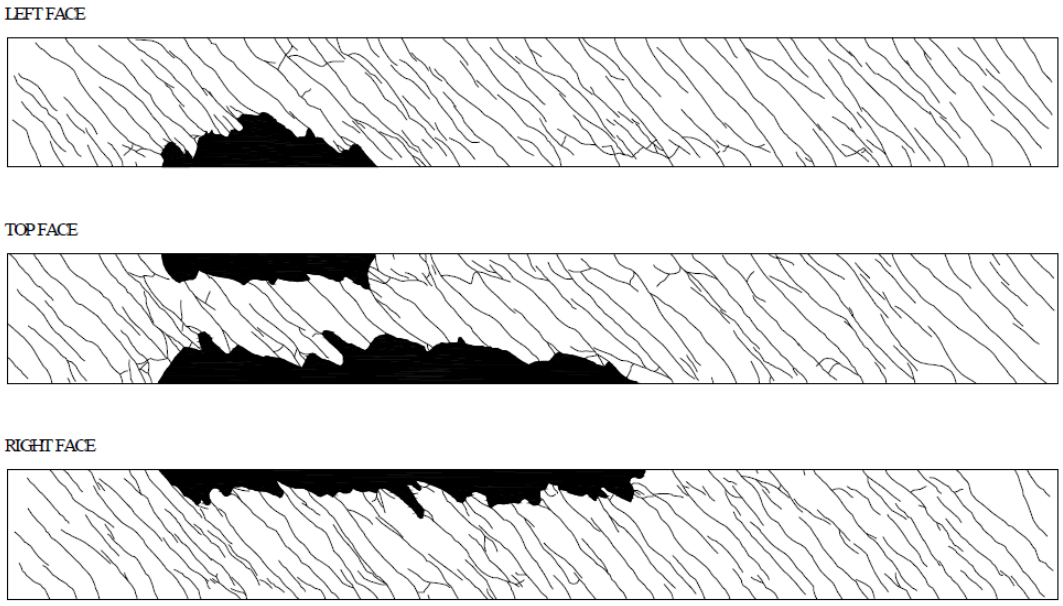

Figure 13. Cracking pattern: Beam D-1.79.

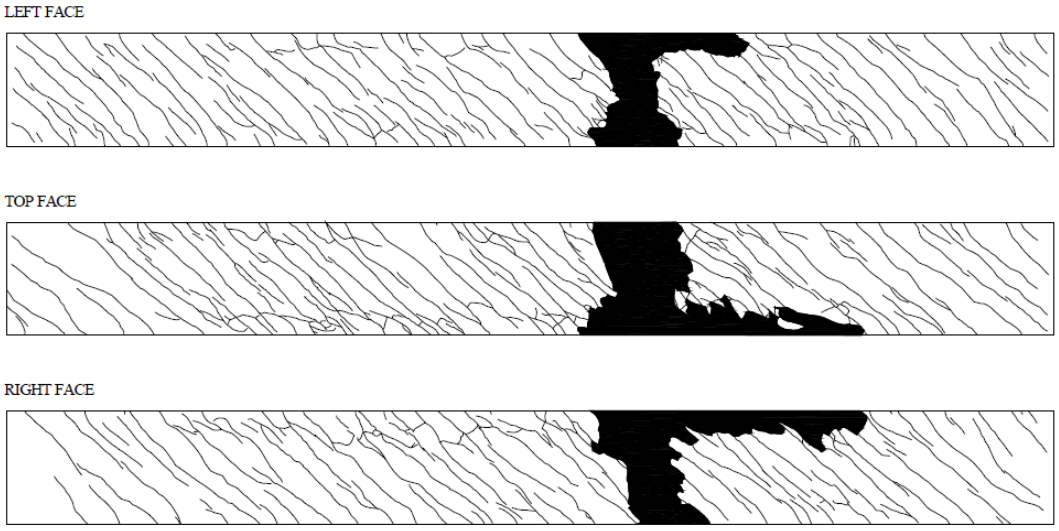

Figure 14. Cracking pattern: Beam D-3.08.

Figures 12–14 do not seem to show a significant influence of the prestress level in the distribution of cracking.

Table 4 presents, for each beam, the average longitudinal distance between cracks (d_m) and the average angle of such cracks to the longitudinal axis of the beams (α_m). Only diagonal cracks that cross the entire width of the faces were considered to compute d_m. Minors cracks or those associated to localized concrete spalling were not accounted. The angles α_m were taken at the mid-width of the faces.

Table 4. Cracking parameters.

Beam	d_m cm	α_m °
D-0	13.0	46.3
D-1.79	12.9	44.8
D-3.08	13.6	44.2

Table 4 confirms that prestress does not seems to influence the distribution of cracking, since the values of d_m are similar for the three beams. The values of α_m varied from 44.2° to 46.3°, not far from the expected theoretical value of 45° for beams with balanced reinforcement and without prestress. For beams with prestress, the referred angle is slightly smaller to the one of the similar beam without prestress. This shows a small influence of prestress (the prestress levels were not high either). It is known that the existence of an axial compressive force in beams symmetrically reinforced under torsion causes the angle of the diagonal cracks to decrease [17].

5. Conclusions

The experimental results obtained with prestressed HSC hollow beams tested in this study showed the effectiveness of longitudinal prestress to delay the cracking and to increase their resistance to torsion. After cracking, the longitudinal prestress reinforcement starts to effectively behave as an ordinary reinforcement, contributing for the internal equilibrium state of the beams.

Despite the limited number of tested beams, the tests showed that the level of longitudinal prestress can influence the failure mode. It was observed that, as the level of prestress increases, the risk of a fragile failure by concrete crushing in the struts becomes higher. Therefore, the level of compressive stresses in the concrete struts must be carefully controlled and the contribution of the prestress reinforcement must not be neglected. This problem becomes more important in HSC beams when compared to NSC beams, because HSC is more fragile when compared to NSC. In fact, the range of the reinforcement ratios that leads to ductile hollow beams under torsion is larger in NSC beams when compared to HSC beams [6].

The use of longitudinal prestress did not result in high differences with respect to the cracking behaviour of the tested beams.

Despite the limited number of tests presented in this study, the reported results show that there are noticeable differences in the behaviour of the tested beams. After this research program, it became now obvious that some particular aspects of the behaviour of prestressed HSC hollow beams need to be further investigated.

Author Contributions: S.L. supervised the experimental program. L.B. supervised the construction of the test beams, performed the experimental tests and analysed the recorded data with the help of M.T.; L.B. wrote the article with review by S.L. and M.T. All authors have read and agreed to the published version of the manuscript.

Funding: No funding supported this work.

Conflicts of Interest: The authors declare no conflict of interest.

References

1. Dahl, K.K.B. *Uniaxial Stress-Strain Curve for Normal and High Strength Concrete*; Report No. 182; Department of Structural Engineering, Technical University of Denmark: Kgs. Lyngby, Denmark, 1992; p. 58.
2. Hsu, T.T.C. *Torsion of Structural Concrete—Behavior of Reinforced Concrete Rectangular Members*; Torsion of Structural Concrete, SP-18; American Concrete Institute: Detroit, MI, USA, 1968; pp. 261–306.
3. Lampert, P.; Thürlimann, B. *Essais de Poutre en Béton Armé Sous Torsion Simple et Flexion Combinées (Tests on Reinforced Concrete Beams under Pure Torsion and Combined Bending)*; Torsion, Bulletin d´Information Nº 71, Comitée Européen du Béton: Brussels, Belgium, 1969; pp. 177–207.
4. Mitchell, D.; Collins, M.P. *Behavior of Structural Concrete Beams in Pure Torsion*; Civil Engineering Publication No.74-06; Department of civil Engineering, University of Toronto: Toronto, ON, Canada, 1974; p. 88.
5. Leonhardt, F.; Schelling, G. *Torsionsversuche na Stahlbetonbalken (Torsion Tests on Reinforced Concrete Beams)*; Bulletin No. 239; Deutscher Ausschuss für Stahlbeton: Berlin, Germany, 1974; p. 122.
6. Bernardo, L.F.A.; Lopes, S.M.R. Torsion in HSC Hollow Beams: Strength and Ductility Analysis. *ACI Struct. J.* **2009**, *106*, 39–48.
7. Jeng, C.H. Unified Softened Membrane Model for Torsion in Hollow and Solid Reinforced Concrete Members: Modeling Precracking and Postcracking Behavior. *J. Struct. Eng.* **2015**, *141*, 04014243. [CrossRef]

8. Bernardo, L.F.A.; Lopes, S.M.R. Behaviour of Concrete Beams under Torsion—NSC Plain and Hollow Beams. *Mater. Struct.* **2008**, *41*, 1143–1167. [CrossRef]
9. Bernardo, L.F.A.; Lopes, S.M.R. Theoretical Behaviour of HSC Sections under Torsion. *Eng. Struct.* **2011**, *33*, 3702–3714. [CrossRef]
10. Lopes, S.M.R.; Bernardo, L.F.A. Twist Behaviour of High-Strength Concrete Hollow Beams—Formation of Plastic Hinges along the Length. *Eng. Struct.* **2009**, *31*, 138–149. [CrossRef]
11. Lopes, S.M.R.; Bernardo, L.F.A. Plastic Rotation Capacity of High-Strength Concrete Beams. *Mater. Struct.* **2003**, *36*, 22–31. [CrossRef]
12. Bernardo, L.F.A.; Lopes, S.M.R. Plastic Analysis of HSC Beams in Flexure. *Mater. Struct.* **2009**, *42*, 51–69. [CrossRef]
13. El-Degwy, W.M.; McMullen, A.E. Prestressed Concrete Tests Compared with torsion Theories. *PCI J.* **1985**, *30*, 96–127.
14. Hsu, T.T.C.; Mo, Y.L. Softening of Concrete in Torsional Members—Prestressed Concrete. *J. Am. Concr. Inst.* **1985**, *82*, 603–615.
15. Wafa, F.F.; Shihata, S.A.; Ashour, S.A.; Akhtaruzzaman, A.A. Prestressed High-Strength Concrete Beams Under Torsion. *J. Struct. Eng.* **1995**, *121*, 1280–1286. [CrossRef]
16. *NP EN 1992–1-1. Eurocode 2: Design of Concrete Structures—Part 1: General Rules and Rules for Buildings*; European Committee for Standardization—CEN: Brussels, Belgium, 2010.
17. Hsu, T.T.C. *Torsion of Reinforced Concrete*; Van Nostrand Reinhold Company: New York, NY, USA, 1984; p. 516.

Capítulo 5

Conclusões e recomendações para estudos futuros

No presente capítulo são apresentadas as principais conclusões de cada trabalho de investigação realizado. No final do capítulo são propostos alguns estudos e trabalhos que podem contribuir para o desenvolvimento na área da torção em vigas de betão estrutural.

5.1. Conclusões

5.1.1. Modelo de Treliça com Ângulo Variável Modificado para vigas com pré-esforço sujeitas à torção.

Neste estudo, o modelo teórico MVATM [3] [4] para vigas de betão armado sujeitas à torção foi generalizado para a analise do comportamento de vigas de betão pré-esforçado sujeitas à torção. Para tal, foram feitas algumas modificações ao modelo MVATM de modo a definir e a implementar um procedimento de cálculo que determine, na integra, a curva $T-\theta$ teórica para vigas de betão pré-esforçado, com secção cheia e vazada, sujeitas à torção.

Neste estudo foi demonstrado que o MVATM generalizado fornece bons resultados quando comparados com resultados experimentais de vigas de betão pré-esforçado sujeitas à torção encontrados na literatura. Já quando comparado com a previsão de outro modelo teórico, designadamente o SMMT [10] [11] [12], o MVATM generalizado fornece previsões melhores para o comportamento real pós-fissuração das vigas.

Assim, o modelo MVATM generalizado pode ser considerado como uma boa contribuição na tentativa da generalização da Analogia da Treliça Espacial [14] para a previsão do comportamento global de vigas de betão pré-esforçado sujeitas à torção.

5.1.2. Avaliação de leis constitutivas médias do betão à tração para prever a transição entre o estado não fissurado e fissurado de vigas de betão armado sujeitas à torção, tendo por base a Analogia da Treliça Espacial.

Neste estudo, o modelo GSVATM [4] foi utilizado para avaliar algumas propostas de leis constitutivas médias para o betão à tração encontradas na literatura. O objetivo deste estudo foi avaliar qual das leis permite a um modelo recente da Analogia da Treliça Espacial prever, de forma mais adequada, a resposta de vigas de betão armado à torção para a fase de baixo

carregamento, designadamente a transição da fase não fissurada para a fase fissurada. A partir dos resultados obtidos, foi possível concluir o seguinte:

- Os resultados obtidos confirmam que a previsão da resposta das vigas de betão armado sujeitas à torção, para a transição da fase não fissurada para a fase fissurada, depende fortemente da lei constitutiva média do betão à tração incorporada no modelo;

- As previsões para o momento torsor de fissuração das vigas com secção cheia são melhores do que as previsões para as vigas de secção vazadas. Para estas últimas observa-se uma maior variabilidade dos resultados, como já foi relatado em estudos anteriores;

- Independentemente da lei constitutiva média utilizada para o betão à tração, o momento torsor de fissuração apresenta uma notável variabilidade de resultados em virtude da forte dependência da resistência à tração do betão;

- Dentro das leis constitutivas médias para o betão à tração estudadas, a lei proposta por Belarbi e Hsu [2] permite prever com segurança o momento torsor de fissuração das vigas de betão armado sujeitas à torção, independentemente do tipo de secção transversal (cheia ou vazada). Este resultado vem confortar vários estudos anteriores, nos quais os autores utilizaram por hipótese esta lei constitutiva média nos seus modelos de treliça espacial.

Os resultados obtidos neste estudo, utilizando o modelo GSVATM como modelo de referência, podem ser extrapolados para outros modelos de treliça para vigas de betão armado sujeitas à torção. Contudo, são necessários novos estudos experimentais sobre os diferentes mecanismos de rotura do betão em torção e respetivas aproximações teóricas para identificar melhor os parâmetros influentes nas fases mais baixas de carregamento, por forma a calibrar melhor os modelos para o estudo da fissuração de vigas de betão armado sujeita à torção.

5.1.3. Refinamento do Modelo de Treliça com Amolecimento com procedimento de cálculo eficiente para vigas de betão armado sujeitas à torção combinada com flexão.

Neste estudo foi apresentado uma versão refinada do CA-STM [8] com uma solução numérica eficiente para o seu procedimento de cálculo. Esta nova versão, designada por CA-STM refinado com procedimento de cálculo eficiente, foi usado para calcular a resposta completa de numerosas vigas de betão armado de referência sujeitas à torção combinada com flexão, cujos resultados experimentais foram encontrados na literatura. A partir dos resultados obtidos ao longo deste estudo, foram obtidas as seguintes conclusões:

- Os refinamentos propostos para o procedimento de cálculo do CA-STM, nomeadamente a incorporação de um conjunto de relações constitutivas médias para os materiais consideradas mais adequadas e um critério mais simples para calcular a armadura longitudinal equivalente em cada painel, mostraram-se apropriados para modelar com razoável precisão a resposta das vigas de betão armado sujeitas à torção combinada com flexão. Tal foi observado para todos os níveis de carregamento, incluindo a transição da fase não fissurada para a fase fissurada;

- Outros refinamentos propostos, como a utilização de um algoritmo alternativo ao uso da técnica original de "tentativa e erro" e a definição de um novo critério para fixar a espessura máxima dos painéis em vigas com secção cheia, conduziu a um procedimento de cálculo mais eficiente e com maior estabilidade numérica. Os resultados numéricos foram obtidos em períodos de tempo muito aceitáveis, sendo o tempo médio de processamento, para as vigas em estudo, de aproximadamente 30 segundos por viga (embora com alguma variação entre vigas), usando um computador corrente (Intel (R) Core (TM) i7-4700MQ CPU @ 2,40 GHz);

- Quando comparado com os vários resultados experimentais de vigas de betão armado ensaiadas à torção combinada com flexão, o CA-STM refinado com procedimento de cálculo eficiente provou ser um modelo confiável para prever o comportamento global dessas vigas, incluindo os pontos-chave de comportamento (pontos de fissuração e último).

O CA-STM refinado com procedimento de cálculo eficiente mostrou ser um modelo relativamente simples e confiável, baseado no modelo de treliça para elementos de betão armado e pode constituir um modelo analítico alternativo a modelos mais complexos. O modelo pode ainda ser facilmente utilizado para elaborar ferramentas computacionais de utilização simples, que ajudem a dimensionar e otimizar elementos estruturais de betão armado.

5.1.4. Ductilidade de vigas de betão armado sujeitas à torção.

Este estudo focou especificamente a ductilidade de torção de vigas de betão armado, com secção transversal retangular cheia e vazada. A partir dos resultados obtidos, foi possível obter as seguintes conclusões:

- O índice de ductilidade torsional utilizado neste estudo mostrou ser adequado para caracterizar a ductilidade em torção de vigas de betão armado e realizar análises comparativas entre a ductilidade de numerosas vigas, cujos resultados foram encontrados na literatura;

- Para vigas de betão armado com secção cheia, a ductilidade torsional aumenta com o aumento da resistência à compressão do betão, enquanto que, para vigas de betão armado com secção vazada a tendência observada é a oposta;

- A ductilidade de torção diminui notavelmente à medida que a taxa de armadura de torção total aumenta. Isto é verdade até que um determinado limite seja alcançado e a partir do qual se observa um comportamento dúctil residual (que é maior, para vigas de secção cheia). O limite da taxa de armadura parece aumentar à medida que a resistência do betão aumenta, com um valor compreendido entre os 2,0-3,0% para vigas de secção cheias e um valor compreendido entre os 1,0–1,5% para vigas vazadas;

- Vigas de betão armado semelhantes com secções transversais cheias e vazadas apresentam diferentes níveis de ductilidade torsional, devido à influência do núcleo de betão. Para uma dada taxa de armadura, as vigas de secção cheia são mais dúcteis do que as vigas de secção vazada. As vigas de secção cheia apresentam ainda um comportamento dúctil para um maior intervalo de taxa de armadura de torção;

- A taxa de armadura total apresenta maior influência na ductilidade torsional quando comparada com a influência da resistência do betão à compressão;

- Para os códigos ACI 318R-14 [1], MC 10 [6] e EC2 [13] observou-se que as regras que definem o cálculo da armadura transversal mínima de torção, para vigas de betão armado com armadura aproximadamente equilibrada, são adequadas para evitar a rotura frágil e prematura dos elementos por armadura insuficiente. Já para o código CSA A23.3–14 [7], este limite parece ser ligeiramente excessivo;

- Os códigos ACI 318R-14 e MC 10, bem como o CSA A23.3-14 embora em menor extensão, são excessivamente restritivos em relação ao limite máximo da armadura transversal de torção, o que conduz à não aceitação de vigas de betão armado que na realidade apresentam um comportamento dúctil em torção. Isso acontece mais em vigas com secção cheia e armadura aproximadamente equilibrada. Dos códigos estudados, o EC2 é o código que mostra ser mais eficiente para definir o limite máximo da armadura transversal de torção. Para as demais normas estudadas, o valor da tensão máxima permitida para as escoras de betão comprimido parece ser muito conservador, sugerindo-se que este limite deva ser revisto.

5.1.5. Resistência à torção de vigas de betão armado – Avaliação de alguns documentos normativos.

Neste artigo foi apresentada uma análise comparativa entre os resultados experimentais do momento torsor último de numerosas vigas de betão armado com secção retangular sujeitas à torção pura, encontradas na literatura consultada, e a previsão do momento torsor resistente dessas mesmas vigas calculado segundo diversos códigos e regulamentos utilizados para o dimensionamento de estruturas de betão. Dos resultados obtidos neste estudo, é possível concluir o seguinte:

- O tipo de secção das vigas, a classe do betão e a taxa de armadura têm influência direta na previsão da capacidade resistente à torção das vigas calculada pelos códigos analisados;

- Os códigos americanos tendem a sobrestimar a resistência à torção pura de vigas de secção cheia com taxas de armadura baixas, prevendo uma rotura teórica frágil e prematura por insuficiência de armadura. O limite da armadura mínima de torção estipulado por estes códigos necessita ser revista, designadamente para a versão mais recente analisada;

- O código MC90 tende a sobrestimar a resistência à torção de vigas com taxas de armaduras elevadas e/ou desequilibradas, independentemente do tipo de secção ou da classe do betão. Para estas vigas, o referido código prevê roturas frágeis por compressão das escoras de betão ou por insuficiente de armadura longitudinal. Como tal, o limite máximo para a armadura não se mostra adequado, uma vez que implica tensões elevadas nas escoras de betão, tal como o limite mínimo de armadura longitudinal, o qual não é suficiente para garantir a resistência das vigas à força longitudinal adicional provocada pelo momento torsor;

- O código MC10 tende a sobrestimar a resistência à torção das vigas construídas com betões de alta resistência, independentemente do tipo de secção. O limite da tensão nas escoras de betão requer ser revista para evitar roturas frágeis por compressão nas escoras de betão;

- Os códigos EC2 e CSA A23.3-04 tendem a sobrestimar a resistência à torção de vigas com taxas de armadura elevadas, independentemente do tipo de secção ou da classe do betão. Também para estes códigos, o limite da tensão nas escoras do betão requer ser revisto para evitar roturas frágeis;

No global e no que toca à previsão da capacidade resistente das vigas em estudo sujeitas à torção pura, o código que demonstrou estar mais do lado da segurança foi o código americano ACI 318R-14, enquanto que o código que demonstrou estar menos do lado da segurança foi o código canadiano CSA A23.3-04. Já o código que demonstrou estar mais perto do comportamento real das vigas e com grau de segurança satisfatório foi o código

ACI 318R-89 (único código, de entre os analisados, cujo modelo base não é a Analogia da Treliça Espacial e atualmente já não está em vigor), enquanto que o código EC2 apresentou resultados médios muito próximos da unidade para o ratio entre o momento torsor resistente real e normativo.

5.1.6. Estudo experimental do comportamento torsional de vigas pré-esforçadas com betões de alta resistência e secção vazada.

Tendo por base o tratamento dos resultados experimentais obtidos em ensaios à torção previamente realizados e envolvendo vigas pré-esforçadas com betões de alta resistência e secções vazadas, foi possível demonstrar a eficácia do pré-esforço longitudinal em retardar a fissuração e aumentar a resistência à torção. Após a fissuração, a armadura de pré-esforço longitudinal passa a comportar-se efetivamente como uma armadura ordinária, contribuindo assim para o estado de equilíbrio interno das vigas. Apesar do número limitado de resultados associados às vigas ensaiadas, os mesmos mostraram que o nível de pré-esforço longitudinal pode influenciar o modo de rutura da viga. Observou-se também que, à medida que o nível de pré-esforço aumenta, o risco de rutura frágil por esmagamento do betão nas escoras também aumenta. Portanto, neste tipo de vigas, o nível de tensões de compressão nas escoras de betão deve ser cuidadosamente controlado e a contribuição da armadura de pré-esforço não deve ser desprezada. Este problema torna-se mais importante em vigas construídas com betões de alta resistência, pois o betão de alta resistência possui um caráter mais frágil do que o betão de resistência normal. De fato, o intervalo de taxas de armadura que levam a que as vigas vazadas tenham um comportamento dúctil sob torção é maior nas vigas construídas por betões de resistência normal do que em vigas construídas por betões de alta resistência [5].

Os resultados mostraram que a utilização do pré-esforço longitudinal não apresentou grandes alterações no comportamento das vigas ensaiadas na fase de fissuração. Contudo, apesar do número limitado de resultados apresentados, os mesmos mostram que existem diferenças percetíveis no comportamento global das vigas ensaiadas. Com este estudo, tornou-se óbvio que alguns aspetos particulares do comportamento de vigas pré-esforçadas com betões de alta resistência e secção vazada precisam de ser mais aprofundados.

5.2. Recomendações para trabalhos futuros.

O presente trabalho contribuiu para o desenvolvimento de campos específicos do estudo do comportamento de vigas de betão estrutural sujeitas à torção. No entanto, vários aspetos ficaram ainda por esclarecer, o que demonstra que a problemática da torção em vigas de betão estrutural constitui ainda uma área de investigação atual e em desenvolvimento. Assim, para cada assunto estudado e apresentado neste trabalho, são sugeridos futuros

estudos que poderão ajudar a compreender melhor e a desenvolver os modelos para vigas de betão estrutural em torção.

Na área da modelação do comportamento de vigas de betão estrutural sujeitas à torção pura e torção combinada com outros esforços, considera-se importante o desenvolvimento dos seguintes estudos:

- Generalização do modelo MVATM para a incorporação de pré-esforço transversal nas paredes de vigas com secção vazada e estudar a sua efetividade nos problemas de torção.

- Novos estudos experimentais focados no comportamento do betão à tração em vigas sujeitas à torção, afim de refinar a respetiva lei constitutiva média. Aprofundar o estudo da fissuração de vigas de betão armado sujeita à torção, em particular a previsão da fissuração para as cargas de serviço.

- Generalização e validação do procedimento CA-STM refinado com procedimento de cálculo eficiente para combinações de carregamento mais gerais.

Na área da segurança ao estado limite último de vigas de betão armado sujeitas à torção, considera-se importante o desenvolvimento dos seguintes estudos:

- Realização de novos ensaios focados especificamente no estudo da ductilidade em torção e na capacidade de rotação plástica em torção de vigas de betão armado com secção cheia e vazada sujeitas;

- Estudo da influência da microfissuração do betão comprimido nas escoras na ductilidade em torção de vigas;

- Refinamento de modelos teóricos baseados na Analogia da Treliça Espacial para o comportamento pós-pico de vigas de betão armado em torção, em particular o comportamento dúctil;

- Alargamento do estudo da ductilidade a vigas pré-esforçadas sujeitas à torção e a vigas com outro tipo de secções para além das retangulares (do tipo “T”, “U” e “L”);

- Estudo de propostas para alteração das disposições normativas dos códigos em vigor com o objetivo de melhorar a fiabilidade do cálculo da resistência e a garantia da ductilidade em torção de vigas de betão armado.

Bibliografia

[1] ACI Committee 318. (2014). *Building code requirements for reinforced concrete (ACI 318-14) and commentary (ACI 318R-14)*. American Concrete Institute, MI. Detroit.

[2] Belarbi, A. and Hsu, T. T. C. (1994). Constitutive laws of concrete in tension and reiforcing bars stiffened by concrete. *Structural Journal of American Concrete Institute*. **91**(4): 465-474.

[3] Bernardo, L. F. A., Andrade, J. M. A. and Lopes, S. M. R. (2012a). Modefied variable angle truss-model for torsion in reinforced concrete beams. *Materials and Structures*. **45**(12): 1877-1902.

[4] Bernardo, L. F. A, Andrade, J. M. A. and Nunes, N. C. G. (2015). Generalized softened variable angle truss-model for reinforcement concrete beams under torsion. *Materials and Structures*. **48**: 2169-2193.

[5] Bernardo, L. F. A. and Lopes, S. M. R. (2009). Torsion in HSC hollow beams: strength and ductility analysis. *ACI Structural Journal*. **106**(1): 39-48.

[6] CEB-FIP. (2013). *Model code for concrete structures 2010*. Comité Euro-International du Béton – Fédération Internationale du Betón. Suisse.

[7] CSA Standard. (2014). *Design of concrete structures – CSA A23.3-14*. Missisauga: e Standards Association.

[8] Greene, G. and Belarbi, A. (2009a). Model for RC members under torsion, bending and shear. I: Theory. *Journal of Engineering Mechanics*. **135**(9): 961-969.

[9] Hsu, T. T. C. (1984). *Torsion of reinforced concrete*. Van Nostrand Reinhold Company.

[10] Jeng, C. H. (2015). Unified softened membrane model for torsion in hollow and solid reinforced concrete members: Modeling precracking and postcracking behavior. *Journal of Structural Engineering*. **141**(10).

[11] Jeng, C. H., Chiu, H. J. and Chen, C. S. (2010). Modelling the initial stresses in prestressed concrete members under torsion. *Structures Congress*; ASCE: Orlando, USA. pp. 1773-1781.

[12] Jeng, C. H. and Hsu, T. T. C. (2009). A softened membrane model for torsion in reinforced concrete members. *Engineering Structures*, **31**: 1944-1954.

[13] NP EN 1992-1-1. (2010). *Eurocode 2: Design of concrete structures – Part 1: General rules and rules for buildings*.

[14] Rausch, E. (1929). *Berechnung des eisenbetons gegen verdrehung (Design of reinforced concrete in torsion)*. Ph.D Thesis. Berlin. 53 pp. (em Alemão, citado em [9]).

Anexos

Anexo I. Código em MATLAB do CA-STM refinado com procedimento de cálculo eficiente

Script para iniciar o CA-STM

```
%////////////////////////////////////////////////////////////////////////
% CA-STM - COMBINED ACTION SOFTENED TRUSS MODEL                         /
%////////////////////////////////////////////////////////////////////////

% INICIO
////////////////////////////////////////////////////////////////////////
tic; clear all; clc; global eds1

% DADOS DE ENTRADA
% ////////////////////////////////////////////////////////////////////
DADOS_INICIAIS;

% EXTENSÃO DE COMPRESSÃO INICIAL DO PAINEL 1//////////////////////////
eds1 = -0.01;

% CÁLCULO DA ESTIMATIVA INICIAL///////////////////////////////////////
EST_CAMCTM(eds1);

% SOLUÇÃO DO SISTEMA//////////////////////////////////////////////////
COMP_CASTM;

% CURVAS CARGA-DEFORMAÇÃO/////////////////////////////////////////////
toc; PLOT_CASTM;
```

Função para a escolha da viga de referência (T+M)

```
function DADOS_INICIAIS
%//////////////////////////////////////////////////////////////////////////
% SELEÇÃO DA VIGA A ANALISAR
%//////////////////////////////////////////////////////////////////////////

disp('Selecione os dados iniciais');
disp(' ');
disp('1  - McMullen_and_Warwaruk_11 (M/T=0)');
disp('2  - McMullen_and_Warwaruk_12');
disp('3  - McMullen_and_Warwaruk_13');
disp('4  - McMullen_and_Warwaruk_14');
disp('5  - McMullen_and_Warwaruk_15');
disp('6  - McMullen_and_Warwaruk_16');
disp('7  - McMullen_and_Warwaruk_21 (M/T=0)');
disp('8  - McMullen_and_Warwaruk_22');
disp('9  - McMullen_and_Warwaruk_23');
disp('10 - McMullen_and_Warwaruk_24');
disp('11 - McMullen_and_Warwaruk_25');
disp('12 - McMullen_and_Warwaruk_31');
disp('13 - McMullen_and_Warwaruk_32');
disp('14 - McMullen_and_Warwaruk_33');
disp('15 - McMullen_and_Warwaruk_34');
disp('16 - McMullen_and_Warwaruk_35');
disp('17 - McMullen_and_Warwaruk_41');
disp('18 - McMullen_and_Warwaruk_42');
disp('19 - McMullen_and_Warwaruk_43');
disp('20 - McMullen_and_Warwaruk_44');
disp('21 - McMullen_and_Warwaruk_45');
disp('22 - McMullen_and_Warwaruk_46');
%
disp('26 - Lampert_and_Thurlimann_TB0');
disp('27 - Lampert_and_Thurlimann_TB1');
disp('28 - Lampert_and_Thurlimann_TB2');
disp('29 - Lampert_and_Thurlimann_TB3');
disp('30 - Lampert_and_Thurlimann_TB4');
disp('31 - Lampert_and_Thurlimann_TB5');
disp('32 - Lampert_and_Thurlimann_TB6');
%
disp('41 - Winston_Onsongo_TBS1');
disp('42 - Winston_Onsongo_TBS2');
disp('43 - Winston_Onsongo_TBS3');
disp('44 - Winston_Onsongo_TBS4');
disp('45 - Winston_Onsongo_TBO2');
disp('46 - Winston_Onsongo_TBO3');
disp('47 - Winston_Onsongo_TBO4');
disp('48 - Winston_Onsongo_TBO5');
disp('49 - Winston_Onsongo_TBU2');
disp('50 - Winston_Onsongo_TBU3');
disp('51 - Winston_Onsongo_TBU4');
disp('52 - Winston_Onsongo_TBU5');
%
disp('73 - Pandit_and_Warwaruk_B-2')
disp('74 - Pandit_and_Warwaruk_B-3')
disp('741 - Pandit_and_Warwaruk_B-4 (M/T=0)')
disp('75 - Pandit_and_Warwaruk_C-1')
disp('76 - Pandit_and_Warwaruk_C-2')
disp('77 - Pandit_and_Warwaruk_C-3')
```

```
disp('771 - Pandit_and_Warwaruk_C-4 (M/T=0)')
disp('78 - Pandit_and_Warwaruk_D-1')
disp('79 - Pandit_and_Warwaruk_D-2')
disp('80 - Pandit_and_Warwaruk_D-3')
disp('801 - Pandit_and_Warwaruk_D-4 (M/T=0)')
disp('81 - Pandit_and_Warwaruk_E-1')
disp('82 - Pandit_and_Warwaruk_E-2')
disp('821 - Pandit_and_Warwaruk_E-3 (M/T=0)')
disp('83 - Goode_and_Helmy_III.1')
disp('84 - Goode_and_Helmy_III.2')
disp('85 - Goode_and_Helmy_III.3')
disp('86 - Goode_and_Helmy_III.4')
disp('87 - Goode_and_Helmy_IV.1')
disp('88 - Goode_and_Helmy_IV.2')
disp('89 - Goode_and_Helmy_IV.3')
disp('90 - Goode_and_Helmy_IV.4')
disp('91 - Goode_and_Helmy_V.1')
disp('92 - Goode_and_Helmy_V.2')
disp('93 - Goode_and_Helmy_V.3')
disp('94 - Goode_and_Helmy_V.4')
disp('95 - Goode_and_Helmy_VI.1')
disp('96 - Goode_and_Helmy_VI.2')
disp('97 - Goode_and_Helmy_VI.3')
disp('98 - Goode_and_Helmy_VI.4')
disp('99 - Collins_et_al_RE1')
disp('100 - Collins_et_al_RE2')
disp('101 - Collins_et_al_RE3')
disp('102 - Collins_et_al_RE4')
disp('103 - Collins_et_al_RE5')
disp('104 - Collins_et_al_RE4x')
disp('105 - Collins_et_al_RU1')
disp('106 - Collins_et_al_RU3Ax')
disp('107 - Collins_et_al_RU2xx')
disp('108 - Collins_et_al_RU3xx')
disp('109 - Collins_et_al_RU3Axx')
disp('110 - Collins_et_al_RU4')
disp('111 - Collins_et_al_RU5')
disp('112 - Collins_et_al_RU5A')
disp('113 - Collins_et_al_RU6')
disp('114 - Kemp_BT2')
disp('115 - Kemp_BT3')
disp('116 - Kemp_BT4')
disp('117 - Kemp_BT5')
disp('1171 - Kemp_TT6 (M/T=0)')
disp('118 - Kemp_BBT3')
disp('119 - Kemp_BBT4')
disp('120 - Kemp_BBT6')
disp('1201 - Kemp_BT1')
disp('121 - Iyengar_and_Rangan_V1')
disp('122 - Iyengar_and_Rangan_V2')
disp('123 - Iyengar_and_Rangan_V3')
disp('124 - Iyengar_and_Rangan_V5')
disp('125 - Iyengar_and_Rangan_V6')
disp('1251 - Iyengar_and_Rangan_V4I (M/T=0)')
disp('126 - Iyengar_and_Rangan_S1II')
disp('127 - Iyengar_and_Rangan_S2I')
disp('128 - Iyengar_and_Rangan_S2II')
disp('129 - Iyengar_and_Rangan_S3')
disp('130 - Iyengar_and_Rangan_S4I')
disp('131 - Iyengar_and_Rangan_S4II')
disp('132 - Iyengar_and_Rangan_S5I')
```

```
disp('133 - Iyengar_and_Rangan_S5II')
disp('1331 - Iyengar_and_Rangan_S6 (M/T=0)')
disp('134 - Iyengar_and_Rangan_L1-2II')
disp('135 - Iyengar_and_Rangan_L2-1II')
disp('136 - Iyengar_and_Rangan_L2-2II')
disp('137 - Iyengar_and_Rangan_L3-1I')
disp('138 - Iyengar_and_Rangan_L3-1II')
disp('139 - Iyengar_and_Rangan_L3-2I')
disp('140 - Iyengar_and_Rangan_L3-2II')
disp('141 - Iyengar_and_Rangan_L4-1')
disp('142 - Iyengar_and_Rangan_L4-2')
disp('143 - Iyengar_and_Rangan_L5-1')
disp('144 - Iyengar_and_Rangan_L5-2')
disp('145 - Iyengar_and_Rangan_L6-1I')
disp('146 - Iyengar_and_Rangan_L6-2I')
disp('1461 - Iyengar_and_Rangan_L1-1 (M/T=0)')


disp(' ');
disp('200 - Introduzir manualmente os dados iniciais');
disp(' ');
disp('0 - Sair');
disp(' ');
IND = input('Escolha uma opção: ');

if IND >= 0
    switch IND
        case 1
            McMullen_and_Warwaruk_11;
        case 2
            McMullen_and_Warwaruk_12;
        case 3
            McMullen_and_Warwaruk_13;
        case 4
            McMullen_and_Warwaruk_14;
        case 5
            McMullen_and_Warwaruk_15;
        case 6
            McMullen_and_Warwaruk_16;
        case 7
            McMullen_and_Warwaruk_21;
        case 8
            McMullen_and_Warwaruk_22;
        case 9
            McMullen_and_Warwaruk_23;
        case 10
            McMullen_and_Warwaruk_24;
        case 11
            McMullen_and_Warwaruk_25;
        case 12
            McMullen_and_Warwaruk_31;
        case 13
            McMullen_and_Warwaruk_32;
        case 14
            McMullen_and_Warwaruk_33;
        case 15
            McMullen_and_Warwaruk_34;
        case 16
            McMullen_and_Warwaruk_35;
        case 17
            McMullen_and_Warwaruk_41;
```

```
case 18
    McMullen_and_Warwaruk_42;
case 19
    McMullen_and_Warwaruk_43;
case 20
    McMullen_and_Warwaruk_44;
case 21
    McMullen_and_Warwaruk_45;
case 22
   McMullen_and_Warwaruk_46;
case 26
    Lampert_and_Thurlimann_TB0;
case 27
    Lampert_and_Thurlimann_TB1;
case 28
    Lampert_and_Thurlimann_TB2;
case 29
    Lampert_and_Thurlimann_TB3;
case 30
    Lampert_and_Thurlimann_TB4;
case 31
    Lampert_and_Thurlimann_TB5;
case 32
    Lampert_and_Thurlimann_TB6;
case 41
    Winston_Onsongo_TBS1;
case 42
    Winston_Onsongo_TBS2;
case 43
    Winston_Onsongo_TBS3;
case 44
    Winston_Onsongo_TBS4;
case 45
    Winston_Onsongo_TBO2;
case 46
    Winston_Onsongo_TBO3;
case 47
    Winston_Onsongo_TBO4;
case 48
    Winston_Onsongo_TBO5;
case 49
    Winston_Onsongo_TBU2;
case 50
    Winston_Onsongo_TBU3;
case 51
    Winston_Onsongo_TBU4;
case 52
    Winston_Onsongo_TBU5;
case 73
    Pandit_and_Warwaruk_B2;
case 74
    Pandit_and_Warwaruk_B3;
case 741
    Pandit_and_Warwaruk_B4;
case 75
    Pandit_and_Warwaruk_C1;
case 76
    Pandit_and_Warwaruk_C2;
case 77
    Pandit_and_Warwaruk_C3;
case 771
```

```
        Pandit_and_Warwaruk_C4;
    case 78
        Pandit_and_Warwaruk_D1;
    case 79
        Pandit_and_Warwaruk_D2;
    case 80
        Pandit_and_Warwaruk_D3;
    case 801
        Pandit_and_Warwaruk_D4;
    case 81
        Pandit_and_Warwaruk_E1;
    case 82
        Pandit_and_Warwaruk_E2;
    case 821
        Pandit_and_Warwaruk_E3;
    case 83
        Goode_and_Helmy_III1;
    case 84
        Goode_and_Helmy_III2;
    case 85
        Goode_and_Helmy_III3;
    case 86
        Goode_and_Helmy_III4;
    case 87
        Goode_and_Helmy_IV1;
    case 88
        Goode_and_Helmy_IV2;
    case 89
        Goode_and_Helmy_IV3;
    case 90
        Goode_and_Helmy_IV4;
    case 91
        Goode_and_Helmy_V1;
    case 92
        Goode_and_Helmy_V2;
    case 93
        Goode_and_Helmy_V3;
    case 94
        Goode_and_Helmy_V4;
    case 95
        Goode_and_Helmy_VI1;
    case 96
        Goode_and_Helmy_VI2;
    case 97
        Goode_and_Helmy_VI3;
    case 98
        Goode_and_Helmy_VI4;
    case 99
        Collins_et_al_RE1;
    case 100
        Collins_et_al_RE2;
    case 101
        Collins_et_al_RE3;
    case 102
        Collins_et_al_RE4;
    case 103
        Collins_et_al_RE5;
    case 104
        Collins_et_al_RE4x;
    case 105
        Collins_et_al_RU1;
```

```
case 106
    Collins_et_al_RU3Ax;
case 107
    Collins_et_al_RU2xx;
case 108
    Collins_et_al_RU3xx;
case 109
    Collins_et_al_RU3Axx;
case 110
    Collins_et_al_RU4;
case 111
    Collins_et_al_RU5;
case 112
    Collins_et_al_RU5A;
case 113
    Collins_et_al_RU6;
case 114
    Kemp_BT2;
case 115
    Kemp_BT3;
case 116
    Kemp_BT4;
case 117
    Kemp_BT5;
case 1171
    Kemp_TT6;
case 118
    Kemp_BBT3;
case 119
    Kemp_BBT4;
case 120
    Kemp_BBT6;
case 1201
    Kemp_BT1;
case 121
    Iyengar_and_Rangan_V1;
case 122
    Iyengar_and_Rangan_V2;
case 123
    Iyengar_and_Rangan_V3;
case 124
    Iyengar_and_Rangan_V5;
case 125
    Iyengar_and_Rangan_V6;
case 1251
    Iyengar_and_Rangan_V4I;
case 126
    Iyengar_and_Rangan_S1II;
case 127
    Iyengar_and_Rangan_S2I;
case 128
    Iyengar_and_Rangan_S2II;
case 129
    Iyengar_and_Rangan_S3;
case 130
    Iyengar_and_Rangan_S4I;
case 131
    Iyengar_and_Rangan_S4II;
case 132
    Iyengar_and_Rangan_S5I;
case 133
```

```
            Iyengar_and_Rangan_S5II;
        case 1331
            Iyengar_and_Rangan_S6;
        case 134
            Iyengar_and_Rangan_L1_2II;
        case 135
            Iyengar_and_Rangan_L2_1II;
        case 136
            Iyengar_and_Rangan_L2_2II;
        case 137
            Iyengar_and_Rangan_L3_1I;
        case 138
            Iyengar_and_Rangan_L3_1II;
        case 139
            Iyengar_and_Rangan_L3_2I;
        case 140
            Iyengar_and_Rangan_L3_2II;
        case 141
            Iyengar_and_Rangan_L4_1;
        case 142
            Iyengar_and_Rangan_L4_2;
        case 143
            Iyengar_and_Rangan_L5_1;
        case 144
            Iyengar_and_Rangan_L5_2;
        case 145
            Iyengar_and_Rangan_L6_1I;
        case 146
            Iyengar_and_Rangan_L6_2I;
        case 1461
            Iyengar_and_Rangan_L1_1;

        case 200
            INTRODUZIR_DADOS;
        case 0
            error('SCRIPT INTERROMPIDO!')
            clc
    end
end
end
```

Função para o cálculo da estimativa inicial

```
function EST_CAMCTM(eds1)
%////////////////////////////////////////////////////////////////////////
% ESTIMATIVA INICIAL - COMPORTAMENTO LINEAR DE UM PAINEL SUBMETIDO      /
%                      A UM ESTADO DE TENSÃO DE CORTE PURO              /
%////////////////////////////////////////////////////////////////////////
global x fcm b h

% Perímetro externo da secção:
pcp = 2*(b+h);

% Área inclusa pelo perímetro externo da secção:
Acp = b*h;

% NBR-6118/2007 - Módulo de elasticidade secante do betão:
Ecc = 0.85*5600*sqrt(fcm);

for i = 1:3
    x(i) = eds1;
end

for i = 4:7
    x(i) = (-eds1)/2;
    x(i+4) = 0;
    x(i+8) = 1;
end
    x(16) = eds1*10^-3*(-Ecc/2)*(Acp^2/pcp);
end
```

Função do CA-STM

```
function F = CASTM(x,eds1)
%////////////////////////////////////////////////////////////////////////
% CA-STM - COMPORTAMENTO NÃO LINEAR DA SECÇÃO                           /
%////////////////////////////////////////////////////////////////////////
global h b t1 t2 t3 t4 Al1 Al2 Al3 Al4 At s fLy fTy Es
global fcm e0 ecr TETA Tcr MyTx MzTx VyTx VzTx NxTx Mz fiL24

% Área inclusa pelo perímetro externo da secção:
Acp = b*h;

% Área bruta da secção:
Ag = (b-t1)*t4 + (h-t2)*t1 + (b-t3)*t2 + (h-t4)*t3;

% Tensão de fissuração do betão:
fcr = 0.5*Ag/Acp*sqrt(fcm);

% Deformação de cedência da armadura longitudinal (1/1000):
eLy = fLy/Es*1000;

% Deformação de cedência da armadura transversal:
eTy = fTy/Es;

% Perímetro externo da secção:
pcp = 2*(b+h);

% Momento torsor de fissuração:
Tcr = 1/3*sqrt(fcm)*(Acp^2/pcp);

% COMBINED ACTION SOFTENED TRUSS MODEL (CA-STM)//////////////////////////
% Relação dos outros esforços com o momento torsor:
Tx = Tcr*x(16);
My = MyTx*Tx;
Mz = MzTx*Tx;
Vy = VyTx*Tx;
Vz = VzTx*Tx;
Nx = NxTx*Tx;

% Espessura do fluxo e deformação interna do painel:
if x(12) < 2
    td1 = x(12)*t1/2;
    ea1 = 0;
else
    td1 = t1;
    ea1 = (x(12) - 2)*eds1*10^-3;
end

if x(13) < 2
    td2 = x(13)*t2/2;
    ea2 = 0;
else
    td2 = t2;
    ea2 = (x(13) - 2)*x(1)*10^-3;
end

if x(14) < 2
```

```
    td3 = x(14)*t3/2;
    ea3 = 0;
else
    td3 = t3;
    ea3 = (x(14) - 2)*x(2)*10^-3;
end

if x(15) < 2
    td4 = x(15)*t4/2;
    ea4 = 0;
else
    td4 = t4;
    ea4 = (x(15) - 2)*x(3)*10^-3;
end

% Base do fluxo de tensões tangenciais:
b0 = b - (td1 + td3)/2;

% Altura do fluxo de tensões tangenciais:
h0 = h - (td2 + td4)/2;

% Área inclusa pelo fluxo de tensões tangenciais:
A0 = b0*h0;

% Deformação principal de compressão nos painéis:
eD1 = (eds1*10^-3 + ea1)/2;
eD2 = (x(1)*10^-3 + ea2)/2;
eD3 = (x(2)*10^-3 + ea3)/2;
eD4 = (x(3)*10^-3 + ea4)/2;

% Curvaturas longitudinais:
fiL13 = (x(8)*10^-3 - x(10)*10^-3)/b0;
fiL24 = (x(9)*10^-3 - x(11)*10^-3)/h0;

% Princípio da invariância das extensões:
eT1 = x(4)*10^-3 + eD1 - x(8)*10^-3;
eT2 = x(5)*10^-3 + eD2 - x(9)*10^-3;
eT3 = x(6)*10^-3 + eD3 - x(10)*10^-3;
eT4 = x(7)*10^-3 + eD4 - x(11)*10^-3;

% Curvaturas transversais:
fiT13 = (eT1 - eT3)/b0;
fiT24 = (eT2 - eT4)/h0;

% Taxa de armadura longitudinal e transversal:
roL1= (Al1/(td1*h0));
roL2= (Al2/(td2*b0));
roL3= (Al3/(td3*h0));
roL4= (Al4/(td4*b0));
roT1= At/(td1*s);
roT2= At/(td2*s);
roT3= At/(td3*s);
roT4= At/(td4*s);


% Coeficiente de amolecimento:
R = 5.8/(sqrt(fcm));
if   R <= 0.9
    R_linha = R;
```

```
else
    R_linha = 0.9;
end

n1 = (roT1*fTy)/(roL1*fLy);
if   n1 <= 1
    n1_linha = n1;
else
    n1_linha = 1/n1;
end
zeta1 = R_linha/(sqrt(1+((0.4*x(4))/n1_linha)));

n2 = (roT2*fTy)/(roL2*fLy);
if  n2 <= 1
    n2_linha = n2;
else
    n2_linha = 1/n2;
end

zeta2 = R_linha/(sqrt(1+((0.4*x(5))/n2_linha)));

n3 = (roT3*fTy)/(roL3*fLy);
if   n3 <= 1
    n3_linha = n3;
else
    n3_linha = 1/n3;
end

zeta3 = R_linha/(sqrt(1+((0.4*x(6))/n3_linha)));

n4 = (roT4*fTy)/(roL4*fLy);
if   n4 <= 1
    n4_linha = n4;
else
    n4_linha = 1/n4;
end

zeta4 = R_linha/(sqrt(1+((0.4*x(7))/n4_linha)));

% Relação entre a resistência à compressão no pico e a resistência
% média:
if  eds1*10^-3 / (zeta1*e0) <= 1
    k1D1 = eds1*10^-3/(zeta1*e0) - (eds1*10^-3)^2/(3*(zeta1*e0)^2);
else
    k1D1 = 1 - zeta1*e0/(3*eds1*10^-3) - (eds1*10^-3 -
zeta1*e0)^3/(3*eds1*10^-3*(4*e0-zeta1*e0)^2);
end

if  x(1)*10^-3 / (zeta2*e0) <= 1
    k1D2 = x(1)*10^-3/(zeta2*e0) - (x(1)*10^-3)^2/(3*(zeta2*e0)^2);
else
    k1D2 = 1 - zeta2*e0/(3*x(1)*10^-3) - (x(1)*10^-3 -
zeta2*e0)^3/(3*x(1)*10^-3*(4*e0-zeta2*e0)^2);
end

if  x(2)*10^-3 / (zeta3*e0) <= 1
    k1D3 = x(2)*10^-3/(zeta3*e0) - (x(2)*10^-3)^2/(3*(zeta3*e0)^2);
else
```

```
    k1D3 = 1 - zeta3*e0/(3*x(2)*10^-3) - (x(2)*10^-3 -
zeta3*e0)^3/(3*x(2)*10^-3*(4*e0-zeta3*e0)^2);
end

if x(3)*10^-3 / (zeta4*e0) <= 1
    k1D4 = x(3)*10^-3/(zeta4*e0)  - (x(3)*10^-3)^2/(3*(zeta4*e0)^2);
else
    k1D4 = 1 - zeta4*e0/(3*x(3)*10^-3) - (x(3)*10^-3 -
zeta4*e0)^3/(3*x(3)*10^-3*(4*e0-zeta4*e0)^2);
end

% Tensão principal de compressão no betão:
sigmaD1 = -zeta1*fcm*k1D1;
sigmaD2 = -zeta2*fcm*k1D2;
sigmaD3 = -zeta3*fcm*k1D3;
sigmaD4 = -zeta4*fcm*k1D4;

% Extensão principal de tração na face externa dos painéis:
ers1 = 2*x(4);
ers2 = 2*x(5);
ers3 = 2*x(6);
ers4 = 2*x(7);

% Relação entre a resistência à tração no pico e a resistência
% média:
if ers1 <= ecr
    k1R1 = ers1/(2*ecr);
else
    k1R1 = ecr/(2*ers1) + ecr^0.4/(0.6*ers1)*((ers1)^0.6 - (ecr)^0.6);
end

if ers2 <= ecr
    k1R2 = ers2/(2*ecr);
else
    k1R2 = ecr/(2*ers2) + ecr^0.4/(0.6*ers2)*((ers2)^0.6 - (ecr)^0.6);
end

if ers3 <= ecr
    k1R3 = ers3/(2*ecr);
else
    k1R3 = ecr/(2*ers3) + ecr^0.4/(0.6*ers3)*((ers3)^0.6 - (ecr)^0.6);
end

if ers4 <= ecr
    k1R4 = ers4/(2*ecr);
else
    k1R4 = ecr/(2*ers4) + ecr^0.4/(0.6*ers4)*((ers4)^0.6 - (ecr)^0.6);
end

% Tensão principal de tração no betão:
sigmaR1 = k1R1*fcr;
sigmaR2 = k1R2*fcr;
sigmaR3 = k1R3*fcr;
sigmaR4 = k1R4*fcr;

% Tensão na armadura trasnversal:
BT1 = (1/(At/(td1*s)))*(fcr/fTy)^1.5;
enT1 = eTy*(0.93-2*BT1);
if eT1 <= enT1
    fT1  = eT1*Es;
```

```
else
    fT1 = fTy*((0.91-2*BT1)+(0.02+0.25*BT1)*(eT1/eTy));
end

BT2  = (1/(At/(td2*s)))*(fcr/fTy)^1.5;
enT2 = eTy*(0.93-2*BT2);
if eT2 <= enT2
    fT2  = eT2*Es;
else
    fT2 = fTy*((0.91-2*BT2)+(0.02+0.25*BT2)*(eT2/eTy));
end

BT3  = (1/(At/(td3*s)))*(fcr/fTy)^1.5;
enT3 = eTy*(0.93-2*BT3);
if eT3 <= enT3
    fT3  = eT3*Es;
else
    fT3 = fTy*((0.91-2*BT3)+(0.02+0.25*BT3)*(eT3/eTy));
end

BT4  = (1/(At/(td4*s)))*(fcr/fTy)^1.5;
enT4 = eTy*(0.93-2*BT4);
if eT4 <= enT4
    fT4  = eT4*Es;
else
    fT4 = fTy*((0.91-2*BT4)+(0.02+0.25*BT4)*(eT4/eTy));
end

% sin(alfaD)^2:
sin21 = ((x(8)*10^-3) - eD1)/((x(4)*10^-3) - eD1);
sin22 = ((x(9)*10^-3) - eD2)/((x(5)*10^-3) - eD2);
sin23 = ((x(10)*10^-3) - eD3)/((x(6)*10^-3) - eD3);
sin24 = ((x(11)*10^-3) - eD4)/((x(7)*10^-3) - eD4);

% cos(alfaD)^2:
cos21 = ((x(4)*10^-3) - (x(8)*10^-3))/((x(4)*10^-3) - eD1);
cos22 = ((x(5)*10^-3) - (x(9)*10^-3))/((x(5)*10^-3) - eD2);
cos23 = ((x(6)*10^-3) - (x(10)*10^-3))/((x(6)*10^-3) - eD3);
cos24 = ((x(7)*10^-3) - (x(11)*10^-3))/((x(7)*10^-3) - eD4);

% sin(alfaD)*cos(alfaD):
sincos1 = sqrt(((x(8)*10^-3) - eD1)*(eT1 - eD1))/((x(4)*10^-3) - eD1);
sincos2 = sqrt(((x(9)*10^-3) - eD2)*(eT2 - eD2))/((x(5)*10^-3) - eD2);
sincos3 = sqrt(((x(10)*10^-3) - eD3)*(eT3 - eD3))/((x(6)*10^-3) - eD3);
sincos4 = sqrt(((x(11)*10^-3) - eD4)*(eT4 - eD4))/((x(7)*10^-3) - eD4);

% Equação de equilíbrio transversal:
F(1) = sigmaD1*sin21 + sigmaR1*cos21 + fT1*(At/(td1*s));
F(2) = sigmaD2*sin22 + sigmaR2*cos22 + fT2*(At/(td2*s));
F(3) = sigmaD3*sin23 + sigmaR3*cos23 + fT3*(At/(td3*s));
F(4) = sigmaD4*sin24 + sigmaR4*cos24 + fT4*(At/(td4*s));

% Cálculo dos Fluxos:
q1 = Tx/(2*A0) + Vy/(2*h0);
q2 = Tx/(2*A0) + Vz/(2*b0);
q3 = Tx/(2*A0) - Vy/(2*h0);
q4 = Tx/(2*A0) - Vz/(2*b0);

% Distorção nos painéis:
gamaLT1 = 2*((x(4)*10^-3) - eD1)*sincos1*sign(q1);
```

```
gamaLT2 = 2*((x(5)*10^-3) - eD2)*sincos2*sign(q2);
gamaLT3 = 2*((x(6)*10^-3) - eD3)*sincos3*sign(q3);
gamaLT4 = 2*((x(7)*10^-3) - eD4)*sincos4*sign(q4);

% Ângulo Teta:
TETA = ((gamaLT1 + gamaLT3)*h0 + (gamaLT2 + gamaLT4)*b0)/(2*A0);

% Curvatura da escora:
curv1a = -((eds1*10^-3) - ea1)/td1;
curv2a = -((x(1)*10^-3) - ea2)/td2;
curv3a = -((x(2)*10^-3) - ea3)/td3;
curv4a = -((x(3)*10^-3) - ea4)/td4;

curv1b = TETA*2*sincos1 - fiL13*cos21 - fiT13*sin21;
curv2b = TETA*2*sincos2 - fiL24*cos22 - fiT24*sin22;
curv3b = TETA*2*sincos3 + fiL13*cos23 + fiT13*sin23;
curv4b = TETA*2*sincos4 + fiL24*cos24 + fiT24*sin24;

F(5) = curv1a - curv1b;
F(6) = curv2a - curv2b;
F(7) = curv3a - curv3b;
F(8) = curv4a - curv4b;

% Tensão tangencial:
tal1a = q1/td1;
tal2a = q2/td2;
tal3a = q3/td3;
tal4a = q4/td4;

tal1b = (-sigmaD1 + sigmaR1)*sincos1*sign(q1);
tal2b = (-sigmaD2 + sigmaR2)*sincos2*sign(q2);
tal3b = (-sigmaD3 + sigmaR3)*sincos3*sign(q3);
tal4b = (-sigmaD4 + sigmaR4)*sincos4*sign(q4);

F(9) = tal1a-tal1b;
F(10) = tal2a - tal2b;
F(11) = tal3a - tal3b;
F(12) = tal4a - tal4b;

% Tensão na armadura longitudinal:
BL1  = (1/(Al1/(td1*h0)))*(fcr/fLy)^1.5;
enL1 = eLy*10^-3 *(0.93-2*BL1);
if x(8)*10^-3 <= enL1
    fL1  = x(8)*10^-3*Es;
else
    fL1 = fLy*((0.91-2*BL1)+(0.02+0.25*BL1)*(x(8)/eLy));
end

BL2  = (1/(Al2/(td2*b0)))*(fcr/fLy)^1.5;
enL2 = eLy*10^-3 *(0.93-2*BL2);
if x(9)*10^-3 <= enL2
    fL2  = x(9)*10^-3*Es;
else
    fL2 = fLy*((0.91-2*BL2)+(0.02+0.25*BL2)*(x(9)/eLy));
end

BL3  = (1/(Al3/(td3*h0)))*(fcr/fLy)^1.5;
enL3 = eLy*10^-3 *(0.93-2*BL3);
if x(10)*10^-3 <= enL3
```

```
    fL3  = x(10)*10^-3*Es;
else
    fL3 = fLy*((0.91-2*BL3)+(0.02+0.25*BL3)*(x(10)/eLy));
end

BL4  = (1/(Al4/(td4*b0)))*(fcr/fLy)^1.5;
enL4 = eLy*10^-3 *(0.93-2*BL4);
if x(11)*10^-3 <= enL4
    fL4  = x(11)*10^-3*Es;
else
    fL4 = fLy*((0.91-2*BL4)+(0.02+0.25*BL4)*(x(11)/eLy));
end

% Equação de equilíbrio longitudinal:
sigmaL1 = sigmaD1*cos21 + sigmaR1*sin21 + fL1*(Al1/(td1*h0));
sigmaL2 = sigmaD2*cos22 + sigmaR2*sin22 + fL2*(Al2/(td2*b0));
sigmaL3 = sigmaD3*cos23 + sigmaR3*sin23 + fL3*(Al3/(td3*h0));
sigmaL4 = sigmaD4*cos24 + sigmaR4*sin24 + fL4*(Al4/(td4*b0));

% Momento fletor no eixo Y:
F(13) = (sigmaL3*td3*h0 - sigmaL1*td1*h0)*b0/2 - My;

% Momento fletor no eixo Z:
F(14) = (sigmaL4*td4*b0 - sigmaL2*td2*b0)*h0/2 - Mz;

% Esforço normal em X (Eq. 62):
F(15) = sigmaL1*td1*h0 + sigmaL2*td2*b0 + sigmaL3*td3*h0 + sigmaL4*td4*b0
- Nx;

% Compatibilização das deformações longitudinais:
ecL13 = (x(8)*10^-3 + x(10)*10^-3)/2;
ecL24 = (x(9)*10^-3 + x(11)*10^-3)/2;

F(16) = ecL13-ecL24;
end
```

Função para o cálculo do comportamento carga-deformação da viga

```
function COMP_CASTM
%////////////////////////////////////////////////////////////////////////
% CÁLCULO DO COMPORTAMENTO CARGA-DEFORMAÇÃO DA SECÇÃO                    /
%////////////////////////////////////////////////////////////////////////
global eds1 Tcr TETAj Tj x TETA fcm FIL24 MZ Mz fiL24 Mzj


% Limites inferiores e superioes para x(1)-x(16):
lb = [-100; -100; -100; 0; 0; 0; 0; 0; 0; 0; 0; 0; 0; 0; 0; 0];
ub = [0; 0; 0; 100; 100; 100; 100; 100; 100; 100; 100; 3; 3; 3; 3; 100];

nmax = 400;
TETAj(nmax) = 0; Tj(nmax)=0;
for i = 1:nmax
    passo =0.01;

    options = optimset('MaxFunEvals',40000,'MaxIter',50000,'TolX',10^-
8,'TolFun',10^-8);
    x = lsqnonlin(@(x) CASTM(x,eds1-passo*i),x,lb,ub,options);
    TETAj(i) = TETA;
    Tj(i) = x(16)*Tcr*1000;
    FIL24(i) = fiL24;
    MZ(i) = Mz*1000;

    lim = min(min(eds1-passo*i,x(1)),min(x(2),x(3)));

    % Critérios de paragem (betão normal e de alta resistência):
    if fcm <= 50
        if lim < -3.5
            TETAj = TETAj(1:i);
            Tj = Tj(1:i);
            break
        end
    else
        if lim <= -( 2.8 + 27 * ((98-fcm)/100)^4)
            TETAj = TETAj(1:i);
            Tj = Tj(1:i);
            break
        end
    end
end
Tj = [0 Tj];
TETAj = [0 TETAj];
Mzj = [0 MZ];
max(Tj)
TETAj(find(Tj==max(Tj)))
max(Mzj)
Mzj(find(Tj==max(Tj)))
end
```

Função para impressão das curvas carga-deformação da viga

```
function PLOT_CASTM
%////////////////////////////////////////////////////////////////////////
% IMPRESSÃO DAS CURVAS CARGA-DEFORMAÇÃO                                  /
%////////////////////////////////////////////////////////////////////////
global TETAexp Texp TETAteo Tteo TETAj Tj aa bb cc dd FIL24 MZ TETAexp_1
Mzexp_1
global Mzexp FIL24exp Mzj TCI_exp MCI_exp TCI_teo MCI_teo TCI_teog
MCI_teog
% Opção
disp('1 - Curva momento torsor-rotação axial');
disp('2 - Curva momento fletor-rotação axial');
disp('3 - Curva momento fletor-curvatura longitudinal');
disp('4 - Curva de interação');
disp(' ');
disp('5 - Voltar ao inicio');
disp('0 - Sair');
disp(' ');
IND = input('Escolha uma opção: ');

% SELEÇÃO DA CURVA/////////////////////////////////////////////////////
while IND > 0
    switch IND
        case 1
            hold on
            plot(TETAexp,Texp,'-rs','LineWidth',2)
            plot(TETAj,Tj,'--b','LineWidth',2)
            plot(TETAteo,Tteo,'-k','LineWidth',1)
            xlabel('\theta (rad/m)');
            ylabel('T_X (kN.m)');
            legend(aa,...
                bb,...
                cc,'Location','southeast');
            grid on
        case 2
            hold on
            plot(TETAexp_1,Mzexp,'-rs','LineWidth',1.5,'MarkerSize',4)
            plot(TETAj,Mzj,'--b','LineWidth',1.5)
            xlabel('\theta (rad/m)');
            ylabel('M_Z (kN.m)');
            legend(aa,cc,'Location','southeast');
            grid on
        case 3
            hold on
            plot(FIL24exp,Mzexp_1,'-rs','LineWidth',1.5,'MarkerSize',4)
            plot(-FIL24,MZ,'--b','LineWidth',1.5)
            xlabel('\phi_L_,_2_4(rad)');
            ylabel('M_Z (kN.m)');
            legend(aa,cc,'Location','southeast');
            grid on
        case 4
            hold on
            plot(MCI_exp,TCI_exp,'-rs','LineWidth',1.5)
            plot(MCI_teo,TCI_teo,'-bs','LineWidth',1.5)
            plot(MCI_teog,TCI_teog,'-ks','LineWidth',1)
            xlabel('M_Z (kN.m)');
            ylabel('T_X (kN.m)');
            axis ([0 300 0 150]) %auto
```

```
            legend(dd,...
                bb,...
                cc,'Location','southeast');
            grid on
        case 5
            if IND == 5
                INICIO;
                break
            end
    end
    disp(' ');
    IND = input('Escolha uma opção: ');
end
tempo = toc;
end
```

Exemplos de funções para os dados experimentais e de alguns resultados para duas vigas

```
function McMullen_and_Warwaruk_22
%////////////////////////////////////////////////////////////////////////
% Dados experimentais viga 2-2 (McMullen e Warwaruk em 1970)
%////////////////////////////////////////////////////////////////////////
global h b t1 t2 t3 t4 Al1 Al2 Al3 Al4 At s fLy fTy Es fcm e0 ecr ecr0
Acp pcp
global TETAexp Texp TETAteo Tteo MyTx MzTx VyTx VzTx NxTx aa bb cc
global TCI_exp MCI_exp TCI_teo MCI_teo TCI_teog MCI_teog  TETAexp_1 Mzexp
FIL24exp Mzexp_1
%////////////////////////////////////////////////////////////////////////
% DADOS DA SECÇÃO
%////////////////////////////////////////////////////////////////////////

% Geometria da secção:
h = 0.30;              % Altura da secção (m)
b = 0.15;              % Base da secção (m)
% Área inclusa pelo perímetro externo da secção:
Acp = b*h;
% Perímetro externo da secção:
pcp = 2*(b+h);
% Espessura máxima dos painéis (m)
t1 = Acp/pcp; t2 = t1; t3 = t1; t4 = t1;

% Quantidade das armaduras:
Al1 = 2.84*10^-4;     % Área da armadura longitudinal no painel 1 (m2)
Al2 = 2.84*10^-4;     % Área da armadura longitudinal no painel 2 (m2)
Al3 = 2.84*10^-4;     % Área da armadura longitudinal no painel 3 (m2)
Al4 = 2.84*10^-4;     % Área da armadura longitudinal no painel 4 (m2)
At = 7.10*10^-5;      % Área da armadura transversal (m2)
s = 0.083;            % Espaçamento da armadura transversal (m)

% Propriedades Mecânicas dos aços:
fLy = 323.365;        % Tensão de cedência da armadura longitudinal (MPa)
fTy = 370.249;        % Tensão de cedência da armadura transversal (MPa)
Es = 200000;          % Módulo de elasticidade dos aços (MPa)

% Propriedades Mecânicas do betão:
fcm = 34.61;          % Resistência média do betão à compressão (MPa)
e0=(-0.7*(fcm)^0.31)*10^-3; % Extensão de compressão do betão
correspondente à tensão máxima (1/1000)
ecr = 0.116;          % Deformação de tração de fissuração do betão
(1/1000)
ecr0 = 4.5;           % Deformação de tração limite do betão (1/1000)

% Relação dos outros esforços com o momento torsor:
MyTx = 0;             % Momento Fletor y / Momento Torsor x
MzTx = 0.5;           % Momento Fletor z / Momento Torsor x
VyTx = 0;             % Esforço Cortante y / Momento Torsor x
VzTx = 0;             % Esforço Cortante z / Momento Torsor x
NxTx = 0;             % Esforço Normal x / Momento Torsor x

%////////////////////////////////////////////////////////////////////////
% DADOS CURVA EXPERIMENTAL E TÉORICA
%////////////////////////////////////////////////////////////////////////
```

```
TETAexp = [0.0000; 0.0082; 0.0126; 0.0161; 0.0205; 0.0289; 0.0389;
0.0485; 0.0627];
Texp = [0.000; 5.423; 5.649; 7.909; 9.151; 11.185; 13.445; 15.591;
17.738];

TETAexp_1 = [0.0000; 0.0082; 0.0126; 0.0161; 0.0205; 0.0289; 0.0389;
0.0485; 0.0627];
Mzexp = [0.000; 2.712; 3.389; 3.954; 4.519; 5.649; 6.666; 7.796; 8.812];

FIL24exp = [];
Mzexp_1 = [];

TETAteo = [0.0000; 0.0013; 0.0129; 0.0260; 0.0354; 0.0442; 0.0483;
0.0560; 0.0596; 0.0615];
Tteo = [0.000; 4.604; 9.927; 13.436; 15.490; 16.814; 17.375; 17.703;
18.119; 18.214];

TCI_exp = [20.449; 19.4324; 18.755; 15.139; 10.168];
MCI_exp = [0; 9.942; 18.755; 30.165; 40.898];
TCI_teo = [19.4705; 17.7858; 16.9302; 13.0901; 13.1451];
MCI_teo = [0; 8.8929; 16.9302; 26.1803; 52.5803];
TCI_teog = [19.8; 18.1; 16.8; 13];
MCI_teog = [0; 9;  16.7; 26];

% Legenda
aa = '2-2 Exp. (M/T = 0.5)';
bb = 'CA-STM';
cc = 'CA-STM [15]';
end
```

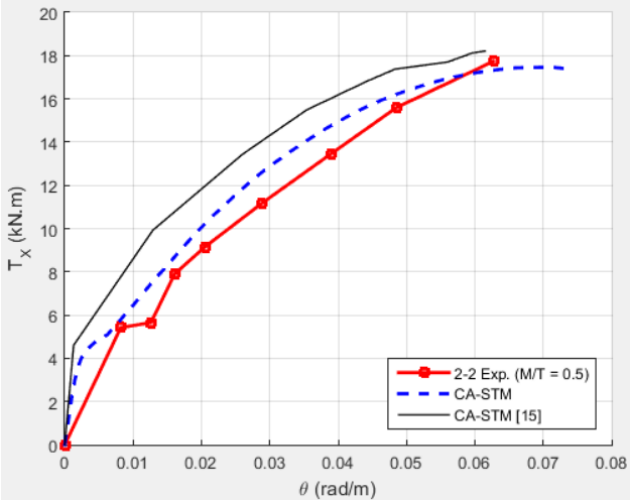

Curvas $T_X - \theta$

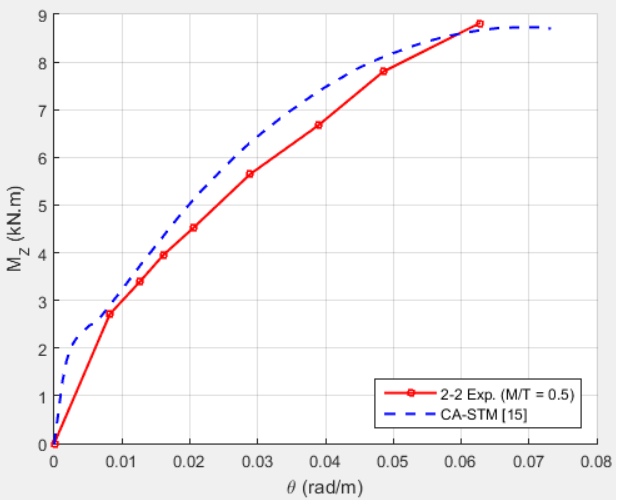

Curva $M_Z - \theta$

```
function Lampert_and_Thurlimann_TB2
%////////////////////////////////////////////////////////////////////////
% Dados experimentais viga TB2 de Lampert e Thurlimann (1969)
%////////////////////////////////////////////////////////////////////////
global h b t1 t2 t3 t4 Al1 Al2 Al3 Al4 At s fLy fTy Es fcm e0 ecr ecr0
global TETAexp Texp TETAteo Tteo aa bb cc dd MyTx MzTx VyTx
global VzTx NxTx TCI_exp MCI_exp TCI_teo MCI_teo TCI_teog MCI_teog
TETAexp_1 Mzexp FIL24exp Mzexp_1
%////////////////////////////////////////////////////////////////////////
% DADOS DA SECÇÃO
%////////////////////////////////////////////////////////////////////////

% Geometria da secção:
h = 0.50;                % Altura da secção (m)
b = 0.50;                % Base da secção (m)
t1 = 0.08; t2 = 0.08;    % Espessura máxima dos painéis 1 e 2 (m)
t3 = 0.08; t4 = 0.08;    % Espessura máxima dos painéis 3 e 4 (m)

% Quantidade das armaduras:
Al1 = 2.262*10^-4;   % Área da armadura longitudinal no painel 1 (m2)
Al2 = 2.262*10^-4;   % Área da armadura longitudinal no painel 2 (m2)
Al3 = 2.262*10^-4;   % Área da armadura longitudinal no painel 3 (m2)
Al4 = 11.31*10^-4;   % Área da armadura longitudinal no painel 4 (m2)
At = 1.131*10^-4;    % Área da armadura transversal (m2)
s = 0.110;           % Espaçamento da armadura transversal (m)

% Propriedades Mecânicas dos aços:
fLy = 390;           % Tensão de cedência da armadura longitudinal (MPa)
fTy = 390;           % Tensão de cedência da armadura transversal (MPa)
Es = 210000;         % Módulo de elasticidade dos aços (MPa)

% Propriedades Mecânicas do betão:
fcm = 27.9;          % Resistência média do betão à compressão (MPa)
e0 = (-0.7*(fcm)^0.31)*10^-3; % Extensão de compressão do betão
correspondente à tensão máxima (1/1000)
ecr = 0.0992;        % Extensão de tração de fissuração do betão (1/1000)
ecr0 = 4.5;          % Extensão de tração limite do betão (1/1000)

% Relação dos outros esforços com o momento torsor:
MyTx = 0;            % Momento Fletor y / Momento Torsor x
MzTx = 2;            % Momento Fletor z / Momento Torsor x
VyTx = 0;            % Esforço Cortante y / Momento Torsor x
VzTx = 0;            % Esforço Cortante z / Momento Torsor x
NxTx = 0;            % Esforço Normal x / Momento Torsor x

%////////////////////////////////////////////////////////////////////////
% DADOS CURVA EXPERIMENTAL E TÉORICA
%////////////////////////////////////////////////////////////////////////

TETAexp = [0.0000; 0.0004; 0.0006; 0.0008; 0.0019; 0.0039; 0.0054;
0.0079;
    0.0092; 0.0178; 0.0252; 0.0319; 0.0393];
Texp = [0.000; 10.000; 15.823; 22.777; 32.000; 42.306; 51.262; 61.234;
    71.000; 77.389; 80.665; 80.665; 81.789];

TETAteo = [0.0000; 0.0001; 0.0017; 0.0047; 0.0078; 0.0130; 0.0160;
0.0178;
    0.0193; 0.0211; 0.0250];
Tteo = [0.000; 13.000; 24.483; 40.617; 55.000; 62.252; 67.582; 68.730;
    68.730; 69.000; 71.000];
```

```
TETAexp_1 = [];
Mzexp = [];

FIL24exp = [0; 0; 0.000007; 0.00036; 0.000839; 0.001256; 0.001772;
0.002322;
    0.002618; 0.003127; 0.0064; 0.009884; 0.013496; 0.01732; 0.021482;
    0.027575; 0.030086; 0.03797];
Mzexp_1 = [0; 25.5; 38; 49.5; 64.5; 83; 103.5; 122; 143; 161.5; 174;
180.5;
    181.5; 183; 185.5; 189; 190.5; 193.5];



TCI_exp = [105.5; 115.3; 81.4; 59.0];
MCI_exp = [0; 146.6; 176.2; 232];
TCI_teo = [108.4; 92.4377; 75.3271; 67.3394 ];
MCI_teo = [0; 92.4377; 150.6541; 249.1557];
TCI_teog = [95.9; 105.9; 70.5];
MCI_teog = [0; 135; 153];

% Legenda
aa = 'TB2 Exp. (M/T = 2.0)';
bb = 'CA-STM';
cc = 'CA-STM [15]';
dd = 'T3, TB1, TB2 e TB3';
end
```

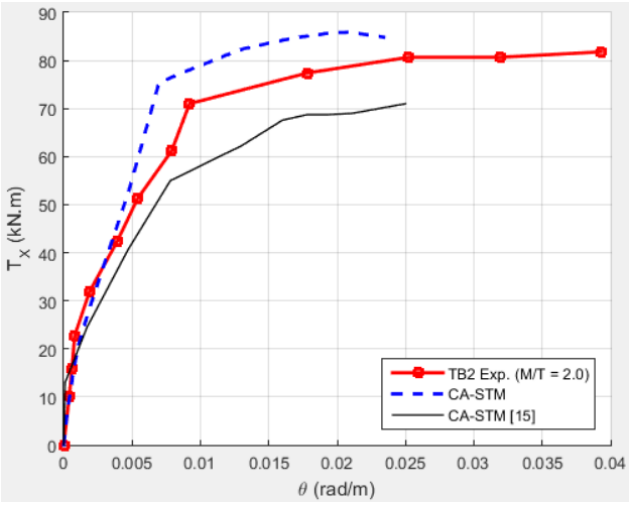

Curvas $T_X - \theta$

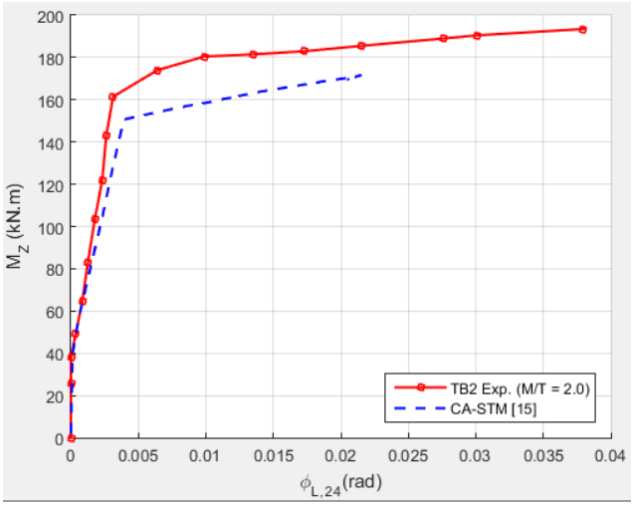

Curva $M_Z - \phi_{L,24}$